

**Development of new Lead-Like Dual Inhibitors of
the cdc2-like Kinase 1 (Clk1) and Dual
Specificity Y-phosphorylation Regulated Kinases
1A and 1B (Dyrk1A and Dyrk1B)**

Dissertation

zur Erlangung des Grades

des Doktors der Naturwissenschaften

der Naturwissenschaftlich-Technischen Fakultät III

Chemie, Pharmazie, Bio- und Werkstoffwissenschaften

der Universität des Saarlandes

von

Dipl. Chem. Christian Schmitt

Saarbrücken, 2014

Tag des Kolloquiums:	8. August 2014
Dekan:	Prof. Dr. Volkhard Helms
Vorsitzender:	Prof. Dr. Claus Jacob
Berichterstatter:	Prof. Dr. R.W. Hartmann Prof. Dr. Johann Jauch
Akad. Mitarbeiter:	Dr. Klaus Hollemeyer

Die vorliegende Arbeit wurde von Juni 2009 bis September 2013 unter Anleitung von Herrn Prof. Dr. Rolf W. Hartmann in der Fachrichtung 8.2 Pharmazeutische und Medizinische Chemie der Naturwissenschaftlich-Technischen Fakultät III der Universität des Saarlandes angefertigt.

Summary

Dyrk1A, a kinase from the CMGC group of kinases was recently identified as potential drug target for the treatment of Down Syndrome (DS) related Alzheimer's Disease. Within the present work a combination of ligand- and structure-based inhibitor design was successfully applied to develop new dual inhibitors of Clk1 and Dyrk1A/1B. Two new compound classes were identified and optimised in terms of potency and selectivity for their target kinases. This approach yielded in three lead-like compounds with exceptional small molecular weight and IC_{50} values of about 100 nM. The good selectivity of the inhibitors was achieved by applying the following strategies:

- Establishment of only one hydrogen bond to the hinge region within the ATP pocket
- Optimisation of ligand shape and distance of H-bond acceptor groups
- Optimisation of the electrostatic complementarity to the kinase ATP pocket

The most active compounds showed activity within living cancer cells which was clearly reduced to modulation of some Dyrk1A/1B and Clk1 dependent pathways. Therefore the new inhibitor scaffolds might serve as new leads for the development of new therapeutics for the treatment of neurodegenerative diseases or cancer.

In parallel, a MALDI triple quadrupole mass spectrometry based kinase assay platform was established which exhibited excellent performance in terms of reproducibility, robustness and high-speed measurements.

Zusammenfassung

Dyrk1A, eine Kinase aus der Familie der CMGC Kinasen wurde als mögliches Target zur Behandlung der Alzheimer Krankheit bei Down Syndrom Patienten beschrieben. In der vorliegenden Arbeit wurde eine Kombination aus struktur- und ligandbasiertem Ansatz erfolgreich angewandt, um neue duale Inhibitoren von Clk1 und Dyrk1A/1B zu entwickeln. Zwei geeignete Verbindungsklassen wurden identifiziert, die durch weitere Optimierung drei selektive Inhibitoren der Zielkinasen hervorbrachten. Die Verbindungen zeichnen sich durch eine kleine molare Masse und IC_{50} Werte im Bereich von 100 nM aus. Deren hohe Selektivität wurde durch die folgenden drei Strategien erreicht:

- Verwendung von nur einem Wasserstoffbrückenakzeptor zu der „hinge region“ der ATP-Bindetasche der Kinase
- Optimierung des Wasserstoffbrückenakzeptorenabstandes, so wie der Molekülgeometrie der Inhibitoren
- Erzeugung elektrostatischer Komplementarität zur ATP Bindetasche

Die aktivsten Verbindungen wiesen zelluläre Aktivität in Krebszellen auf. Dieser Effekt konnte eindeutig auf die Modulierung Dyrk1A/Dyrk1B und Clk1 abhängiger Signalwege zurückgeführt werden. Daher können die Verbindungen als neue Leitverbindungen zur Entwicklung von Medikamenten zu Behandlung neurodegenerativer Erkrankungen und Krebs dienen.

Parallel dazu wurde ein auf MALDI-Massenspektrometrie basierender Kinaseassay etabliert, der durch exzellente Leistung in Bezug auf Reproduzierbarkeit, Robustheit und Messgeschwindigkeit überzeugte.

Publications included in this thesis

The present thesis is divided into four publications which are referred to in the text by capital letters A to D.

- A.** Design and Synthesis of a library of lead-like 2,4-bisheterocyclic substituted thiophenes as selective Dyrk/Clk inhibitors. Christian Schmitt, Dagmar Kail, Marica Mariano, Martin Empting, Nadja Weber, Tamara Paul, Rolf W. Hartmann, Matthias Engel; *PlosOne* **2014**, 9, e87851

- B.** Hydroxybenzothiophene ketones as novel mRNA splicing modulators: potent inhibition of Dyrk1A but not of Clk1/4 alone results in high efficacy. Christian Schmitt, Parisa Miralinaghi, Marica Mariano, Rolf W. Hartmann and Matthias Engel; *Medicinal Chemistry Letters*, **2014**

- C.** Screening Dyrk1A inhibitors by MALDI-QQQ mass spectrometry. Systematic comparison to established radiometric, luminescence and LC-UV-MS assays. David Gode, Christian Schmitt , Matthias Engel , Dietrich A. Volmer; *Analytical and Bioanalytical Chemistry*, **2014**, DOI: 10.1007/s00216-014-7703-1

- D.** 6-Hydroxybenzothiophene ketones: potent inhibitors of 17 β -hydroxysteroid dehydrogenase type 1 (17 β -HSD1) due to favorable molecule geometry and conformational pre-organization. Miralinaghi Parisa, Schmitt Christian, Hartmann, R. W, Frotscher Martin, Engel Matthias. *ChemMedChem*, **2014**, DOI: 10.1002/cmdc.201402050

Contribution Report

The author wishes to clarify his contributions to the publications **A–D** in the thesis.

- A.** The author significantly contributed to the inhibitor design concept. The author planned, synthesised and characterised most of the new kinase inhibitors. In addition, the author planned and performed most of the *in vitro* assays. The author performed molecular docking experiments and analysed the data. Furthermore the author significantly contributed to the interpretation of the results and wrote the manuscript.

- B.** The author significantly contributed to the planning, synthesis, and characterisation of most compounds. The author significantly contributed to the conception and analysis of the real-time PCR experiments. The author performed most of the kinase assays and interpreted the results. The author wrote the manuscript.

- C.** The author significantly contributed to the experimental design of the study. The author conceived and performed the kinase assays. The author significantly contributed to the analysis of the data and wrote parts of the manuscript.

- D.** The author significantly contributed to the design, synthesis, and characterization of the new compounds as 17- β -HSD1 inhibitors. The author significantly contributed to the interpretation of the results and wrote parts of the manuscript.

Abbreviations

Å	Angstrom
µM	Micromole per liter
17β-HSD	17β-Hydroxysteroid Dehydrogenase
ABL	Tyrosine-protein kinase ABL1
ADP	Adenosine diphosphate
AGC	PKA, PKG and PKC
ALL	Acute lymphoblastic leukemia
ASF	Alternative splicing factor
Asp	Aspartate
ATP	Adenosine triphosphate
CAMK	Ca ²⁺ /calmodulin-dependent protein kinases
Clk	Cdc2-like kinases
CDK	Cyclin-dependent kinase
c-Jun	Transcription factor AP-1
CK1	Casein kinase 1
CK2α	Casein kinase 2 alpha
CMGC	Cyclin-dependent kinases, mitogen-activated protein kinases, glycogen synthase kinases and CDK-like kinases (CLKs)
CML	Chronic myeloid leukemia
c-Myc	Myc proto-oncogene protein
CSF1R	Colony stimulating factor 1 receptor
Cyclic AMP	Cyclic adenosine monophosphate
DFG	Aspartate, Phenylalanine and Glycine
Dyrk	Dual Specificity Tyrosine phosphorylation regulated Kinase
EC ₅₀	Concentration required to induce 50 % of the maximal effect after a specific exposure time
EGFR	Epidermal growth receptor kinase
EPH	Ephrin type-A receptor 1
EPHB4	Receptor protein tyrosine kinase EphB4
ERBB2	Receptor tyrosine-protein kinase erbB-2
FDA	Food and Drug Administration
FGR	Tyrosine-protein kinase Fgr
FLT3	Receptor-type tyrosine-protein kinase FLT3
FYN	Tyrosine-protein kinase Fyn
GC	Gas chromatography
GIST	Gastrointestinal stromal tumors
Glu	Glutamate
Gsk3β	Glycogen synthase kinase 3 beta
HCK	Tyrosine-protein kinase HCK
HPLC	High performance liquid chromatography
IC ₅₀	Concentration required to induce 50 % inhibition
INDY	Inhibitor of Dyrk kinases
KIT	Mast/stem cell growth factor receptor Kit
K _m	Michaelis-Menten constant
LCK	Lymphocyte cell-specific protein-tyrosine kinase
LogP	Octanol/water partition coefficient
LYN	Tyrosine-protein kinase Lyn
Lys	Lysine
MALDI	Matrix assisted laser desorption ionization

MS	Mass spectrometry
mTORC1	Mammalian target of rapamycin complex 1
NMR	Nuclear magnetic resonance
NSCLC	Non-small cell lung cancer
p27kip1	Cyclin-dependent kinase inhibitor 1B
PDGFR β	Platelet-derived growth factor receptor
PKA	Protein kinase A
pK _a	Acid dissociation constant
pNET	Pancreatic neuroendocrine tumors
PSA	Polar surface area
QqQ	Triple quadrupole
RAF	RAF proto-oncogene serine/threonine-protein kinase
RCC	Renal cell carcinoma
RET	Proto-oncogene tyrosine-protein kinase receptor Ret
RGC	Receptor Guanylate cyclase
RSD	Relative standard deviation
SAR	Structure activity relationship
Ser	Serine
SH2	Src homology 2 domain
SH3	Src homology 3 domain
SPF45	Alternative splicing factor 45
SRC	Proto-oncogene tyrosine-protein kinase Src
SRp55	Serine/arginine-rich splicing factor 6
STE	Human homologs of the yeast sterile 7, sterile 11 and sterile 20 kinases
Thr	Threonine
TK	Tyrosine kinases
TKL	Tyrosine kinase-like
VEGFR	Vascular endothelial growth factor receptor
YES	Tyrosine-protein kinase Yes

Table of Contents

1.	Introduction	1
1.1	Protein Kinases	1
1.2	Structural features of protein kinases	4
1.3	Activation of Protein Kinases	7
1.4	Dyrk kinases	8
1.4.1	Dyrk1A	9
1.4.2	Dyrk1B	12
1.4.3	Dyrk2	12
1.4.4	Dyrk3 and Dyrk4	13
1.5	Cdc2-like kinases (Clks)	14
1.6	Dyrk1A inhibitors	15
1.6.1	Synthetic inhibitors	15
1.6.2	Dyrk1A inhibitors from natural sources	17
1.7	Inhibitors of other Dyrks	18
1.7.1	Dyrk1B inhibitors	18
1.7.2	Dyrk2, Dyrk3, and Dyrk4 inhibitors	18
1.8	Clk1 inhibitors	19
2.	Aim of the Thesis	21
3.	Results	23
3.1	Publication A: Design and Synthesis of a Library of Lead-Like 2,4-Bisheterocyclic Substituted Thiophenes as Selective Dyrk/Clk Inhibitors	23
3.2	Publication B: Dual Clk1/Dyrk1A inhibition is required for efficient mRNA splicing manipulation. Discovery of a new inhibitor scaffold.	71
3.3	Publication C: Screening Dyrk1A inhibitors by MALDI-QqQ mass spectrometry. Systematic comparison to established radiometric, luminescence and LC-UV-MS assays	82
3.4	Publication D: 6-Hydroxybenzothiophene ketones: potent inhibitors of 17 β -hydroxysteroid dehydrogenase type 1 (17 β -HSD1) due to favorable molecule geometry and conformational pre-organization	103
4.	Final Discussion	133
4.1	Inhibitor Design Concept	133
4.2	Publication A: Design and Synthesis of a focused library of novel dual Dyrk1A and Dyrk1B inhibitors	136
4.3	Publication B: Discovery of 5-hydroxybenzothiophene ketones as novel dual inhibitors of cdc2-like kinases and Dyrk1A/1B	144
4.4	Classification of the novel inhibitor classes compared to known reference inhibitors	147
4.5	Publication C: Comparison of a MALDI-QqQ mass spectrometric kinase assay with radiometric, luminescence and LC-UV-MS kinase assays	149
4.6	Publication D: Hydroxybenzothiophene ketones as new 17- β -HSD1 inhibitors	153
5.	References	157
6.	Acknowledgements	172
7.	Appendix	173
8.	Lebenslauf	208

1. Introduction

1.1 Protein Kinases

About 1.7 % of the whole human genome encodes for protein kinases which play a significant role in cellular signalling. In 2002, Manning *et al.* identified 478 human eukaryotic kinase and 40 atypical kinase genes. They classified the 478 protein kinases into 9 groups, which contains different kinase families that can be further divided into several subfamilies (Manning *et al.*, 2002). The classification based on the comparison of the amino acid sequence within the catalytic domain and supported by knowledge of additional properties, including known biological functions and sequence similarity outside of the catalytic domains (Manning *et al.*, 2002).

Protein kinases catalyse the transfer of the γ -phosphate group of ATP to the hydroxyl group of serine, threonine and tyrosine residues within a substrate peptide or protein (Figure 1.1). Although kinases can be classified as serine/threonine specific and tyrosine specific kinases there are many representatives which show dual specificity (e.g. Dyrks (Walte *et al.*, 2013) and mitogen activated protein kinase kinases (Raingeaud *et al.*, 1995)). The transient protein phosphorylation is one of the most important posttranslational modifications (Adams, 2001) and can be regarded as universal molecular switch of almost all cellular processes (Graves and Krebs, 1999). Thus kinases are key players in signal transduction pathways and regulate many cellular mechanisms, such as growth, differentiation, proliferation and apoptosis (Traxler and Furet, 1999).

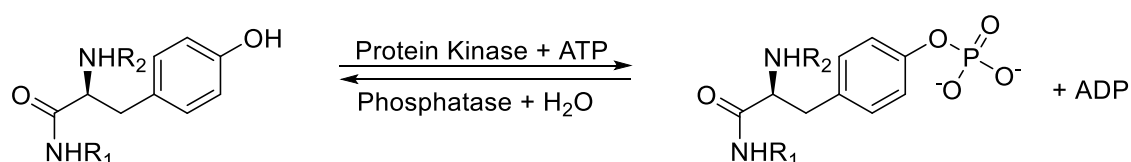


Figure 1.1: The protein kinase mediates the phosphorylation reaction of a substrate peptide/protein with ATP. The reaction yields a phosphopeptide/protein and adenosine diphosphate (ADP). Phosphatases catalyse the cleavage of the phosphoric acid monoesters and deactivate the signal triggered by the protein kinase.

Deregulation of kinase activity or mutations in kinase genes are responsible for the outcome of many human diseases, in particular inflammatory diseases, neurological diseases (e.g. Alzheimer's disease and Parkinson's disease), metabolic disorders (e.g. diabetes type 2), vascular diseases and many types of cancer (Chico *et al.*, 2009; Lahiry *et al.*, 2010). Protein kinases rank among the most important drug targets and demand for 20 to 30% of some industrial drug discovery programmes and essentially three strategies for kinase inhibition are known (Cohen, 2002). These attack points are summarized as follows:

- Peptide substrate binding site
- Allosteric pockets
- ATP binding site

Today, there are a vast number of small molecule kinase inhibitors in different stages of clinical trials and some of them are approved as drugs by the FDA (Table 1.1). Nearly all efforts in kinase inhibitor research are focussed on the treatment of cancer. Although Ser/Thr kinases were identified to have critical roles in tumour progression they attracted less attention than tyrosine kinases and all anti-cancer kinase inhibitors on market target on tyrosine kinases (Fedorov et al., 2007).

Table 1.1: Examples of marketed kinase inhibitors approved by the FDA (Matthews and Gerritsen, 2010)

Drug	Company	Target	Kinase	Indication	Approval (FDA)
Imatinib, Gleevec®	Novartis	ABL, KIT, PDGFR	TK	ALL, CML, GIST	2001
Dasatinib, Sprycel®	Bristol-Myers Squibb	ABL, EPH, FYN, LCK, SRC, PDGFR	TK	ALL, CML	2006
Nilotinib, Tasisign®	Novartis	ABL, KIT, PDGFR, EPHB4, FGR, FYN, HCK, LCK, LYN, SRC, YES	TK	CML	2007
Gefitinib, Iressa®	AstraZeneca	EGFR	TK	NSCLC	2003
Rapamune	Wyeth	mTORC1	Ser/Thr	immunosuppressiva	1999
Torisel	Wyeth	mTORC1	Ser/Thr	Advanced renal Cell carcinoma	2007
Erlotinib, Tarceva®	OSI/Gentech	EGFR	TK	NSCLC, pancreatic cancer	2004
Lapatinib, Tykerb®	GlaxoSmithKline	EGFR, ERBB2	TK	Breast cancer	2007
Sorafenib, Nexavar®	Bayer	RAF, VEGFR, FLT3, KIT, RET, PDGFR β	TK	Hepatocellular and renal carcinoma	2005
Sunitinib, Sutent®	Pfizer	VEGFR, FLT3, KIT, RET, PDGFR, CSF1R	TK	GIST, RCC, pNET	2006

Dependent on their mode of action kinase inhibitors can be roughly divided into 5 classes (Cox et al., 2010; Lamba and Ghosh, 2012; Liu and Gray, 2006):

- Type I inhibitors are competitive to ATP binding site and binding is independent of the kinase activation state.
- Type I ½ inhibitors are similar to type I inhibitors but in addition they exploit a hydrophobic back pocket for binding.
- Type II inhibitors use the ATP binding site and an additional “allosteric” pocket which is exclusively accessible in inactive kinases (DFG-out) and buried in active kinases (DFG-in).
- Type III inhibitors bind into the “allosteric” pocket adjacent to the ATP cleft, which is also used by type II inhibitors and prevent the kinase to adopt its active state. Type III inhibitors undergo no interactions within the ATP pocket.
- Type IV inhibitors exploit allosteric pockets distant from the ATP binding site.
- Type V inhibitors are bivalent inhibitors that combine different features from the other inhibitor classes (Lamba and Ghosh, 2012; van Linden et al., 2013).

Figure 1.2 schematically illustrates the mode of action of type I, type II and type III inhibitors. Most kinase inhibitors currently identified in the course of drug discovery programs binds to the adenine binding region and compete with ATP for binding. To anchor within this pocket, these small molecule inhibitors take advantage of at least one of three possible hydrogen bonds in the so called hinge region, a short peptide chain the N-terminal lobe and the C-terminal lobe of the kinase (Ghose et al., 2008; Traxler and Furet, 1999). Despite of this highly conserved binding site present in all kinases it is possible to develop rather selective ATP competitive inhibitors but the exact molecular mechanism remains elusive. However, a major difficulty to obtain *in vivo* efficient competitive kinase inhibitors are the K_m^{ATP} values of the kinases varying between 0.1 μ M to 1 mM (Dennis et al., 2001; Sadler et al., 2004). In combination with the high intracellular ATP concentration ranging from 1 to 5 mM, kinase targets with K_m^{ATP} values below 10 μ M are more suitable to be affected by ATP-noncompetitive inhibitors which are independent from the surrounding ATP concentration (Cohen, 2002; Traut, 1994).

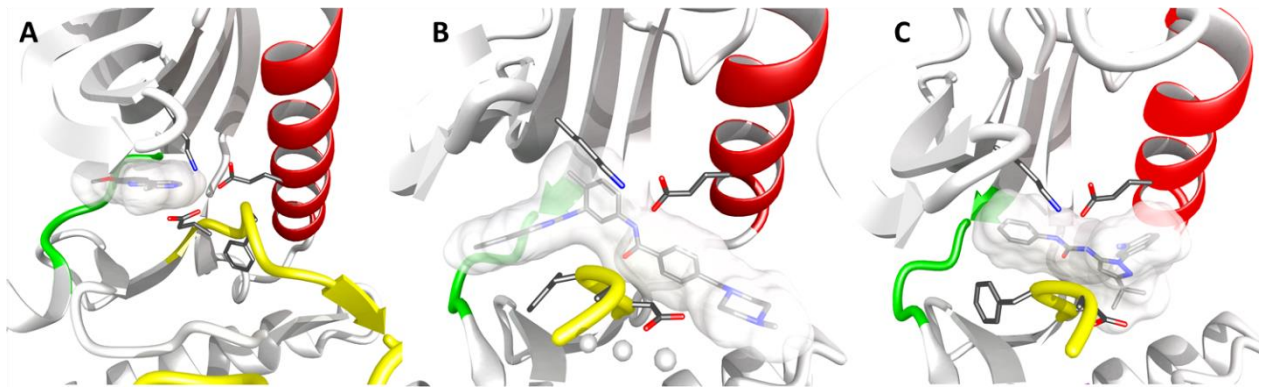


Figure 1.2: Representation of Type I, Type II and Type III mode of action. The hinge region is shown in green, the highly conserved α -C helix is shown in red, and the activation loop harbouring the DFG loop is shown in yellow. A) Type I inhibitor (harmine) in the ATP binding cleft of Dyrk1A (PDB code: 3ANR). The kinase is in its active state (also referred as DFG-in); B) Type II inhibitor (imatinib) bound to the crystal structure of cSrc (PDB code: 2OIQ); the activation loop cannot adopt the active conformation and the phenylalanine residue of the DFG loop points into the ATP cleft; C) Type III inhibitor (RL37) bound to cSrc (PDB code: 3F3U); the inhibitor binds to a pocket adjacent to the ATP binding site where it prevents the active conformation.

1.2 Structural features of protein kinases

The 3D-structure of the Ser/Thr kinase, protein kinase A (PKA or cyclic AMP dependent kinase) was resolved in 1991 by Knighton *et al.* (Knighton *et al.*, 1991a, 1991b). It was the first structure of a protein kinase determined by X-ray crystallography and since then 1252 ligand-bound kinase X-ray structures were deposited in the protein data base (PDB, www.pdb.org) (Bernstein *et al.*, 1977; van Linden *et al.*, 2013). All protein kinases are composed of two spatially different subdomains consisting of the N-terminal and the C-terminal lobe. The N-terminal lobe contains five antiparallel β -strands and one absolutely conserved α -helix, namely the α C-helix. The designation α C-helix originates from the structure of PKA, where the N-terminal lobe contains three helices, the α A-, α B- and α C-helix (Knighton *et al.*, 1991a). The less conserved C-terminal lobe harbours the substrate peptide binding region which is predominantly α -helical without specific structural arrangement. Figure 1.2 shows the X-ray structure of the murine protein kinase A (PKA) with ADP and a substrate peptide in the active state which represents the common 3-D structure of all protein kinases (Madhusudan *et al.*, 2002). Both lobes are connected by a short peptide chain referred to as the hinge region. This structure motif is embedded in the cleft between the N-terminal and the C-terminal lobe and is essential for ATP binding. Therefore it is not surprising that the conformation of this short amino acid sequence is highly conserved and provides usually one backbone hydrogen donor flanked by two backbone hydrogen acceptor groups (Ghose *et al.*, 2008).

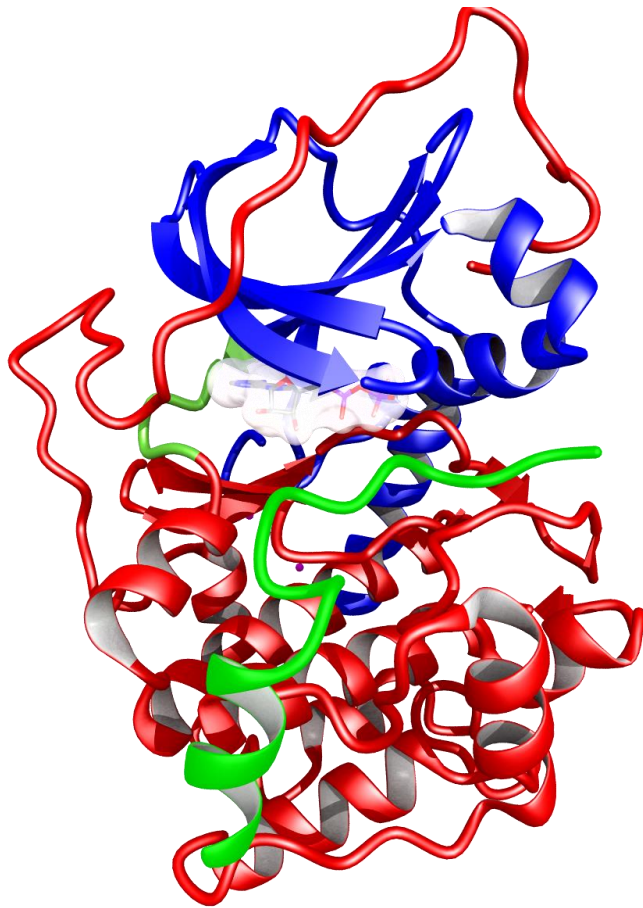


Figure 1.3: Common features of protein kinases by means of the active mouse protein kinase A in complex with ADP and a substrate peptide (PDB-code: 1L3R). The N-terminal lobe is connected with the C-terminal lobe (red) via the hinge region (green). The nucleotide is buried in the cleft between the two lobes and the adenine ring is fixed to the hinge region by two H-bonds. The substrate peptide (light green) binds to the surface of the C-terminal lobe.

ATP uses in general a hydrogen donor acceptor tandem to target the hinge region whereas the H-bond acceptor group in front of the ATP pocket remains free. An exception is represented by the family of Pim kinases, harbouring a PXP sequence motif within the hinge region. The proline residue lacks of the hydrogen bond donor function and ATP can exploit only one hydrogen bond acceptor function to bind to the hinge region (Qian et al., 2005). Figure 1.3 depicts the general architecture of the ATP binding pocket by means of the X-ray structure of PKA. In 1999, Traxler and Furet defined a pharmacophore of the kinase nucleotide binding pocket which comprised of five different features (Traxler and Furet, 1999). These features are also shown in Figure 1.4 and are indicated by the white circles.

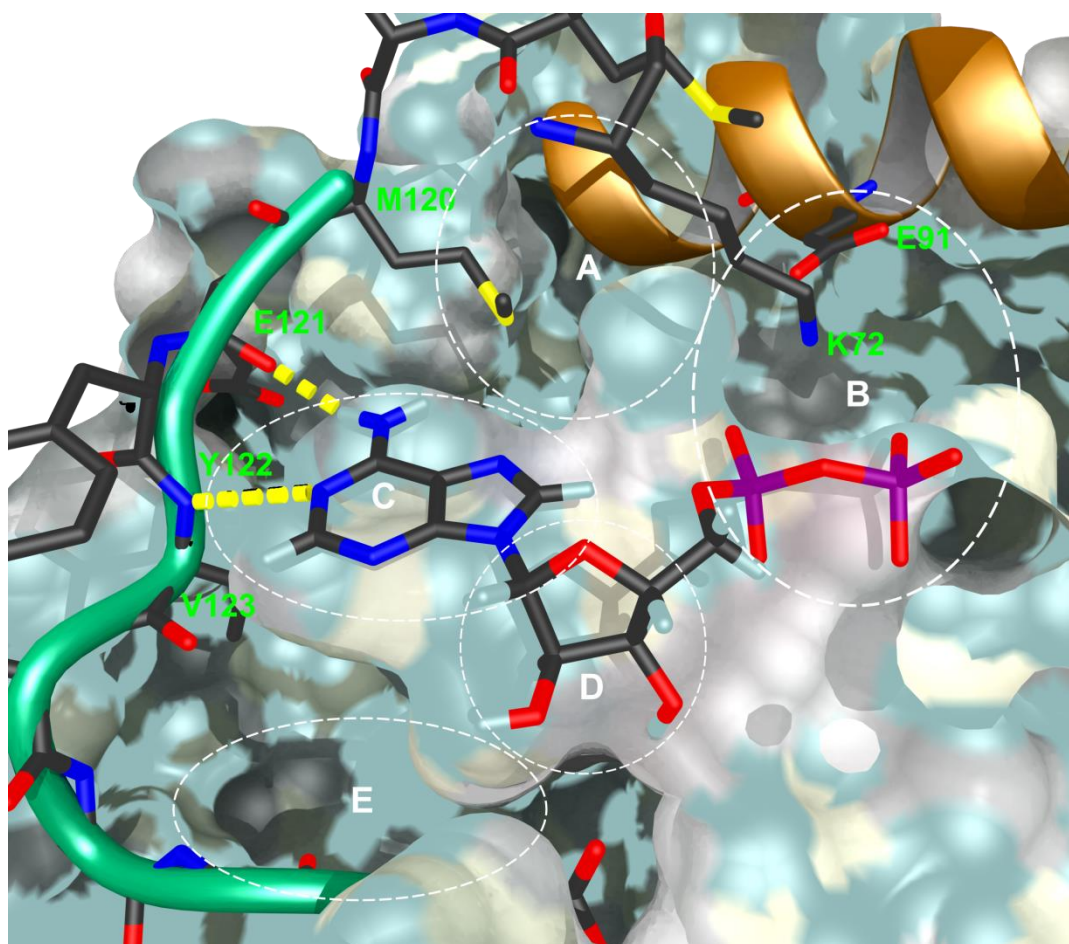


Figure 1.4: Representation of the ATP-pocket of protein kinase A in its active conformation. The linker and hinge region is shown as green lobe. The conserved α -helix is illustrated in gold in the background. The different pocket areas are indicated as white circles. (A) Back hydrophobic or specificity pocket, (B) conserved salt bridge and phosphate binding region, (C) adenine binding region, (D) sugar binding pocket, (E) front pocket.

- **Hydrophobic back pocket (A):** The pocket is located in the spatial extension of the N7-amino group of the adenine moiety but is not used by ATP for binding. The size of the pocket and its accessibility are limited by the bulkiness of the so called gatekeeper residue (methionine in case of PKA). Therefore this hydrophobic region has been used to tune the specificity of kinase inhibitors (type I $\frac{1}{2}$ inhibitors). Compound SB203580 is a prominent example which exploits the back hydrophobic pocket to gain specificity for the p38 α MAP kinase (Tong et al., 1997; Wang et al., 1998; Wilson et al., 1997). This exploration was supported by mutation studies where the gatekeeper residue was replaced by the larger methionine and the smaller alanine respectively (Wilson et al., 1997).
- **Salt bridge and phosphate binding region (B):** This part of the ATP pocket is exposed to the surrounding water and contains the highly conserved salt bridge between Lys72 (PKA

numbering) and Glu91, which is crucial for the active conformation of kinases. Asp184 is required for the binding of the Mg^{2+} ions that are crucial for the phosphorylation reaction. Glu91 stabilises the proper conformation of Lys72, which adjusts Asp184 by a salt bridge. In addition the lysine residue fixes the position of the α - and β -phosphate groups of ATP (Huse and Kuriyan, 2002).

- **Adenine binding region (C):** The adenine binding region has a predominantly hydrophobic character flanked by the polar hinge recognition site (Ghose et al., 2008). All ATP competitive inhibitors bind to this region.
- **Sugar pocket (D):** The ribose pocket is adjacent to the adenine binding region and some EGFR kinase inhibitors show important interactions with this region (Traxler et al., 1996).
- **Front pocket (E):** The front pocket is a rather small hydrophobic area between the adenine binding region and the solvent and is not used by ATP. This area can be used to enhance the potency as well as the specificity of some kinase inhibitors.

1.3 Activation of Protein Kinases

All protein kinases can switch between a catalytically active (open) and a catalytically inactive (closed) conformation (Karlsson et al., 1993; Zheng et al., 1993). Kinases catalyse the same reaction and underlie very sharp conformational constraints which result in closely related active conformations (Figure 1.3). In contrast the conformation of inactive kinases is not limited and there are diverse activation mechanisms among the different kinase classes (Huse and Kuriyan, 2002). Therefore they have mainly two key regulatory elements, consisting of the α C-helix which is located in the N-terminal lobe and the activation loop, which is part of the C-terminal lobe. Both elements are crucial for the appropriate kinase folding that is required for substrate binding. The activation loop normally comprises of 20-30 amino acids and harbours the conserved Asp-Phe-Gly (DFG) sequence.

Since most kinases underlie phosphorylation of their activation segment, this post-translational modification represents the best known mechanism of protein kinase activation. The phosphorylation of the activation segment induces a conformational change of the DFG peptide and stabilises the active conformation of the kinase by establishment of electrostatic interaction with conserved arginine residues (Nolen et al., 2004). In the inactive state, the aspartate residue (Asp) is turned away from the ATP pocket and the phenylalanine residue (Phe) is pointed into the ATP cleft or into the solvent. This state, commonly referred as DFG-out, prevents the highly conserved salt

bridge between lysine Lys72 and glutamate Glu91 by displacing the α C-helix from the active site. In the active state, commonly referred to as DFG-in, the aspartate shifts into its proper position and the phenylalanine side chain rotates into a hydrophobic pocket, enabling the reformation of the conserved salt bridge and repositioning of the α C-helix. The number and position of phosphorylation sites on the activation segment is not fixed and varies from kinase to kinase (Huse and Kuriyan, 2002).

As mentioned before, some groups of kinases underlie other regulation mechanisms distinct from the activation segment phosphorylation/ dephosphorylation switch. These mechanisms include C-terminal regulation, N-terminal regulation and protein-protein interactions.

C-terminal regulation can be controlled either by C-terminal inhibitory domains which have been found in the calcium/calmodulin-dependent kinase I and the large muscle protein titin (Goldberg et al., 1996; Mues et al., 1999) or by C-terminal activation domains which could be found in AGC kinases (Gold et al., 2006). Both domains affect the proper orientation of the α C-helix and the formation of the conserved lysine-glutamate salt bridge which is crucial for catalytic activity.

N-terminal regulation of kinases is often controlled by a small juxtamembrane sequence which has several potential phosphorylation sites that are needed for auto-inhibitory control. The juxtamembrane sequence binds to the surface of the N- and C- terminal lobe and stabilises a catalytic inactive conformation of the kinase. Phosphorylation of the juxtamembrane segment triggers the dissociation of the complex between kinase and the N-terminal juxtamembrane lobe and allows the kinase to adopt an active conformation (Griffith et al., 2004; Huse and Chen, 1999; Huse et al., 2001; Wybenga-Groot et al., 2001).

The last two important regulation mechanisms are represented by protein-protein interactions and other intramolecular interactions. A prominent example for regulation by protein-protein interactions is the class of cyclin-dependent kinases (CDK). The appropriate orientation of the α C-helix is controlled by a specific interaction of the kinase domain with cyclin. Only in presence of cyclin the kinase can adopt its active conformation (De Bondt et al., 1993). The SRC kinases are non-receptor tyrosine kinases which are regulated by intramolecular interactions of different domains. In the inactive state, the kinase exists in a compact structure with close interactions between the SH2, SH3 and the kinase domain. In presence of an activator the compact structure opens and enables kinase activation by phosphorylation of the activation loop (Xu et al., 1999).

1.4 Dyrk kinases

Dual specificity tyrosine (Y)-phosphorylation regulated kinases (Dyrks) belong to the CMGC superfamily and six members were identified, Dyrk1A, 1B, 2, 3, 4A, and 4B (Becker et al., 1998). CMGC implies for its principal kinase families: Cyclin-dependent kinases (CDKs), mitogen-activated protein kinases (MAPKs), glycogen synthase kinases (GSKs), and CDK-like kinases (CLKs). CMGC kinases are serine/threonine kinases but several members of the superfamily autophosphorylate on specific tyrosine residues to evolve full activity (Ben-David et al., 1991; Howell et al., 1991; Kentrup et al., 1996). The Dyrk kinases, like other members of the CMGC superfamily, are dependent on the autophosphorylation mechanism in their activation loop to develop full enzymatic activity. Earlier studies suggested that tyrosine autophosphorylation of Dyrk kinases occurs during the translation of the protein and the specificity for tyrosine residues is lost in the mature kinase (Lochhead et al., 2005).

However, a newer study on Dyrk1A suggests that tyrosine autophosphorylation can also happen after translation and is not limited to the activation loop (Walte et al., 2013). After autophosphorylation, the specificity for tyrosine residues is not completely lost, but depends on a particular kinase conformation. The authors suggested two different kinase conformations, one with serine/threonine specificity and one with tyrosine specificity, which are in a dynamic equilibrium (Walte et al., 2013). Dyrk1A, Dyrk1B, and Dyrk2 have been most extensively investigated regarding their biological function (Becker, 2012).

1.4.1 Dyrk1A

Dyrk1A attracted more attention than the both congeners Dyrk1B and Dyrk2 due to its supposed contribution to the development of Alzheimer-like neurodegenerative diseases observed in individuals suffering from Down Syndrome (DS). The gene for Dyrk1A is located within the Down Sndrome Critical Region (DSCR) of chromosome 21 (Aranda et al., 2011; Becker and Joost, 1999; Becker and Sippl, 2011). Due to the extra-copy of chromosome 21, Down Syndrome patients have an up to 1.5 fold increased Dyrk1A level compared to the Dyrk1A level of healthy individuals (Kimura et al., 2007a; Wegiel et al., 2008). Dyrk1A was identified to phosphorylate the microtubule-associated tau protein on at least 11 sites and acts as priming kinase for glycogen-synthase-kinase (GSK)3 β (Kurabayashi et al., 2010; Liu et al., 2008; Ryoo et al., 2007; Woods et al., 2001). The hyperphosphorylation of tau protein caused by elevated Dyrk1A levels is suggested as one key step in the formation of neurotoxic neurofibrillary tangles observed in Alzheimer's Disease (Johnson and Stoothoff, 2004; Steinhilb et al., 2007). In addition, Dyrk1A also phosphorylates on the alternative

splicing factor (ASF) and the serine/arginine-rich protein 55 (SRp55). The phosphorylation shifts the sensitive ratio between 4R- and 3R-tau (4 repeat and 3 repeat tau) isoforms by reducing the transcription of exon 10 to an increased level of 3R-tau. This modification forces back the ASF into its nuclear speckles and removes ASF from the site of mRNA transcription (Qian et al., 2011; Shi et al., 2008). The imbalance between the both tau isoforms affect the protein stability, which facilitate the aggregation and precipitation of tau protein resulting in the formation of neurofibrillary tangles (Liu and Gong, 2008; Smith et al., 2012; Wegiel et al., 2011a). Clk1, another CMGC kinase was also identified to affect Tau alternative splicing (see chapter 1.5). Dyrk1A was also found to phosphorylate on Thr668 of β -amyloid precursor protein (APP), a modification which is necessary for APP cleavage (Ryoo et al., 2008). The cleavage of APP is the first step in the formation of amyloid β and increased amyloid β concentrations are discussed to additionally activate the Dyrk1A transcription, resulting in an acceleration of amyloid β formation (Kimura et al., 2007a; Park et al., 2007). The resulting tauopathies and β -amyloidosis cause the decrease of cognitive functioning and loss of neuronal cells in Alzheimer's Disease progression (Figure 1.5). Aberrant Dyrk1A activity has also been associated with other neurodegenerative diseases like Parkinson Disease (PD). Dyrk1A phosphorylates α -synuclein and facilitates its aggregation to build Lewy bodies found in Parkinson Disease but also in Alzheimer's Disease (Kim et al., 2006a). In a recent study Dyrk1A was found to be overexpressed in EGFR-dependent glioblastoma cell lines (Pozo et al., 2013). The treatment of the glioblastoma cells with two validated Dyrk1A inhibitors significantly reduced the tumour cell growth. In addition, Dyrk1A stabilises HPV16E7 by phosphorylation on two threonine residues and increases the mutation potential of HPV16 infected cells (Liang et al., 2008). Therefore, pharmacological inhibition of Dyrk1A is a promising strategy for the treatment of Down Syndrome (DS) related Alzheimer's Disease (AD), other neurological pathologies, and maybe in some types of cancer. Despite of the high interest in the development of new Dyrk1A inhibitors, there is currently little known about potential adverse target-based effects. Especially for the treatment of neurodegenerative diseases the goal is to decrease the elevated Dyrk1A activity to that of healthy individuals (Smith et al., 2012).

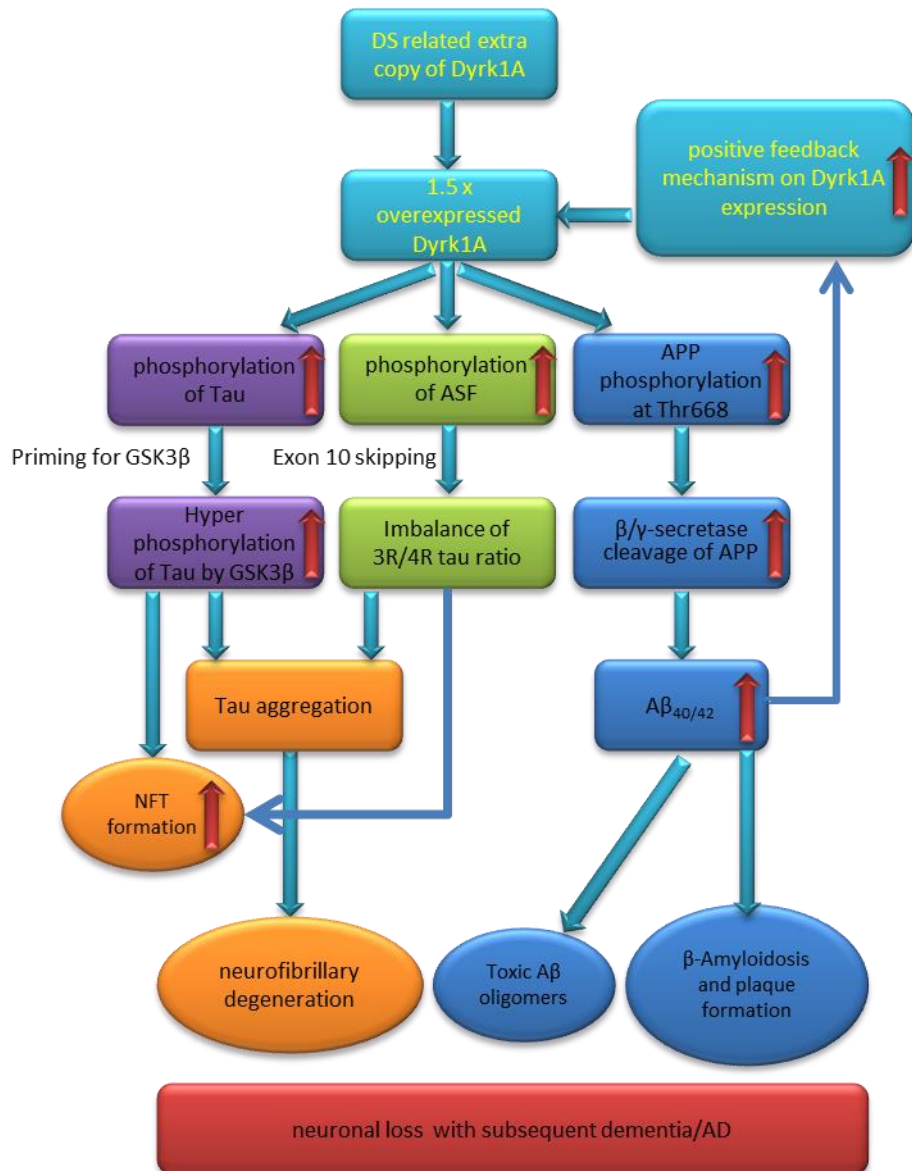


Figure 1.5: Assumed contribution of Dyrk1A to the development of Down Syndrome related neurodegeneration. Dyrk1A triggers two pathways leading to neurofibrillary tangles by phosphorylation of Tau and alternative splicing factor (ASF). Phosphorylation on amyloid- β precursor protein (APP) discloses a pathway responsible for toxic amyloid- β oligomers and β -amyloidosis. Neurofibrillary degeneration and β -amyloidosis cause loss of neuronal cells leading to dementia and Alzheimer's Disease (Wegiel et al., 2011b).

1.4.2 Dyrk1B

Dyrk1B, the closest related kinase to Dyrk1A is mainly expressed in skeletal muscle, testes heart, and brain cells but shows a strong overexpression in some tumour cell lines (Lee et al., 2000). Dyrk1B was found to be essential for differentiation of myoblasts by stabilising p27kip1 and prevention of apoptosis under physiological conditions (Mercer et al., 2005). Several types of cancer, including pancreatic cancer, exploit the anti-apoptotic function of Dyrk1B. Due to the elevated expression of this kinase, tumour cells are able to reversibly switch in the G₀ state of the cell cycle. This allows the cells to re-enter the cell cycle later and to escape from eradication by chemotherapeutic agents (Hu et al., 2011; Jin et al., 2009). The increased activity of Dyrk1B leads to higher phosphorylation rate of the cell cycle regulators cyclin D1 and the cyclin-dependent kinase 2 (CDK2) inhibitor p27kip1 (Deng et al., 2004; Jin et al., 2009; Zou et al., 2004). The phosphorylation of threonine 286 or threonine 288 by Dyrk1B highlights cyclin D1 for proteasomal degradation whereas p27kip1 is stabilised by phosphorylation of serine 10 (Zou et al., 2004). It has been suggested that Dyrk1A mediates the same phosphorylation on cyclin D1 which highlights the cell cycle regulator for nuclear export and ubiquitinylation (Becker, 2012; Blockeel et al., 2011). In view of the treatment of cancer, co-inhibition of both Dyrk1A and Dyrk1B might be a useful strategy to intervene into the tumour cell cycle. Dyrk1B also mitigates the effects of reactive oxygen species in quiescent pancreatic cancer cells impeding cell damaging and induction of apoptosis (Deng et al., 2009a).

1.4.3 Dyrk2

The reported roles of Dyrk2 especially in tumour biology are discussed controversial. Dyrk2 mRNA was identified to be overexpressed in esophageal and lung adenocarcinomas (Miller et al., 2003) and the Dyrk2 gene was overexpressed in malignant gastrointestinal stromal tumours (Koon et al., 2004). But more recent studies suggest an antiproliferative function of Dyrk2. The stable knockdown of Dyrk2 in human cancer cells accelerated the cell cycle progression resulting in a higher proliferation rate. Dyrk2 is required as priming kinase for GSK3 β which phosphorylates the cell cycle promoters c-Jun and c-Myc and marks them for proteasomal degradation (Taira et al., 2012). Without the Dyrk2 mediated priming phosphorylation GSK3 β is not able to phosphorylate c-Jun and c-Myc for degradation (Figure 1.6). In human breast cancer cells Dyrk2 has been also identified as a marker for invasiveness, where the down regulation of Dyrk2 leads to an accumulation of Snail protein and subsequent increased invasion (Mimoto et al., 2013). The final phosphorylation of Snail protein for ubiquitinylation and degradation is made by GSK3 β . Another mechanism of Dyrk2 is the modulation and stabilisation of p53 tumour suppressor protein, which induces apoptosis after severe DNA damage (Taira et al., 2007; Yoshida, 2008). Furthermore the elimination of Dyrk2 expression in

breast cancer may hamper the proteasomal degradation of telomerase (Jung et al., 2013). The development of Dyrk2 selective small molecule inhibitors could be an opportunity to elucidate the precise role of Dyrk2 in biological pathways especially of these critical in cancer development.

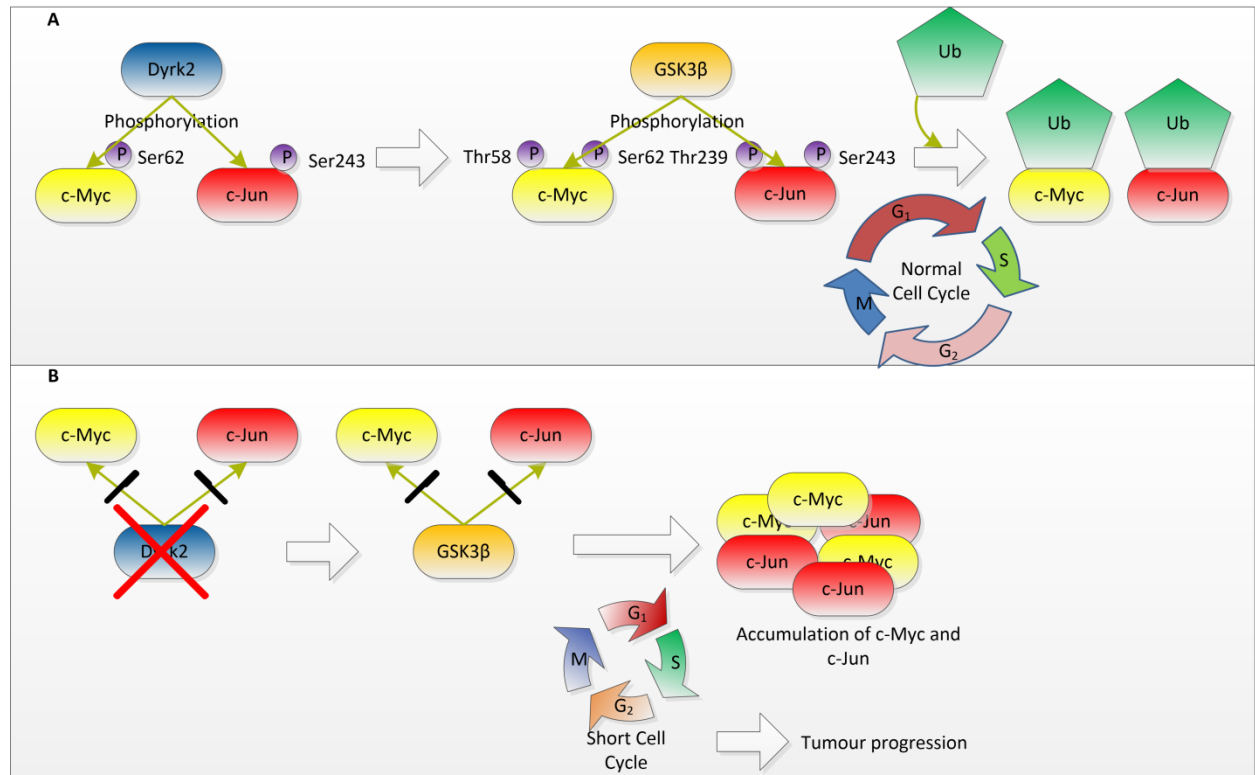


Figure 1.6: A) In normal Dyrk2 phosphorylates c-Jun and c-Myc in the late G₁-phase. GSK3β is then able to further phosphorylate both substrates. The phosphorylated proteins are recognized by ubiquitin (Ub) for degradation; B) Dyrk2 is down regulated in tumour cells. This prevents subsequent phosphorylation by GSK3β in the late G₁-phase. C-Jun and C-Myc accumulate and shorten the G₁-phase resulting in a higher proliferation rate. Figure was adapted from Taira *et al.* (Taira et al., 2012).

1.4.4 Dyrk3 and Dyrk4

There are only little reports about the roles of Dyrk3 and Dyrk4. Dyrk3 is mainly expressed in erythroid and erythropoietin – responsive cells. There it is located in the nucleus and controls the cell cycle by phosphorylation of histones (Geiger et al., 2001; Lord et al., 2000). In a profiling of tyrosine phosphorylation in an anaplastic large cell lymphoma cell line, Dyrk3 was found to be prominently phosphorylated in this cell line (Rush et al., 2005). This finding suggests that Dyrk3 might have an enhanced activity in lymphoma cells. In future studies it has to be clarified if Dyrk3 could be a valuable pharmacological target. Dyrk4A and 4B are the least studied of all Dyrk isoforms; no substrate has been discovered so far for these kinases. A recent study identified several Dyrk4 isoforms resulting from alternative splicing events. The isoforms show different subcellular

localization which could have a regulatory mechanism (Papadopoulos et al., 2011). Furthermore overexpression of Dyrk family members in primary neurons revealed that Dyrk3 and Dyrk4 increased dendritic branching (Slepak et al., 2012).

1.5 Cdc2-like kinases (Clks)

Cdc2-like kinases also belong to the CMGC group of kinases and are activated by autophosphorylation on specific tyrosine residues, whereas substrate modulation exclusively takes place on serine/threonine residues (Becker et al., 1998). The Cdc2-like family members form two subfamilies comprising of Clk1/Clk4 and Clk2/Clk3 respectively (Nayler et al., 1997). Cdc2-like kinases phosphorylate on serine/arginine – rich (SR) splicing proteins modulating their function and localization in the nucleus (Colwill et al., 1996; Duncan et al., 1997). The reversible phosphorylation of the SR proteins is a prerequisite for their ability to associate with the RNA and to provide mRNA splice sites (Misteli et al., 1998). Alternative Splicing alters the inclusion or exclusion of exons yielding in different isoforms of proteins. Therefore, there is increasing evidence that alternative splicing is involved in the development of numerous diseases, including neurodegenerative diseases and cancer (Dowjat et al., 2007; Fischer et al., 2004; Garcia-Blanco et al., 2004; Liu and Gong, 2008; Qian et al., 2011; Shi et al., 2008; Ward and Cooper, 2010; Wegiel et al., 2011a).

However, Clk1-4 have been identified to influence the 3R/4R tau ratio by phosphorylation on the corresponding splicing factors SRp55 and ASF and promoting an increased exon 10 skipping (Hartmann et al., 2001). A recent study identified Clk1 to influence the cell migration and invasion of ovarian cancer cells by phosphorylation of the alternative splicing factor 45 (SPF45) (Liu et al., 2013). Up-regulation of Clk1 activity induces overexpression of SPF45 which stimulates ovarian cancer cell invasion, whereas the inhibition of Clk1 accelerated the proteasomal degradation of SPF45. Thereby, the development of small molecules that selective control a specific splicing signal pathway by inhibition or modulation of Clk1 in combination with Dyrk1A could be an innovative approach for the development of mRNA splicing modifiers (Fedorov et al., 2011; Muraki et al., 2004; Shi et al., 2008). Additionally, Clk1 could be a promising target for the treatment of tauopathies, cancer, and other diseases caused by aberrant splicing events.

1.6 Dyrk1A inhibitors

Dyrk1A is the best studied Dyrk kinase and the efforts for development and identification of new inhibitors mainly focused on this kinase. Dyrk1A inhibitors currently identified are natural products, derivatives thereof, and synthetic compounds.

1.6.1 Synthetic inhibitors

The first target-oriented design of Dyrk1A inhibitors yielded a pyrazolidine-dione **1** (Table 1.2). The scaffold was previously identified from a virtual screening approach (Kim et al., 2006b; Koo et al., 2009). Compound selectivity was only evaluated against a small panel of eight kinases lacking the closely related kinases Dyrk1B and Clk1/4.

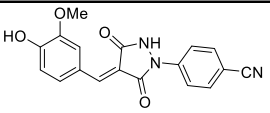
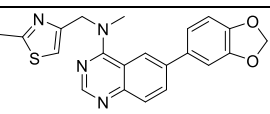
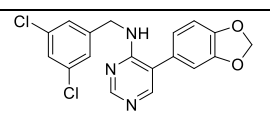
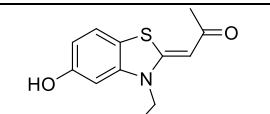
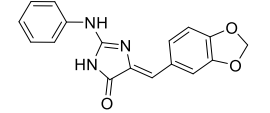
Another class of synthetic Dyrk1A inhibitors is represented by a series of 6-arylquinazolin-4-amines which were initially investigated as new inhibitors of Cdc2like kinases (Mott et al., 2009). Quinazoline based small molecules were originally developed as tyrosine kinase inhibitors resulting in the market EGFR inhibitor erlotinib (Tarceva®) for the treatment of pancreatic and non-small-cell cancer (<http://www.tarceva.com/patient/considering/index.jsp>). The substituents on the central 6-arylquinazolin-4-amine scaffold were varied resulting in the identification of compound **2** as highly potent Dyrk1A inhibitor (Rosenthal et al., 2011). Compound **2** was identified as rather selective for Clks and Dyrks against a panel of 442 kinases. In addition, the same group examined substituted pyrimidine based inhibitors as Clk and Dyrk inhibitors yielding in compound **3** with a good selectivity profile in the same panel of kinases (Coombes et al., 2013).

The benzothiazole **4**, also referred as INDY, was identified in the course of a high throughput screening as highly potent Dyrk1A inhibitor (Ogawa et al., 2010). Evaluation of INDY against a set of 66 kinases revealed cross-inhibition of several other kinases, including Clk1, Ck1 δ , and Pim1. INDY is closely related to TG003, the first Clk1 inhibitor identified which also displayed a moderate inhibitory potency against Dyrk1A (Muraki et al., 2004).

Marine organisms represent rich sources of pharmacological interesting chemical scaffolds with anti-proliferative, anti-microbial, and anti-inflammatory properties (Blunt et al., 2010). Among the vast number of marine natural products, the alkaloids Variolin B, Leucettamine B, and Meridianin E exhibited kinase inhibitory potency. Meridianin E was initially identified as a moderate kinase inhibitor and showed activity against several kinases including CDKs, GSK α , and some PKCs (Gompel et al., 2004). Variolin B which has also pro-apoptotic activity was highly active against CDKs (Simone

et al., 2005). In a first approach to develop new cyclin-dependent kinase inhibitors, Meridianins and Variolins were synthetically combined resulting in Meriolins which were also Dyrk1A inhibitors (Echalier et al., 2008). In addition a series of meridianin derivatives was designed and synthesized for evaluation of their anti-proliferative activity (Akue-Gedu et al., 2009; Giraud et al., 2011a). Within this compound series the specificity of the compounds moved from CDKs to Dyrk1A and Clk1. The most potent Dyrk1A and Clk1 inhibitor in this study showed an IC₅₀ value of 34 nM, but no data of a reference inhibitor was provided. Starting from the marine alkaloid Leucettamine B which possess a selective inhibition towards Dyrk and Clk kinases, a structure-activity relationship (SAR) study of Leucettamine B derivatives, so-called leucettines, revealed leucettine L41 **5** as potent Clk1 and Dyrk1A inhibitor (Debdab et al., 2011).

Table 1.2: Synthetic Dyrk1A inhibitors identified in target-oriented design approaches

Structure		IC ₅₀ (Dyrk1A)/(n M)	[ATP] (μM)	Ref. Compound	Dyrk1A transcript	Lit.
	1	78 % @ 10μM ¹	5	Harmine	Full length	(Koo et al., 2009)
	2	14	10	TG003	Not reported	(Rosenthal et al., 2011)
	3	282	10	TG003	Not reported	(Coombes et al., 2013)
	4	230	10	Harmine	truncated	(Ogawa et al., 2010)
	5	40	15	harmine	truncated	(Debdab et al., 2011)

¹ harmine was 12 fold less potent against Dyrk1A as previously described by Bain *et al.* (Bain et al., 2007).

In a subsequent selectivity screening of **5** against a panel of 402 kinases, cross-inhibition of several kinases, including other CMGC kinases was revealed (Tahtouh et al., 2012). The observed neuroprotective effect of leucettine L41 could not be associated to inhibition of a specific kinase and

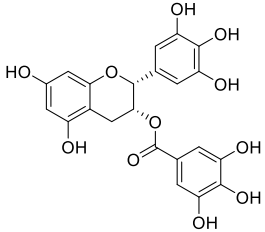
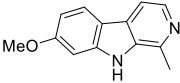
exclude possible additional targets other than protein kinases (Tahtouh et al., 2012). Another class of marine natural product based Dyrk1A inhibitors was designed starting from Lamellarin D, a rather promiscuous kinase and topoisomerase I inhibitor with strong cytotoxic activity against cancer cell lines (Marco et al., 2005; Neagoie et al., 2012). The most potent Lamellarin D derivative exhibited an IC₅₀ value of about 70 nM against Dyrk1A. But again no data of a reference inhibitor with known potency has been provided; therefore the potency of this inhibitor class cannot be evaluated by comparison with other potent Dyrk1A inhibitors. The selectivity of the compounds in this study was only probed towards CDK5 and GSK3 β and inhibition of other can be assumed.

1.6.2 Dyrk1A inhibitors from natural sources

The first natural product Dyrk1A inhibitor identified was Epigallocatechin gallate (EGCg), **6**, one of the main polyphenolic substances in green tea (Table 1.3). EGCg inhibits Dyrk1A *in vitro* with an IC₅₀ of 330 nM (Bain et al., 2003). The specificity of EGCg **6** was evaluated against a panel of 28 related protein kinases. Only p38 regulated/activated kinase (PRAK) was significantly inhibited with an IC₅₀ of about 1 μ M by EGCg **6** (Bain et al., 2003). The efficacy of the ATP non-competitive EGCg **6** (Adayev et al., 2006) was examined in *in vivo* studies on mice overexpressing Dyrk1A (Guedj et al., 2009; De la Torre et al., 2013). Administration of green tea extracts containing mainly EGCg **6** improved hippocampal-dependent learning and synaptic plasticity in Ts65Dn mice, which represent a well-established Down syndrome model (De la Torre et al., 2013; Reeves et al., 1995). In addition to its action on kinase activity EGCg **6** shows a multitude of further effects. These include antibacterial (Anand et al., 2006; Friedman et al., 2006; Yamamoto et al., 2004; Yoda et al., 2004), antiviral (Chang et al., 2003; Weber et al., 2003; Yamaguchi et al., 2002), and antifungal (Hirasawa and Takada, 2004) properties as well as anti-inflammatory (Oz et al., 2013) and anticancer properties by inhibition of topoisomerase I/II and the anti-apoptotic protein Bcl-xl (Lei and Hong-Yu, 2007; Leone et al., 2003; Suzuki et al., 2001). However the applicability of EGCg as Dyrk1A inhibitor is limited due to the complex pharmacokinetics and low bioavailability which is limited by extensive phase II metabolism and the susceptibility to active efflux pumps (Lambert et al., 2007). Harmine **7** is a β -carboline alkaloid which can be isolated from different plants, especially from the Syrian rue (*Peganum harmala*) and from the South American soulvine (*Banisteriopsis caapi*). Originally, it has been identified as a highly potent monoamine oxidase A inhibitor (K_i = 5nM) (Kim et al., 1997) but in 2007 Bain and co-workers discovered harmine **7** as quite powerful Dyrk1A inhibitor displaying an *in vitro* IC₅₀ value of about 80 nM (Table 1.3) (Bain et al., 2007). Despite of its low molecular weight harmine **7** turned out to be a rather selective ATP competitive Dyrk1A inhibitor. In the first study, the

selectivity of harmine **7** was evaluated using 69 related protein kinases (Bain et al., 2007). In this initial screening only Dyrk2 and Dyrk3 were found to be significantly inhibited by harmine **7** but with about 10 fold lower extent. In subsequent studies Dyrk1B, Cdc2-like kinases, and casein kinases were identified as additional targets of harmine **7** (Tahtouh et al., 2012). As pointed out before harmine **7** affects some other kinases in their activity, but it can be currently regarded as the most useful Dyrk1A inhibitor identified due to its good oral bioavailability. Furthermore the efficiency of harmine **7** to block the phosphorylation of tau protein on different serine and threonine residues in cell culture and *in vitro* phosphorylation assays was independently confirmed by two research groups (Frost et al., 2011; Göckler et al., 2009). However, the quite powerful monoamine oxidase A inhibition prevents its direct application as kinase inhibitor in the brain (Kim et al., 1997; Miralles et al., 2005; Pozo et al., 2013). In addition to the reported monoamine oxidase inhibition, some controversial discussions about cytotoxic and genotoxic effects of harmine **7** exist that can be referred to the planar tricyclic structure which might intercalate DNA (Boeira et al., 2001, 2002; Jimenez et al., 2008).

Table 1.3: Potent natural product Dyrk1A inhibitors

Structure		IC ₅₀ (Dyrk1A)/(nM)	[ATP] (μM)	Ref. Compound	Dyrk1A transcript	Lit.
	6	330	50		truncated	(Bain et al., 2003)
	7	80	50	-	truncated	(Bain et al., 2007)

1.7 inhibitors of other Dyrks

1.7.1 Dyrk1B inhibitors

In contrast to the large number of Dyrk1A inhibitors, only few small molecule inhibitors especially for Dyrk1B were reported. Many of the Dyrk1A small molecule inhibitors described above were also identified as highly efficient Dyrk1B inhibitors. This finding can be attributed an overall high sequence homology between Dyrk1A and Dyrk1B of about 85 %. In literature, only two small molecules are described as Dyrk1B inhibitors (Ashford et al., 2014; Ewton et al., 2011a). The

compound developed by Ashford and co-workers was more potent towards Dyrk1A than Dyrk1B than harmine, which was used as reference compound and showed a good selectivity within a panel of 400 kinases (Ashford et al., 2014). The compound published by Ewton and co-workers in 2011 was even more potent towards Dyrk1A and also screened against a panel of 317 kinases but no information whether Clk1 was included in the screening or not has been provided (Ewton et al., 2011a).

1.7.2 Dyrk2, Dyrk3, and Dyrk4 inhibitors

Although the development of selective Dyrk2 inhibitors might be an opportunity to understand the specific role of this kinase in cancer development, little attention has been spent on the development of selective Dyrk2 inhibitors. Some acridine analogues were identified as strong Dyrk2 inhibitors by Cuny and co-workers in 2010 in the course of the development of haspin inhibitors (Cuny et al., 2010).

The specific roles of these kinases are still not investigated and therefore no attention has been spent on the development of specific Dyrk3 and Dyrk4 inhibitors. In case of leucettine L41 (**5**) an IC_{50} of 0.32 μ M for Dyrk3 and 0.52 μ M for Dyrk4 was reported (Tahtouh et al., 2012).

1.8 Clk1 inhibitors

A benzothiazole named TG003 was identified in 2004 through a screening of a small molecule compound library as first Clk1 inhibitor with an IC_{50} value of about 20 nM (Muraki et al., 2004). Treatment of living cells with the compound induced different splice variants of the SC35 and the Clk/Sty gene in comparison to untreated cells (Muraki et al., 2004). As mentioned before TG003 was later reported to inhibit Dyrk1A as well (Mott et al., 2009).

Another compound referred to KH-CB19 was also identified as highly potent dual Clk1/Dyrk1A inhibitor which was inspired from the alkaloid Bauerine C (Fedorov et al., 2011). The specificity of KH-CB19 was evaluated against a panel of 129 human protein kinases using a thermal shift assay (Fedorov et al., 2011). In a subsequent study Leucettine L41 (**5**) was also identified as dual inhibitor of Clk1 and Dyrk1A with an IC_{50} value of 71 nM against Clk1 (Debdab et al., 2011; Tahtouh et al., 2012). Further highly potent and selective Clk/Dyrk inhibitors, including 6-arylquinazolines and aryl-substituted aminopyrimidines were reported (Coombs et al., 2013; Mott et al., 2009; Rosenthal et al., 2011). Although, these compounds were highly active against Clk1 and Dyrk1A and the specificity of these compound classes was impressive, no cellular activity data were provided for these

2. Aim of the Thesis

Life expectancy of the world population dramatically increased over the past century especially in the industrialized countries. As a consequence the rising incidence of neurodegenerative diseases like dementia is one of the increasing challenges for the health systems in future. Alzheimer's Disease (AD) is the most common pathological manifestation of dementia owning two characteristic features consisting of

- a. β -amyloid plaques and
- b. intracellular neurofibrillary tangles, composed of hyperphosphorylated tau protein (Yankner, 1996).

Only little is known about the mechanisms triggering the Alzheimer's Disease process but the pathological alterations in brain start in a very early stage of life (<http://www.nia.nih.gov/alzheimers/topics/alzheimers-basics>). Individuals suffering from Down syndrome often develop Alzheimer's disease-like symptoms by the end of their third decade of life. This observation can be attributed to an extra-copy of the Dyrk1A gene which is located within the Down Syndrome critical region (DSCR) of chromosome 21. As mentioned before the CMGC kinase Dyrk1A is crucial for the proper brain development, but persistent trisomy-driven overexpression lead to mental retardation and impaired brain development. The hyperphosphorylation of tau protein by Dyrk1A and other kinases leads to the formation of the neurotoxic neurofibrillary tangles which could be also found in AD patients.

A new innovative strategy to potentially enhance the life span of DS patients is the pharmacological inhibition of Dyrk1A kinase in brain to a normal physiological level using selective small molecule inhibitors. The identification of harmine as highly potent Dyrk1A inhibitor demonstrated that very small, compact molecules can act as rather selective ATP competitive small molecule kinase inhibitors. However the usefulness of harmine to act as a central nervous system active kinase inhibitor is considerably limited due to its strong inhibition of monoamine oxidase A. Hence, the first goal of this work was the identification of new Dyrk1A inhibitors starting from our in-house compound library void of classical kinase inhibitor scaffolds which was screened against Dyrk1A. Therefore we considered only compounds from which we expected an ATP competitive mode of action. To gain selectivity over related kinases we decided to choose compounds which were only able to form one hydrogen bond to the hinge region. The compound selection was supported by a pharmacophore model created from the ATP pocket of the Dyrk1A crystal structure. Starting from the hit compound one of the major goals of this work was then the development of

small, drug-like molecules. As the compounds should target Dyrk1A within the central nervous system (CNS) they should have a low molecular weight, as well good physicochemical properties. These properties include a good solubility, a moderate lipophilicity, and only H-bond donor group which enhance probability of surmounting the blood brain barrier. To further develop the initial hit compounds two different strategies were applied. The first strategy involved the systematic variation of peripheric substituents, whereas the second approach covered the exchange of the central core. In both cases structure activity relationships (SAR) were derived. The aim was to improve the potency as well as the selectivity against other kinase families from the kinome tree.

In a second project, a MALDI triple quadrupole mass spectrometric kinase assay should be established and compared to conventional radiometric and luminescence based kinase assays for reproducibility and robustness. Furthermore its applicability to high throughput campaigns was evaluated.

3. Results

3.1 Design and Synthesis of a Library of Lead-Like 2,4-Bisheterocyclic Substituted Thiophenes as Selective Dyrk/Clk Inhibitors.

Christian Schmitt, Dagmar Kail, Marica Mariano, Martin Empting, Nadja Weber, Tamara Paul, Rolf W. Hartmann, Matthias Engel

Reprinted from PLoS ONE **2014**, 9, e87851

Copyright: © 2014 Schmitt et al. This is an open-access article distributed under the terms of the Creative Commons Attribution License

Publication A

3.1.1 Abstract

The Dyrk family of protein kinases is implicated in the pathogenesis of several diseases, including cancer and neurodegeneration. Pharmacological inhibitors were mainly described for Dyrk1A so far, but in fewer cases for Dyrk1B, Dyrk2 or other isoforms. Herein, we report the development and optimization of 2,4-bisheterocyclic substituted thiophenes as a novel class of Dyrk inhibitors. The optimized hit compounds displayed favorable pharmacokinetic properties and high ligand efficiencies, and inhibited Dyrk1B in intact cells. In a larger selectivity screen, only Clk1 and Clk4 were identified as additional targets of compound **48**, but no other kinases frequently reported as off-targets. Interestingly, Dyrk1A is implicated in the regulation of alternative splicing, a function shared with Clk1/Clk4; thus, some of the dual inhibitors might be useful as efficient splicing modulators. A further compound (**29**) inhibited Dyrk1A and 1B with an IC_{50} of 130 nM, showing a moderate selectivity over Dyrk2. Since penetration of the central nervous system (CNS) seems possible based on the physicochemical properties, this compound might serve as a lead for the development of potential therapeutic agents against glioblastoma. Furthermore, an inhibitor selective for Dyrk2 (**24**) was also identified, which might be suitable as a pharmacological tool to dissect Dyrk2 isoform-mediated functions.

KEYWORDS

Lead-like library, Ligand efficiency, Dyrk kinase family, automated parallel synthesis

3.1.2 Introduction

The Dyrk family of kinases belongs to the CMGC superfamily and comprises five members, Dyrk1A, 1B, 2, 3, 4A and 4B [1]. The name is an abbreviation for “dual-specificity tyrosine-(Y)-phosphorylation regulated kinase”, based on the observation that autophosphorylation at a tyrosine residue in the activation loop is required for the activation of the kinase, while all observed substrate phosphorylations proceed at serine/threonine residues [2].

Dyrk1A was identified as a major kinase phosphorylating the microtubule-associated tau protein, often functioning as a priming kinase for glycogen-synthase kinase (GSK)3 β [3-6]. Hyperphosphorylation of tau protein is believed to be one of the triggering factors for neurodegeneration because it leads to the formation of neurotoxic neurofibrillary tangles [7, 8]. In particular, Dyrk1A is discussed to be causally involved in the development of Alzheimer-like neurodegenerative diseases in Down Syndrome patients, where the kinase is 1.5-fold overexpressed due to its location in the so-called Down Syndrome Critical Region on chromosome 21 [5, 9, 10]. An additional pathogenic mechanism contributing to the development of tauopathies in Down Syndrome is the altered splicing of tau protein pre-mRNA which results in an imbalance between 3R-tau and 4R-tau isoforms. This imbalance is caused by the increased phosphorylation of the alternative splicing factor (ASF) and of the Serine/Arginine-rich Protein 55 (SRp55) by Dyrk1A that leads to a reduced inclusion of tau exon 10 [11-15].

Skipping of tau exon 10 was also reported to be enhanced through the action of cdc-like kinase 1 (Clk1) [16], a dual specificity kinase from the CMGC kinase group, which is often affected by Dyrk1A inhibitors and *vice versa* [17-21]. Interestingly, both kinases appear to phosphorylate SRp55, suggesting that both might be involved in the pathogenesis of tauopathies [16].

The most closely related isoform, Dyrk1B, is rather ubiquitously expressed, but particularly strong in skeletal muscle tissue and in several types of cancer [22, 23]. One of the known physiological roles of Dyrk1B is the regulation of muscle cell regeneration after damage [24, 25]. In tumors, Dyrk1B exerts an anti-apoptotic function as it mediates some of the survival signals activated by the K-Ras oncoprotein [26]. In addition, Dyrk1B inhibits cell cycle progression in G0/G1 in some tumor cells by phosphorylation of p27Kip1. As a consequence, this protein is retained in the nucleus, where it inhibits cyclin-dependent kinase (CDK)2 [27, 28]. Depletion of cyclin D1 by targeting the protein to proteosomal degradation is another mechanism by which Dyrk1B blocks the cell cycle [29], a function which might be shared with Dyrk1A [30, 31]. Hence, tumor cells are maintained in quiescence, allowing them to escape the eradication by chemotherapeutic agents [32, 33]. In

addition, both Dyrk1A and 1B (but not Dyrk2) are functionally linked with E3 ubiquitin ligases [34-36], suggesting that they may target the same proteins for proteosomal degradation as part of a fail-safe mechanism. In virus-induced cancers, Dyrk1A may play a role as an important anti-apoptotic factor, as has been demonstrated in HPV16-immortalized keratinocytes and cervical lesions [37]. Malignant cervical lesions contain significantly more Dyrk1A than normal tissue. Importantly, a recent study validated Dyrk1A as a new target in EGFR-dependent glioblastoma; inhibition of Dyrk1A promoted degradation of EGFR and sharply decreased tumor cell growth and viability [38]. Altogether, there is increasing evidence that inhibition of Dyrk1B, possibly in combination with Dyrk1A, might represent a promising, yet underexploited anti-tumor strategy.

The reported roles of Dyrk2 in the tumor biology appear rather controversial. The corresponding gene was originally identified as the most frequently amplified and overexpressed gene in lung adenocarcinomas and esophageal carcinoma [39]. In addition, overexpression of Dyrk2 was found to be associated with tumor progression in gastrointestinal stromal tumors [40]. However, more recent studies point to a reduced or abolished Dyrk2 expression in multiple human tumor types, which correlates with invasiveness in the case of human breast cancer [41]. In non-small cell lung carcinomas, Dyrk2 expression was identified as a marker that correlated with induction of apoptosis in response to chemotherapeutic treatment [42], which is possibly mediated through co-activation of the p53 tumor suppressor protein [43]. Furthermore, abrogation of Dyrk2 expression had been shown to result in the activation of telomerase activity [44], and in the stabilization of the c-Jun and c-Myc proto-oncogenes [41]. However, in the light of all these potential tumor suppressor activities it is fair to ask why Dyrk2 is strongly overexpressed in several tumor entities. This question could effectively be addressed using selective small molecule inhibitors.

In general, relatively few reports were published on the remaining Dyrk isoforms. Dyrk3 has also been shown to attenuate apoptosis in response to cytokine withdrawal in hematopoietic cells of erythroid lineage [45, 46]. Future studies will show if it might be a potential pharmacological target in lymphomas, since a profiling of tyrosine phosphorylation in cancer cells identified Dyrk3 (and Dyrk1A) as prominently tyrosine-phosphorylated proteins in an anaplastic large cell lymphoma cell line, suggesting that these kinases might be abnormally activated in lymphoma cells [47].

Dyrk4A and 4B are the least studied of all Dyrk isoforms; no substrate has been discovered so far for these kinases. Dyrk4 was recently identified in a neuronal overexpression screen as a kinase which increased the number of dendritic branches in hippocampal neurons [48].

Among the published Dyrk inhibitors, the natural product harmine proved to be most useful due to its selectivity for Dyrk1A and – with 3-fold lower potency – for Dyrk1B [49]. However, it is an even more potent inhibitor of monoamine oxidase A, impeding its applicability for studies in the brain [38, 50, 51]. Furthermore, some controversy exists in literature on potential genotoxic effects of harmine that were attributed to its flat tricyclic structure which might intercalate DNA [52-54]. Several further inhibitor classes were published, which potently inhibited Dyrk1A. However, these compounds were either not selective for the Dyrk family, or no selectivity data were provided [49, 55-60]. While it can be challenging to develop selective ATP-competitive kinase inhibitors, the example of harmine has demonstrated that in the case of the Dyrk isoforms, this might be achievable using very small, compact molecules. In contrast to the situation with Dyrk1A, only few small molecule inhibitors were reported for the other Dyrk family members. A pyrido[2,3-d]pyrimidine derivative was published as a Dyrk1B inhibitor; however it was three times more potent toward Dyrk1A and also inhibited microtubule affinity-regulating kinase (MARK)1 in a small counter screen [32]. This series was extended in a recent report, however, selectivity data or evidence for an inhibition of the target kinases in cells were not provided [61]. Some acridine analogs were found to potently inhibit Dyrk2, with only few kinases being affected outside the CMGC family [62].

In the present report, we describe the design and synthesis of a focused library of a new class of dual Dyrk/Clk1/4 inhibitors, which displayed a high degree of selectivity over other kinase families. The new compounds exhibited high ligand efficiencies and favorable physicochemical properties. Moreover, evidence for an inhibition of Dyrk1B in intact cells was provided by several cell-based assays.

3.1.3 Materials and Methods

Biology

Dyrk1B and Clk1 were purchased from Life Technologies (LOT # 877059G, Catalog # PV4649 and LOT # 943590A, Catalog # PV3315). Casein kinase 2 (CK2) substrate peptide was purchased from Millipore (LOT # JBC1949760, Catalog # 12-330); cOmplete Mini Protease inhibitor cocktail tablets were purchased from Roche. Woodtide substrate peptide and RS repeat substrate peptide were custom synthesized at the Department of Medical Biochemistry and Molecular Biology, Saarland University, Homburg, Germany.

Protein expression and purification

An expression plasmid encoding the catalytic domain of human Dyrk1A fused to an N-terminal hexahistidine-tag (termed pET45b-Dyrk1A-cd) was constructed as described in the Supporting Information section. Human hexahistidine-tagged Dyrk1A (His₆-Dyrk1A) and glutathione S-transferase (GST)-fused Dyrk2 were both expressed in *Escherichia coli*. *E. coli* BL21(DE3) cells were co-transformed using either the pET45b-Dyrk1A-cd or the pGEX-2TK-Dyrk2 (gift from W. Becker, Aachen) expression plasmid together with the pRARE plasmid (Novagen), carrying genes of human tRNAs which are rare in *E. coli*. to increase the yield of recombinant proteins. The transformed bacteria were grown in LB medium containing 50 µg/mL ampicillin and 25 µg/mL chloramphenicol. Protein expression was induced by addition of 0.5 mM isopropyl β-D-thiogalactopyranoside (IPTG) overnight at 18°C. Cell pellets were resuspended in lysis buffer (50 mM Tris/HCl, pH 7.4, 0.27 M Sucrose, 1 mM sodium orthovanadate, 10 mM β-glycerophosphate disodium salt, 1 mM DTT, 50 mM NaF, 1 % Triton X 100, cOmplete Mini Protease inhibitor cocktail tablets) and lysed by sonication. His₆-Dyrk1A was purified by affinity chromatography using Ni²⁺-Sepharose beads (GE Healthcare Bio Sciences, LOT # 10038389) as follows: the cleared cell lysate was gently stirred with the beads overnight at 4°C. Then the beads were filled into an empty chromatography column and the column washed three times with 10 volumes lysis buffer, followed by one wash with lysis buffer containing 20 mM imidazole. After another wash using 50 mM Tris/HCl, pH 7.2, and 100 mM NaCl, the bound proteins were eluted using 50 mM Tris/HCl, pH 7.2, 100 mM NaCl, 1 mM DTT, 200 mM imidazole, and 0.1 mM EGTA. The proteins were dialyzed against the same buffer without imidazole, 20% glycerol was added, and the proteins snap frozen in dry ice/isopropanol and stored at -80 °C. GST-Dyrk2 fusion protein was purified from the lysate using glutathione-agarose beads (Machery-Nagel, LOT # 1212001) essentially as described previously for GST-PKCζ. [63]

Kinase assays

Dyrk1A, Dyrk1B, Dyrk2, CK2α and Clk1 kinase reactions were performed in a reaction buffer containing 50 mM Tris/HCl, pH 7.4, 0.1 mM EGTA, 0.5 mM DTT, 10 mM MgCl₂, 100 µM ATP and 0.33 µM [γ -³²ATP] as well as the appropriate substrate peptides, which were 100 µM Woodtide for the Dyrk isoforms (KKISGRLSPIMTEQ-NH₂), 60 µM CK2 substrate peptide (RRRDDDSDDD-NH₂, from Millipore) for CK2α or RS repeat peptide (GRSRSRSRSRSRSR) for Clk1. The CK2α protein was a kind gift of M. Montenarh (Homburg). The kinase reactions were performed at 30 °C for 15 min and terminated by spotting 5 µL of the reaction mixture onto a P81 phosphocellulose membrane

(Whatman). The membrane was washed four times with 0.3 % phosphoric acid and one time with acetone and dried. The dry membrane was exposed in a cassette to a Phosphor Screen Imaging Plate (FujiFilm) and the signals detected by scanning of the imaging plate in a Fuji FLA-3000 PhosphorImager. The spots were quantified using AIDA software (Raytest, Version 3.52) to determine the activities of the kinases in the assay reactions. For IC₅₀ determinations, eight concentrations of each compound were used in triplicates, and the percentage of inhibition at 5 μM was also calculated from the average of triplicate values. IC₅₀ values were calculated by fitting the data with Origin Pro 8.6 (OriginLabs). The IC₅₀ values given in the tables are representative of at least two independent determinations.

ROS Assay

U2OS osteosarcoma cells were plated on six well cell culture plates (5×10^5 cells/well). The cells were starved for 24 hours in McCoy's medium containing 0.5 % fetal calf serum (FCS) and incubated for 48 hours with four different concentrations of compound **29** in McCoy's medium also containing 0.5 % FCS. The final DMSO concentration in each well was 0.1 %. Cells were washed with phosphate-buffered saline (PBS) and incubated for 30 min at 37 °C in the dark with 10 μM Dihydroethidium (DHE) in PBS and washed with PBS. The cells were then trypsinized, collected by centrifugation, and lysed with lysis buffer (100 mM Tris/HCl, pH 7.3, 2 mM EGTA, 2 % Triton X100). The amount of ethidium produced by reactive oxygen species (ROS) was quantified by measuring the fluorescence (Ex485, Em620) in a POLARstar plate reader (BMG Labtech, Offenburg, Germany). Values obtained for different compound concentrations were compared using the two-sided Student's t-test; levels of significance are indicated in the Figure as asterisks.

Determination of logP, pK_a and logS parameters

The physicochemical parameters were determined on a Sirius T3 machine (Sirius Analytical machines, East Sussex, UK) by automated titration according to the manufacturer's instructions.

Caspase-3 Assay

U2OS osteosarcoma cells were seeded in a 96 well flat bottom plate (15×10^3 cells/well). The cells were starved for at least 24 hours in McCoy's medium containing 0.5 % FCS and incubated for 48

hours with four different concentrations of **11**, **29** and **48** in McCoy's medium containing 0.5 % FCS. The induction of caspase-3/7 activity was measured using the Promega Caspase-Glo 3/7 assay system (Promega, LOT 0000054568). The resulting luciferase reaction signals that are proportional to the caspase induction were measured in a POLARstar plate reader (BMG Labtech, Offenburg, Germany). In a control experiment using purified luciferase and substrate, we verified that the tested compounds did not inhibit the luciferase enzymatic activity itself. Values obtained for different compound concentrations were compared using the two-sided Student's t test; levels of significance are indicated in the Figure by asterisks.

Real-Time PCR

U2OS cells were seeded in 6 well flat bottom plates (5×10^5 cells/well) and grown to confluency. The cells were then starved for 48 hours in McCoy's medium containing 0.5 % FCS and incubated for 72 hours with compounds **29** and **48** or DMSO in McCoy's medium containing 0.5 % FCS; the medium containing the compounds or DMSO, respectively, was refreshed each day, and each concentration applied in triplicates. The cells were then harvested and total RNA isolated using the RNeasy Mini Kit (Qiagen, Cat. No. 74104). 1 μ g of total RNA was transcribed to cDNA using the QuantiTect Rev. Transcription Kit (Qiagen, Cat. No. 205311), and 20 ng of cDNA used per Real-Time (RT)-PCR experiment (assuming quantitative reverse transcription). RT-PCR was performed in a StepOnePlus Real-Time PCR System (Life Technologies) using the SYBR green RT-PCR Kit (Peqlab, Cat. No. 07-KK4603-01) according to the manufacturer's protocol, using the following cycling conditions: initial denaturation: 95 °C, 40 sec, followed by 45 cycles of denaturation at 95 °C, 2 sec, and annealing/extension at 60 °C, 40 sec. The following primer pairs were used: β -actin: 5'-TGC GTG ACA TTA AGG AGA AG-3' and 5'-GTC AGG CAG CTC GTA GCT CT-3' [64]; CDH4: 5'-CAA CCT GAA CGC CAT CAA CAT C-3' and 5'-CGC AAG CTG AGT TGG GCA TAG-3' [65]; FGF2: 5'-CAA GCG GCT GTA CTG CAA AAA-3' and 5'-GTT CGT TTC AGT GCC ACA TAC-3' [66]; BIM: 5'-TCA GCG CCT TTG TGA GGA G-3' and 5'-CAG GCA AGG ATC AGG TAG GTG-3' (PrimerBank ID: 50593007c2, [67]); TRADD: 5'-GCT GTT TGA GTT GCA TCC TAG C-3' and 5'-CCG CAC TTC AGA TTT CGC A-3' (PrimerBank ID: 115387096c1, [67]); FasL: 5'-TGC CTT GGT AGG ATT GGG C-3' and 5'-GCT GGT AGA CTC TCG GAG TTC-3' (PrimerBank ID: 4557328c1, [67]); SOD2: 5'-CGA CCT GCC CTA CGA CTA CG-3' and 5'-TGA CCA CCA CCA TTG AAC TT-3' [68]; CP: 5'-CCC TGG AGA ATG GAT GCT CA-3' and 5'-CTA ACA TGC TTC CCA CGG ATA TT-3' [69].

ViaLight™ Toxicity Assay

V79 hamster lung fibroblast cells were plated at a density of 45,000 cells per well in a white 96 well plate and allowed to adhere and grow for 24 hours. The compounds were then applied as dilutions in cell culture medium (DMEM with 10% FCS and penicillin/streptomycin mix) at a final concentration of 5, 10, and 20 µM, respectively. The plate was further incubated for 48 hours at 37 °C in a humidified atmosphere containing 5% CO₂. The ATP level was detected with a LONZA ViaLight™ Plus Kit according to protocol 1 of the vendor's instructions. Luminescence was measured in a POLARstar plate reader (BMG Labtech, Offenburg, Germany). The background luminescence was obtained from equally treated, cell-free wells containing serum, and subtracted from all values. Inhibition values obtained for different compound concentrations were compared using the two-sided Student's t-test; levels of significance are indicated in the Figure by asterisks.

Metabolic Stability Assay

The assay was performed with liver microsomes from male Sprague-Dawley rats (BD Bioscience, Catalog # 452501) and half-lives of the compounds calculated essentially as previously described, [70] except that the compounds were used at a final concentration of 0.5 µM. The samples were analyzed by LC-MS/MS analysis on a TSQ Quantum Access MAX (Thermo Fisher Scientific) using 0.5 µM amitriptyline as an internal standard. The microsomal intrinsic clearance (Cl_{int}) estimates were calculated according to Obach [71] using the formula $Cl_{int} = 0,69314718 / t_{1/2 \text{ microsomal}} * (\text{mL incubation volume} / \text{mg microsomal protein}) * (\text{mg microsomal protein} / \text{g liver}) * (\text{g liver} / \text{kg body weight})$. In the assay, the incubation volume was 0.2 ml, containing 0.045 mg microsomal protein, and the following literature values for male Sprague-Dawley rats were used for the calculation: 23.3 mg microsomal protein / g liver, 8.0 g liver weight, 180 g body weight. [72] From the Cl_{int} values, the blood clearance rate was calculated using the formula $Cl_{blood} = Q * (1 - e^{-Cl_{int}/Q})$ (Obach, 1999) with $Q = 55.2 \text{ ml/min/kg}$ (rat hepatic blood flow, taken from Ref. [73]). This formula disregards serum and microsomal protein binding events; however it had given the best predictions for weakly basic and neutral compounds [71].

Docking studies

The multi-step *in silico* experiment employing local docking and molecular dynamics simulations was performed with YASARA structure using a self-written command sequence (macro) with the

AMBER03 force field [74-76]. First, the crystal structure of Dyrk1A in complex with harmine (PDB accession code: 3ANR) was loaded into the software. Then, the ligand was removed and a grid box of approximately 9 nm³ was set up around the active site of the enzyme for the subsequent local docking experiment using the built-in AutoDock 4 algorithm [77]. Compound **29** possesses two rotatable bonds which link both heterocyclic substituents to the thiophene core. This rather small degree of rotational freedom was systematically sampled *via* 100 conformers using 10 rotamers for each bond. Each of these structures was subjected to a rigid docking experiment to the prepared Dyrk1A enzyme structure using 999 individual docking runs.

The ten best ligand-enzyme structures of the previous step were then simulated in 0.9% (m/v) NaCl (aq.) at 298 K and pH 7.4 for 50 μ sec with fixed backbone atoms. After energy minimization, the resulting complexes were subjected to a final rigid local docking experiment using a smaller grid box which extended 1 Å around the ligand atoms. Ligand–receptor interactions of this structure as well as the parent Dyrk1A–harmine complex were analyzed with MOE 2010 and images were rendered with POVRay.

Chemistry. *General chemical methods.*

Chemical starting material was purchased from Sigma-Aldrich, CombiBlocks or Alfa Aesar and used without further purification. Synthesis of the focused library was performed by an ISYNTH robotic platform from Chemspeed Technologies. Purity of the compounds was determined using an Agilent 1100 series HPLC system from Agilent Technologies, a GC Trace Ultra from Thermo or a Waters autopurification system from Waters Corporation. The purity of the compounds used in the biological assays was \geq 95%. Mass spectra (ESI) were measured on an AB Sciex Qtrap2000 from AB Sciex or a Waters 3100 Mass detector from Waters Corporation. Mass spectra (EI) were measured on a DSQ II from Thermo. ¹H and ¹³C NMR spectra were recorded on either a Bruker DRX-500 (¹H, 500 MHz; ¹³C, 126 MHz) instrument at 300 K or on a Bruker Fourier300 (¹H, 300 MHz; ¹³C, 75 MHz) NMR spectrometer at 300 K in the deuterated solvents indicated. IR spectra were recorded on a Perkin Elmer Spectrum 100 FT-IR spectrometer, Perkin Elmer, Rodgau, Germany. Flash column chromatography was performed using silica gel 60 (Merck, 35-70 μ m). Reaction/flash monitoring was done by thin layer chromatography (TLC) on ALUGRAM SIL G/UV₂₅₄ (Macherey-Nagel) employing UV detection.

Procedure for the synthesis of 3-(4-bromothiophen-2-yl)pyridine i: 1 g (8.14 mmol) of 3-Pyridylboronic acid was dissolved under nitrogen in 10 mL of dioxane and 4 mL of water. To this

solution 1.97 g (8.14 mmol) of 2, 4-dibromothiophene, 0.376 g (0.325 mmol) of tetrakis(triphenylphosphine)Palladium(0) and 1.72 g (16.28 mmol) of sodium carbonate were added successively. The mixture was heated to reflux and the reaction progress was monitored by TLC. After completion of the reaction the crude product was washed with water and brine, dried over magnesium sulfate and purified by flash column chromatography eluting with ethyl acetate/hexane 1:5 to yield 1.3 g (67 %) of 3-(4-bromothiophen-2-yl)pyridine as a white solid. ^1H NMR (500 MHz, Methanol- d_4) δ (ppm) 7.41 - 7.51 (m, 3 H) 8.02 (dt, $J=7.96$, 0.75 Hz, 1 H) 8.46 - 8.50 (m, 1 H) 8.76 - 8.81 (m, 1 H); ^{13}C NMR (126 MHz, Methanol- d_4) δ (ppm) 112.06, 125.02, 125.63, 128.51, 131.22, 134.89, 142.31, 146.92, 149.56; Purity (FID): 99 %, t_{R} : 6.69 min; MS (EI), m/z $[\text{M}]^+$: 239.87 calc.: 238.94.

Procedure for the synthesis of [5-(pyridin-3-yl)thiophen-3-yl]boronic acid ii: To a solution of 2.64 g (11 mmol) of **i** in anhydrous toluene/THF under nitrogen atmosphere 3.3 mL (14.3 mmol) of triisopropyl borate were added followed by a careful addition of 5.72 mL (14.3 mmol) *n*-BuLi (2.5 M in hexanes) at -78 °C (yellow to orange) over 45 min. The reaction was stirred at bath temperature for half an hour before adjusting the bath to -25 °C. After 5 min 28.6 mmol of 2 M HCl were added and the mixture was stirred for half an hour at RT, before being transferred to a separatory funnel with 15 mL of water and 9 mL of THF. The organic layer was separated, extracted with 9 mL of water and the aqueous phases were adjusted to pH 7 with 5 M NaOH (2.1 mL, precipitation), before being extracted with THF (3 \times 15 mL). The combined organic layers were dried (MgSO_4) and concentrated. The crude crystals were directly used without further purification.

Procedure for the synthesis of 5-(4-bromothiophen-2-yl)-1,3-oxazole iii: (Modified from Besselievre et al. 2008 [78]) To a solution of 2.5 g (13.1 mmol) of 4-bromo-2-thiophenecarbaldehyde in 10 mL of methanol, 2.81 g (14.4 mmol) toluenesulfonylmethyl isocyanide and 3.62 g (26.2 mmol) of potassium carbonate were added. The mixture was heated for 4h to reflux. The solvent was evaporated in vacuo and the residue was poured into ice water. The precipitate was filtered off and dried. The crude product was recrystallized from hexane and directly used without further purification. ^1H NMR (300 MHz, DMSO- d_6) δ (ppm) 7.46 - 7.63 (m, 2H) 7.76 (s, 1H) 8.43 (s, 1 H), ^{13}C NMR (75 MHz, DMSO- d_6) δ (ppm) 110.33, 122.84, 124.61, 127.22, 130.98, 145.34, 152.16; Purity (FID): > 99 %, MS(EI), t_{R} : 5.42 min, m/z $[\text{M}]^+$: 228.77, calc. 228.92.

Procedure for the synthesis of 5-(4-bromothiophen-2-yl)pyrimidine iv: 0.62 g (5 mmol) of 5-pyrimidineboronic acid was diluted in a mixture of degassed dioxane/water (5:1) under nitrogen atmosphere. To this solution 1.34 g (5 mmol) of 2,4-dibromothiophene, 0.289 g (0.25 mmol) of tetrakis(triphenylphosphine)palladium(0) and 1.59 g (15 mmol) of Na_2CO_3 were added successively.

The mixture was heated to 90°C and stirred for two days. After completeness of the reaction the crude mixture was poured into water and extracted with diethyl ether. The combined organic layers were washed with brine, dried over Na₂SO₄, filtered off and the solvent was removed under reduced pressure. The crude product was purified by flash column chromatography eluting with ethyl acetate/cyclohexane (1:3) to give 0.55 g (46 %) of 5-(4-bromothiophen-2-yl)pyrimidine as yellow crystals. ¹H-NMR (300 MHz, CDCl₃): δ = 7.30–7.34 (m, 1H), 7.34–7.37 (m, 1H), 8.92 (d, *J* = 0.6 Hz, 2H), 9.17 (s, 1H). ¹³C-NMR (75 MHz, CDCl₃): δ = 111.51, 124.33, 127.59, 127.85, 137.44, 153.44 (2C), 157.93; MS (ESI+): *m/z* (%) = 284 (13) [M+ACN+H⁺], 282 (12) [M+ACN+H⁺], 244 (13), 243 (100) [M+H⁺], 242 (12), 241 (100) [M+H⁺], calc. 240.94.

Procedure for the synthesis of 2-(trimethylsilyl)-1,3-thiazole v: 22.4 mL (56 mmol) of n-buthyllithium was added to 100 mL of dry diethyl ether and cooled to -78°C. Subsequently a solution of 8.2 g (50 mmol) of 2-bromothiazole in 80 mL of diethyl ether were added dropwise over 30 min and stirred for 30 min at -78 °C. Then, a solution of 5.43 g of trimethylsilylchloride in 80 mL of diethyl ether was added dropwise and stirred for an additional hour at -78°C. The reaction mixture was allowed to warm to room temperature and saturated NaHCO₃ solution (70 mL) was added. The organic phase was separated, dried over Na₂SO₄ and the solvent was removed under reduced pressure. The crude product was purified by vacuum distillation (0-10 mbar, bp 65-67°C) to yield 4.6 g (59 %) of a colorless oil. ¹H-NMR (300 MHz, CDCl₃): δ = 0.42 (s, 9H), 7.53 (dd, *J* = 3.0, 0.7 Hz, 1H), 8.12 (d, *J* = 3.0 Hz, 1H), ¹³C-NMR (75 MHz, CDCl₃): δ = -0.98, 121.34, 145.73, 174.37. Data are in accordance to Literature [79].

Procedure for the synthesis of 5-(tetramethyl-1,3,2-dioxaborolan-2-yl)-1,3-thiazole vi: A solution of 4.4 g (28 mmol) 2-(trimethylsilyl)-1,3-thiazole in dry THF was cooled to -78°C. Then, 13.4 mL (33.6 mmol) n-buthyllithium were added dropwise over 20 min. After 15 min, 6.32 g (33.6 mmol) of triisopropylborate were added dropwise and the solution was stirred for 90 min at -78°C. The solution was allowed to warm to room temperature and stirred for additional 30 min. Then 3.3 g (28 mmol) of pinacol, solved in 10 mL of dry THF was added and after 10 minutes the pH was adjusted to 5 with glacial acetic acid. The crude product was extracted with cyclohexane and dried under reduced pressure to yield 5.04 g of crude 5-(tetramethyl-1,3,2-dioxaborolan-2-yl)-1,3-thiazole. ¹H-NMR (300 MHz, CDCl₃): δ = 1.27–1.38 (m, 12H), 8.33 (s, 1H), 8.99 (s, 1H), ¹³C-NMR (75 MHz, CDCl₃): δ = 24.69 (4C), 84.50 (2C), 152.57, 158.20. 1 C not det. NMR data are in accordance to literature [80].

Procedure for the synthesis of 5-(4-bromothiophen-2-yl)-1,3-thiazole vii: 0.95 g (4.5 mmol) of 5-(tetramethyl-1,3,2-dioxaborolan-2-yl)-1,3-thiazole were dissolved in a degassed mixture of dioxane/water (3:1) under nitrogen atmosphere. To this solution 1.09 g (4.5 mmol) of 2,4

dibromothiophene, 0.29 g (0.25 mmol) of tetrakis(triphenylphosphine)palladium(0) and 1.22 g (11.5 mmol) of Na₂CO₃ were added and the reaction mixture was stirred for 2 days at 90°C. After completion of the reaction, the mixture was poured into water and extracted with diethyl ether. The combined organic layers were washed with water and brine, dried over Na₂SO₄ and the solvent was removed in vacuo. The crude product was purified by column flash chromatography eluting with ethyl acetate/cyclohexane (1:10). ¹H-NMR (300 MHz, CDCl₃): δ = 7.12 (d, *J* = 1.4 Hz, 1H, Ar_m-H), 7.19 (d, *J* = 1.4 Hz, 1H), 7.97 (s, 1H), 8.73 (d, *J* = 0.5 Hz, 1H). ¹³C-NMR (75 MHz, MeOD): δ = 110.57, 122.76, 128.22, 130.14, 133.48, 139.91, 152.27. Purity: ~ 65 %, *t*_R = 7.56 min; MS (ESI⁺): *m/z* (%) = 289 (17) [M+ACN+H⁺], 287 (14) [M+ACN+H⁺], 250 (20), 249 (23), 248 (100) [M+H⁺], 247 (2), 246 (100) [M+H⁺], calc. 245.90. The product was used for the synthesis of **48** without further purification.

Procedure for the synthesis of compound 4: 152.4 mg (1.24 mmol) 3-pyridylboronic acid were dissolved under nitrogen in 10 mL dioxane and 2 mL water and stirred at room temperature. To this solution 150mg (0.62mmol) 2, 4-dibromothiophene, 72 mg (0.062 mmol) tetrakis(triphenylphosphine)palladium(0) and 265 mg (2.5 mmol) sodium carbonate were added successively. The mixture was stirred and heated to 100°C for 18 h. The reaction progress was monitored by TLC. After completion of the reaction, the mixture was cooled down to room temperature and the crude product was poured into water and extracted with diethyl ether (4 x). The combined organic extracts were washed with water and brine, dried over magnesium sulfate and the solvent was removed in vacuo. The crude product was purified by flash column chromatography eluting with ethyl acetate and 1% Methanol to give 93 mg (63 %) of **4** as a colorless solid. mp 110-111°C; IR (neat) 3047, 1469, 1125, 1022, 796, 696, 617 cm⁻¹; ¹H NMR (300 MHz, DMSO-*d*₆) δ (ppm) 9.01 (dd, *J* = 0.75, 1.68 Hz, 1H), 8.94 (dd, *J* = 0.65, 2.33 Hz, 1H), 8.47 - 8.50 (m, 1H), 8.45 - 8.47 (m, 1H), 8.18 (d, *J* = 1.49 Hz, 1H), 8.10 - 8.16 (m, 1H), 8.04 - 8.10 (m, 2H), 7.42 - 7.45 (m, 1H), 7.38 - 7.42 (m, 1H); ¹³C NMR (75 MHz, DMSO-*d*₆) δ (ppm) 123.30, 124.26, 124.37, 124.56, 129.94, 130.90, 133.14, 133.70, 139.78, 141.26, 146.69, 147.66, 148.84, 149.25; Purity (UV @254 nm): 99.1 %, *t*_R: min; MS (ESI), *m/z* [M+H]⁺: ; calc. 238,06

Procedure for the synthesis of compound 20: 87 mg (0.42 mmol) of 3-bromoquinoline were dissolved in 10 mL of dry THF under nitrogen and the resulting solution was cooled to -78°C. To this solution 1.1 eq. (0.46 mmol, 184 μL) of *n*-buthyllithium was added in drops. The mixture was stirred for 1 hour at -78°C, then 1.2 eq. (0.5 mmol, 136 μL) of tributyl borate were added slowly and the mixture was stirred for 1.5 hours at -78°C. The mixture was allowed to warm up to room temperature. Then 2.5 eq. of Na₂CO₃ (1.3 mmol, 137 mg), 4 mol % of tetrakis(triphenylphosphine)palladium(0) (0.017 mmol, 19.4 mg), 100mg (0.42 mmol) of 3-(4-bromothiophen-2-yl)pyridine and 4 mL of water were

added successively and the mixture was heated to reflux overnight. The reaction progress was monitored by TLC analysis. The reaction was stopped and poured into water. The crude product was extracted with ethyl acetate and the combined organic layer was washed with water and brine, dried over magnesium sulfate and the solvent was removed in vacuo. The crude product was purified by flash column chromatography eluting with ethyl acetate/hexane 1:5 to give 70 mg (58 %) of **20** as a light yellow solid. mp 198-199°C; IR 3058, 1571, 1319, 1125, 1022, 798, 700, 615 cm⁻¹; ¹H NMR (500 MHz, Methanol-*d*₄) δ (ppm) 7.36 (ddd, *J*=7.90, 5.00, 0.95 Hz, 1H) 7.47–7.51 (m, 1 H) 7.62 (ddd, *J*=8.35, 6.94, 1.42 Hz, 1 H) 7.84 (d, *J*=7.88 Hz, 1 H) 7.86 (d, *J*=1.58 Hz, 1 H) 7.89 (d, *J*=8.51 Hz, 1 H) 7.92 (d, *J*=1.26 Hz, 1 H) 8.01 (dt, *J*=8.04, 1.81 Hz, 1 H) 8.36 (dd, *J*=4.89, 1.42 Hz, 1 H) 8.45 (d, *J*=1.89 Hz, 1 H) 8.78 (d, *J*=2.21 Hz, 1 H) 9.07 (d, *J*=2.21 Hz, 1 H); ¹³C NMR (126 MHz, Methanol-*d*₄) δ (ppm) 124.00, 124.73, 125.61, 128.56, 128.95, 129.46, 129.69, 129.83, 130.93, 132.05, 133.99, 134.92, 140.87, 142.47, 146.98, 147.71, 149.15, 149.80; Purity (FID): 96.7 %, *t*_R: 10.15 min; MS (EI), *m/z* [M]⁺: 288.01 calc.: 288.072.

General Procedure for the synthesis of focused libraries on the ISYNTH Chemspeed system: The corresponding arylboronic acids / arylbromides (0.30 mmol) for diversification were manually pre-filled into 20 mL disposable vials and placed on the ISYNTH. Cs₂CO₃ was added by an SDU (solid dosing unit). The interior of the vials was brought under protective gas atmosphere by repeated cycles of evacuation and flushing with argon. Water (0.75 mL) and stock solutions of the thiophene core (0.33 mmol in 1.25 mL of DMF) as well as Pd(dppf)Cl₂ (0.015 mmol in 1.0 mL of DMF) were dispensed into each vial under a slight argon stream employing a 4-needle head attached to 10 mL syringes. Afterwards, the vials were automatically sealed and heated to 80 °C under reflux for 15 h. After completion of the reaction 6 mL of water and 5 mL of diethyl ether were added to each vial. Solid matter was manually removed by filtration. The phase separation area was determined visually and the value (height in mm) entered. Separation of the organic phase and extraction of the aqueous one (twice with 6 mL of ethyl acetate) was performed by the ISYNTH robotic platform. MgSO₄ was automatically added to the combined organic layers for drying and filtered off manually. The solvent was evaporated and the crude product was purified by preparative HPLC on a Waters Autopurification System employing a C-18 column (Waters X-Bridge OBD 19 x 150 mm, 5 μm) with a flow rate of 20 mL/min and respective 10 min gradients [solvents A (water + 0.1% formic acid) / solvent B (acetonitrile / 0.1% formic acid)].

3-methyl-5-[5-(pyridin-3-yl)thiophen-3-yl]pyridine 5: yield: 61%, mp 106-107°C; IR (neat) 3100, 1420, 1125, 1024, 807, 703, 613 cm⁻¹; ¹H-NMR (300 MHz, CDCl₃): δ (ppm) 2.40 (s, 3H), 7.36 (dd, *J* = 7.9, 4.9 Hz, 1H) 7.52 (d, *J* = 1.3 Hz, 1H), 7.61 (d, *J* = 1.5 Hz, 1H), 7.72–7.77 (m, 1H), 7.92 (dt, *J* = 8.0, 2.0 Hz,

1H), 8.35–8.41 (m, 1H), 8.54 (dd, $J = 4.8, 1.5$ Hz, 1H), 8.69 (d, $J = 2.1$ Hz, 1H), 8.91 (d, $J = 2.4$ Hz, 1H). ^{13}C -NMR (75 MHz, CDCl_3): δ (ppm) 18.37, 122.10, 122.99, 123.89, 130.16, 131.02, 133.42, 133.74, 134.83, 139.55, 141.53, 143.60, 146.19, 147.84, 148.17; Purity(UV): 99 %, t_{R} : 3.28 MS (ESI+): m/z (%) = 255 (6), 254 (20), 253 (100) $[\text{M}+\text{H}^+]$, calc. 253.07.

3-methoxy-5-[5-(pyridin-3-yl)thiophen-3-yl]pyridine **8**: yield: 50%, mp 132-133°C; IR (neat) 3072, 1456, 1296, 1121, 1022, 799, 696, 612 cm^{-1} ; ^1H NMR (300 MHz, Methanol- d_4): δ (ppm) 8.85 - 8.93 (m, 1H), 8.42 - 8.54 (m, 2H), 8.07 - 8.20 (m, 2H), 7.93 - 7.99 (m, 1H), 7.85 - 7.92 (m, 1H), 7.65 - 7.74 (m, 1H), 7.47 (dd, $J = 4.94, 6.99$ Hz, 1H), 3.87 - 3.99 (m, 3H); ^{13}C NMR (75 MHz, Methanol- d_4): δ (ppm) 56.43, 119.75, 124.27, 124.87, 125.66, 132.13, 133.81, 135.00, 136.77, 139.96, 140.74, 142.38, 147.02, 149.16, 158.05. Purity (UV): 98 %, t_{R} = 4.05 min; MS (ESI+): m/z (%) = 271 (21), 270 (57), 269 (100) $[\text{M}+\text{H}^+]$, calc. 269.07.

3-fluoro-5-[5-(pyridin-3-yl)thiophen-3-yl]pyridine **15**: yield: 21%, mp 186-187°C; IR (neat) 3069, 1417, 1185, 1142, 1023, 805, 697, 615 cm^{-1} ; ^1H -NMR (300 MHz, CDCl_3): δ (ppm) 8.92 (d, $J = 2.42$ Hz, 1H), 8.72 (t, $J = 1.58$ Hz, 1H), 8.57 (dd, $J = 1.49, 4.84$ Hz, 1H), 8.43 (d, $J = 2.79$ Hz, 1H), 7.87 - 7.95 (m, 1H), 7.57 - 7.63 (m, 2H), 7.55 - 7.57 (m, 1H), 7.35 (ddd, $J = 0.75, 4.84, 8.01$ Hz, 1H); ^{13}C -NMR (75 MHz, CDCl_3): δ (ppm) 120.11 (d, $J = 18.7$ Hz, 1C), 122.72, 122.75, 123.72, 129.74, 132.63 (d, $J = 3.9$ Hz, 1C), 133.03, 136.78 (d, $J = 23.2$ Hz, 1C), 138.51 (d, $J = 3.9$ Hz, 1C), 142.31, 143.36 (d, $J = 4.0$ Hz, 1C), 146.96, 149.12, 159.69 (d, $J = 257.1$ Hz, 1C); Purity (UV): 99 %, t_{R} : 5.11 min; MS (ESI+): m/z (%) = 259 (12), 258 (36), 257 (100) $[\text{M}+\text{H}^+]$, calc. 257.05.

1-[5-[5-(pyridin-3-yl)thiophen-3-yl]pyridin-3-yl]ethan-1-one **17**: yield: 39%, mp 166-167°C; IR (neat) 3079, 1419, 1124, 1023, 798, 695, 617 cm^{-1} ; ^1H -NMR (300 MHz, CDCl_3): δ (ppm) 2.68 (s, 3 H) 7.37 (ddd, $J=8.0, 4.9, 0.7$ Hz, 1 H) 7.59 - 7.64 (m, 1 H) 7.64 - 7.68 (m, 1 H) 7.88 - 7.98 (m, 1 H) 8.39 - 8.46 (m, 1 H) 8.55 (dd, $J=4.8, 1.5$ Hz, 1 H) 8.91 (d, $J=2.4$ Hz, 1 H) 9.04 (d, $J=2.2$ Hz, 1 H) 9.07 (d, $J=1.9$ Hz, 1 H); ^{13}C -NMR (75 MHz, CDCl_3): δ (ppm) 26.85, 122.81, 122.85, 123.90, 129.93, 131.37, 132.35, 132.65, 133.41, 138.62, 142.06, 146.33, 148.19, 148.45, 150.76, 163.65, 196.41; Purity (UV): 98 %, t_{R} : 4.55 min; MS (ESI+): m/z (%) = 283 (7), 282 (18), 281 (100) $[\text{M}+\text{H}^+]$, calc. 281.07.

5-[5-(pyridin-3-yl)thiophen-3-yl]pyridine-3-carboxamide **19**: yield: 13%, mp 217-218°C; IR (neat) 3346, 1679, 1467, 1126, 1026, 802, 701, 617 cm^{-1} ; ^1H NMR (300 MHz, Methanol- d_4): δ (ppm) 9.10 (d, $J = 2.24$ Hz, 1H), 8.96 (d, $J = 1.86$ Hz, 1H), 8.93 (d, $J = 1.68$ Hz, 1H), 8.63 (t, $J = 2.14$ Hz, 1H), 8.50 (dd, $J = 1.40, 4.94$ Hz, 1H), 8.18 (ddd, $J = 1.68, 2.61, 7.64$ Hz, 1H), 8.07 (d, $J = 1.49$ Hz, 1H), 8.01 (d, $J = 1.49$ Hz, 1H), 7.52 (ddd, $J = 0.84, 4.94, 8.01$ Hz, 1H); ^{13}C NMR (75 MHz, Methanol- d_4) δ (ppm) 124.73, 124.75, 125.72, 131.54, 132.08, 132.87, 134.39, 135.11, 140.11, 142.85, 147.10, 148.07, 149.34,

150.42, 169.76; Purity(UV): 96 %, t_R : 5.47 min MS (ESI+): m/z (%) = 284 (14), 283 (38), 282 (100) [M+H⁺], calc. 282.06.

3-[4-(1,3-thiazol-5-yl)thiophen-2-yl]pyridine 29: yield: 48%, mp 114-115°C; IR (neat) 3091, 1418, 1122, 1021, 798, 698, 600 cm⁻¹; ¹H-NMR (300 MHz, CDCl₃): δ (ppm) 8.89 (dd, J = 0.65, 2.33 Hz, 1H), 8.69 - 8.76 (m, 1H), 8.55 (dd, J = 1.49, 4.84 Hz, 1H), 7.99 - 8.06 (m, 1H), 7.88 (ddd, J = 1.68, 2.42, 7.82 Hz, 1H), 7.50 (d, J = 1.49 Hz, 1H), 7.42 (d, J = 1.30 Hz, 1H), 7.33 (ddd, J = 0.84, 4.84, 7.92 Hz, 1H); ¹³C-NMR (75 MHz, CDCl₃): δ (ppm) 122.06, 123.24, 123.69, 129.66, 132.73, 133.04, 133.48, 139.31, 141.77, 146.80, 148.94, 151.48; Purity(UV): 99 %, t_R : 4.72 min, MS (ESI+): m/z (%) = 247 (15), 246 (34), 245 (100) [M+H⁺], calc. 245.01.

3-[4-(1-methyl-1H-pyrazol-4-yl)thiophen-2-yl]pyridine 30: yield: 21 %, mp 119-120°C; IR (neat) 3103, 1420, 1129, 1023, 807, 703, 610 cm⁻¹; ¹H-NMR (300 MHz, CDCl₃): δ (ppm) 3.94 (s, 3H), 7.23 (d, J = 1.1 Hz, 1H), 7.32 (dd, J = 8.0, 4.8 Hz, 1H), 7.43 (d, J = 1.1 Hz, 1H), 7.57 (s, 1H), 7.70 (s, 1H), 7.88 (dt, J = 8.0, 1.9 Hz, 1H), 8.52 (dd, J = 4.8, 1.4 Hz, 1H), 8.89 (d, J = 2.2 Hz, 1H); ¹³C-NMR (75 MHz, CDCl₃): δ (ppm) 39.02, 118.23, 118.72, 123.22, 123.69, 126.99, 130.30, 133.00, 134.58, 136.93, 140.74, 146.67, 148.42; Purity(UV): 96.2 %, t_R : 4.10 min; MS (ESI+): m/z (%) = 244 (9), 243 (24), 242 (100) [M+H⁺], calc. 242.07.

3-[5-(1,3-oxazol-5-yl)thiophen-3-yl]pyridine 33: yield: 18%, mp 86-87°C; IR (neat) 3075, 1415, 1129, 1027, 816, 706, 618 cm⁻¹; ¹H-NMR (300 MHz, CDCl₃): δ (ppm) 7.28 (s, 1H), 7.31-7.39 (m, 1H), 7.47-7.52 (m, 1H), 7.58 (d, J = 1.2 Hz, 1H), 7.84-7.91 (m, 2H), 8.56 (dd, J = 5.2, 1.1 Hz, 1H), 8.87 (d, J = 2.2 Hz, 1H); ¹³C-NMR (75 MHz, CDCl₃): δ (ppm) 121.55, 121.75, 123.11, 123.66, 130.83, 130.97, 133.45, 139.52, 146.48, 147.54, 148.69, 150.11; Purity(UV): 96 %, t_R : 3.69 min; MS (ESI+): m/z (%) = 231 (7), 230 (16), 229 (100) [M+H⁺], calc. 229.04.

5-[4-(pyridin-3-yl)thiophen-2-yl]pyrimidine 41: yield: 47%, mp 173-174°C; IR (neat) 3045, 1416, 1104, 1027, 814, 708, 618 cm⁻¹; ¹H-NMR (300 MHz, CDCl₃): δ (ppm) 9.16 (s, 1H), 9.00 (s, 2H), 8.90 (dd, J = 0.56, 2.24 Hz, 1H), 8.59 (dd, J = 1.49, 4.84 Hz, 1H), 7.92 - 7.92 (m, 1H), 7.90 (ddd, J = 1.68, 2.42, 8.20 Hz, 1H), 7.67 (d, J = 1.30 Hz, 1H), 7.62 (d, J = 1.30 Hz, 1H), 7.37 (ddd, J = 0.75, 4.84, 7.82 Hz, 1H), ¹³C-NMR (75 MHz, CDCl₃): δ (ppm) 122.95, 123.70, 123.92, 128.26, 130.79, 133.48, 137.77, 140.36, 147.58, 148.86, 153.47 (2C), 157.66; Purity(UV): 98 %, t_R : 4.29 min; MS (ESI+): m/z (%) = 242 (5), 241 (15), 240 (100) [M+H⁺], calc. 240.05.

3-[5-(1,3-thiazol-5-yl)thiophen-3-yl]pyridine 48: yield: 35 %, mp 69-70°C ; IR (neat) 3052. 1480, 1128, 1023, 769, 706, 612 cm⁻¹; ¹H-NMR (300 MHz, CDCl₃): δ (ppm) 7.33 - 7.41 (m, 1 H) 7.45 - 7.50 (m, 2 H) 7.85 - 7.93 (m, 1 H) 8.03 (s, 1 H) 8.53 - 8.61 (m, 1 H) 8.72 - 8.78 (m, 1 H) 8.85 - 8.91 (m, 1 H); ¹³C-NMR

(75 MHz, CDCl₃): δ (ppm) 152.0, 148.4, 147.3, 139.7, 139.5, 134.4, 133.7, 132.0, 131.0, 124.5, 123.8, 121.6; Purity(UV): 99 %, t_R : 4.08 min, MS (ESI+): m/z (%) = 247 (10), 246 (16), 245 (100) [M+H⁺], calc. 245.01.

3.1.4 Results and Discussion

Identification of screening hits and lead generation. In order to discover novel inhibitors for the family of Dyrk kinases, we screened an in house library lacking any compounds with typical kinase inhibitor motifs at a concentration of 10 μ M. During this campaign, hit compound **1** (Figure 1) was identified as a moderate inhibitor of Dyrk1A, exhibiting an IC₅₀ of 2.0 μ M. In order to assess the selectivity, a first counter screen was performed using casein kinase 2 (CK2 α), a related kinase from the same CMGC family which was frequently shown to have overlapping active hits [81,82]. Compound **1** proved to be rather inactive towards CK2 α (15% inhibition at 5 μ M). To explore first structure–activity relationships, we synthesized compound **2** as an analogue of compound **1** bearing both hydroxyl groups in the *meta*-position. This substitution pattern abolished the biological activity of the molecule (10 % inhibition at 5 μ M), suggesting that the positions of the hydroxyl groups might be crucial for hydrogen bond interactions. The constitutional isomer **3** of compound **1** showed comparable activity against Dyrk1A, but, interestingly, led to a significant loss of selectivity over CK2. This suggested that by altering the position of the sulfur atom in the thiophene core, it might be possible to influence the selectivity. We also tested 2,5-disubstituted thiophenes with similar phenolic substituents, but these compounds were all inactive (data not shown). The phenolic hydroxyl groups represented not only a weak spot for phase II metabolism, they were also responsible for the inhibitory activity of the hit compound against 17 β -hydroxysteroid dehydrogenase 1 (HSD1), for which it had been originally designed [70].

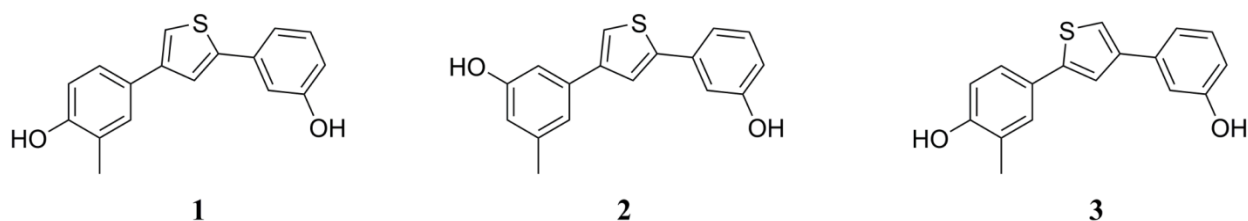


Figure 1: Structure of the hit compound **1** and two newly synthesized derivatives.

In addition, hydrogen bond donor functions are negatively correlated with the ability to cross the blood–brain barrier [83], and a comparison of our hit compound with previously reported Dyrk

inhibitors showed that hydrogen bond donor functions are not required for potent inhibition [49, 84]. Therefore, we aimed at replacing the hydrogen bond donor function of the hydroxyls by acceptor functions. Firstly, the methoxy-substituted analogue of compound **3** was tested which was available as a precursor compound. However, this derivative was completely inactive against Dyrk1A. A comparison with previously reported Dyrk inhibitors suggested that the distance of the hydrogen bond acceptor functions might be too large [49, 84]. Therefore, we decided to compact the bisphenol thiophene structure by including the hydrogen bond acceptor functions in aryl heterocycles, which logically led to 3-pyridyl rings.

Table 1: Distances between the two hydrogen bond acceptor functions^a

Compound	Range of distances between H-bond acceptor functions [Å]
1	10.65 – 12.36
4	7.78 – 9.38
Harmine	7.85

^aThe Energy was minimized using Chem3D Pro (Version 13.0.0.3015; Method: MM2). The ranges denote the distances measured in different conformers of similar energy.

The resulting new compound class featured two hydrogen bond acceptor groups in a spatial distance comparable to that of the earlier described Dyrk1A inhibitor harmine (Table 1, Figure S1). The prototype bispyridyl derivative **4** (Figure 2) turned out to be three times more potent towards Dyrk1A than the hit compound **1** (IC₅₀ = 0.7 μM). Replacing one of the 3-pyridine rings by a 3-methoxy-substituted phenyl did not recover the biological activity, indicating again that the distance between the hydrogen bond acceptor functions is crucial for activity. In contrast to many known kinase inhibitor scaffolds, our novel lead compound **4** did not contain a tandem hydrogen bond donor/ acceptor moiety, which could establish a strong affinity anchor with the highly conserved hinge region backbone, but on the other hand might compromise selectivity. Importantly, compound **4** did not affect the activity of CK2α, indicating that a decent degree of selectivity could be expected.

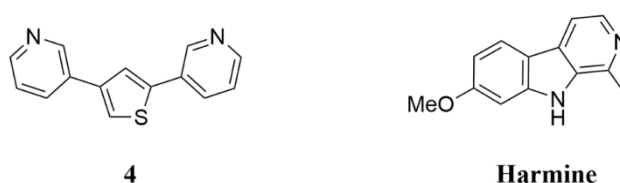
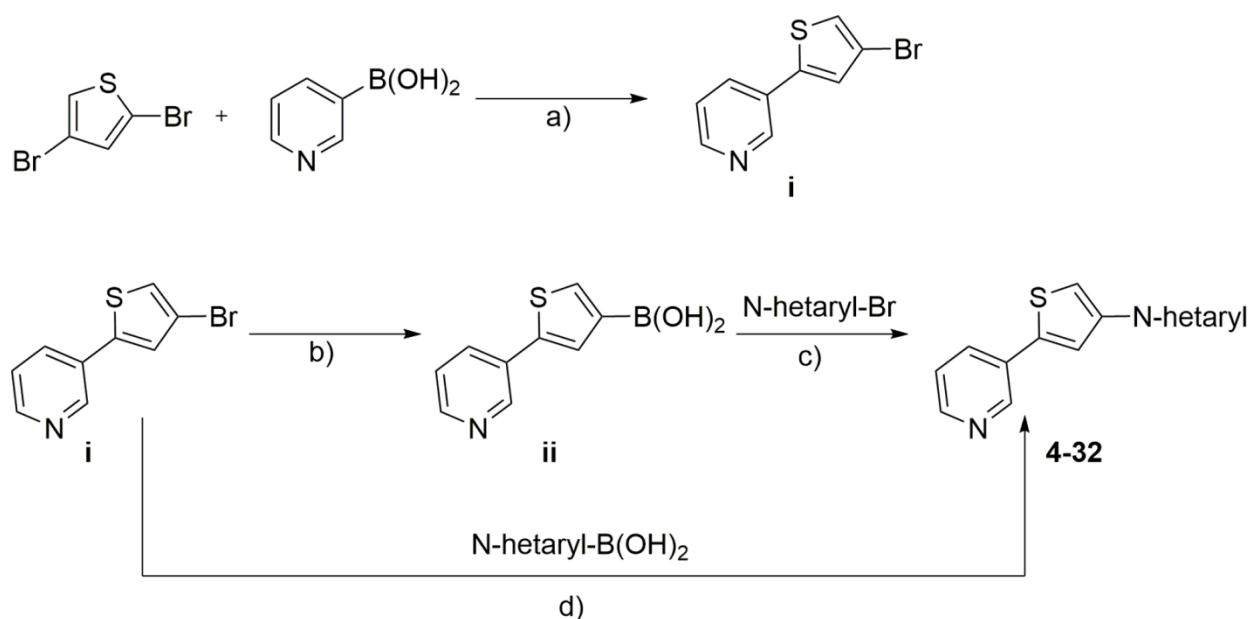


Figure 2: Structures of the Dyrk inhibitor **4 (this study) and harmine (originally isolated from *Peganum harmala*).**

It seemed straightforward to investigate whether the binding affinity of **4** could be increased by optimization of both the position and the strength of the two hydrogen bond acceptor functions. In addition, already small differences in the angle and distance between these functions might translate into significant binding preferences for the one versus the other Dyrk isoform. Furthermore, independent modulation of the electrostatic potential as well as the steric properties of the exterior ring systems provided another means to optimize the selectivity profile.

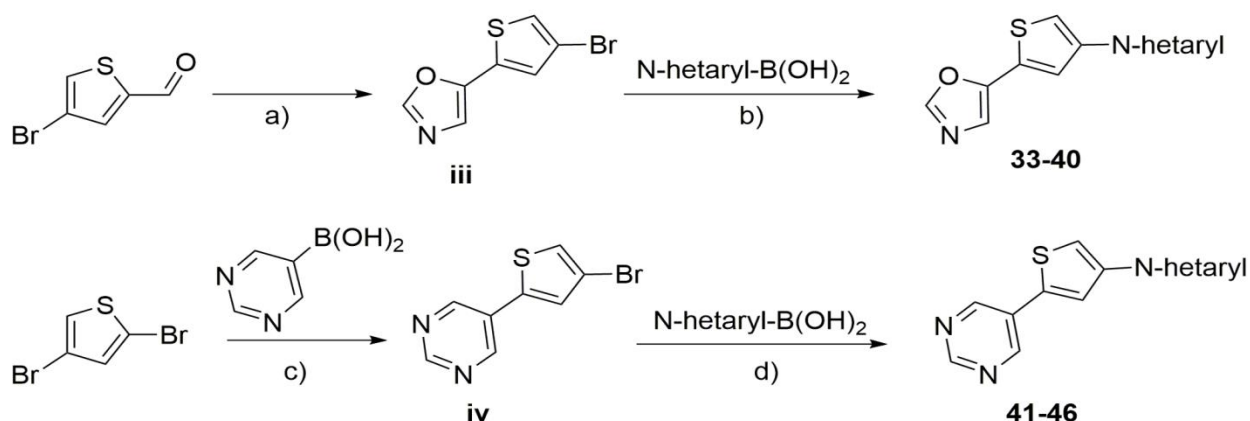
Scheme 1: Synthesis of target compounds 4 to 32^a



^aReagents and conditions: a) Na_2CO_3 , $\text{Pd}(\text{PPh}_3)_4$, Dioxane/Water, Reflux, 15 hours; b) $(i\text{PrO})_3\text{B}$, $n\text{BuLi}$, Toluene/THF, -78°C , 75 min, 2 M HCl, -25°C , 30 min; c) N-heteroaryl bromide, CS_2CO_3 , $\text{Pd}(\text{dppf})\text{Cl}_2$, DMF/Water, Reflux, 15 hours; d) N-heteroaryl boronic acid, CS_2CO_3 , $\text{Pd}(\text{dppf})\text{Cl}_2$, DMF/Water, Reflux, 15 hours.

Chemistry. A diverse set of aromatic azaheterocycles was attached to the 2- and 4-position of the thiophene core. Since the compounds were conveniently accessible by consecutive Suzuki cross coupling reactions [85], it was possible to adapt the synthesis to an automated robotic system for diversification purposes. A series of N-heteroaryl bromides or boronic acids was selected, including pyridine isomers, substituted pyridines, pyrimidines, pyridinone, five-membered heterocycles e.g. pyrazoles, thiazoles, oxazoles and fused heterocycles, with molecular masses below 140 g/mol, so that the final compounds would not exceed a mass of 300 g/mol. All building blocks were commercially available for prices below US\$ 50 per gram.

Scheme 2: Synthesis of target compounds **33** to **46**^a

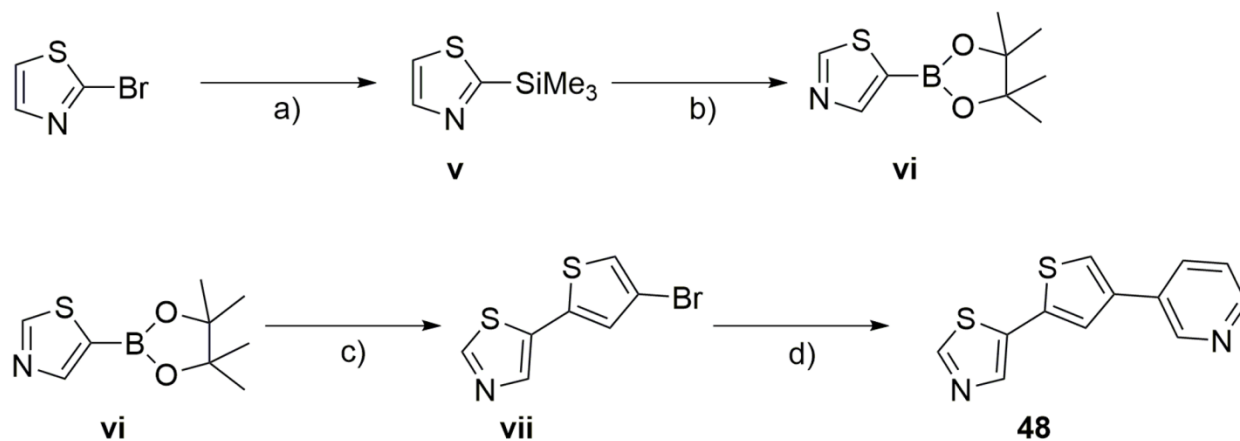


^aReagents and conditions: a) Toluensulfonylmethyl isocyanide, Na_2CO_3 , Methanol, Reflux, 4 hours; b) Cs_2CO_3 , $\text{Pd}(\text{dppf})\text{Cl}_2$, DMF/Water; Reflux, 15 hours; c) Na_2CO_3 , $\text{Pd}(\text{PPh}_3)_4$, Dioxane/Water, 90°C , 48 hours; d) Cs_2CO_3 , $\text{Pd}(\text{dppf})\text{Cl}_2$, DMF/Water; Reflux, 15 hours.

Starting from compound **4**, we synthesized three compound series. Within the first series we kept the 3-pyridyl moiety in 2-position of the thiophene core constant and varied the substituent in 4-position of the central core (compounds **5** to **32**). Scheme 1 outlines the synthetic route for compounds **5** to **32**. 2,4-Dibromothiophene was reacted with 3-pyridylboronic acid to yield (**i**). Compound (**i**) was either directly reacted with an appropriate heteroaryl boronic acid or first converted to the corresponding boronic acid (**ii**) and subsequently reacted with an appropriate heteroaryl bromide to yield compounds **5** to **32**. Scheme 2 illustrates the synthesis of compound series 2 (compounds **33** to **40**) and 3 (compounds **41** to **46**). Series 2 was furnished with an oxazole moiety in 2-position of the thiophene core, which could be easily introduced by reaction of 4-bromo-2-thiophenecarbaldehyde with Toluensulfonylmethyl isocyanide (TosMIC). The resulting precursor (**iii**) was directly used for the synthesis of compounds **33** to **40** by a subsequent Suzuki cross coupling reaction. In series 3, a pyrimidine moiety was introduced in 2-position of the central thiophene core by reaction of 5-pyrimidine boronic acid with 2,4-dibromothiophene. The resulting intermediate (**iv**) was used in a subsequent Suzuki cross coupling to yield compounds **41** to **46**. In addition to the compound series named above, we synthesized an additional molecule, bearing the 3-pyridyl moiety in 4-position of the thiophene core (Scheme 3). The resulting compound **48** represented an isomer of compound **29**, where the relative position of the sulfur atom is moved by 1 atom. Therefore, 2-bromo-thiazole was reacted with trimethylsilyl chloride to yield (**v**), which was converted to the

corresponding boronic ester (**vi**). Suzuki cross coupling of (**vi**) with 2,4-dibromothiophene yielded (**vii**), which was reacted with 3-pyridyl boronic acid to compound **48**.

Scheme 3: Synthesis of Compound 48^a



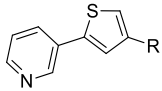
^aReagents and conditions: a) nBuLi, diethyl ether, -78°C, 60 min; trimethylsilylchloride, -78°C, 60 min; b) nBuLi, THF, -78°C, 35 min; (*i*PrO)₃B, -78°C, 90 min; pinacol, RT, 10 min; c) Dibromothiophene, Na₂CO₃, Pd(PPh₃)₄, Dioxan/Water, 90°C; d) 3-Pyridylboronic acid, Cs₂CO₃, Pd(dppf)Cl₂, DMF, Reflux.

Biological activity. Compound **4** is directed to the ATP-binding site. Because the synthesized compounds have not been described in the context of kinase inhibition yet, we first investigated the potential mechanism of inhibition. Given that the two hydrogen bond acceptor functions in **4** were superimposing with those in harmine (cf. Figure S1, Supporting Information), it was most likely that the compounds would also target the ATP-binding site, although they did not exhibit a fully coplanar shape. In a kinetic experiment, we were able to confirm that Dyrk1A was inhibited by **4** in a clearly ATP- competitive manner (Figure S2, Supporting information). Hence, for the discussion of the structure–activity relationships (SAR), it was assumed that the compounds were addressing the ATP-binding pocket.

Structure-activity relationships of the 2,4-bisheterocyclic substituted thiophenes. Starting from **4**, we first investigated the influence of different heterocycles in 4-position of the central thiophene on the biological activity while the 3-pyridyl in 2-position was preserved. The biological activities of this first compound series are shown in Table 2, with the most potent compounds being highlighted in blue. Firstly we probed the impact of an additional methyl group in the variable part of the compound. Compounds **5** to **7** featured 3-pyridyl moieties bearing a methyl substituent at different positions.

Compound **5** maintained approximately the activity towards Dyrk2, whereas a slight loss of activity was observed towards Dyrk1A and 1B. The selectivity against CK2 was not affected. For compound **6** and **7**, we observed a significant loss of activity towards the Dyrk kinases. In the case of **6**, the sixfold decrease in affinity is probably caused by the methyl group in *ortho*-position to the thiophene linkage. This presumably forced the pyridine ring to rotate out of plane which was not tolerated by the binding pocket. In compound **7**, the *para*-methyl presumably caused a steric clash within the ATP pocket, thus preventing the compound from assuming an optimal binding position. The impact of the *para*-methyl group was less pronounced with Dyrk2 and resulted only in a twofold loss in activity. We also introduced an additional hydrogen bond acceptor function in *meta*-position to the nitrogen (**8**). This modification enhanced the activity towards Dyrk1B and Dyrk2, whereas the potency towards Dyrk1A was similar to that of **4**. A sterically more demanding, flexible residue like an ethoxy group (**10**) was not tolerated at this position. Similarly to **7**, the spatial requirements of the methoxy group in the *para*-position to the thiophene linkage (**9**) led to a complete loss of activity towards the Dyrk isoforms. Apparently, the electron density at the pyridine nitrogen could not be efficiently enhanced, because the electron donating substituents were not tolerated at the relevant position. To further investigate the optimal relative position of the pyridyl nitrogen, we introduced the 4-pyridyl at one side, resulting in compounds **11** and **12**. This completely abolished the biological activity, confirming that the position of and distance between the hydrogen bond acceptor functions was critical to the activity. The next step was to switch from electron-donating substituents to electron-withdrawing substituents in the 3-pyridyl ring. To this end, we introduced nicotinitrile, 3-trifluoromethylpyridyl, 3-fluoropyridyl, 3-chloropyridyl, 3-acetylpyridyl, nicotinic acid methyl ester, and nicotinamide as thiophene-4-substituents (**13** - **19**). As a result, we found that the nitrile and the trifluoromethyl group were not tolerated well in all tested Dyrk kinases, whereas fluorine and chlorine affected the biological activity only slightly compared with compound **4**, thus offering a potential option to increase the metabolic stability.

Table 2: Biological activity of 3-(thiophen-2-yl)pyridine derivatives with diversification at the 4-position of the thiophene core

					
Compound	Structure	IC ₅₀ [μM] ^a			
		Dyrk1A	Dyrk1B	Dyrk2	CK2α
4		0.7	0.7	0.7	18.5 %

5		0.9	1.2	0.6	5 %
6		4.4	8.0	10 % (1 μ M)	0 %
7		4.7	3.4	1.6	0 %
8		0.7	0.3	0.2	16 %
9		36	34	No inhibition	0 %
10		45 %	6 % (1 μ M)	22 % (1 μ M)	0 %
11		10 %	10 %	20 %	0 %
12		23 %	No inhibition	37.5 %	n.d.
13		2.6	30 %	44 %	3 %
14		3.1	5.4	3	0 %
15		0.9	1.4	0.4	0 %
16		1.2	1.9	0.7	14 %
17		0.9	1.1	0.9	0 %
18		1.2	1.7	1.5	14 %
19		0.9	1.5	0.3	4.2 %
20		1.1	0.9	1.8	27 %
21		3.5	3.2	2.9	6 %

22		1.8	3.5	1.8	0 %
23		1.3	1.4	0.3	0 %
24		37 %	13 % (1μM)	0.6	7 %
25		4 %	n.d.	n.d.	n.d.
26		No inhibition	No inhibition	27 %	n.d.
27		No inhibition	No inhibition	31 %	n.d.
28		31 %	n.d.	6.7	n.d.
29		0.1	0.1	0.4	0 %
30		0.3	0.4	0.2	9.5 %
31		44 %	9.1	5.1	n.d.
32		2.2	0.6	0.4	0 %

^aGiven are mean values of at least two independent experiments, S.D. < 10 %. Compounds exhibiting an IC₅₀ value below 1 μM towards Dyrk1A are highlighted in blue. Percent values indicate the percentage of inhibition at 5 μM if not stated otherwise (other test concentrations are indicated in brackets).

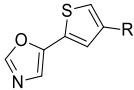
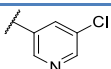
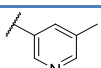
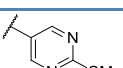
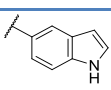
None of the substitutions provoked CK2 inhibition, indicating that the scaffold – though being small – did not bind to the ATP binding pocket of this related kinase. We also introduced a quinoline (**20**) and an isoquinoline moiety (**21**) into the 4-position of the thiophene to enhance the hydrophobicity and extend the aromatic system. The quinoline derivative was slightly more active than the isoquinoline, which was probably related to the different spatial orientation of the additional hydrophobic π-system (Figure S3). We assumed that both moieties protrude into different areas of the ATP pocket. However, they probably prevented an optimal hydrogen bond interaction so that the potency was actually reduced compared with **4**. We also examined the influence of an additional

hydrogen bond acceptor function by synthesis of a pyrimidine-substituted thiophene **22**. This modification decreased the potency toward the target kinases, which may have been caused by an inappropriate electrostatic potential and/or attenuated hydrogen bond acceptor strength of the nitrogen involved in hydrogen bonding [86]. On the other hand, the positional isomer **41** (Table 4, see further below) restored the activity towards Dyrk1A, however with a two times lower potency towards Dyrk2. Hence, the regioisomeric pair of compounds **22** and **41** provided another example that the relative position of the sulfur in the thiophene core had an influence on the potency and selectivity.

A further extension of the pyridine in 4-position by disubstitution (**23**) or by annelation (**24**) significantly enhanced the selectivity for Dyrk2. Within the three screened Dyrk family members, compound **24** was specific for Dyrk2.

Compounds **25** to **27** were completely inactive against the Dyrk kinases. Since we found that the introduction and modification of a six-membered ring systems did not achieve a significant increase in potency towards Dyrk1A and Dyrk1B, we decided to introduce five-membered ring systems in the 4-position of the thiophene core. While the thiazole derivative **28**, with the nitrogen being located in 2-position relative to the thiophene linkage, was inactive against Dyrk1A/B and weakly inhibited Dyrk2 ($IC_{50} = 6.7 \mu\text{M}$), the positional isomer **29** turned out to be a potent inhibitor of all Dyrk kinases with a preference for Dyrk1A/B. When tested in parallel in our assay, the IC_{50} values for **29** and the reference compound harmine were almost identical. The 5 to 7-fold enhancement of the potency (towards Dyrk1A and 1B, respectively) compared with the pyridine analogue **4** was remarkable, given the fact that the hydrogen bond acceptor strength of the thiazole is weaker than that of the pyridine [86].

Table 3: Biological activity of 2-(thiophen-2-yl)oxazole derivatives with diversification at the 4-position of the thiophene core

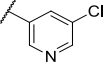
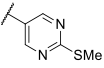
Name	R	IC ₅₀ [μM] ^a			
		Dyrk1A	Dyrk1B	Dyrk2	CK2α
					
33		0.8	1	1.34	0 %
34		0 %	18 %	12 %	-
35		1.2	1.1	1.5	-15 %
36		25 %	40 %	16 %	-
37		7 %	21 %	5 %	-
38		1.5	2.2	1.5	-20 %
39		20 %	8.07	19 %	-
40		18 %	9 %	30 %	-

^aSee footnote of Table 2.

Probably the angle of the nitrogen toward the hydrogen bond donor is more favorable than with the pyridine, thus compensating for its reduced acceptor strength. Introduction of a methyl pyrazole also yielded one of the most potent inhibitors of this series (**30**). However, the selectivity switched to Dyrk2. In contrast, compound **31**, bearing a methyl imidazole moiety with the methyl group in *ortho*-position to the thiophene linkage, displayed a largely reduced activity against all Dyrk kinases. The methyl group probably forced the ring to rotate out of plane, thus abolishing the favorable co-planar conformation, similar to compound **6**. Extension of the favorable imidazole ring to the imidazo[1,2-

a]pyridine produced compound **32** with a distinct selectivity profile, showing good inhibition of Dyrk1B and Dyrk2 but significantly reduced activity toward Dyrk1A.

Table 4: Biological activity of 5-(thiophen-2-yl)pyrimidine derivatives with diversification at the 4-position of the thiophene core

Name	R	IC ₅₀ [μM] ^a			
		Dyrk1A	Dyrk1B	Dyrk2	CK2α
41		0.9	1.8	3.5	0 %
42		1 %	5 %	0 %	-
43		5	2.2	3.8	-15 %
44		2 %	27 %	27 %	-
45		8 %	20 %	-24 %	-
46		9 %	33 %	15 %	-

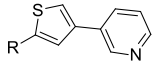
^aSee footnote of Table 2.

In parallel to the compounds from series 1 (Table 2), we synthesized two additional compound classes (Tables 3 and 4). The pyridine in 2-position was replaced by oxazole (Table 3) and by pyrimidine (Table 4), respectively, while the 4-position was varied by a set of different heterocycles. Within these series we identified four Dyrk inhibitors with IC₅₀ values around 1 μM. Compound **33** and **41** were equally active towards Dyrk1A. However, the pyrimidine-substituted congener **41** displayed a superior selectivity (cf. discussion of the matched isomer **22** above). Interestingly, in this series, the introduction of a methyl group in *meta*-position to the thiophene connection of the pyridine substituent (**43**) decreased the biological activity as well as the selectivity profile within the Dyrk family. Introduction of a chlorine substituent also abolished the activity (**34** and **42**). These

substituent effects are in sharp contrast to those seen with the bis-pyridyl derivatives **5** and **16**, demonstrating that they are specifically dependent on the type of the partner heterocycle at the other thiophene position. Notably, none of the oxazole derivatives reached the potency range of the thiazole congeners **29** and **48** (see below), even though both heterocycles exhibit a comparable hydrogen bond acceptor strength [86]. However, compared with the oxazole ring system, the thiazole ring displays a higher aromatic character as a major difference. The Bird Index (BI), a measure for aromaticity relative to benzene (BI 100), has a value of 79 for thiazole, which is closer to pyridine (BI 86) than that of oxazole (BI 47) [87]. In consequence, the π -electrons are less delocalized in the oxazole ring but more confined to the double bonds, thus decreasing potential surface for CH- π interactions with the aliphatic side chains of the ATP binding pocket in Dyrk1A/B. Interestingly, though, we found later that the oxazole compound **33** was still accepted by the Clk1 ATP binding site (Table 9 and see below), conferring some selectivity for the latter kinase. In contrast, the thiazole congeners **29** and **48** turned out to be dual inhibitors of Dyrks and Clk1/4 (Table 9 and see under "Selectivity Profile").

Inspired by the distinct results obtained with the isomeric pair **22** and **41**, we also synthesized isomers of **21** and **29** in which the relative position of the sulfur atom in the thiophene core was changed. This modification led to compound **47** and **48**, respectively (Table 5). Interestingly, the activity of **48** towards Dyrk1A and Dyrk1B was not affected compared to **29**, but the Dyrk2 activity was increased tenfold. Compound **47** was slightly more potent than the first isomer **21**, but without major changes in the selectivity profile. Altogether, our results suggested that depending on the size and type of the heterocycles, the thiophene scaffold allowed modulation of both selectivity and potency simply by interchanging the positions of the thiophene substituents. Thiazole was found to generate potent compounds both at the 2- and the 4-position of the thiophene core in the disubstituted inhibitors. Expectedly, high ligand efficiencies were calculated for both thiazole compounds **29** and **48** (Table S1). According to these results, the design of future refined libraries of Dyrk inhibitors might include a thiazole ring in combination with other azaheterocycles.

Table 5: Biological activities of compounds 47 and 48 possessing a changed relative position of the thiophene sulfur compared to their regioisomers 21 and 29

					
Compound	Structure	IC ₅₀ [μM] ^a			
		Dyrk1A	Dyrk1B	Dyrk2	CK2α
47		1.5	2.4	1.2	3 %
48		0.1	0.07	0.04	0 %

^aSee footnote of Table 2.

Evaluation of the Drug-like properties. The major indication for Dyrk1A inhibitors are neurodegenerative diseases such as Alzheimers disease [4, 5, 9, 10]. Thus, it is prerequisite for those inhibitors to cross the blood–brain barrier. In the literature, several physicochemical properties of CNS–active drugs and lead compounds have been analyzed, thus providing parameters to estimate the probability of a brain penetration [83]. To this end, we experimentally determined the physicochemical properties of compound **4** including logP, pK_a and logS. The obtained data were then compared with the corresponding calculated physicochemical properties (Table 6). Since the predicted parameters were in a good agreement with the experimental data for the prototype compound **4**, we decided to calculate the most important predictive parameters of our best compounds and compared them to those of the CNS–active inhibitor harmine (Table S2). Almost all calculated parameters showed ideal values, with the number of hydrogen bond donors being even more favorable than in the case of harmine. Only the calculation of the size of the polar surface area (PSA) [88] raised the question as to whether the thiophene sulfur should be included or not. However, since the calculation of the molecular electrostatic potential of each compound revealed no particular polarity for the aromatic sulfur atom (data not shown), it might be correct to exclude the sulfur from the calculation, however both values are given in Table S2. Altogether, the probability of CNS penetration was predicted to be high.

Table 6: physicochemical properties of compound 4

Physicochemical property	Experimental	calculated
logP	2.47	2.61 ^a
pK_{a1}	3.48	4.23 ^a
pK_{a2}	4.8	4.86 ^a
logS	-2.67	-2.81 ^b
Solubility mg/ml	0.50	0.37 ^b

^aCalculation was performed using JChem for Excel (Version 6.0, 2013, ChemAxon Ltd., www.ChemAxon.com);

^bCalculation was performed using ACD/Percepta 2012 (ACD/Labs).

Evaluation of metabolic stability. In addition to the assessment of the physicochemical parameters, the most potent lead compounds **29**, **30** and **48** were evaluated for their phase I metabolic stability using rat liver microsomes. Samples were taken at defined time points, and the remaining percentage of parent compound was determined by LC-MS/MS. Half-life and intrinsic clearance were calculated and compared to the two reference compounds diazepam and diphenhydramine, but also to harmine (Table 7). All of the new lead compounds but not harmine showed significantly longer half-lives than the antihistaminic drug diphenhydramine. In particular, compound **30** was considerably more stable than harmine and showed a good half-life and predicted clearance ranging between those obtained for the drugs diphenhydramine and diazepam. The two isomeric compounds **29** and **48** displayed a similar metabolic stability and were slightly more stable than harmine.

Table 7: Metabolic stability of compounds 29, 30 and 48 and reference compounds against rat liver microsomes^a.

Compound	Half-life [min]	Cl _{blood} ^b [mL/min/kg]
Harmine	18	53
29	27	49
30	53	34
48	31	47
Diphenhydramine	17	53
Diazepam	96	25

^a 0.225 mg/mL protein, NADP⁺-regenerating system, [inhibitor]: 0.5 μM, incubation at 37 °C, samples taken at 0, 15, 30, and 60, 90 min, determination of parent compound by MS. ^b Cl_{blood}: estimated blood clearance in rats as calculated based on *in vitro* intrinsic clearance. The values are representative for two independent experiments that essentially gave the same results.

Cell-based functional and toxicity assays. Having observed a potent inhibition of Dyrk1B, and because Dyrk1B inhibitors which are more potent than harmine had barely been reported, we performed different assays to evaluate the ability of our compounds to inhibit Dyrk1B in cells. It was previously shown that the inhibition of Dyrk1B in tumor cell lines in which this kinase is overexpressed triggers the activation of the caspase signaling cascade resulting in apoptosis [89], and causes an increased production of reactive oxygen species (ROS) also contributing to cell destruction [90]. For our experiments, we chose the U2OS sarcoma cell line as a model, in which a strong overexpression of Dyrk1B had been demonstrated [89]. The cells were starved and incubated with the most potent inhibitors from our series and in addition with one inactive congener (**11**) as a further control. The activity of caspase-3/7 was measured as an indicator of apoptosis induction after 48 hours. We found that compounds **29** and **48**, which had inhibited purified Dyrk1B with IC₅₀ values of 100 and 70 nM, respectively, triggered a clear increase of the caspase-3/7 activity in a concentration–dependent manner (Figures 3A and 3B). Notably, the induction of caspase-3/7 by **29** was observed already at a concentration of 0.5 μM, although the values at this concentration failed to reach statistical significance.

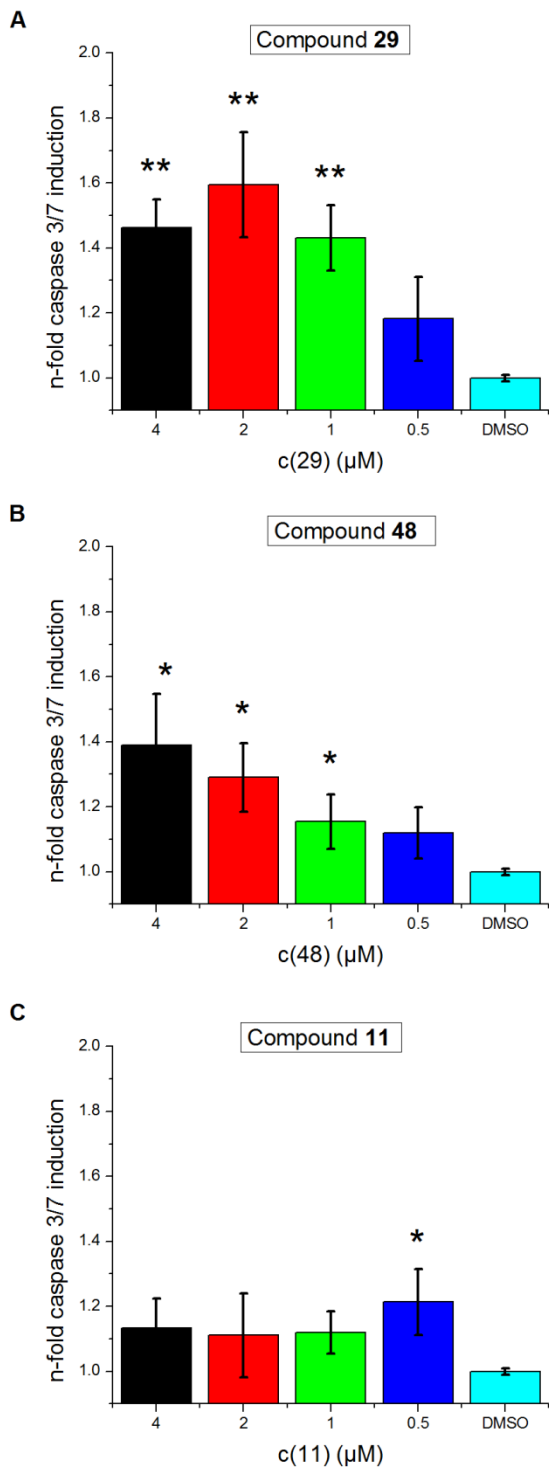


Figure 3: The Dyrk1B inhibitors 29 and 48 induce Caspase 3/7 activity in U2OS cells. U2OS cells were incubated overnight with the indicated concentrations of the active inhibitors 29 (A) and 48 (B), which resulted in a concentration-dependent increase of Caspase-3/7 activity. In contrast, incubation with the inactive congener 11 (C) slightly enhanced the background caspase activity independent of the compound concentration. Values from one out of three separate experiments are shown that gave essentially similar results. The standard deviation is given as γ -error bar. One asterisk indicates significance with a p value < 0.05 , two asterisks indicate significance $p < 0.01$.

In contrast, the Dyrk1B–inactive analogue **11** caused only a slight increase of the caspase-3/7 activity compared with the DMSO control, which however, did not show a concentration–dependency, suggesting that it was a non-specific effect (Figure 3C). The effects observed with **29** and **48** were fully consistent with an inhibition of Dyrk1B in this tumor cell line, which was previously reported to respond by an increased apoptosis rate after down-regulation of Dyrk1B by siRNA [89].

Another known biological consequence of Dyrk1B inhibition in tumor cells is the increased generation of ROS [90]. The ability of our most potent compound **29** to trigger this response in U2OS cells was tested using the cell permeable dihydroethidium as an indicator dye. In the presence especially of the superoxide anion radical ($O_2^{\cdot-}$), this dye is oxidized to 2-hydroxyethidium, giving rise to increased fluorescence after intercalating with the cellular DNA [91]. Indeed, **29** considerably enhanced the fluorescence of the reporter dye in a concentration–dependent manner, already starting at 0.2 μ M (Figure 4). This result was indicative of an increased production of ROS as a consequence of Dyrk1B inhibition.

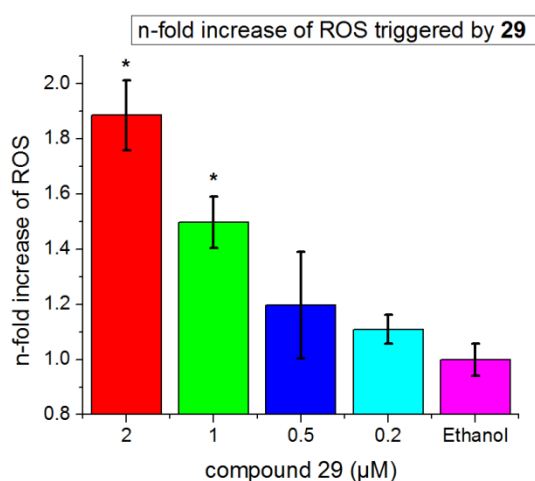


Figure 4: The Dyrk1B inhibitor **29** triggers the production of reactive oxygen species in U2OS cells. Incubation of U2OS cells with **29** caused an increased intracellular conversion of dihydroethidium to the stronger fluorescent ethidium, indicating raised levels of reactive oxygen species compared with the ethanol control. Data shown are representative of two independent experiments. Asterisks indicate statistical significance (p value < 0.05).

To provide further evidence that Dyrk1B was the intracellular target of our compounds, we analyzed by Real-Time PCR whether they would modulate some major Dyrk1B–regulated gene expressions in the expected manner. To this end, we selected a comprehensive set of genes representing the distinct Dyrk1B-dependent gene regulatory pathways that were previously reported in literature. For instance,

Dyrk1B phosphorylates the class II histone deacetylase (HDAC)5, leading to a reduced nuclear accumulation and suspended biological function of this epigenetic modifier, thus ensuing an increased transcription of a number of genes [92,93]. We selected CDH4 (cadherine-4) and FGF2 (basic fibroblast growth factor), whose transcription was found to be clearly suppressed by HDAC5 activity in a large microarray analysis [66]. Treatment of U2OS cells with our Dyrk1B inhibitors was therefore expected to induce a down-regulation of these genes due to increased migration of HDAC5 to the nucleus. Indeed, both **29** and **48** caused a slight reduction of the mRNA expression, which was somewhat more pronounced with FGF2 (Table 8). Furthermore, Dyrk1B was implicated in the down regulation of the FoxO family of transcription factors; siRNA-mediated knockdown of Dyrk1B in ovarian cancer cells resulted in apoptosis accompanied by nuclear translocation of FoxO1 and/or FoxO3A as well as increased BIM (BH3-only member of the BCL-2 family) and TRADD (Tumor necrosis factor receptor type 1-associated DEATH domain protein) expression, as well as caspase-3 and PARP cleavage [94].

Table 8: Modulation of Dyrk1B-regulated gene expressions by compounds 29 and 48 as analyzed by Real-Time PCR^a

Target gene mRNA	29		48	
	5 μ M	10 μ M	5 μ M	10 μ M
CDH4	-1,4 \pm 0.2	-1,5 \pm 0.3	-1,4 \pm 0.1	-1,5 \pm 0.2
FGF2	-1,4 \pm 0.1	-1,8 \pm 0.2	-1,7 \pm 0.1	-1,7 \pm 0.3
BIM	2,4 \pm 0.2	2,5 \pm 0.4	2,7 \pm 0.3	2,6 \pm 0.5
TRADD	2,5 \pm 0.3	3,0 \pm 0.3	1,2 \pm 0.2	3,0 \pm 0.6
FasL	1,2 \pm 0.1	2,7 \pm 0.4	1,2 \pm 0.1	1,9 \pm 0.3
SOD2	-2,3 \pm 0.2	-2,3 \pm 0.3	-2,4 \pm 0.1	-2,1 \pm 0.4
CP	-2,7 \pm 0.3	-2,9 \pm 0.6	-2,0 \pm 0.3	-2,2 \pm 0.4

^aValues indicate fold up-regulation (positive numbers) or down-regulation (negative numbers) of mRNA expression, relative to DMSO-treated cells. Given are mean values of at least two independent experiments, n=3, \pm S.D..

In addition, it was reported that Dyrk1A co-localizes with FoxO and may phosphorylate FKHR (Forkhead in rhabdomyosarcoma) at Ser329, decreasing the ability of FKHR to stimulate gene transactivation and reducing its nuclear localization. In agreement, treatment of fibroblasts with the

Dyrk1A/B inhibitor harmine resulted in elevated FoxO-DNA binding activity and increased nuclear accumulation [95]. Hence, the effect of our inhibitors on FoxO signaling was monitored by analyzing the expressions of the transcriptional targets BIM, TRADD and FasL (Fas ligand). In full accordance with the mentioned reports, incubation of U2OS cells with our inhibitors resulted in an increased expression of all three pro-apoptotic genes (Table 8), although a concentration dependency was not clearly seen in the case of the BIM expression. However, it is possible that BIM was already maximally transactivated at the lowest concentration of each inhibitor tested.

Altogether, using the complementary approach of apoptotic gene expression analysis, we were able to confirm that the compounds induce apoptosis, in agreement with the activation of caspase 3/7 (Figure 3). According to previous findings, the release of FoxO repression by pharmacological inhibition of Dyrk1B might be the responsible pathway, at least partially. In the light of the potentially synergistic roles of Dyrk1A and Dyrk1B in the suppression of FoxO function, dual inhibitors of both Dyrk isoforms, such as those presented here, might be even more effective.

In addition, Dyrk1B was described to increase the expression of antioxidant enzymes by an as yet unidentified pathway. Specifically, it was reported that shRNA-induced silencing of Dyrk1B led to a reduced mRNA expression of the antioxidant genes superoxide dismutase (SOD)2 and ferroxidase (also called ceruloplasmin, CP) in pancreatic cancer cell lines, accompanied by an increase in ROS levels [90]. As can be seen from Table 8, the mRNA expression of both SOD2 and CP was reduced more than twofold in the presence of the compounds compared to the DMSO control. Like in the case of BIM, there was only a weak concentration dependency – if at all – at the concentrations chosen for the experiment. Again, a possible explanation could be that the maximum suppression of transcription might already have been reached at 5 μ M. This is supported by the fact that a slight increase of ROS production was already observed at 0.2 μ M of compound **29** (Figure 4).

Collectively, the results of our transcription profiling, obtained with seven different genes from three different Dyrk1B-regulated pathways, were in full agreement with the previous literature reports. Moreover, the profiling data were consistent with the results from our biochemical assays regarding Caspase3/7 activation (Figure 3) and ROS production (Figure 4). Hence the transcription profiling provided strong evidence that compounds **29** and **48** indeed targeted Dyrk1B in the U2OS cells.

To further rule out a general cytotoxicity of the compounds, we tested the potential effects on cell growth of V79 hamster lung fibroblasts as a model for non-tumor cells which do not depend on overexpressed Dyrks. Cellular ATP levels were determined as a measure for cell viability and

proliferation using a luminescence-coupled assay. As shown in Figure 5, harmine appeared to be slightly toxic already at 5 μM , whereas compounds **29** and **48** showed no influence on cell viability at this concentration. However, there was no significant difference anymore at the higher concentrations (10 and 20 μM). Thus, all active dual Dyrk/Clk inhibitors seemed to affect cell growth, whereas a control compound (**11**) of the same chemotype but without effect on Dyrk kinases (in the cell-free assays) showed no influence. We thus concluded that at least part of the effect shown by all Dyrk/Clk inhibitors at higher concentrations might be mechanism-related. One possible explanation might be that mitochondrial ATP production was slightly reduced at higher concentrations of the compounds due to the increased ROS generation as a consequence of SOD2 down-regulation (see also above) [96].

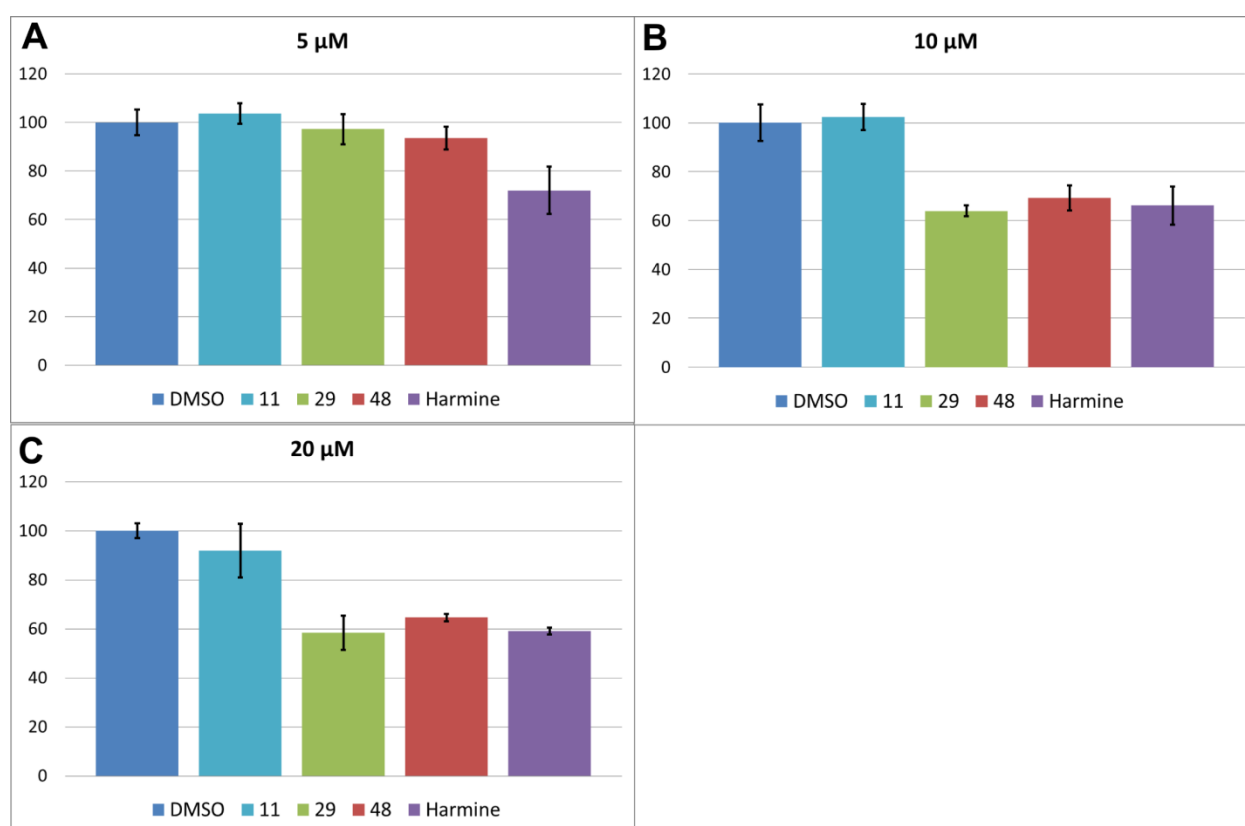


Figure 5: Influence of the Dyrk inhibitors **29** and **48** at three different concentrations (A-C) on the cell growth of V79 hamster lung fibroblasts in comparison to harmine. Compound **11** is of the same chemotype as **29** and **48** but was inactive with respect to Dyrk/Clk inhibition. Intracellular ATP levels were quantified as a measure for cell viability and proliferation rates. Results of one out of three independent experiments are presented, which all showed the same tendency. The standard deviation is indicated as y-error bars. Asterisks indicate statistical significance (p value < 0.05).

Binding model. To get a better insight in the binding mechanism of our compound class, we performed a multi-step *in silico* study employing local docking and molecular dynamics simulations with our lead compound **29**. The cocrystal structure of harmine and Dyrk1A was used as a template (PDB accession Code: 3ANR). The results were compared with the binding mode of harmine within the ATP pocket. As depicted in Figure 6, compound **29** is anchored between the conserved Lys188 and the hinge region residue Leu241 via two hydrogen bonds. In addition, we found two CH- π interactions involving Lys188 and Val306 and two edge-to-face CH- π interactions with the Phe238 benzene ring. Interestingly, **29** only takes advantage of the adenine and the phosphate binding regions, offering a high potential to expand the inhibitor to target additional areas within the ATP pocket. These further ligand modifications could enhance the potency but also the selectivity within the Dyrk family and against Clk1 if needed. The predicted binding pose for **29** also provided another potential explanation why the pyridine analogue of **29**, compound **4**, was considerably less active: for steric reasons, the larger pyridine ring is expected to prevent a similarly deep docking in the ATP pocket, thus impairing the CH- π interactions with the Phe238 benzene ring. The cocrystallized harmine exploits the same hydrogen bonds to Dyrk1A. However, we could detect only one CH- π interaction between Val306 and harmine (Figure 6C). These less extensive interactions with the aliphatic side chains and Phe238 are probably compensated by the energetically more favorable angles of the hydrogen bonds established by harmine. A second reason could be the higher hydrogen bond acceptor strength of 2-methylpyridine (pK_{BHX} : 2.03) compared to 1,3-thiazole (pK_{BHX} : 1.37), compensating for the fewer CH- π interactions [86].

Selectivity profile. During lead optimization, we routinely determined the inhibitory activity towards three Dyrk isoforms and against CK2 α as a primary counter screen. The latter kinase was not appreciably inhibited by any of the compounds. Further frequently reported off-targets for Dyrk inhibitors comprise Clks, PIM1, HIPK2 and PKD2 [56, 81, 82, 97]. Therefore, we tested the selectivity of our five most potent compounds especially against these kinases and in addition against further kinases representing each subfamily of the human kinome (Tables S3 and S4, and Figures S3 and S4, Supporting Information). Table S4 contains an extended kinase list to assess the selectivity of the most potent compounds **29** and **48**. As can be seen from Tables S3 and S4, no other kinase was inhibited to the same degree as the Dyrk kinases, with the exception of Clk1/4. This coupled inhibitory activity was consistent with former reports: all Dyrk1A and Dyrk1B inhibitors as published to date, and for which selectivity data were provided, also displayed Clk1 inhibition with similar potency, while other kinases were affected at variable degrees [17-20, 84, 98]. This was also true for harmine, which showed an IC_{50} for Clk1 of 0.2 μM (Table 9). Hence, our lead compounds were still among the most selective Dyrk inhibitors.

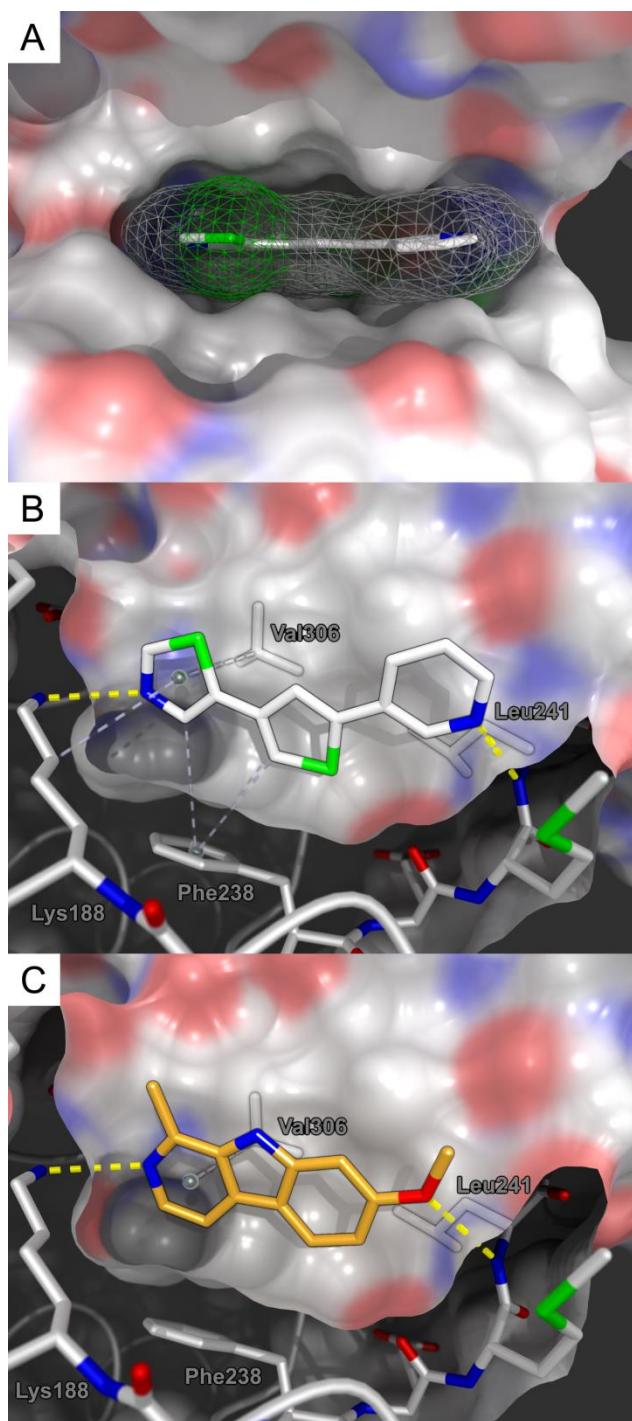


Figure 6: Predicted structure of the inhibitor-enzyme complex of 29 and Dyrk1A (A and B) in comparison with the corresponding cocrystal structure of harmine (C; PDB accession code: 3ANR). (A) Spatial orientation and space-filling (wireframe) of compound 29 within the ATP pocket of Dyrk1A. The compound adopts an approximately co-planar conformation with a good shape complementarity to the binding cleft. (B) Top view of the ATP pocket from the N-terminus. Compound 29 is anchored between Lys188 and Leu241 via two hydrogen bonds. Two CH- π interactions are formed with Val306 and a Lys188 methylene, respectively, and two with Phe238. (C) Binding mode of harmine within the ATP pocket. Harmine targets Lys188 and Leu241 via hydrogen bonds as well but establishes only one CH- π interaction in the crystal structure (with Val306). Blue: nitrogen, green: sulfur, red: oxygen, light grey: receptor carbon atoms, white: carbon atoms of 29, orange: carbon atoms of harmine, hydrogen is omitted for clarity. Receptor surface is cut in B and C.

In the case of compound **29**, the MAP kinase MNK1 was also markedly inhibited (83% at 5 μ M). Interestingly, this inhibitory activity was rather abolished in compound **48**, which differs from **29** only by the relative position of the thiophene sulfur. In the light of this rather unexpected finding, it might be worth investigating the role of the thiophene sulfur in the generation of inhibitory activity against MNK1, and also to screen our library to identify further potential inhibitors of MNK1 with reduced activity against Dyrks and Clks. MNK1 was validated as a potential target in glioblastoma by Brian Hemmings' group [99]. Since Dyrk1A was also proposed as a new target in EGFR-dependent glioblastoma [38], compound **29** might even be considered a new lead for the development of dual Dyrk1A/MNK1 inhibitors to defeat this aggressive subset of brain tumors. The next most strongly inhibited kinase in our panel was PIM1. The IC₅₀ values of **30**, **33** and **48** for PIM1 were all about 5 μ M, which was, e.g. in the case of compound **48**, 50 times higher than that for the Dyrk1B inhibition.

Altogether, the new inhibitors displayed a good selectivity for the Dyrk family of kinases, qualifying them as promising lead compounds.

Table 9: Potency of the dual Dyrk/Clk inhibitors 29, 30, 33, 41 and 48 against the target kinases.

Kinases		29	30	33	41	48	Harmine
Dyrk1A	IC ₅₀ [nM]	130	300	810	880	100	100
	% inhibition @ 5 μ M	90 %	99 %	84 %	85 %	97 %	98 %
Dyrk1B	IC ₅₀ [nM]	100	410	1000	1800	70	228
	% inhibition @ 5 μ M	100 %	100 %	83 %	70 %	100 %	98 %
Dyrk2	IC ₅₀ [nM]	430	190	1300	3400	40	3000
	% inhibition @ 5 μ M	93 %	100 %	77 %	57 %	100 %	68 %
Clk1	IC ₅₀ [nM]	130	160	420	610	110	220
	% inhibition @ 5 μ M	96 %	92 %	88 %	86 %	94 %	97 %

^aGiven are mean values of at least two independent experiments, S.D. < 10 %.

Relative potencies within the Dyrk/Clk target family. Among the most potent compounds **29** and **48**, **48** was slightly more active against Dyrk1B than against Clk1, while **29** was equally potent towards Dyrk1A, 1B and Clk1, but exhibited some selectivity against Dyrk2 (Table 9). However, in the case of **33**, Clk1 was the main target (though the potency was only moderate). A further extension of the 5-thiophenyl oxazole series, to which **33** belongs, might thus yield selective Clk1 inhibitors. In the larger selectivity screening, Clk4 was identified as an additional target within the Clk family (see Table S4 and below) whereas Clk2 and -3 were only slightly affected, if at all. Based on the high degree of identity between Clk1 and -4 (but not between Clk1 and Clk2/3), similar potencies of our compounds can be expected towards Clk1 and Clk4.

3.1.5 Conclusions

The novel kinase inhibitor class of 2,4-bisheterocyclic substituted thiophenes possesses a flexible scaffold, which allowed the independent optimization of both molecule ends using a large set of commercially available heterocyclic moieties, consisting of five- and six-membered rings and annelated ring systems. Automated parallel synthesis of several focused libraries of compounds accelerated the optimization of the potency and selectivity while increasing the ligand efficiency, thus resulting in lead-like molecules [100]. Our two most potent inhibitors, **29** and **48**, exhibited an activity towards Dyrk1A similar to that of the first-in-class inhibitor harmine (Table 9), however, at a somewhat reduced cytotoxic potential.

Within the tested panel of kinases, the inhibitors displayed a good selectivity for the ATP binding pockets of the Dyrk and Clk1/4 family. This was probably achieved by a combination of the following strategies: (i) Establishment of only one hydrogen bond each with the hinge region and the conserved lysine, respectively; thus, even small shifts in the optimum spatial arrangements of the donor moieties in the protein will result in a large drop of the binding affinity. (ii) Generation of the optimum shape and electrostatic complementarity by identifying the appropriate combination of azaheterocycles in our parallel synthesis campaign. Further fine-tuning of potency and selectivity was achieved by a simple change of the relative position of the thiophene sulfur. Both isomeric compounds **29** and **48** might serve as potential leads for the development of new anti-cancer therapeutics due to their inhibitory activity against Dyrk1A and -1B, which we also demonstrated in intact cells; **29** might offer an additional advantage in the case of glioblastoma, due to the simultaneous inhibition of Dyrk1A and Mnk1, which were both validated as new promising targets for this tumor entity [38, 99]. Furthermore, compound **24** was selective for Dyrk2 ($IC_{50} = 0.63 \mu M$)

among the three Dyrk family members tested. Thus, we anticipate that with our focused library approach, it might also be possible to generate inhibitors of the Dyrk3 and 4 isoforms as well, for which no chemical inhibitors have been reported yet, and no crystal structures are available. So far it is not clear whether selectivity against Clk1 can be achieved at all for ATP-competitive Dyrk inhibitors. However, the dual Dyrk1A/Clk1 inhibitory activity might even provide higher efficacy for the treatment of tauopathies, because both kinases are inducing alternative splicing to generate tau species with enhanced pathogenic potential.

ASSOCIATED CONTENT

Supporting Information

Synthetic procedures and analytical data of compounds **2, 3, 6, 7, 9-14, 16, 18, 21-24, 26-28, 31, 32, 34-40, 42-47** are given, the construction of the pET45b-Dyrk1A-cd expression plasmid is described, and supplementary Figures S1, S2, S3 and Tables S1, S2, S3, and S4 are shown.

AUTHOR INFORMATION

Corresponding Author

*Phone: +49 681 302 70312. Fax: +49 681 302 70308. E-mail: ma.engel@mx.uni-saarland.de.
Website: <http://www.pharmmedchem.de>.

Notes

The data presented herein are the result of a scientific collaboration with PharmBioTec GmbH, which is a Spin-Off company of the Saarland University. No commercial interest was involved. Therefore, this collaboration does not alter our adherence to all the PLOS ONE policies on sharing data and materials.

ACKNOWLEDGMENT

We thank the Deutsche Forschungsgemeinschaft (DFG) for financial support to M.E. (EN381/3-1). We are also grateful to Prof. Dr. Walter Becker (RWTH Aachen, Germany) for discussions and for

providing us with the expression plasmid for Dyrk2, and to Prof. Dr. Matthias Montenarh (Medical Biochemistry, University of Saarland, Homburg, Germany) for his gift of CK2 α .

3.1.6 References

1. Becker W, Weber Y, Wetzel K, Eirmbter K, Tejedor FJ, et al. (1998) Sequence characteristics, subcellular localization, and substrate specificity of DYRK-related kinases, a novel family of dual specificity protein kinases. *J Biol Chem* 273: 25893–25902.
2. Becker W, Joost HG (1999) Structural and functional characteristics of Dyrk, a novel subfamily of protein kinases with dual specificity. *Prog Nucleic Acid Res Mol Biol* 62: 1–17.
3. Woods YL, Cohen P, Becker W, Jakes R, Goedert M, et al. (2001) The kinase DYRK phosphorylates protein-synthesis initiation factor eIF2B ϵ at Ser539 and the microtubule-associated protein tau at Thr212 for DYRK as a glycogen synthase kinase 3-priming kinase. *Biochem J* 355: 609–615.
4. Ryoo S-RR, Jeong HK, Radnaabazar C, Yoo J-JJ, Cho H-JJ, et al. (2007) DYRK1A-mediated hyperphosphorylation of Tau. A functional link between Down syndrome and Alzheimer's Disease. *J Biol Chem* 282: 34850–34857.
5. Liu F, Liang Z, Wegiel J, Hwang Y-WW, Iqbal K, et al. (2008) Overexpression of Dyrk1A contributes to neurofibrillary degeneration in Down syndrome. *FASEB J* 22: 3224–3233.
6. Kurabayashi N, Hirota T, Sakai M, Sanada K, Fukada Y (2010) DYRK1A and glycogen synthase kinase 3 β , a dual-kinase mechanism directing proteasomal degradation of CRY2 for circadian timekeeping. *Mol Cell Biol* 30: 1757–1768.
7. Johnson G V, Stoothoff WH (2004) Tau phosphorylation in neuronal cell function and dysfunction. *J Cell Sci* 117: 5721–5729.
8. Steinhilb ML, Dias-Santagata D, Fulga TA, Felch DL, Feany MB (2007) Tau phosphorylation sites work in concert to promote neurotoxicity in vivo. *Mol Biol Cell* 18: 5060–5068.
9. Kimura R, Kamino K, Yamamoto M, Nuripa A, Kida T, et al. (2007) The DYRK1A gene, encoded in chromosome 21 Down syndrome critical region, bridges between beta-amyloid production and tau phosphorylation in Alzheimer's Disease. *Hum Mol Genet* 16: 15–23.
10. Wegiel JJ, Dowjat K, Kaczmarek W, Kuchna I, Nowicki K, et al. (2008) The role of overexpressed DYRK1A protein in the early onset of neurofibrillary degeneration in Down syndrome. *Acta Neuropathol* 116: 391–407.
11. Shi J, Zhang T, Zhou C, Chohan MO, Gu X, et al. (2008) Increased dosage of Dyrk1A alters alternative splicing factor (ASF)-regulated alternative splicing of tau in Down syndrome. *J Biol Chem* 283: 28660–28669.

12. De Graaf K, Czajkowska H, Rottmann S, Packman LC, Lilischkis R, et al. (2006) The protein kinase DYRK1A phosphorylates the splicing factor SF3b1/SAP155 at Thr434, a novel in vivo phosphorylation site. *BMC Biochem* 7: 7.
13. Álvarez M, Estivill X, de La Luna S (2003) DYRK1A accumulates in splicing speckles through a novel targeting signal and induces speckle disassembly. *J Cell Sci* 116: 3099–3107.
14. Yin X, Jin N, Gu J, Shi J, Zhou J, et al. (2012) Dual-specificity tyrosine phosphorylation-regulated kinase 1A (Dyrk1A) modulates serine/arginine-rich protein 55 (SRp55)-promoted Tau exon 10 inclusion. *J Biol Chem* 287: 30497–30506.
15. Wegiel J, Kaczmarek W, Barua M, Kuchna I, Nowicki K, et al. (2011) Link between DYRK1A overexpression and several-fold enhancement of neurofibrillary degeneration with 3-repeat tau protein in Down syndrome. *J Neuropathol Exp Neurol* 70: 36–50.
16. Hartmann a M, Rujescu D, Giannakouros T, Nikolakaki E, Goedert M, et al. (2001) Regulation of alternative splicing of human tau exon 10 by phosphorylation of splicing factors. *Mol Cell Neurosci* 18: 80–90.
17. Giraud F, Alves G, Debiton E, Nauton L, Théry V, et al. (2011) Synthesis, protein kinase inhibitory potencies, and in vitro antiproliferative activities of meridianin derivatives. *J Med Chem* 54: 4474–4489.
18. Rosenthal AS, Tanega C, Shen M, Mott BT, Bougie JM, et al. (2011) Potent and selective small molecule inhibitors of specific isoforms of Cdc2-like kinases (Clk) and dual specificity tyrosine-phosphorylation-regulated kinases (Dyrk). *Bioorg Med Chem Lett* 21: 3152–3158.
19. Mott BT, Tanega C, Shen M, Maloney DJ, Shinn P, et al. (2009) Evaluation of substituted 6-arylquinazolin-4-amines as potent and selective inhibitors of Cdc2-like kinases (Clk). *Bioorg Med Chem Lett* 19: 6700–6705.
20. Fedorov O, Huber K, Eisenreich A, Filippakopoulos P, King O, et al. (2011) Specific CLK inhibitors from a novel chemotype for regulation of alternative splicing. *Chem Biol* 18: 67–76.
21. Debdab M, Carreaux F, Renault S, Soundararajan M, Fedorov O, et al. (2011) Leucettines, a class of potent inhibitors of Cdc2-like kinases and dual specificity, tyrosine phosphorylation regulated kinases derived from the marine sponge leucettamine B: modulation of alternative pre-RNA splicing. *J Med Chem* 54: 4172–4186.
22. Mercer SE, Friedman E (2006) Mirk/Dyrk1B: a multifunctional dual-specificity kinase involved in growth arrest, differentiation, and cell survival. *Cell Biochem Biophys* 45: 303–315.
23. Friedman E (2007) Mirk/Dyrk1B in cancer. *J Cell Biochem* 102: 274–279.
24. Mercer SE, Ewton DZ, Deng X, Lim S, Mazur TR, et al. (2005) Mirk/Dyrk1B mediates survival during the differentiation of C2C12 myoblasts. *J Biol Chem* 280: 25788–25801.
25. Deng X, Ewton DZ, Pawlikowski B, Maimone M, Friedman E (2003) Mirk/dyrk1B is a Rho-induced kinase active in skeletal muscle differentiation. *J Biol Chem* 278: 41347–41354.

26. Jin K, Park S, Ewton DZ, Friedman E (2007) The survival kinase Mirk/Dyrk1B is a downstream effector of oncogenic K-ras in pancreatic cancer. *Cancer Res* 67: 7247–7255.
27. Deng X, Mercer SE, Shah S, Ewton DZ, Friedman E (2004) The cyclin-dependent kinase inhibitor p27Kip1 is stabilized in G(0) by Mirk/dyrk1B kinase. *J Biol Chem* 279: 22498–22504.
28. Vervoorts J, Luscher B (2008) Post-translational regulation of the tumor suppressor p27(KIP1). *Cell Mol Life Sci* 65: 3255–3264.
29. Zou Y, Ewton DZ, Deng X, Mercer SE, Friedman E (2004) Mirk/dyrk1B kinase destabilizes cyclin D1 by phosphorylation at threonine 288. *J Biol Chem* 279: 27790–27798.
30. Yabut O, Domogauer J, D’Arcangelo G (2010) Dyrk1A overexpression inhibits proliferation and induces premature neuronal differentiation of neural progenitor cells. *J Neurosci* 30: 4004–4014.
31. Becker W (2012) Emerging role of DYRK family protein kinases as regulators of protein stability in cell cycle control. *Cell Cycle* 11: 3389–3394.
32. Ewton DZ, Hu J, Vilenchik M, Deng X, Luk KC, et al. (2011) Inactivation of mirk/dyrk1b kinase targets quiescent pancreatic cancer cells. *Mol Cancer Ther* 10: 2104–2114.
33. Hu J, Nakhla H, Friedman E (2011) Transient arrest in a quiescent state allows ovarian cancer cells to survive suboptimal growth conditions and is mediated by both Mirk/dyrk1b and p130/RB2. *Int J Cancer* 129: 307–318.
34. Skurat A V, Dietrich AD (2004) Phosphorylation of Ser640 in muscle glycogen synthase by DYRK family protein kinases. *J Biol Chem* 279: 2490–2498.
35. Mazmanian G, Kovshilovsky M, Yen D, Mohanty A, Mohanty S, et al. (2010) The zebrafish dyrk1b gene is important for endoderm formation. *Genesis* 48: 20–30.
36. Miyata Y, Nishida E (2011) DYRK1A binds to an evolutionarily conserved WD40-repeat protein WDR68 and induces its nuclear translocation. *Biochim Biophys Acta* 1813: 1728–1739.
37. Chang HS, Lin CH, Yang CH, Yen MS, Lai CR, et al. (2007) Increased expression of Dyrk1a in HPV16 immortalized keratinocytes enable evasion of apoptosis. *Int J Cancer* 120: 2377–2385.
38. Pozo N, Zahonero C, Fernández P, Liñares JM, Ayuso A, et al. (2013) Inhibition of DYRK1A destabilizes EGFR and reduces EGFR-dependent glioblastoma growth. *J Clin Invest* 123: 2475–2487.
39. Miller CT, Aggarwal S, Lin TK, Dagenais SL, Contreras JI, et al. (2003) Amplification and overexpression of the dual-specificity tyrosine-(Y)-phosphorylation regulated kinase 2 (DYRK2) gene in esophageal and lung adenocarcinomas. *Cancer Res* 63: 4136–4143.
40. Koon N, Schneider-Stock R, Sarlomo-Rikala M, Lasota J, Smolkin M, et al. (2004) Molecular targets for tumour progression in gastrointestinal stromal tumours. *Gut* 53: 235–240.
41. Taira N, Mimoto R, Kurata M, Yamaguchi T, Kitagawa M, et al. (2012) DYRK2 priming phosphorylation of c-Jun and c-Myc modulates cell cycle progression in human cancer cells. *J Clin Invest* 122: 859–872.

42. Yamashita S, Chujo M, Moroga T, Anami K, Tokuishi K, et al. (2009) DYRK2 expression may be a predictive marker for chemotherapy in non-small cell lung cancer. *Anticancer Res* 29: 2753–2757.
43. Taira N, Nihira K, Yamaguchi T, Miki Y, Yoshida K (2007) DYRK2 is targeted to the nucleus and controls p53 via Ser46 phosphorylation in the apoptotic response to DNA damage. *Mol Cell* 25: 725–738.
44. Jung H-Y, Wang X, Jun S, Park J-I (2013) Dyrk2-associated EDD-DDB1-VprBP E3 ligase inhibits telomerase by TERT degradation. *J Biol Chem* 288: 7252–7262.
45. Geiger JN, Knudsen GT, Panek L, Pandit AK, Yoder MD, et al. (2001) mDYRK3 kinase is expressed selectively in late erythroid progenitor cells and attenuates colony-forming unit-erythroid development. *Blood* 97: 901–910.
46. Lord KA, Creasy CL, King AG, King C, Burns BM, et al. (2000) REDK, a novel human regulatory erythroid kinase. *Blood* 95: 2838–2846.
47. Rush J, Moritz A, Lee KA, Guo A, Goss VL, et al. (2005) Immunoaffinity profiling of tyrosine phosphorylation in cancer cells. *Nat Biotechnol* 23: 94–101.
48. Slepak TI, Salay LD, Lemmon VP, Bixby JL (2012) Dyrk kinases regulate phosphorylation of doublecortin, cytoskeletal organization, and neuronal morphology. *Cytoskelet* 69: 514–527.
49. Bain J, Plater L, Elliott M, Shpiro N, Hastie CJ, et al. (2007) The selectivity of protein kinase inhibitors: a further update. *Biochem J* 408: 297–315.
50. Kim H, Sablin SO, Ramsay RR (1997) Inhibition of monoamine oxidase A by beta-carboline derivatives. *Arch Biochem Biophys* 337: 137–142.
51. Miralles A, Esteban S, Sastre-Coll A, Moranta D, Asensio VJ, et al. (2005) High-affinity binding of beta-carbolines to imidazoline I2B receptors and MAO-A in rat tissues: norharman blocks the effect of morphine withdrawal on DOPA/noradrenaline synthesis in the brain. *Eur J Pharmacol* 518: 234–242.
52. Boeira JM, da Silva J, Erdtmann B, Henriques JA (2001) Genotoxic effects of the alkaloids harman and harmine assessed by comet assay and chromosome aberration test in mammalian cells in vitro. *Pharmacol Toxicol* 89: 287–294.
53. Boeira JM, Viana AF, Picada JN, Henriques JA (2002) Genotoxic and recombinogenic activities of the two beta-carboline alkaloids harman and harmine in *Saccharomyces cerevisiae*. *Mutat Res* 500: 39–48.
54. Jimenez J, Riveron-Negrete L, Abdullaev F, Espinosa-Aguirre J, Rodriguez-Arnaiz R (2008) Cytotoxicity of the beta-carboline alkaloids harmine and harmaline in human cell assays in vitro. *Exp Toxicol Pathol* 60: 381–389.
55. Pin F, Buron F, Saab F, Colliandre L, Bourg S, et al. (2011) Synthesis and biological evaluation of 2,3-bis(het)aryl-4-azaindole derivatives as protein kinase inhibitors. *MedChemComm* 2: 899–903.

56. Tahtouh T, Elkins JM, Filippakopoulos P, Soundararajan M, Burgy G, et al. (2012) Selectivity, Cocrystal Structures, and Neuroprotective Properties of Leucettines, a Family of Protein Kinase Inhibitors Derived from the Marine Sponge Alkaloid Leucettamine B. *J Med Chem* 55: 9312–9330.
57. Akue-Gedu R, Debiton E, Ferandin Y, Meijer L, Prudhomme M, et al. (2009) Synthesis and biological activities of aminopyrimidyl-indoles structurally related to meridianins. *Bioorg Med Chem* 17: 4420–4424.
58. Koo KA, Kim ND, Chon YS, Jung M-SS, Lee B-JJ, et al. (2009) QSAR analysis of pyrazolidine-3,5-diones derivatives as Dyrk1A inhibitors. *Bioorg Med Chem Lett* 19: 2324–2328.
59. Loidreau Y, Marchand P, Dubouilh-Benard C, Nourrisson MR, Duflos M, et al. (2012) Synthesis and biological evaluation of N-arylbenzo[b]thieno[3,2-d]pyrimidin-4-amines and their pyrido and pyrazino analogues as Ser/Thr kinase inhibitors. *Eur J Med Chem* 58C: 171–183.
60. Debray J, Bonte S, Lozach O, Meijer L, Demeunynck M (2012) Catalyst-free synthesis of quinazolin-4-ones from (hetero)aryl-guanidines: application to the synthesis of pyrazolo[4,3-f]quinazolin-9-ones, a new family of DYRK1A inhibitors. *Mol Divers* 16: 659–667.
61. Anderson K, Chen Y, Chen Z, Dominique R, Glenn K, et al. (2013) Pyrido[2,3-d]pyrimidines: Discovery and preliminary SAR of a novel series of DYRK1B and DYRK1A inhibitors. *Bioorg Med Chem Lett* 23: 6610–6615.
62. Cuny GD, Robin M, Ulyanova NP, Patnaik D, Pique V, et al. (2010) Structure-activity relationship study of acridine analogs as haspin and DYRK2 kinase inhibitors. *Bioorg Med Chem Lett* 20: 3491–3494.
63. Fröhner W, Lopez-Garcia L a, Neimanis S, Weber N, Navratil J, et al. (2011) 4-benzimidazolyl-3-phenylbutanoic acids as novel PIF-pocket-targeting allosteric inhibitors of protein kinase PKC ζ . *J Med Chem* 54: 6714–6723.
64. Hoppstädter J, Diesel B, Eifler LK, Schmid T, Brüne B, et al. (2012) Glucocorticoid-induced leucine zipper is downregulated in human alveolar macrophages upon Toll-like receptor activation. *Eur J Immunol* 42: 1282–1293.
65. Du C, Huang T, Sun D, Mo Y, Feng H, et al. (2011) CDH4 as a novel putative tumor suppressor gene epigenetically silenced by promoter hypermethylation in nasopharyngeal carcinoma. *Cancer Lett* 309: 54–61.
66. Urbich C, Rössig L, Kaluza D, Potente M, Boeckel J-N, et al. (2009) HDAC5 is a repressor of angiogenesis and determines the angiogenic gene expression pattern of endothelial cells. *Blood* 113: 5669–5679.
67. Spandidos A, Wang X, Wang H, Seed B (2010) PrimerBank: a resource of human and mouse PCR primer pairs for gene expression detection and quantification. *Nucleic Acids Res* 38: D792–D799.
68. Yara S, Lavoie J-C, Beaulieu J-F, Delvin E, Amre D, et al. (2013) Iron-ascorbate-mediated lipid peroxidation causes epigenetic changes in the antioxidant defense in intestinal epithelial cells: impact on inflammation. *PLoS One* 8: e63456.

69. Wang K-K, Liu N, Radulovich N, Wigle D a, Johnston MR, et al. (2002) Novel candidate tumor marker genes for lung adenocarcinoma. *Oncogene* 21: 7598–7604.
70. Bey E, Marchais-Oberwinkler S, Werth R, Negri M, Al-Soud YA, et al. (2008) Design, synthesis, biological evaluation and pharmacokinetics of bis(hydroxyphenyl) substituted azoles, thiophenes, benzenes, and aza-benzenes as potent and selective nonsteroidal inhibitors of 17beta-hydroxysteroid dehydrogenase type 1 (17beta-HSD1). *J Med Chem* 51: 6725–6739.
71. Obach RS (1999) Prediction of human clearance of twenty-nine drugs from hepatic microsomal intrinsic clearance data: An examination of in vitro half-life approach and nonspecific binding to microsomes. *Drug Metab Dispos* 27: 1350–1359.
72. Kato R, Gillette J (1965) Effect of Starvation on NADPH-Dependant Enzymes in Liver Microsomes of Male and Female Rats. *J Pharmacol Exp Ther* 150: 279–284.
73. Davies B, Morris T (1993) Physiological parameters in laboratory animals and humans. *Pharm Res* 10: 1093–1095.
74. Duan Y, Wu C, Chowdhury S, Lee MC, Xiong G, et al. (2003) A Point-Charge Force Field for Molecular Mechanics Simulations of Proteins Based on Condensed-Phase. *J Comput Chem* 24: 1999–2012.
75. Krieger E, Darden T, Nabuurs SB, Finkelstein A, Vriend G (2004) Making optimal use of empirical energy functions: force-field parameterization in crystal space. *Proteins* 57: 678–683.
76. Avrutina O, Fittler H, Glotzbach B, Kolmar H, Empting M (2012) Between two worlds: a comparative study on in vitro and in silico inhibition of trypsin and matriptase by redox-stable SFTI-1 variants at near physiological pH. *Org Biomol Chem* 10: 7753–7762.
77. Morris GM, Goodsell DS, Halliday RS, Huey R, Hart WE, et al. (1998) Automated Docking Using a Lamarckian Genetic Algorithm and an Empirical Binding Free Energy Function. *J Comput Chem* 19: 1639–1662.
78. Besselièvre F, Mahuteau-Betzer F, Grierson DS, Piguel S (2008) Ligandless Microwave-Assisted Pd/Cu-Catalyzed Direct Arylation of Oxazoles. *J Org chem* 73: 3278–3280.
79. Dondoni A, Fantin G, Fogagnolo M, Medici A (1988) Synthesis of (Trimethylsilyl)thiazoles and Reactions with Carbonyl Compounds. Selectivity Aspects and Synthetic Utility'. *J Org Chem* 3: 1748–1761.
80. Primas N, Bouillon A, Lancelot J-C, El-Kashef H, Rault S (2009) Synthesis of 5-arylthiazoles. Comparative study between Suzuki cross-coupling reaction and direct arylation. *Tetrahedron* 65: 5739–5746.
81. Bain J, McLauchlan H, Elliott M, Cohen P (2003) The specificities of protein kinase inhibitors: an update. *Biochem J* 371: 199–204.
82. Anastassiadis T, Deacon SW, Devarajan K, Ma H, Peterson JR (2011) Comprehensive assay of kinase catalytic activity reveals features of kinase inhibitor selectivity. *Nat Biotechnol* 29: 1039–1045.

83. Wager TT, Chandrasekaran RY, Hou X, Troutman MD, Verhoest PR, et al. (2010) Defining Desirable Central Nervous System Drug Space through the Alignment of Molecular Properties, in Vitro ADME, and Safety Attributes. *ACS Chem Neurosci* 1: 420–434.
84. Ogawa Y, Nonaka Y, Goto T, Ohnishi E, Hiramatsu T, et al. (2010) Development of a novel selective inhibitor of the Down syndrome-related kinase Dyrk1A. *Nat Comm* 1: 86.
85. Miyaura N, Yanagi T, Suzuki A (1981) The Palladium-Catalyzed Cross-Coupling Reaction of Phenylboronic Acid with Haloarenes in the Presence of Bases. *Synth Comm* 11: 513–519.
86. Laurence C, Brameld K a, Graton J, Le Questel J-Y, Renault E (2009) The pK(BHX) database: toward a better understanding of hydrogen-bond basicity for medicinal chemists. *J Med Chem* 52: 4073–4086.
87. Bird CW (1992) Heteroaromaticity, 5, a unified aromaticity index. *Tetrahedron* 48: 335–340.
88. Ertl P, Rohde B, Selzer P (2000) Fast calculation of molecular polar surface area as a sum of fragment-based contributions and its application to the prediction of drug transport properties. *J Med Chem* 43: 3714–3717.
89. Yang C, Ji D, Weinstein EJ, Choy E, Hornicek FJ, et al. (2010) The kinase Mirk is a potential therapeutic target in osteosarcoma. *Carcinogenesis* 31: 552–558.
90. Deng X, Ewton DZ, Friedman E (2009) Mirk/Dyrk1B maintains the viability of quiescent pancreatic cancer cells by reducing levels of reactive oxygen species. *Cancer Res* 69: 3317–3324.
91. Rothe G, Valet G (1990) Flow cytometric analysis of respiratory burst activity in phagocytes with hydroethidine and 2',7'-dichlorofluorescein. *J Leukoc Biol* 47: 440–448.
92. Deng X, Ewton DZ, Li S, Naqvi A, Mercer SE, et al. (2006) The kinase Mirk/Dyrk1B mediates cell survival in pancreatic ductal adenocarcinoma. *Cancer Res* 66: 4149–4158.
93. Deng X, Ewton DZ, Mercer SE, Friedman E (2005) Mirk/dyrk1B decreases the nuclear accumulation of class II histone deacetylases during skeletal muscle differentiation. *J Biol Chem* 280: 4894–4905.
94. Gao J, Yang X, Yin P, Hu W, Liao H, et al. (2012) The involvement of FoxO in cell survival and chemosensitivity mediated by Mirk/Dyrk1B in ovarian cancer. *Int J Oncol* 40: 1203–1209.
95. Bartholome A, Kampkötter A, Tanner S, Sies H, Klotz L-O (2010) Epigallocatechin gallate-induced modulation of FoxO signaling in mammalian cells and *C. elegans*: FoxO stimulation is masked via PI3K/Akt activation by hydrogen peroxide formed in cell culture. *Arch Biochem Biophys* 501: 58–64.
96. Melov S, Coskun P, Patel M, Tuinstra R, Cottrell B, et al. (1999) Mitochondrial disease in superoxide dismutase 2 mutant mice. *PNAS* 96: 846–851.
97. Pagano MA, Bain J, Kazimierczuk Z, Sarno S, Ruzzene M, et al. (2008) The selectivity of inhibitors of protein kinase CK2: an update. *Biochem J* 415: 353–365.

98. Wang D, Wang F, Tan Y, Dong L, Chen L, et al. (2012) Discovery of potent small molecule inhibitors of DYRK1A by structure-based virtual screening and bioassay. *Bioorg Med chem Lett* 22: 168–171.
99. Grzmil M, Morin P, Lino MM, Merlo A, Frank S, et al. (2011) MAP kinase-interacting kinase 1 regulates SMAD2-dependent TGF- β signaling pathway in human glioblastoma. *Cancer Res* 71: 2392–2402.
100. Teague S, Davis A, Leeson P, Oprea T (1999) The Design of Leadlike Combinatorial Libraries. *Angew Chem (Int Ed)* 38: 3743–3748.

3.2 Dual Clk1/Dyrk1A inhibition is required for efficient mRNA splicing manipulation. Discovery of a new inhibitor scaffold.

Christian Schmitt, Parisa Miralinaghi, Marica Mariano, Rolf W. Hartmann and Matthias Engel

The manuscript was submitted to *ACS Medicinal Chemistry Letters* and is in the revision process

Publication B

3.2.1 Abstract

ABSTRACT: Alternative splicing allows cells to produce isoforms of a specific protein which originates from the same gene. Serine- and arginine-rich proteins control the mechanisms of alternative splicing and are therefore modulated by the action of different protein kinases including Clk1 and Dyrk1A. Activation of splicing factors through aberrant action of Clk1 and Dyrk1A are suspected to result in an imbalance of specific protein isoforms. Within this study we describe the development of a new selective dual Clk1 and Dyrk1A inhibitor which was able to manipulate the alternative splicing of selected genes in cells with submicromolar potencies. The thorough optimization of the hit compound yielded in an exceptional small molecule inhibitor providing excellent ligand efficiency. Furthermore, our results suggested that dual inhibition of Clk1 and Dyrk1A significantly increased the mRNA splicing manipulation compared to inhibition of Clk1 alone.

3.2.2 Results

The cdc2-like kinase 1 (Clk1) and the dual specificity tyrosine-phosphorylation-regulated kinase 1A (Dyrk1A) are serine/threonine protein kinases belonging to the CMGC group of kinases. Both kinases were identified to induce alternative splicing by phosphorylation of several serine- and arginine-rich (SR) splicing proteins.¹⁻⁵ Alternative splicing expands the mRNA diversity leading to protein isoform expression. In addition, alternative splicing is also a mechanism to alter the binding behavior between proteins and regulates their localization and enzymatic activity.⁶ There is a growing evidence that deregulated mRNA splicing is implicated in the outcome and progression of numerous diseases including neurodegeneration, cancer, and HIV.⁷⁻⁹ Dyrk1A, which is 1.5 fold overexpressed in Down syndrome (DS) brain promotes aberrant tau pre-mRNA splicing and hyperphosphorylation of tau protein leading to the formation of neurotoxic neurofibrillary tangles.^{10,11} The specific role of Clk1 in neurodegenerative diseases is not clear so far. Indeed, overlapping specificity for the splicing factors AF2/ASF, SC35, and SRp55 which are involved in tau splicing has been reported.^{3,5,12} Clk1 seems to be also involved in cell migration and invasion of ovarian cancer cells by

phosphorylation of the alternative splicing factor SPF45.¹³ There is a growing interest to generate specific splicing modulators aiming to recover normal transcription in some diseases. In order to achieve this goal, splice sites can be targeted by antisense oligonucleotides or by modifying splicing signal nodes using small molecules. Especially small molecules are more suitable for the treatment of central nervous system disorders, where oligonucleotides have rather limited applicability. Dual inhibition of the structural highly similar kinases Clk1 and Dyrk1A may have a therapeutic utility for treatment of tauopathies, inter alia due to imbalanced 3R/4R tau ratio caused by impaired splicing events.^{5,10} Several published kinase inhibitors, including harmine and TG003 were dual Clk1 and Dyrk1A inhibitors (Figure 1).^{14–22}

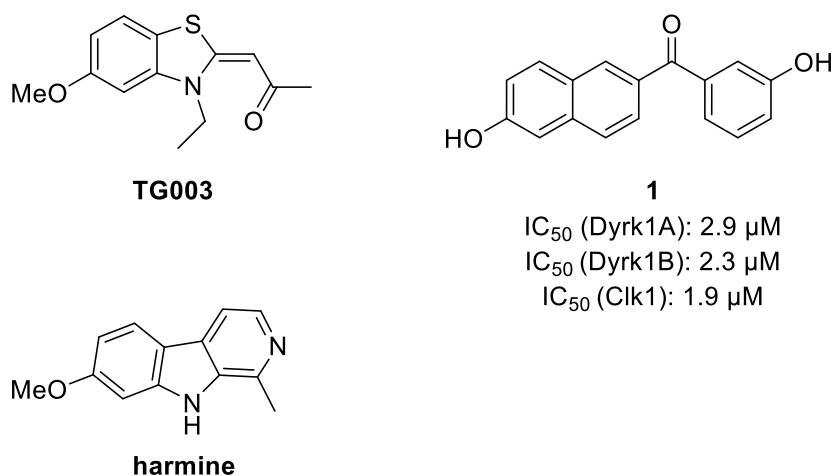


Figure 1: Reported Clk1 and Dyrk1A inhibitors and the newly identified dual Clk/Dyrk inhibitor **1**.

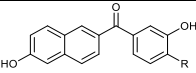
TG003 was initially described as potent Clk1 inhibitor which modified splicing of SC35 and Clk/Sty gene transcripts in cells.²⁰

Herein we describe the discovery of a new class of potent and selective dual Clk and Dyrk1A/1B inhibitors. Additionally, we provide evidence that dual inhibition of Clk1 and Dyrk1A increased the transcription of alternative spliced pre-mRNA of selected genes cells more efficiently than Clk1 inhibition alone.

Screening of our in-house collection of diverse enzyme inhibitors revealed a 6-hydroxynaphthalene ketone **1** (Figure 1) as a moderate Dyrk1A and Clk1 inhibitor. Importantly, **1** did not affect Dyrk2, which functions as a negative regulator of cell proliferation *in vitro* and suppressor of tumor progression *in vivo*.²³ Thus, prompted by the good selectivity against this “untouchable” Dyrk

isoform, we decided to optimize the naphthalene based inhibitors **1-3** in terms of potency and selectivity (Table 1). Therefore, the less drug-like naphthalene core was bioisosterically replaced with benzothiophene, benzofuran and indole, considering in each case the two possible hydroxyl positions (Tables 2 and 3). The 6-hydroxyl-substituted compounds **4** to **9** (Table 2) exhibited no improvement of potency or selectivity compared to the naphthalene-based inhibitors. Interestingly though, the activity of **4** towards the target kinases was increased by tenfold by swapping the hydroxyl group from the 6- to the 5-position on the benzothiophene core yielding **10** (Table 3). Inhibition of Clk1 was slightly preferred, displaying an IC₅₀ of about 100 nM. Since such beneficial effect was not observed for any of the benzofuran- and indole-based analogues (**11**, **12**, **13**, **15**), further optimization efforts focused on the 5-hydroxy-benzothiophene ketones. To explore the effect of the phenyl ring substitution pattern, the 3-hydroxyl group was moved to the *para*-position in **14**, which significantly decreased the Dyrk1A inhibition by about tenfold; however, the Clk1 inhibitory potency was less affected.

Table1: Inhibitory potency of naphthalene-based inhibitors

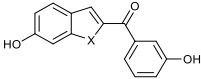
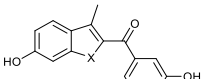
						
Compound	R	IC ₅₀ [μM]/ % inhibition @ 5μM ^a				
		Dyrk1A	Dyrk1B	Dyrk2	Clk1	Ck2α
1	H	2.9	2.3	30 %	1.9	19 %
2	Me	2.9	3.1	23 %	1	11 %
3	F	7.6	0.9	17 %	1	14 %

^a[ATP] = 100 μM

Introduction of an additional *para*-methyl group (**16**) doubled the potency towards Dyrk1A and Clk1 compared with **10**. While **16** was the most potent compound of this series, its isomer **17** was considerably less potent, even less than **14**, suggesting a steric clash of the *meta*-methyl group with the ATP binding pocket. Interestingly, the introduction of fluorine in the phenyl moiety (**18**) dramatically increased the selectivity for Clk1 (IC₅₀ = 50 nM) over Dyrk1A (IC₅₀ = 2.0 μM), suggesting a favorable interaction of the fluorine with the Clk1 but not the Dyrk1A binding pocket. Alternatively, conformational constraints effected by the *ortho*-substitution might produce a better shape complementarity to the Clk1 binding site. A comparison of **21** and **22** with **10** revealed that the

hydroxyl group at the benzo-thiophene but not at the phenyl moiety was essential to the inhibitory activity.

Table 2: Inhibitory potencies of 6-hydroxybenzoheterocyclic inhibitors

						
Compound	X	IC ₅₀ [μM]]/ % inhibition @5μM ^a				
		Dyrk1A	Dyrk1B	Dyrk2	Clk1	Ck2α
4	S	4.5	4	49 %	1	15 %
5	O	2.4	3.8	34 %	1.4	16 %
6	NH	20	45 %	15 %	54 %	24 %
7	NMe	36	-	24 %	35 %	8 %
						
		Dyrk1A	Dyrk1B	Dyrk2	Clk1	Ck2α
		8	S	1.3	1.6	51 %
9	O	2.3	2.8	39 %	1.4	34 %

^a[ATP] = 100 μM

The present data suggest that the 3-hydroxyl function at the phenyl did not essentially contribute to the binding affinity. Indeed, compound **23**, in which the phenyl ring was replaced by methyl exhibited the highest inhibitory potency besides of **16**. This finding provided evidence that the phenyl ring might even impede an optimum protein-ligand interaction. Therefore smaller aliphatic moieties instead of the aryl systems might be alternatives for structural extensions to get new more active and selective inhibitors. Bearing in mind its low molecular mass (192.2 g/mol), **23** probably represented an optimal ligand for the ATP binding pockets of Dyrk1A and Clk1, as indicated by its exceptionally high ligand efficiency of 0.74. The Weinreb amide **25**, also lacking the phenol ring, turned out to be nearly as potent against Clk1 as **23**, but was considerably less active against Dyrk1A and Dyrk1B. **25** was thus identified as a potential new lead for the development of selective Clk1 inhibitors.

Table 3: Inhibitory potencies of 5-hydroxybenzoheterocyclic inhibitors

Compound	X	R ₁	R ₂	R ₃	IC ₅₀ [μM]]/ % inhibition @5μM				
					Dyrk1A	Dyrk1B	Dyrk2	Clk1	Ck2α
10	S	OH	H	H	0.4	0.2	49 %	0.1	12 %
11	O	OH	H	H	3.1	6.1	34 %	1.9	21 %
12	NH	OH	H	H	15	41 %	24 %	2	22 %
13	NMe	OH	H	H	3.4	2.7	25 %	2.1	31 %
14	S	H	OH	H	3.4	0.8	25 %	0.3	33 %
15	O	H	OH	H	9.7	1.3	38 %	1.5	17 %
16	S	OH	Me	H	0.2	0.2	50 %	0.05	10 %
17	S	Me	OH	H	11	7	8 %	25 %	-
18	S	OH	H	F	2	0.4	30 %	0.05	20 %
19	S	OH	F	H	1.2	0.4	27 %	0.3	15 %
20	S	CN	H	H	6	2.3	6 %	0.4	10 %
21	S	H	H	H	2	1	37 %	0.2	13 %
22	S	-	-	-	42	6 %	15 %	-	24 %
23	S	-	-	-	0.2	0.1	46 %	0.06	9 %
24	S	-	-	-	10 %	40 %	-7 %	47 %	-
25	S	-	-	-	0.9	1.6	41 %	0.1	-
TG003					0.83	-	-	0.17	-

^a[ATP] = 100 μM

A 6-hydroxybenzothiazole isomer of **10** had been previously described as a highly potent inhibitor of 17β-hydroxysteroid dehydrogenase type 1 (17β-HSD1).²⁴ Therefore, we tested our structurally similar benzothiophene-based inhibitors for this potential off-target activity. Indeed, several compounds were identified as potent 17β-HSD1 inhibitors. However, although **16** turned out to be a 17β-HSD1 inhibitor (IC₅₀ = 195 nM), **23** and **25** were completely inactive towards this enzyme (Table

S2, Supporting Information), thus excluding side effects on the steroidal biosynthesis by our most active compound **23**.

TG003 which is a dual Clk1/Dyrk1A inhibitor was previously described as mRNA splicing modifier.²⁰ As mentioned before, the target-oriented modification of splicing could be a promising approach for the treatment of severe disorders like Alzheimer's disease, where an appropriate therapy is not yet available. We expected good cellular activity of **16** and **23** due to their good inhibitory potency within our cell free kinase assay even at 100 μ M ATP which was significantly above the reported K_M values of the target kinases Dyrk1A (Table S3). Therefore we developed a qPCR assay to evaluate the cellular potencies of our best compounds to manipulate splicing of selected genes. It was of further interest to compare the efficiencies of our dual Clk1/Dyrk1A inhibitors with a more Clk1 selective inhibitor. Initially, **16** and **18**, **23**, and the reference compound TG003 were incubated with a model cell line, immortal embryonic fibroblasts (STO), which had been previously employed to demonstrate the effects of the reference compound TG003 on mRNA splicing. The influence of the compounds on Clk1/Sty and SC35 mRNA splicing by Clk1 and Dyrk1A inhibition was first assessed by RT-PCR. The dual inhibitors **16**, **23**, and TG003 but not the Clk1 inhibitor **18** increased the production of the larger 274 bp Clk/Sty transcript coding for the catalytically active full-length Clk1.¹ The production of the shorter transcript (183 bp) coding for the truncated form of Clk1 decreased after inhibition of Clk1 and Dyrk1A (Figure S1 A, supporting information). In addition, the dual kinase inhibitors **16**, **23**, and TG003 slightly decreased the 668 bp transcript of SC35 (Figure S1 B, supporting information). These observations were in accordance to the published results for TG003.²⁰ Considering the low potency of **18** against Dyrk1A while the Clk1 inhibitory activity was fully retained, this result gave the first hint that inhibition of Clk1 alone was much less effective in splicing modification of Clk/Sty and SC35 pre-mRNA. However, the effect of **16** and **23** on Clk/Sty splicing was more pronounced obviously than for SC35 splicing (Figure S1, supporting information). Therefore we decided to use only the Clk/Sty pre-mRNA in a qPCR experiment to quantify the cellular potencies of **16**, **23**, and **25** to inhibit Clk1 and Dyrk1A. **25** was chosen due to its dual kinase inhibitory potency comparable to TG003 which was used as reference in the assay (Table 4). **23** triggered a significant response of the Clk1-pre-mRNA splicing already at sub-micromolar concentrations ($C_{5\text{-fold}} = 1.1 \mu\text{M}$), followed by **16**. In particular, both compounds, being efficient dual Dyrk1A/Clk1 inhibitors, were more potent than the amide analogue **25**, which was equally active against Clk1 but not against Dyrk1A in the cell free assay (Table 3). Assuming that there were no major differences in cell permeation between the compounds, these data suggested an additive effect of simultaneous Dyrk1A and Clk1 inhibition on the modulation of alternative splicing of the Clk1 pre-mRNA. In support of this presumption, significantly higher concentrations of

TG003 than of **16** or **23** were needed to elicit a clear response, correlating with the less potent inhibition of Dyrk1A ($IC_{50} = 830$ nM, cf. Table 3). Interestingly, the maximum achievable induction of Clk1 pre-mRNA splicing was a compound-specific variable; hence the calculated EC_{50} values appeared to be of limited significance.

Table 4. Induction of Clk/Sty mRNA alternative splicing triggered by 16, 23, and 25 in comparison to TG003.

	TG003	23	16	25
$C_{5\text{-fold}}$ (μM) ^a	3.1	1.1	1.9	2.4
EC_{50} (μM) ^b	6.6	8.9	1.8	2.1
max. induction ^c	17	21.4	9.5	8.1

^a concentration required to induce a 5-fold increase of the alternative Clk1 transcript levels as determined by qPCR, S.D. \leq 10%; ^b concentration required for half-maximal induction of the alternative Clk1 mRNA splicing, S.D. \leq 10%; ^c maximum increase of alternative Clk1 transcripts achievable with the inhibitors (fold increase over DMSO-treated samples), S.D. $<$ 20%. Shown are means of three independent experiments performed in triplicates.

TG003 and the Clk1 inhibitor KH-CB19 were previously described to block the phosphorylation of several splicing factors mediated by Clk1, including SRp75, SRp55, SF2/ASF, and SC35.¹⁵ It is therefore reasonable to expect that **16** and **23** have not only an effect on the splicing of the mRNAs examined within this study but influence some additional splicing factors mentioned before by blocking their Clk1 and Dyrk1A mediated phosphorylation. **16** and **23** showed good selectivity for the Clks and Dyrks in a panel comprising of 31 kinases covering all kinase groups of the kinome. The kinases were carefully selected and contained all reported off-targets for Clk1 and Dyrk1A inhibitors. **23** was slightly less selective than **16** (Tables S3 and S4) owning a similar inhibitory potency among the closely related cdc2-like kinases Clk1-4 and a moderate potency against the atypical kinase haspin (Table S5). Haspin was reported to be also affected by Clk1 and Dyrk inhibitors.²⁵ The selectivity of **16** and **23** to manipulate the splicing of the selected genes was not examined within this study. Therefore it might be possible that the new kinase inhibitor scaffold is able to influence the Clk1 and Dyrk1A mediated splicing of other genes. To identify one of them might be in the scope of future studies.

In conclusion, we developed a new dual inhibitor of Clks and Dyrks with exceptionally high ligand efficiency and notable cellular efficacy. In comparison to the first reported dual Clk1 and Dyrk1A inhibitor TG003, **16** and **23** were more efficient to manipulate splicing of the Clk/Sty and SC35 pre-mRNA transcripts indicating that potent dual inhibition of Clk1 and Dyrk1A results in an intensified splicing modulation. Given the good cellular potencies, especially with **23** we provide a tool to further explore mRNA splicing events that are controlled by Clk1 and Dyrk1A.

The new compound class might be a useful tool to further explore the specific roles of Clk1 and Dyrk1A mediated splicing with regard to the development of several pathologies caused by an imbalance of particular mRNAs. Due to the low molecular weight and the good aqueous solubility **23** offers the opportunity to further optimize the potency as well as the selectivity for the target kinases. The elimination of the unwanted 17 β -HSD1 inhibition could also be realized in compound **23**.

AUTHOR INFORMATION

Corresponding Authors

*M. E.: E-mail: ma.engel@mx.uni-saarland.de; phone: +4968130270312.

Author Contributions

C.S, P.M., M.M., and M.E. designed and performed research. The manuscript was written through contributions of all authors. / All authors have given approval to the final version of the manuscript.

Funding Sources

We are grateful for the financial support by the DFG to M.E. (EN 381/3-1).

ACKNOWLEDGMENT

The authors thank Mrs. Nadja Weber and Tamara Paul for their assistance in performing alternative splicing assays.

ASSOCIATED CONTENT

Supporting Information. Experimental details for all assays and syntheses, supplementary Tables S1–S4 and Figure S1. This material is available free of charge via the Internet at <http://pubs.acs.org>.

ABBREVIATIONS

CMGC, cyclin-dependent kinases, mitogen-activated protein kinases, glycogen-synthase kinases, and CDC-like kinases; SR proteins, serine- and arginine-rich family of splicing proteins; qPCR, real time PCR

3.2.3 References

- (1) Duncan, P. I.; Stojdl, D. F.; Marius, R. M.; Bell, J. C. In vivo regulation of alternative pre-mRNA splicing by the Clk1 protein kinase. *Mol cell biol* **1997**, *17*, 5996–6001.
- (2) Nowak, D. G.; Woolard, J.; Amin, E. M.; Konopatskaya, O.; Saleem, M. A.; Churchill, A. J.; Ladomery, M. R.; Harper, S. J.; Bates, D. O. Expression of pro- and anti-angiogenic isoforms of VEGF is differentially regulated by splicing and growth factors. *J. Cell Sci.* **2008**, *121*, 3487–3495.
- (3) Qian, W.; Liang, H.; Shi, J.; Jin, N.; Grundke-Iqbal, I.; Iqbal, K.; Gong, C.-X.; Liu, F. Regulation of the alternative splicing of tau exon 10 by SC35 and Dyrk1A. *Nucleic Acids Res.* **2011**, *39*, 6161–6171.
- (4) Ding, S.; Shi, J.; Qian, W.; Iqbal, K.; Grundke-Iqbal, I.; Gong, C.-X.; Liu, F. Regulation of alternative splicing of tau exon 10 by 9G8 and Dyrk1A. *Neurobiol. Aging* **2012**, *33*, 1389–1399.
- (5) Yin, X.; Jin, N.; Gu, J.; Shi, J.; Zhou, J.; Gong, C.-X.; Iqbal, K.; Grundke-Iqbal, I.; Liu, F. Dual-specificity tyrosine phosphorylation-regulated kinase 1A (Dyrk1A) modulates serine/arginine-rich protein 55 (SRp55)-promoted Tau exon 10 inclusion. *J Biol Chem* **2012**, *287*, 30497–30506.
- (6) Kelemen, O.; Convertini, P.; Zhang, Z.; Wen, Y.; Shen, M.; Falaleeva, M.; Stamm, S. Function of alternative splicing. *Gene* **2013**, *514*, 1–30.
- (7) Garcia-Blanco, M. a; Baraniak, A. P.; Lasda, E. L. Alternative splicing in disease and therapy. *Nat. biotechnol.* **2004**, *22*, 535–546.
- (8) Ward, A. J.; Cooper, T. A. The pathobiology of splicing. *J. Pathol.* **2010**, *220*, 152–163.
- (9) Wong, R.; Balachandran, A.; Mao, A.; Dobson, W.; Gray-Owen, S.; Cochrane, A. Differential effect of CLK SR Kinases on HIV-1 gene expression: potential novel targets for therapy. *Retrovirology* **2011**, *8*, 47.
- (10) Wegiel, J.; Kaczmarek, W.; Barua, M.; Kuchna, I.; Nowicki, K.; Wang, K.-C.; Wegiel, J.; Yang, S. M.; Frackowiak, J.; Mazur-Kolecka, B.; Silverman, W. P.; Reisberg, B.; Monteiro, I.; de Leon, M.; Wisniewski, T.; Dalton, A.; Lai, F.; Hwang, Y.-W.; Adayev, T.; Liu, F.; Iqbal, K.; Iqbal, I.-G.; Gong, C.-X. Link between DYRK1A overexpression and several-fold enhancement of neurofibrillary degeneration with 3-repeat tau protein in Down syndrome. *J Neuropathol Exp Neurol* **2011**, *70*, 36–50.
- (11) Dowjat, W. K.; Adayev, T.; Kuchna, I.; Nowicki, K.; Palmieriello, S.; Hwang, Y. W.; Wegiel, J. Trisomy-driven overexpression of DYRK1A kinase in the brain of subjects with Down syndrome. *Neurosci Lett* **2007**, *413*, 77–81.

- (12) Shi, J.; Zhang, T.; Zhou, C.; Chohan, M. O.; Gu, X.; Wegiel, J.; Zhou, J.; Hwang, Y.-W.; Iqbal, K.; Grundke-Iqbal, I.; Gong, C.-X.; Liu, F. Increased dosage of Dyrk1A alters alternative splicing factor (ASF)-regulated alternative splicing of tau in Down syndrome. *J Biol Chem* **2008**, *283*, 28660–28669.
- (13) Liu, Y.; Conaway, L.; Rutherford Bethard, J.; Al-Ayoubi, A. M.; Thompson Bradley, A.; Zheng, H.; Weed, S. a; Eblen, S. T. Phosphorylation of the alternative mRNA splicing factor 45 (SPF45) by Clk1 regulates its splice site utilization, cell migration and invasion. *Nucleic Acids Res.* **2013**, *41*, 4949–4962.
- (14) Tahtouh, T.; Elkins, J. M.; Filippakopoulos, P.; Soundararajan, M.; Burgy, G.; Durieu, E.; Cochet, C.; Schmid, R. S.; Lo, D. C.; Delhommel, F.; Oberholzer, A. E.; Pearl, L. H.; Carreaux, F. F.; Bazureau, J.; Knapp, S.; Meijer, L.; Ralf, S.; Pearl, H. Selectivity, Cocrystal Structures, and Neuroprotective Properties of Leucettines, a Family of Protein Kinase Inhibitors Derived from the Marine Sponge Alkaloid Leucettamine B. *J Med Chem* **2012**, *55*, 9312–9330.
- (15) Fedorov, O.; Huber, K.; Eisenreich, A.; Filippakopoulos, P.; King, O.; Bullock, A. N.; Szklarczyk, D.; Jensen, L. J.; Fabbro, D.; Trappe, J.; Rauch, U.; Bracher, F.; Knapp, S. Specific CLK inhibitors from a novel chemotype for regulation of alternative splicing. *Chem. Biol.* **2011**, *18*, 67–76.
- (16) Giraud, F.; Alves, G.; Debiton, E.; Nauton, L.; Théry, V.; Durieu, E.; Ferandin, Y.; Lozach, O.; Meijer, L.; Anizon, F.; Pereira, E.; Moreau, P. Synthesis, protein kinase inhibitory potencies, and in vitro antiproliferative activities of meridianin derivatives. *J. Med. Chem.* **2011**, *54*, 4474–4489.
- (17) Mott, B. T.; Tanega, C.; Shen, M.; Maloney, D. J.; Shinn, P.; Leister, W.; Marugan, J. J.; Inglese, J.; Austin, C. P.; Misteli, T.; Auld, D. S.; Thomas, C. J. Evaluation of substituted 6-arylquinazolin-4-amines as potent and selective inhibitors of cdc2-like kinases (Clk). *Bioorg Med Chem Lett* **2009**, *19*, 6700–6705.
- (18) Rosenthal, A. S.; Tanega, C.; Shen, M.; Mott, B. T.; Bougie, J. M.; Nguyen, D.-T.; Misteli, T.; Auld, D. S.; Maloney, D. J.; Thomas, C. J. Potent and selective small molecule inhibitors of specific isoforms of Cdc2-like kinases (Clk) and dual specificity tyrosine-phosphorylation-regulated kinases (Dyrk). *Bioorg Med Chem Lett* **2011**, *21*, 3152–8.
- (19) Coombs, T. C.; Tanega, C.; Shen, M.; Wang, J. L.; Auld, D. S.; Gerritz, S. W.; Schoenen, F. J.; Thomas, C. J.; Aubé, J. Small-molecule pyrimidine inhibitors of the cdc2-like (Clk) and dual specificity tyrosine phosphorylation-regulated (Dyrk) kinases: development of chemical probe ML315. *Bioorg Med Chem Lett* **2013**, *23*, 3654–3661.

- (20) Muraki, M.; Ohkawara, B.; Hosoya, T.; Onogi, H.; Koizumi, J.; Koizumi, T.; Sumi, K.; Yomoda, J.; Murray, M. V.; Kimura, H.; Furuichi, K.; Shibuya, H.; Krainer, A. R.; Suzuki, M.; Hagiwara, M. Manipulation of alternative splicing by a newly developed inhibitor of Clks. *J Biol Chem* **2004**, *279*, 24246–24254.
- (21) Ogawa, Y.; Nonaka, Y.; Goto, T.; Ohnishi, E.; Hiramatsu, T.; Kii, I.; Yoshida, M.; Ikura, T.; Onogi, H.; Shibuya, H.; Hosoya, T.; Ito, N.; Hagiwara, M. Development of a novel selective inhibitor of the Down syndrome-related kinase Dyrk1A. *Nat. Comm* **2010**, *1*, 86.
- (22) Bain, J.; Plater, L.; Elliott, M.; Shpiro, N.; Hastie, C. J.; McLauchlan, H.; Klevernic, I.; Arthur, J. S.; Alessi, D. R.; Cohen, P. The selectivity of protein kinase inhibitors: a further update. *Biochem J* **2007**, *408*, 297–315.
- (23) Taira, N.; Mimoto, R.; Kurata, M.; Yamaguchi, T.; Kitagawa, M.; Miki, Y.; Yoshida, K. DYRK2 priming phosphorylation of c-Jun and c-Myc modulates cell cycle progression in human cancer cells. *J Clin Invest* **2012**, *122*, 859–872.
- (24) Spadaro, A.; Frotscher, M.; Hartmann, R. W. Optimization of hydroxybenzothiazoles as novel potent and selective inhibitors of 17 β -HSD1. *J Med Chem* **2012**, *55*, 2469–2473.
- (25) De Antoni, A.; Maffini, S.; Knapp, S.; Musacchio, A.; Santaguida, S. A small-molecule inhibitor of Haspin alters the kinetochore functions of Aurora B. *J Cell Biol* **2012**, *199*, 269–284.

3.3 Screening Dyrk1A inhibitors by MALDI-QqQ mass spectrometry. Systematic comparison to established radiometric, luminescence and LC-UV-MS assays

David Gode, [Christian Schmitt](#), Matthias Engel, Dietrich A. Volmer

Reprinted with permission from *Analytical and Bioanalytical Chemistry*, **2014**, DOI: 10.1007/s00216-014-7703-1

Copyright: © 2014 Springer.

Publication C

3.3.1 Abstract

Enzyme-catalyzed reactions play key roles in disease pathology, thus making them relevant subjects of therapeutic inhibitor screening experiments. Matrix-assisted laser desorption/ionization (MALDI) assays have demonstrated to be able to replace established screening approaches. They offer increased sample throughput but care must be taken to avoid instrumental bias from differences in ionization efficiencies. We compared a MALDI-triple-quadrupole (QqQ) method for the Dyrk1A peptide substrate woodtide to LC-MS, LC-UV, luminescence and radiometric assays. MALDI measurements were performed on a MALDI-QqQ instrument in the multiple-reaction monitoring mode. Different MALDI conditions were investigated to address whether matrix type, sample support and MRM or SIM-based detection conditions can be used to accommodate the molar responses of substrate peptide and its phosphorylated form. UV detection served as a reference method. The impact of MALDI matrix on IC 50 values was small, even considering that matrix preparations were used that are known to alleviate response differences. IC 50 values determined by MALDI were ca. twofold lower than those determined by LC-UV. Although MALDI generated lower ion yields for the phosphorylated peptide than for the peptide substrate, we found that a correction of compound potencies was readily possible using correction factors based on unbiased LC-UV results. A thorough method development delivered a robust assay with excellent performance ($Z' > 0.91$) that was close to that seen for LC-UV.

3.3.2 Introduction

Kinases play key roles in signal transduction pathways and regulate many cellular mechanisms, such as growth, differentiation, proliferation and apoptosis [1]. Deregulation of kinase activity or mutations in kinase genes are therefore involved in many human diseases, in particular inflammatory and neurological diseases (e.g. Alzheimer's Disease and Parkinson's Disease), metabolic disorders (e.g. type 2 diabetes), vascular diseases and many types of cancer [2,3]. The dual

specificity tyrosine phosphorylation regulated kinase 1A (Dyrk1A) is a member of the DYRK family of protein kinases, which comprises five family members, Dyrk1A, 1B, 2, 3, 4A, and 4B [4]. Dyrks belong to the CMGC group of kinases.

Dyrk1A shows specificity for serine/threonine residues of substrates and autophosphorylates tyrosine [5]. The autophosphorylation of a highly conserved tyrosine residue within its activation loop is required for activity and occurs during or immediately after protein translation [6, 7]. Dyrk1A was identified to phosphorylate the microtubule-associated protein tau at multiple sites and acts as priming kinase for glycogen synthase kinase 3 [8]. Due to its location in the Down syndrome critical region of the human chromosome 21, the kinase is 1.5-fold overexpressed in individuals suffering from Down's syndrome [9, 10]. The hyperphosphorylation of tau is responsible for the formation of insoluble, stable aggregates of tau protein resulting in the so-called neurofibrillary tangles [11–14]. Neurofibrillary degeneration through aggregation of tau protein and β -amyloidosis causes loss of neurons, which leads to the pathological indications of Alzheimer's Disease in individuals suffering from Down's Syndrome [11, 15]. The discovery of these physiological roles made Dyrk1A a promising target for the development of therapeutic inhibitors.

Screening for potential inhibitors is the important first step in the drug discovery process. Several techniques are available for screening purposes, each with its own advantages and disadvantages. An overview of established screening techniques was given by von Ahsen and Bömer [16]. The summary does not cover MS-based approaches, however, indicating that mass spectrometry has not yet been fully considered as a suitable screening technique, probably due to the general perception of MS being only a medium throughput technique. A previous report of a MALDI-triple quadrupole (QqQ)-based enzyme activity assay showed, however, that reasonable results are achievable with an analysis speed of *ca.* 9 min per 384-well plate. Considering a HTS screen of one million compounds using triplicates of single concentrations, this would result in 48 days total measurement time (excluding data analysis and sample preparation). This places MALDI screening, assuming a high level of automation, in a time frame segment that is generally considered to be compatible with HTS methodologies (1-3 months for one million compounds) [17]. Of course, the primary limitation of the MALDI measurement speed currently is the sample preparation and therefore the above time frames will only be achievable if the speed of the sample preparation matches that of the MALDI measurements.

Multiplexed analysis by mass spectrometry techniques was also shown to be readily possible by combining phosphorylation and esterase assay [18], which has allowed the application of MS-based approaches in academic high-throughput screening environments [19]. A comprehensive review

covering the role of mass spectrometry in enzyme assays, with particular attention to desorption techniques, was provided by Greis *et al.* [20]. While MALDI can reach the speed requirements of HTS techniques, liquid separation-based systems are usually not fast enough, although focused screening techniques have been readily demonstrated [21]. Deng and Sanyal provided an overview of these developments with a focus on separation-based techniques [22]. Irrespective of their measurement speed, MS-based screening assays are crucial when molecular identity-based screening or confirmatory information is needed.

Monitoring of enzymatic reactions by MALDI has been successfully demonstrated for both small molecule substrates [23–26] and peptides [27–29]. These techniques necessitate a linear relationship of substrate and product response or rely on absolute quantitation. Absolute quantitation, of course, requires a suitable internal standard such as an isotope-labeled substrate as demonstrated by Bungert *et al.* [30]. While this usually leads to excellent agreement with other reference methods, the need for isotope-labeled compounds adds complexity and raises assay cost significantly. It therefore seems preferable to develop workflows that do not rely on stable isotope standards, in particular for assays involving isolated enzymes. Rathore *et al.* successfully linearized the response ratios in a MRM-based AChE inhibitor assay by balancing the response of a 1:1 mixture of substrate and product [31]. A recent report introduced tryptophanyl-arginin-tagged peptide substrates of c-Abl kinase, acetylated with deuterium labeled acetic anhydride [29]. It was stated by the authors, that the use of deuterium-labeled substrate peptides delivered results in excellent agreement to other reports. The majority of MALDI assays, however, have used no internal standardization, since intensity ratios of phosphorylated and un-phosphorylated peptides were linear over a wide concentration range [28, 32]. The limiting factor of these quantitative assays is the lower compound response of the phosphorylated peptides *versus* their un-phosphorylated counterparts. This has led to an underestimation of the phosphorylated substrate [33–35] and thus to an apparent higher inhibition. Craig *et al.* assumed that response differences in positive ion mode originate from differences of iso-electric points caused by the introduction of the negatively-charged phosphate group [33]. A similar but less pronounced under-representation was found for a phosphopeptide bearing 8 basic moieties [32]. A study investigating 136 ROCK2 substrate peptides found consistently lower signal levels for phosphopeptides and correlation of MALDI results to a radiometric method improved as the number of basic residues increased [36]. It was shown that there was no clear causal link between ionization polarity and ionization/detection efficiency of phosphopeptides [37]. Inconsistent results can be found in the literature for the PKA substrate peptide kemptide. While deviations from reference methods were found in one study [33], another

investigation reported good agreement [38]. Such deviations are generally believed to originate from binding of phosphopeptides to steel surfaces [39–41].

The aim of this study was the optimization of a MALDI-QqQ-based readout of the inhibitory potency of Dyrk1A inhibitors and the comparison with other established assay techniques, namely radiometric, luminescence and LC-UV-MS assays. Four new candidate drugs and one suitable reference compound were chosen for the experiments. Three different MALDI matrices were tested for their impact on assay outcome, and MRM was compared to the SIM mode, to further elucidate experimental conditions that best resemble the actual substrate to product ratios.

3.3.3 Experimental

Reagents and chemicals

α -cyano-hydroxy cinnamic acid (CHCA, 99%), sDHB (9:1 mixture of 2,5-dihydroxybenzoic acid, and 2-hydroxy-5-methoxybenzoic acid, 99%), 3-Hydroxypicolinic acid (HPA, 99%), Ethylene glycol-bis(2-aminoethylether)-N,N',N'-tetraacetic acid (EGTA, 97%), 2-Amino-2-(hydroxymethyl)-1,3-propanediol (Tris, 99.8%), anhydrous magnesium chloride (98%), ACS grade hydrochloric acid, LC-MS-grade acetonitrile, LC-MS grade formic acid (FA) and trifluoroacetic acid (TFA) were obtained from Sigma-Aldrich (Steinheim, Germany). Organic-free, deionized water was generated by an Elga PureLab Ultra genetic (Griesheim, Germany) water purification system. Woodtide was prepared by an in house facility (>95% purity). Substances labeled as CS375, SE26, C7E, and PM15 were synthesized as described in [42]. All substances were purified to >95% purity. μ -focus MALDI target plates (900 μ m focusing spot) were purchased from Hudson Surface Technologies (Old Tappan, New Jersey, USA).

Protein expression and purification

Dyrk1A was prepared as described in reference [42]. Briefly, the catalytic domain of Dyrk1A fused to an N-terminal hexahistidine-tag was cloned into a pET expression vector (termed pET45b-Dyrk1A-cd) and expressed in *E. coli* BL21 (DE3) cells. To this end, BL21 (DE3) cells were transformed using the pET45b-Dyrk1A-cd expression plasmid and the transformed bacteria were grown in LB medium. Protein expression was induced by addition of 0.5 mM IPTG overnight at 18°C. Bacteria cells were lysed by sonication and the lysates were purified by affinity chromatography using Ni²⁺-Sepharose beads (GE Healthcare Bio Sciences, LOT # 10038389). The eluted Dyrk1A was dialyzed and aliquots of 5 μ l were snap frozen in dry ice/isopropanol and stored at -80 °C.

Radioassay

Dyrk1A kinase reactions were performed in a reaction buffer containing 50 mM Tris/HCl, pH 7.4, 0.1 mM EGTA, 0.5 mM DTT, 10 mM MgCl₂, 100 μM ATP and 0.33 μM, 2 μCi [γ -³²P]-ATP as well as 100 μM woodtide substrate peptide (KKISGRLSPIMTEQ-NH₂) at a final volume of 20 μl per reaction well. The activity of recombinant Dyrk1A in the assays was 0.1 mU per reaction well. The kinase reactions were carried out at 30 °C for 15 min and terminated by spotting 5 μL of the reaction mixture onto a P81 phosphocellulose membrane (Whatman). The membrane was washed four times with 0.3 % phosphoric acid and one time with acetone and dried. The dry membrane was exposed in a cassette to a Phosphor Screen Imaging Plate (FujiFilm) and the signals detected by scanning of the imaging plate in a Fuji FLA-3000 PhosphorImager. The spots were quantified using AIDA software (Raytest, Version 3.52). For IC₅₀ determinations, 10 concentrations of each compound were used in triplicate reactions.

Luminescence

Dyrk1a activity was measured as residual ATP consumption in 384 well plates using the Kinase-Glo[®] assay kit (Promega) following vendors instructions. The assay was carried out as described in the preceding paragraph with a total volume of 20 μL but without [γ -³²P]-ATP. The kinase reactions were stopped by the addition of 5 μl of a harmine solution resulting in a final concentration of 5 μM. Both reagents, provided with the kit, were added and luminescence was measured on a POLARstar Omega plate reader from BMG Labtech (Ortenberg, Germany) after an additional 15 minutes. For IC₅₀ determinations, 10 concentrations of each compound were used in triplicate reactions that were measured 4 times.

MALDI-QqQ

MALDI experiments were performed on an AB Sciex FlashQuant Workstation comprising a QTRAP 4000 quadrupole-linear ion trap and intermediate pressure MALDI source (Concord, ON, Canada). The MALDI source was equipped with a diode-pumped, q-switched, pulsed solid-state Nd:YLF laser (349 nm, 5 ns pulse width) capable of operating with a repetition rate up to 1 kHz. All experiments were performed using the following settings: source gas flow, 15 (arbitrary units); plate voltage, 140 V; collision activated dissociation (CAD) gas pressure, high; collision energy (CE), 100 V for MRM experiments, 20 V for experiments in SIM mode; collision cell exit potential (CXP), 10 V, laser repetition rate 800 Hz; laser energy 50% for CHCA and CHCA/HPA (approximately 190 J·m⁻²) and 80% for DHB (approximately 340 J·m⁻²). Raster speed was 2 mm·s⁻¹ in all experiments (~2 s per spot). Quantitative data were acquired by peak area measurements of the time-dependent MRM or SIM traces (dwell time, 10 ms; transition, precursor ion m/z 1587.9 [M+H]⁺ → m/z 1442.8 for woodtide

and 1667.9 $[M+H]^+ \rightarrow m/z$ 1442.8 for phosphorylated woodtide; the product ion at m/z 1442.8 corresponds to either b_{13} or the $y_{13}-H_2O$ fragment of woodtide). Experiments for method development were performed in SIM mode exclusively. Assay conditions were as described for the radiometric assay with some exceptions: a total volume of 100 μ L was used and no radioactive ATP was added. The kinase reactions were stopped by adding 5 μ L of an aqueous solution containing 5 vol-% TFA, and 5 μ L of each well was then added to 50 μ L of matrix solution and the remaining part was used for LC-UV-MS measurements. MALDI plates were prepared by manual spotting of 1 μ L on the corresponding target plates (stainless steel for CHCA, Hudson μ Focus plate [900 μ m] for DHB and CHCA/HPA).

HPLC-UV-MS

HPLC was carried out on a Shimadzu Prominence UFLC_{XR} (Duisburg, Germany) high pressure gradient system, equipped with two LC-20AD_{XR} pumps, SIL-20AC_{XR} temperature-controlled autosampler (10 °C), CTO-20AC column thermostat, and G1314A variable wavelength detector from Agilent (Waldbronn, Germany) coupled to a QTRAP 2000 triple quadrupole mass spectrometer (AB Sciex). The LC system was modified by adding a mixing column (4.6 \times 60 mm, V=420 μ L) (G1312-87330, Agilent) to obtain a stable baseline for UV detection. UV data was acquired and analyzed with Chromeleon 6.8 (Dionex-Softron, Germering, Germany). The LC system was controlled with Analyst 1.6 (AB Sciex). LC separations were performed using 10 μ L injections on a Dionex Acclaim C18 HPLC column (2.1 \times 150 mm, 3 μ m) at 40°C and a flow rate of 0.8 mL min⁻¹. Mobile phases were (A) water + 0.1% formic acid and (B) acetonitrile + 0.1% formic acid. Gradient conditions were as follows: 0-1.9 min, 10-35% B; 1.9-2 min, 35-90% B; 2-3.5 min, 90% B; 3.5-3.6 min, 10% B; 3.6-7.1 min, 10% B. The eluent stream was diverted to waste from 0-1.4 min and 2.6-7.1 min using a switching valve. Source and voltage settings for the MS were as follows: curtain gas, 50 (arbitrary units); CAD gas pressure, 6 (arbitrary units); spray gas (gas 1) pressure 50 (arbitrary units), heater gas (gas 2) pressure 80 (arbitrary units); needle voltage, +5500 V; source temperature 500 °C; declustering potential, 90 V, collision energy 15 V, CXP, 30 V. Data was acquired in SIM mode (dwell time, 100 ms; transition, precursor ion m/z 794.5 $[M+H]^+ \rightarrow m/z$ 794.5 for woodtide; precursor ion m/z 834.5 $[M+H]^+ \rightarrow m/z$ 834.5 for phosphorylated woodtide).

Data Analysis

Curve fitting, IC₅₀ determinations and statistical data analysis were performed using Origin Pro 9.1 (OriginLab, Northampton, UK). Homogeneity of variances was tested using Levene's test ($\alpha=0.05$). Multiple comparison of means for heteroscedastic data was accomplished using the Multicomp

package for R (R Core Team (2013), R: A language and environment for statistical computing, R Foundation for Statistical Computing, Vienna, Austria, <http://www.R-project.org/>.) recently introduced by Herberich et al. [48].

3.3.4 Results and Discussion

A MALDI-QqQ-based readout platform was developed in this study and applied to determine the inhibitory potency of five Dyrk1A inhibitors. Initially, three matrices were investigated and experimental conditions optimized for the inhibitor MALDI assay. Mass spectral data acquisition was investigated in both MRM and SIM modes and the resulting data were used to find optimum experimental conditions for the actual substrate to product ratios. Finally, the MALDI-QqQ assay was compared to several established assay techniques, namely radiometric, luminescence and LC-UV-MS assays.

Optimization of type and concentration of matrix compound

The choice of a proper matrix compound for MALDI is essential for the successful outcome of any MALDI assay [37] and a strong influence has also been shown for the relative response ratios of several substrate/product peptides during MALDI analyses [41]. In one study, CHCA was found to deliver very irreproducible relative response ratios [37]. The same study described that differences in response behavior upon changing the matrix were pronounced for some peptides while others were barely affected [37]. Unfortunately, the underlying principles could not be readily explained and optimization therefore required a trial-and-error approach for minimizing these differences. The general applicability of CHCA for quantitative MALDI, however, has been demonstrated in a number of studies [43–45] and several MALDI-TOF and MALDI-QqQ-based enzyme assays using CHCA as matrix compound have been reported [18,25,28,31,38]. The broad applicability of CHCA has made this compound the natural choice as MALDI matrix for small molecule analysis. Super DHB (sDHB), which is a mixture of 9:1 mixture of 2,5-dihydroxybenzoic acid, and 2-hydroxy-5-methoxybenzoic acid, and a combination of CHCA and 3-hydroxypicolinic acid (HPA) were chosen in this study to account for potential phosphate losses during laser desorption/ionization [46,47], as it was previously demonstrated that both matrices were able to prevent these undesired fragmentation reactions. A series of experiments was initially performed to find the optimal experimental conditions for each matrix. Acetonitrile (ACN) was chosen as solvent and aqueous mixtures were prepared using 30, 50 and 70 % (v/v) ACN. The matrices were investigated at concentration levels of 20, 10, 5, 1 and 0.5 mg/mL.

A matrix concentration level of 1 mg/mL was chosen to compensate for the reduced spot sizes of the focusing plates. The focusing plate typically exhibited spot sizes of 0.9 mm for liquid deposits of 1 μ L (50% ACN) compared to *ca.* 2 mm using a standard stainless steel plate. The matrix concentration of 5 mg/mL, which delivered excellent reproducibility on stainless steel (Figure 1), was therefore scaled down using the area ratio (\sim 5) to achieve very similar surface coverage and reproducibility of the measurements as for the stainless steel plates. Figure 1 shows experimental results for CHCA on both target types. RSD and signal intensities refer to the unphosphorylated peptide; reproducibility for the phosphorylated form and their ratio was also monitored (see Experimental). It can be seen that matrix concentrations of 1 and 0.5 mg/mL led to low absolute signal intensities and high relative standard deviations on standard stainless steel. Contrary to our expectations, results for these concentrations were highly irreproducible for the μ -focus plate as well. The reason for this discrepancy becomes obvious from the light microscope images (Figure 1). Deposition of 1 μ L of a solution of 5 mg/mL CHCA on stainless steel yielded small, homogeneously distributed crystals, resulting in a measurement reproducibility of 12 % RSD. Deposition of the same volume on the μ -focus plate but with the matrix concentration reduced by a factor of 5 delivered isolated spots of highly aggregated crystals (57 % RSD).

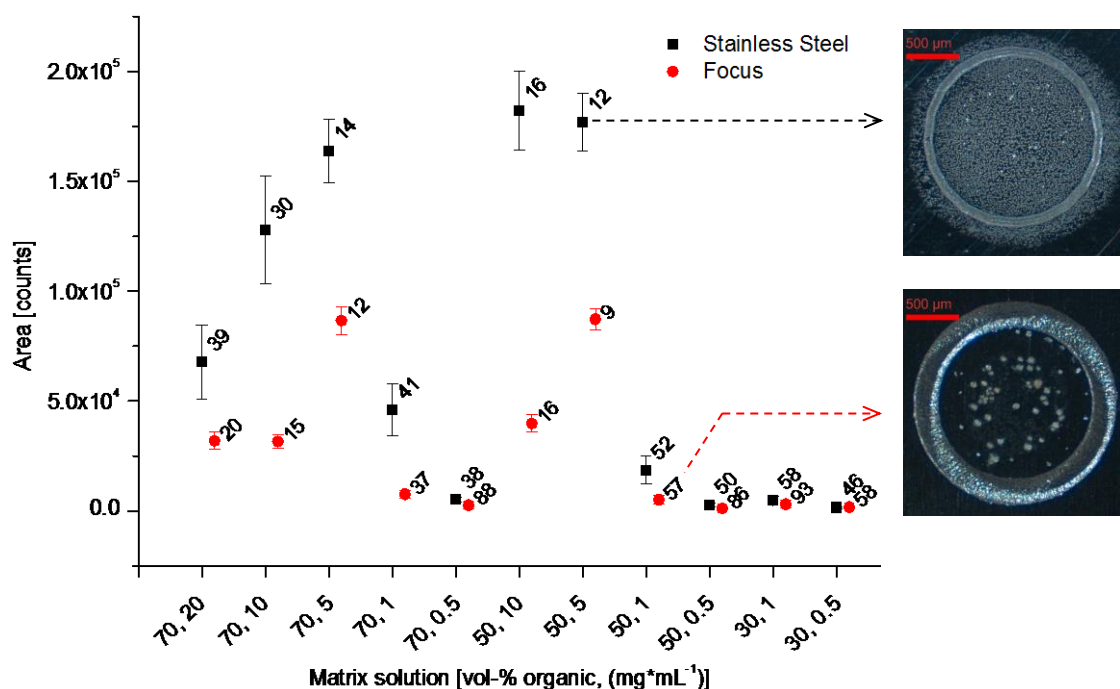


Figure 1: Matrix optimization for CHCA. The experimental data were acquired on standard stainless steel (black squares) and Hudson μ -focus plates (red circles). Error bars are 95% confidence intervals of the mean ($N=12$, $t=2.201$). Data are labeled with the respective relative standard deviations. The right hand side of the diagram shows light microscopic images for two selected conditions. The difference of spot area sizes for these two plates was approximately a factor of 5. Scaling down the matrix concentration by this factor did not result in comparable surface coverage for the focusing plate, however, due to the tendency to form larger crystals on the focusing plate. Missing combinations of solvent and matrix concentration are due to the limited solubility of CHCA.

Response and reproducibility were found to be less influenced by the choice of organic solvent and CHCA concentration for the focusing plate. The experiments for larger CHCA concentrations seen in Figure 1 all exhibited comparable standard deviations and the differences of means were not statistically significant. The same experiments for the steel plate showed pronounced differences in relative standard deviations and differences of mean peak areas were found to be significant. Due to the heteroscedasticity of the data, pair-wise comparisons were performed using the Multicomp package for R recently introduced by Herberich et al. [48] Even though the μ -focus plate allowed for easier method development, the signal levels were consistently lower as compared to stainless steel; by a factor of 2 for the mean peak areas at their respective optimum conditions without significant differences in relative standard deviations. Based on these findings, we chose stainless steel as sample support for all subsequent experiments with CHCA as matrix at a concentration of 5 mg/mL in 50 % ACN. Very small signal levels accompanied by high relative standard deviations were found for the lowest two matrix concentrations and for the mixtures containing 70% water. The same tendency was seen for other combinations of organic solvent, matrix and sample support. For

example, sDHB exhibited RSD values >30% at 1 and 0.5 mg/mL on both sample supports. Figure 2 summarizes results for sDHB and CHCA-HPA mixtures. CHCA and HPA were mixed in a volumetric ratio of 1:1 in all experiments as suggested by Zhou *et al.* [47]. A solvent composition of 70 % ACN at 20 mg/mL of both matrix compositions showed only a slight but significant difference in peak areas, with comparable standard deviations for both sample supports.

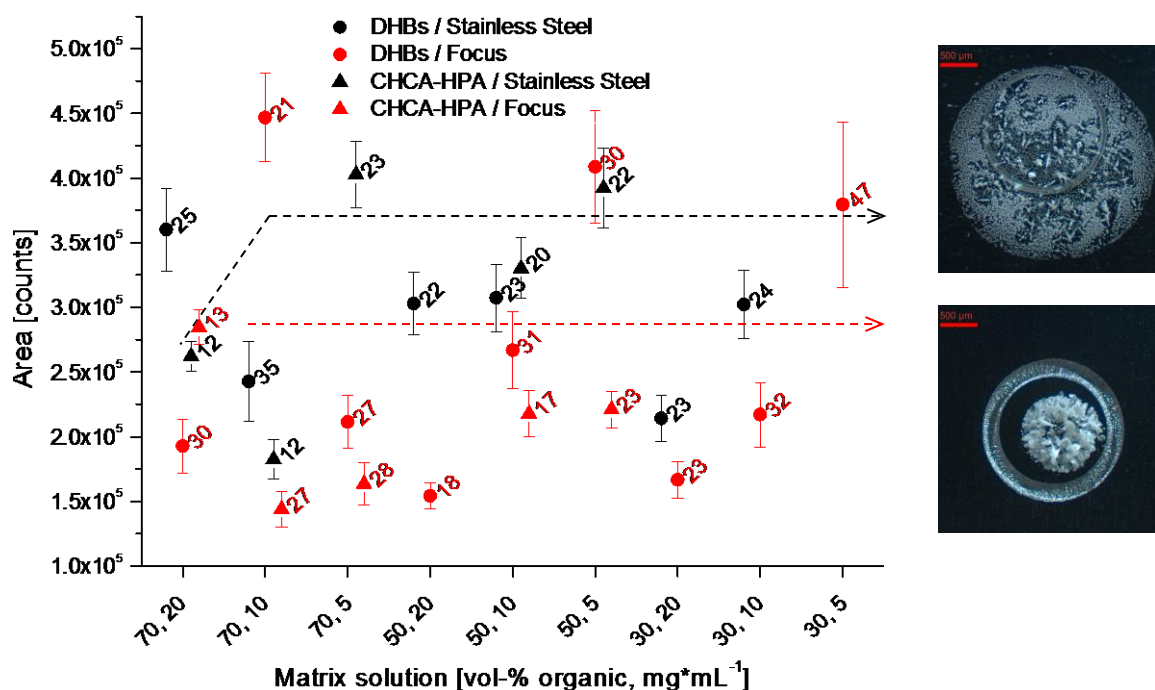


Figure 2: Matrix optimization for DHBs (circles) and 1:1 mixtures of HPA and CHCA (triangles). The experimental data were acquired on standard stainless steel (black) and Hudson μ -focus plates (red). Error bars are 95% confidence intervals of the mean ($N=12$, $t=2.201$). Data are labeled with the respective relative standard deviations. The two light microscopic images show that the sponge-like crystallization behavior under conditions similar to those described in [47] were not observed in our experiments.

Almost all other conditions gave significant increases of standard deviation. Larger peak areas for 5 mg/mL in 70 and 50 % acetonitrile on stainless steel, for example, were accompanied by significant increases (at the 95 % level) of variability from 12 % to 22 and 23 % RSD, respectively. A sponge like crystal formation as reported in [47] was observed, even though the conditions used for matrix preparation were identical. The matrix mixture tended to crystallize in needle-like crystal shapes at higher concentration levels on both sample supports. An almost linear decrease of peak areas was seen at concentration levels of 20 and 10 mg/mL when the organic component was reduced from

70 % to 30 % acetonitrile. The optimum signal stability and ion intensity was found for 10 mg/mL sDHB in 70 % acetonitrile on a μ -focus plate.

Influence of volume/total peptide concentration and general assay conditions

1, 0.75 and 0.5 μ L of the matrix/reaction mix were spotted onto the targets, corresponding to amounts of *ca.* 9, 6.75 and 4.75 pmol total peptide per spot. No significant difference in means and variance were seen for sDHB and HPA/CHCA. Contrasts of means for CHCA were found to be significant. However, the minor differences in relative peak areas for the smaller volumes of 0.75 and 0.5 μ L can be regarded negligible in comparison to 1 μ L (change of +2 % for 1 and 0.5 μ L) and are additionally accompanied by a significant increase of variance.

Experiments for a single inhibitor were performed in the same day using the same aliquots of reagents to allow for a proper comparison of the assay techniques. Assay conditions were optimized following the general principles as outlined in [49]. Briefly, assay conditions were loosely based on work by Göckler et al. [50]. ATP and substrate peptide concentrations above the K_m values were chosen to ensure a linear time-dependency of the conversion. A sufficient conversion is necessary to achieve convenient Z' values. MALDI, LC-MS and LC-UV assays were performed using the same wells. A small portion of the quenched reaction mixture was dedicated to the MALDI assay, while the remainder was used for LC measurements. Radio and luminescence assays were carried out separately due to the specific reagent and safety requirements.

Comparison of MRM and SIM modes

The most abundant product ions were determined in a series of CID experiments with increasing collision energy. Two instrumental protocols were implemented during assay development. The most intense product ions for each peptide were chosen for the first protocol, while the second protocol comprised CID settings that gave a sufficiently intense product ion that both peptides had in common. Highly distorted results were obtained using the most intense product ions m/z 1460 $[\gamma_{13}/b_{13}+H_2O]^+$ for the substrate peptide and m/z 1570 $[M+H-H_3PO_4]^+$ for the phosphorylated peptide (data not shown). This was caused by the known effect that peptides bearing a phospho-group at serine dissociate in a highly sequence-dependent manner [51]. Furthermore, generally low energy CID spectra of phosphorylated peptides are dominated by neutral losses of the phosphate group [52,53]. MRM results obtained using the same product ion at m/z 1442 $[\gamma_{13}-H_2O/b_{13}]^+$ for both substrate and product were found to be in agreement with the expected behavior and were thus used in all subsequent experiments.

Peptide S (YLIEDNEYTARQGA) and kemptide (LRRASLG) were found to deliver biased results for the unphosphorylated substrate. Peptide C (YIHLEKKYVRRDSG), in contrast, was detected without bias [33]. Similar ionization and detection efficiencies were found for tryptophan-modified phosphostide-1 (WAPGTIEKKRSNAMKK-MKSIEQHRNVKGY) and peak ratios from MALDI and HPLC assays were found to be 0.917 [33]. The extent of underestimation for p-kemptide of 0.89 reported in [28] is comparable to the previous report mentioned above [33]. Kemptide was also used as a substrate in a MALDI-QqQ study and interestingly no differences of IC_{50} values were observed compared to a fluorescence assay [38]. The peptide used in this study, woodtide, exhibits 3 basic moieties and a pI value of 10. Considering the above-mentioned studies, we expected response differences and hence IC_{50} values determined by MALDI to differ from those determined by unbiased methods. UV detection of phosphorylated peptides and their unphosphorylated counterparts at 214 nm was demonstrated in several kinase assays as an unbiased detection technique [32,33,54] and peak area ratios determined by UV detection can be used to establish correction factors for exact molar ratios [41]. The unbiased nature and excellent repeatability of HPLC-UV prompted us to choose this technique as reference method in our comparison. Figure 3 illustrates typical assay outcomes for all investigated techniques. Prediction and confidence bands for MALDI results were wider than those observed for the HPLC assays and a slight increase in variance was seen for decreasing inhibitor concentrations. It was generally found that root mean square error for fit results were comparable (ranging from 1.4 to 2.1) in SIM mode, while data acquired in MRM mode delivered fit results with moderately higher RMSE values, especially for sDHB (RMSE, 2-4). The correlation diagram shown in Figure 4 summarizes all experiments, while Table 1 lists the IC_{50} values for five compounds investigated using ten assay approaches. IC_{50} values are listed together with confidence and prediction intervals. Confidence intervals refer to the actual data set and illustrate the interval that covers all possible fit functions. Prediction intervals define a broader range, additionally covering variability introduced by repeating an experiment; they are therefore used to compare IC_{50} values. It is obvious that all MALDI-based methods showed an excellent linear correlation among each other with R values better than 0.998 and only small deviations from the median line. The low degree of scatter underlines the excellent reproducibility of the MALDI assay. The strictly linear relationships and the largely indifferent IC_{50} values (Table 1) determined by MALDI-QqQ demonstrate that matrix and detection mode only have a slight influence on IC_{50} .

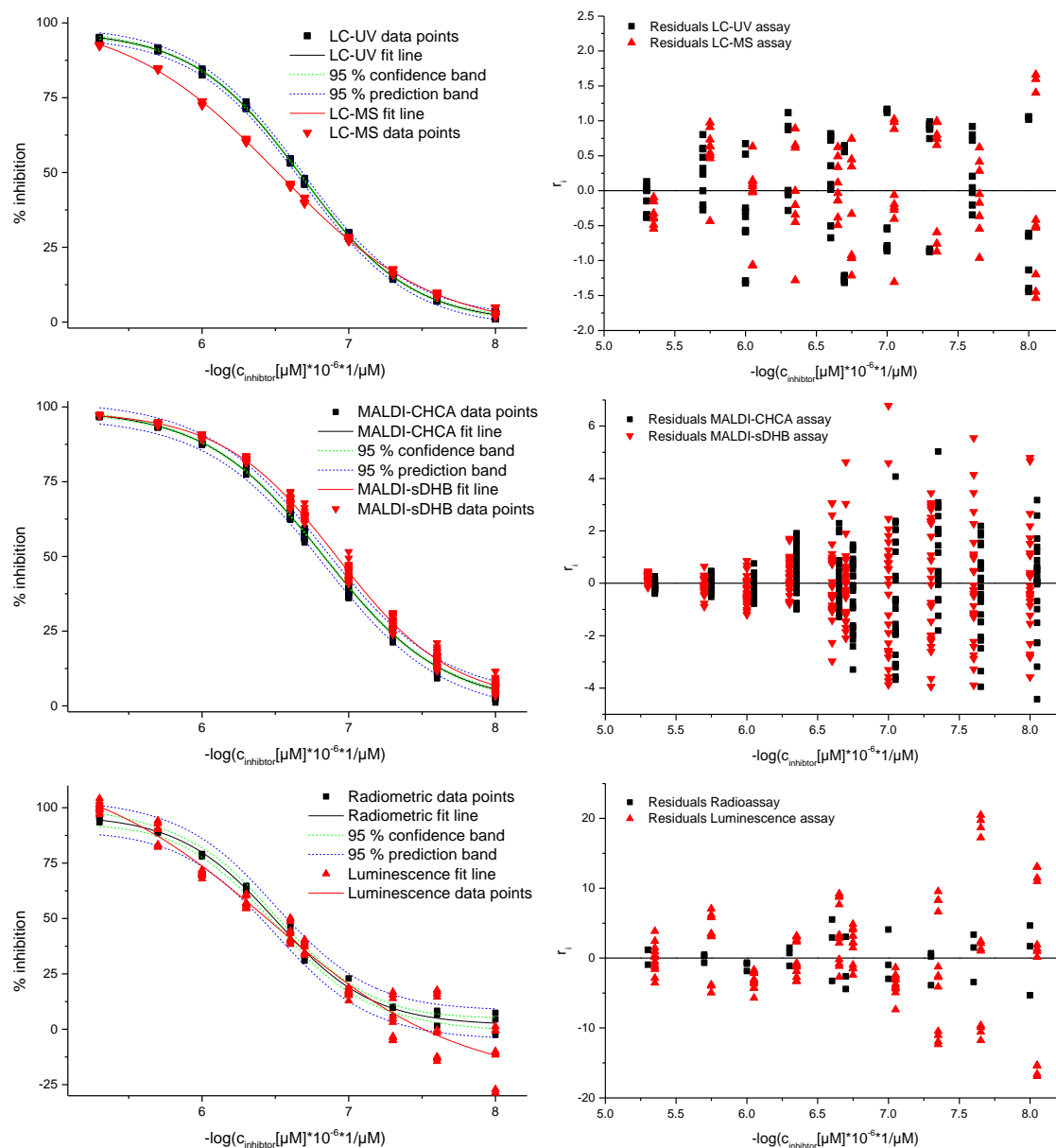


Figure 3: Exemplary IC_{50} curves for compound CS375 determined by MALDI, LC-UV, LC-MS, radiometric and luminescence assays. Other MALDI assay conditions are left out for the sake of clarity. HPLC-based assays and the radiometric assay exhibit a constant variance pattern, while residuals for MALDI and luminescence assays increase with decreasing inhibitor concentration.

We found that a correction of IC_{50} values using correction factors based on HPLC-UV results was readily possible. For CHCA and a mixture of CHCA and HPA, correction factors were reasonably small and fell within the range of 1.5 - 1.8. Correction factors for DHB ranged between 1.7 and 1.8; applying a mean correction factor led to numbers that always fell in the range of the prediction band of the corresponding LC-UV data. The correlation of MALDI with all other investigated techniques resembled a concave function, originating from the underrepresentation of the unphosphorylated peptide. Z' values for MALDI were found to be >0.9 in SIM mode, a value that is usually considered to be excellent [55]. The numbers were comparable to HPLC-based assays. Other reports using

MALDI-QqQ found Z' values from 0.6 to 0.8 [18, 38]. Data acquired in MRM mode showed comparable Z' values, except for DHB (Table 1). Z' values seen for our radiometric and luminescence assay were largely comparable to other reports [56] and were ranging from 0.44 to 0.71. IC₅₀ values for both techniques were indifferent, with higher observed variance for the luminescence assay.

Table 1: IC₅₀ values and statistical parameters for the 5 investigated inhibitors. (N=27 for MALDI, N=9 for LC, N=3 for Radiometry, N=12 for Luminescence). IC₅₀ values were determined from a Boltzmann fit $\{(y = A2 + (A1-A2)/(1 + \exp((x-x0)/dx))\}$ of inhibition values for 10 concentration values of inhibitor. Curve fitting procedures, two sample t-tests and power calculations were performed using Origin 9.1. Z' values were determined for each assay individually by using the 5 μ M inhibitor concentration (near 100 % inhibition in all cases) as background and the respective uninhibited reference reaction as the value that defines the upper limit of the dynamic range. T-tests refer to a one-sided two sample t-test performed on the two inhibitor concentrations of 250 and 200 μ M (green=significant difference, red=no significant difference, $\alpha=0,05$).

Substance	Essay technique	IC ₅₀ (nM)	Confidence interval ($\alpha=0.05$)	Prediction interval ($\alpha=0.05$)	Z'	t-test	power	power N=6	power N=54
C7E	CHCA SIM	397	400 393	445 355	0.94		1.00	0.947	
	CHCA MRM	396	400 390	451 348	0.94		1.00	0.902	
	DHBs SIM	381	385 378	430 338	0.94		1.00	0.941	
	DHBs MRM	440	450 431	553 351	0.85		1.00	0.608	
	HPA SIM	388	393 383	445 339	0.95		1.00	0.941	
	HPA MRM	461	467 453	539 395	0.91		1.00	0.916	
	LC-MS	794	813 774	902 700	0.96		1.00	0.998	1.00
	LC-UV	689	700 679	741 642	0.98		1.00	0.999	1.00
	Radiometry	918	1014 835	1214 709	0.70		0.706		1.00
	Luminescence	917	986 854	1317 615	0.71		0.968	0.541	1.00
PM15	CHCA SIM	252	254 251	280 227	0.95		1.00	1.00	
	CHCA MRM	245	248 243	270 223	0.93		1.00	0.999	
	DHBs SIM	234	236 231	261 209	0.93		1.00	1.00	
	DHBs MRM	273	279 267	349 214	0.80		1.00	0.496	
	HPA SIM	254	256 252	279 232	0.95		1.00	0.999	
	HPA MRM	291	293 288	326 259	0.91		1.00	0.950	

	LC-MS	494	504 485	535 455	0.98		1.00	1.00	1.00
	LC-UV	411	413 408	432 391	0.98		1.00	1.00	1.00
	Radiometry	561	607 519	732 434	0.70		0.460		1.00
	Luminescence	707	778 646	1203 436	0.81		0.940	0.390	0.999
CS375	CHCA SIM	148	149 147	164 134	0.91		1.00	1.00	
	CHCA MRM	134	136 133	150 120	0.91		1.00	0.997	
	DHBs SIM	121	123 120	138 107	0.91		1.00	0.975	
	DHBs MRM	142	146 139	181 112	0.80		1.00	0.463	
	HPA SIM	121	122 120	136 107	0.89		1.00	0.975	
	HPA MRM	168	171 166	200 142	0.90		1.00	0.846	
	LC-MS	306	308 302	327 285	0.94		1.00	1.00	1.00
	LC-UV	219	220 217	232 207	0.96		1.00	1.00	1.00
	Radiometry	331	360 306	428 256	0.73		0.605		1.00
	Luminescence	361	393 334	644 204	0.86		0.999	0.658	1
Harmine	CHCA SIM	80	81 79	92 69	0.92		1.00	0.958	
	CHCA MRM	84	84 82	96 73	0.92		1.00	0.904	
	DHBs SIM	78	79 77	90 68	0.93		1.00	0.971	
	DHBs MRM	76	77 75	87 66	0.93		1.00	0.911	
	HPA SIM	86	87 86	97 77	0.92		1.00	0.991	
	HPA MRM	87	88 86	98 78	0.91		1.00	0.942	
	LC-MS	168	172 165	191 148	0.96		1.00	1.00	1.00
	LC-UV	140	143 137	158 125	0.97		1.00	1.00	1.00
	Radiometry	169	186 153	235 121	0.91		0.439		1.00
	Luminescence	192	212 174	307 119	0.45		0.225		0.934
SE 26	CHCA SIM	205	208 203	236 179	0.92		1.00	0.864	
	CHCA MRM	190	192 187	220 164	0.91		1.00	0.873	
	DHBs SIM	188	191 185	224 157	0.90		1.00	0.987	

DHBs MRM	213	219 208	280 162	0.82		1.00	0.690	
HPA SIM	208	209 207	229 189	0.96		1.00	0.999	
HPA MRM	234	237 231	269 204	0.91		1.00	0.810	
LC-MS	389	395 383	431 352	0.97		1.00	1.00	1.00
LC-UV	327	330 324	351 305	0.98		1.00	1.00	1.00
Radiometry	388	434 351	570 264	0.80		0.483	1.00	
Luminescence	501	526 476	672 372	0.90		1.00	0.898	1.00

As supplement to Z' values, we performed one-sided two sample t-tests for two concentrations that were close to each other and within the range of x-values, where a pronounced change in y occurs (250 and 200 μM). Test powers were calculated and complemented by calculation of hypothetical powers for the least common denominator ($N=6$) and for the highest sample size ($N=54$). These values served as a means to quantify the ability of each assay to differentiate between two concentration levels for identical sample numbers. The lowest sample number had to be applied for radiometric IC_{50} determinations, as 40 was the upper limit of reactions that could be accomplished by manual pipetting [57]. HPLC-based assays gave the highest Z' scores and hypothetical test powers at the lowest sample number were always higher than 99.8 %. Unlike MALDI, ESI ionization favors the phosphorylated peptide over the unphosphorylated form in agreement with Steen *et al.* [35]. A constant bias of 1.2 ($\text{IC}_{50, \text{MS}}/\text{IC}_{50, \text{UV}}$) was found for MS and UV detection. The observed response differences were – as mentioned in the previous paragraph – in agreement with other reports. Several cases of preferred ionization of phosphorylated over unphosphorylated peptides using MALDI have been reported [28, 32, 33, 37, 41] and these differences did [26] or did not [37] correlate well with molecular properties. Response differences have varied with the choice of MALDI matrix in some cases while insignificant changes of ionization efficiency were observed for others [37]. The same unpredictable behavior was also found for electrospray ionization [35, 37]. In addition to the ionization process, adsorption phenomena on steel surfaces can further influence the observed ratios [39]. From these findings, it is clear that the ionization efficiency is highly sequence and instrumentation dependent and that there is no simple way for prediction of the outcome.

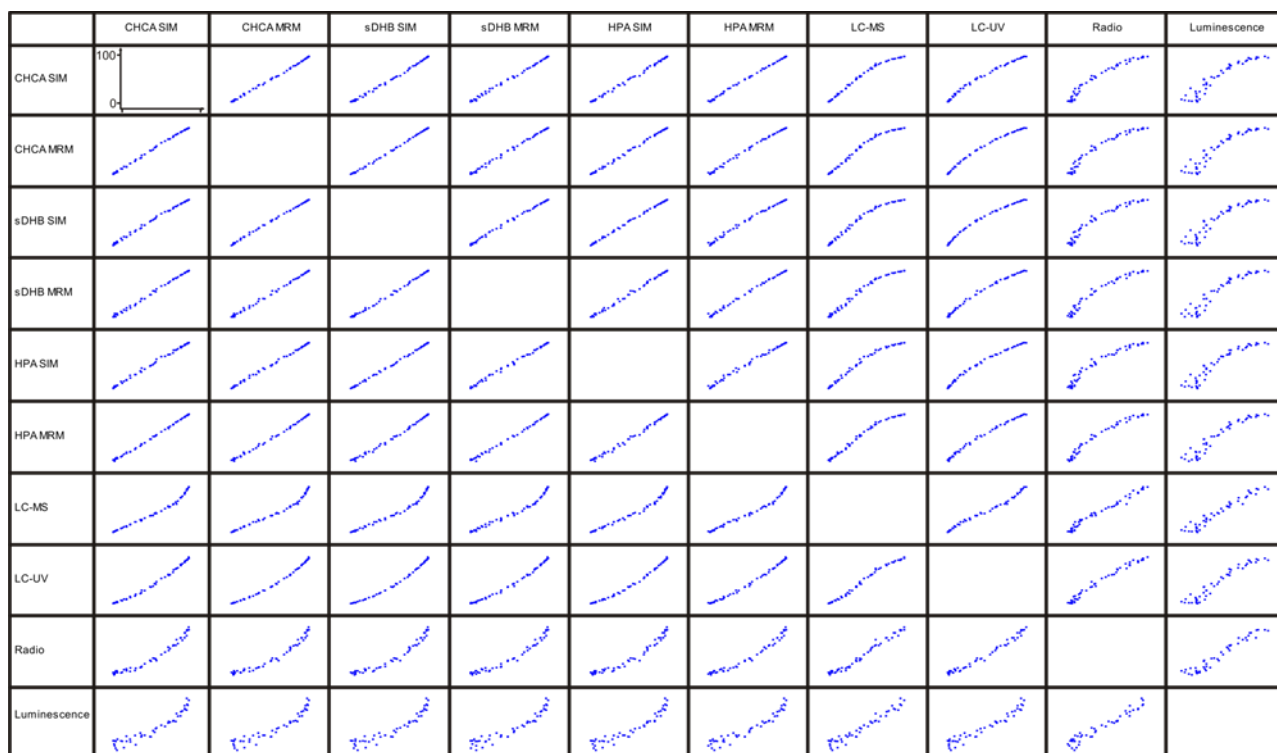


Figure 4: Correlation diagram constructed using mean inhibition ratios for all experiments. x and y scales given in the upper left cell apply to all data. Scales are % inhibition.

3.3.5 Conclusions

In this study we have shown the implementation of a high-speed MALDI assay for measuring the inhibitory potency of Dyrk1A inhibitors using a dedicated MALDI triple quadrupole platform. This instrumental platform offers high duty cycle data acquisition modes such as SIM and MRM over conventional MALDI instruments. After optimizing MALDI conditions to accommodate the differential response behavior of substrate peptide and its phosphorylated form, we compared the optimized assay to LC-MS, LC-UV, luminescence and radiometric assays. UV detection served as a reference method. Interestingly; the impact of the different MALDI matrices on IC_{50} values was very small, even considering that certain matrix preparations were used that normalize response differences. In general, IC_{50} values determined by MALDI were about 2-fold lower than those determined by LC-UV. A thorough method development delivered a robust assay with excellent performance ($Z' > 0.91$) that was close to that seen for LC-UV.

The excellent performance of the MALDI assay was complemented by additional advantages provided by the particular instrument used here; *viz.*, the high-speed, high repetition rate solid-state laser QqQ platform. This instrument platform measured high-quality mass spectral information in a fraction of the time required with conventional MALDI instruments. The analysis of a single spot was

performed in ca. 2 s as opposed to the 3.3 s reported for conventional MALDI [58]. In other words, a 384-well target plate of the inhibitor assay can be completely analyzed in approximately 14 min, and even faster speeds have been demonstrated by Rathore *et al.* [38]. This makes this MALDI assay particularly attractive to high throughput applications. In total, forty 384-well plates were measured during the course of our proof-of-concept study with no significant reduction of analyte peak areas from quality control reactions.

Acknowledgements

DAV acknowledges research support by the Alfried Krupp von Bohlen und Halbach-Stiftung.

3.3.6 References

- [1] P. Traxler and P. Furet, *Pharmacol. Ther.*, 1999, **82**, 195–206.
- [2] L. K. Chico, L. J. Van Eldik and D. M. Watterson, *Nat. Rev. Drug Discov.*, 2009, **8**, 892–909.
- [3] P. Lahiry, A. Torkamani, N. J. Schork and R. a Hegele, *Nat. Rev. Genet.*, 2010, **11**, 60–74.
- [4] W. Becker, Y. Weber, K. Wetzel, K. Eirnbter, F. J. Tejedor and H. G. Joost, *J. Biol. Chem.*, 1998, **273**, 25893–25902.
- [5] S. Himpel, P. Panzer, K. Eirnbter, H. Czajkowska, M. Sayed, L. C. Packman, T. Blundell, H. Kentrup, J. Grötzinger, H. G. Joost and W. Becker, *Biochem. J.*, 2001, **359**, 497–505.
- [6] P. A. Lochhead, G. Sibbet, N. Morrice and V. Cleghon, *Cell*, 2005, **121**, 925–936.
- [7] W. Becker and H. G. Joost, *Prog. Nucleic Acid Res. Mol. Biol.*, 1999, **62**, 1–17.
- [8] Y. L. Woods, P. Cohen, W. Becker, R. Jakes, M. Goedert, X. Wang and C. G. Proud, *Biochem. J.*, 2001, **355**, 609–615.
- [9] W. K. Dowjat, T. Adayev, I. Kuchna, K. Nowicki, S. Palmieriello, Y.-W. Hwang and J. Wegiel, *Neurosci. Lett.*, 2007, **413**, 77–81.
- [10] J. Guimerá, C. Casas, C. Pucharcòs, A. Solans, A. Domènech, A. M. Planas, J. Ashley, M. Lovett, X. Estivill and M. A. Pritchard, *Hum. Mol. Genet.*, 1996, **5**, 1305–1310.
- [11] F. Liu, Z. Liang, J. Wegiel, Y.-W. Hwang, K. Iqbal, I. Grundke-Iqbal, N. Ramakrishna and C.-X. Gong, *FASEB J.*, 2008, **22**, 3224–3233.

- [12] G. V. W. Johnson and W. H. Stoothoff, *J. Cell Sci.*, 2004, **117**, 5721–5729.
- [13] M. L. Steinhilb, D. Dias-Santagata, T. A. Fulga, D. L. Felch and M. B. Feany, *Mol. Biol. Cell*, 2007, **18**, 5060–5068.
- [14] J. Wegiel, W. K. Dowjat, W. Kaczmarek, I. Kuchna, K. Nowicki, J. Frackowiak, B. Mazur Kolecka, J. Wegiel, W. P. Silverman, B. Reisberg, M. Deleon, T. Wisniewski, C.-X. Gong, F. Liu, T. Adayev, M.-C. Chen-Hwang and Y.-W. Hwang, *Acta Neuropathol.*, 2008, **116**, 391–407.
- [15] J. Wegiel, C.-X. Gong and Y.-W. Hwang, *FEBS J.*, 2011, **278**, 236–245.
- [16] O. von Ahsen and U. Bömer, *Chembiochem*, 2005, **6**, 481–490.
- [17] R. Macarron, M. N. Banks, D. Bojanic, D. J. Burns, D. A. Cirovic, T. Garyantes, D. V. S. Green, R. P. Hertzberg, W. P. Janzen, J. W. Paslay, U. Schopfer and G. S. Sittampalam, *Nat. Rev. Drug Discov.*, 2011, **10**, 188–195.
- [18] R. Rathore, P. Pribil, J. J. Corr, W. L. Seibel, A. Evdokimov and K. D. Greis, *J. Biomol. Screen.*, 2010, **15**, 1001–1007.
- [19] S. L. Nelson, *Drug Discov. Today Technol.*, 2008, **5**, e29–e33.
- [20] K. D. Greis, *Mass Spectrom. Rev.*, 2007, **26**, 324–339.
- [21] T. P. Roddy, C. R. Horvath, S. J. Stout, K. L. Kenney, P.-I. Ho, J.-H. Zhang, C. Vickers, V. Kaushik, B. Hubbard and Y. K. Wang, *Anal. Chem.*, 2007, **79**, 8207–8213.
- [22] G. Deng and G. Sanyal, *J. Pharm. Biomed. Anal.*, 2006, **40**, 528–538.
- [23] Z. Xu, S. Yao, Y. Wei, J. Zhou, L. Zhang, C. Wang and Y. Guo, *J. Am. Soc. Mass Spectrom.*, 2008, **19**, 1849–1855.
- [24] T. Cai, L. Zhang, H. Wang, J. Zhang and Y. Guo, *Anal. Chim. Acta*, 2011, **706**, 291–296.
- [25] G. P. Hooff, J. J. A. van Kampen, R. J. W. Meesters, A. van Belkum, W. H. F. Goessens and T. M. Luider, *J. Proteome Res.*, 2012, **11**, 79–84.
- [26] Z. Xu, H.-Y. Wang, S.-X. Huang, Y.-L. Wei, S.-J. Yao and Y.-L. Guo, *Anal. Chem.*, 2010, **82**, 2113–2118.
- [27] J. F. Jung, R. J. Mears, C. A. G. N. Montalbetti, T. S. Coulter, A. Golebiowski, A. N. Carr, O. Barker, K. D. Greis, S. Zhou, E. Dolan and G. F. Davis, *Bioorg. Med. Chem.*, 2011, **19**, 2742–2750.

- [28] K. D. Greis, S. Zhou, T. M. Burt, A. N. Carr, E. Dolan, V. Easwaran, A. Evdokimov, R. Kawamoto, J. Roesgen and G. F. Davis, *J. Am. Soc. Mass Spectrom.*, 2006, **17**, 815–822.
- [29] N. Kondo and S. Nishimura, *Chemistry*, 2009, **15**, 1413–1421.
- [30] D. Bungert, E. Heinzle and A. Tholey, *Anal. Biochem.*, 2004, **326**, 167–175.
- [31] R. Rathore, J. J. Corr, D. T. Lebre, W. L. Seibel and K. D. Greis, *Rapid Commun. Mass Spectrom.*, 2009, **23**, 3293–3300.
- [32] H. Matsumoto, E. S. Kahn and N. Komori, *Anal. Biochem.*, 1998, **260**, 188–194.
- [33] A. G. Craig, C. A. Hoeger, C. L. Miller, T. Goedken, J. E. Rivier and W. H. Fischer, *Biol. Mass Spectrom.*, 1994, **23**, 519–528.
- [34] J. Chen, Y. Qi, R. Zhao, G. W. Zhou and Z. J. Zhao, *Anal. Biochem.*, 2001, **292**, 51–58.
- [35] H. Steen, J. A. Jebanathirajah, J. Rush, N. Morrice and M. W. Kirschner, *Mol. Cell. Proteomics*, 2006, **5**, 172–181.
- [36] A. Tsuchiya, D. Asai, J.-H. Kang, T. Mori, T. Niidome and Y. Katayama, *Anal. Biochem.*, 2012, **421**, 773–775.
- [37] L. Parker, A. Engel-Hall, K. Drew, G. Steinhardt, D. L. Helseth, D. Jabon, T. McMurry, D. S. Angulo and S. J. Kron, *J. Mass Spectrom.*, 2008, **43**, 518–527.
- [38] R. Rathore, J. J. Corr, G. Scott, P. Vollmerhaus and K. D. Greis, *J. Biomol. Screen.*, 2008, **13**, 1007–1013.
- [39] R. Tuytten, F. Lemièrre, E. Witters, W. Van Dongen, H. Slegers, R. P. Newton, H. Van Onckelen and E. L. Esmans, *J. Chromatogr. A*, 2006, **1104**, 209–221.
- [40] S. Liu, C. Zhang, J. L. Campbell, H. Zhang, K. K.-C. Yeung, V. K. M. Han and G. A. Lajoie, *Rapid Commun. Mass Spectrom.*, 2005, **19**, 2747–2756.
- [41] J. Gropengiesser, B. T. Varadarajan, H. Stephanowitz and E. Krause, *J. Mass Spectrom.*, 2009, **44**, 821–831.
- [42] C. Schmitt, D. Kail, M. Mariano, M. Empting, N. Weber, T. Paul, R. W. Hartmann and M. Engel, *PLoS One*, 2014, **9**, e87851
- [43] L. Sleno and D. A. Volmer, *Rapid Commun. Mass Spectrom.*, 2005, **19**, 1928–1936.

- [44] L. Sleno and D. A. Volmer, *Rapid Commun. Mass Spectrom.*, 2006, **20**, 1517–1524.
- [45] L. Sleno and D. A. Volmer, *Anal. Chem.*, 2005, **77**, 1509–1517.
- [46] P. Kapkova, E. Lattova and H. Perreault, *Anal. Chem.*, 2006, **78**, 7027–7033.
- [47] L.-H. Zhou, G.-Y. Kang and K. P. Kim, *Rapid Commun. Mass Spectrom.*, 2009, **23**, 2264–72.
- [48] E. Herberich, J. Sikorski and T. Hothorn, *PLoS One*, 2010, **5**, e9788.
- [49] J. Glickman, *Assay Guidance Manual, Eli Lilly & Company and the National Center for Advancing Translational Sciences*, 2012, 1-19.
- [50] N. Göckler, G. Jofre, C. Papadopoulos, U. Soppa, F. J. Tejedor, W. Becker and N. Gockler, *FEBS J.*, 2009, **276**, 6324–6337.
- [51] P. M. Gehrig, B. Roschitzki, D. Rutishauser, S. Reiland and R. Schlapbach, *Rapid Commun. Mass Spectrom.*, 2009, **23**, 1435–1445.
- [52] M. Rožman, *J. Mass Spectrom.*, 2011, **46**, 949–955.
- [53] P. J. Boersema, S. Mohammed and A. J. R. Heck, *J. Mass Spectrom.*, 2009, **44**, 861–878.
- [54] A. Gratz, C. Götz and J. Jose, *Electrophoresis*, 2010, **31**, 634–640.
- [55] J.-H. Zhang, *J. Biomol. Screen.*, 1999, **4**, 67–73.
- [56] C. Tanega, M. Shen, B. T. Mott, C. J. Thomas, R. MacArthur, J. Inglese and D. S. Auld, *Assay Drug Dev. Technol.*, 2009, **7**, 606–614.
- [57] C. J. Hastie, H. J. McLauchlan and P. Cohen, *Nat. Protoc.*, 2006, **1**, 968–971.
- [58] L. Hu, G. Jiang, S. Xu, C. Pan and H. Zou, *J. Am. Soc. Mass Spectrom.*, 2006, **17**, 1616–1619.

3.4 6-Hydroxybenzothiophene ketones: potent inhibitors of 17 β -hydroxysteroid dehydrogenase type 1 (17 β -HSD1) due to favorable molecule geometry and conformational pre-organization

Parisa Miralinaghi^{a,c,d}, Christian Schmitt^{a,c}, Rolf W. Hartmann^b, Martin Frotscher^a, Matthias Engel^{a,*}

Reprinted with permission from *ChemMedChem* **2014**, DOI: 10.1002/cmdc.201402050

Copyright: © Wiley VCH

Publication D

Abstract

The inhibition of 17 β -hydroxysteroid dehydrogenase type 1 (17 β -HSD1), which catalyzes the conversion of estrone to the potent estrogen receptor agonist estradiol (E2), is discussed as a novel therapeutic approach for the treatment of estrogen-dependent diseases. Because the reduction of E2 would be basically limited to the target tissues, this approach is expected to cause fewer side effects than the currently employed anti-hormonal therapies. Recently, we reported on 6-hydroxybenzothiazole ketones as a new class of 17 β -HSD1 inhibitors with a notable activity/selectivity profile. In an attempt to further optimize these parameters, we modified the benzothiazole core by a systematic bioisosteric replacement. Thus, we were able to identify the new 6-hydroxybenzothiophene derivative **26** which displayed a stronger inhibition of 17 β -HSD1 (IC₅₀ = 13 nM) and was also more selective than the benzothiazole analog **A**. Using *ab initio* calculations, we found that the higher potency of **26** was probably due to a more favorable conformational pre-organization of the scaffold for binding to the enzyme.

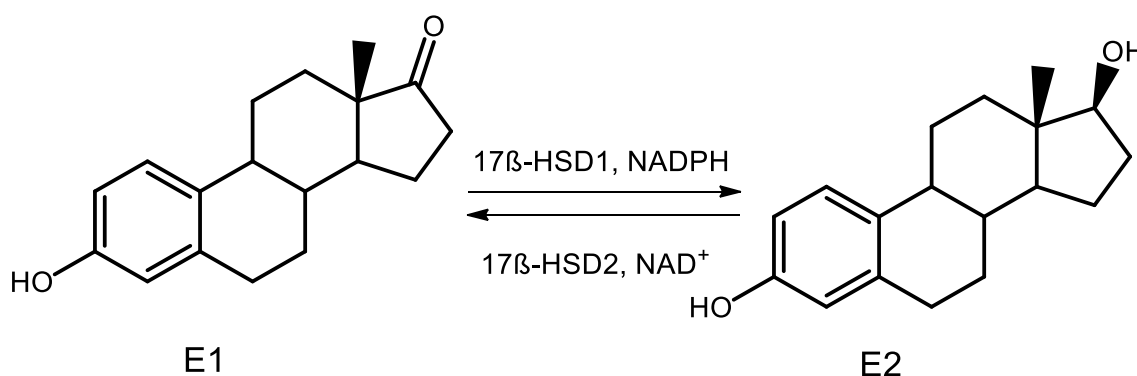
Introduction

17 β -hydroxysteroid dehydrogenase type 1 (17 β -HSD1: EC 1.1.1.62) is a soluble cytosolic enzyme which catalyzes the transformation of the weak estrogen estrone (E1) to the most potent estrogen, estradiol (E2), (chart 1). Estradiol plays a crucial role in the development, differentiation and function of the female reproduction system.^[1] On the other hand, it was found that high intracellular E2 concentrations have a major impact on the development and progression of estrogen-dependent diseases (EDD) like breast cancer,^[2,3] endometriosis,^[4] and endometrial hyperplasia.^[5] 17 β -HSD1 is a homodimeric enzyme with a subunit mass of 34.9 KDa.^[6] It is described to be overexpressed at mRNA level in breast cancer tissue and endometriotic lesions.^[7–10] Inhibition of this enzyme results in an estrogen decrease in the target cells, and hence should be associated with fewer side effects as with current hormonal therapies, for instance using aromatase inhibitors (AI)^[11–13] or GnRH analogues, which lower estrogen levels in the whole body leading to unwanted side effects.^[14–16] Consequently, 17 β -HSD1 is a promising target for the treatment of EDD. Potential 17 β -HSD1 inhibitors should not affect 17 β -HSD2, an enzyme that acts as a biological counterpart, catalyzing the reverse reaction of E2 to E1. Thus, 17 β -HSD1 inhibitors must be screened for selectivity toward 17 β -

HSD2. Until now, two main classes of 17β -HSD1 inhibitors have been reported: steroidal^[17–19] and non-steroidal inhibitors. With respect to non-steroidal inhibitors, five different scaffolds showed interesting biological profiles: bishydroxyphenyl arenes,^[20–22] heterocyclic substituted biphenols,^[23] hydroxyphenyl naphthols,^[24–27] thienopyrimidinones,^[28,29] and flavones.^[30] However, no 17β -HSD1 inhibitors have entered clinical trials so far. As seen in several X-ray structures, the 17β -HSD1 enzyme structure consists of a rigid cofactor binding pocket and a narrow, hydrophobic substrate binding site with two polar areas: His221/Glu282 on one side and Ser142/Tyr155 on the other side, which in co-crystals interact with the oxygens in the 3- and 17-hydroxy group of E2, respectively.^[31,32] As no co-crystal structure with non-steroidal inhibitors is available, computational studies were applied to unravel their binding modes,^[21,33–37] supporting the original design concept that hydroxyl functions at a suitable distance could replace the oxygens present in the substrate.^[20,24]

Recently, we reported on hydroxybenzothiazole as a new template of potent non-steroidal 17β -HSD1 inhibitors.³¹ In the case of the bishydroxyphenyl arene class of inhibitors,^[21] the nature of the heterocyclic core was found to be crucial for the potency against 17β -HSD1. Since the role of the heterocyclic core in the hydroxybenzothiazole ketone class had not been investigated before, we envisaged the bioisosteric replacement of the heterocyclic part (“core hopping”) in order to discover alternative scaffolds with improved potency and selectivity. In the following, synthesis, biological evaluation and structure–activity relationships (SAR) of new 17β -HSD1 inhibitors will be described.

Chart 1. Interconversion of Estrone (E1) to Estradiol (E2)

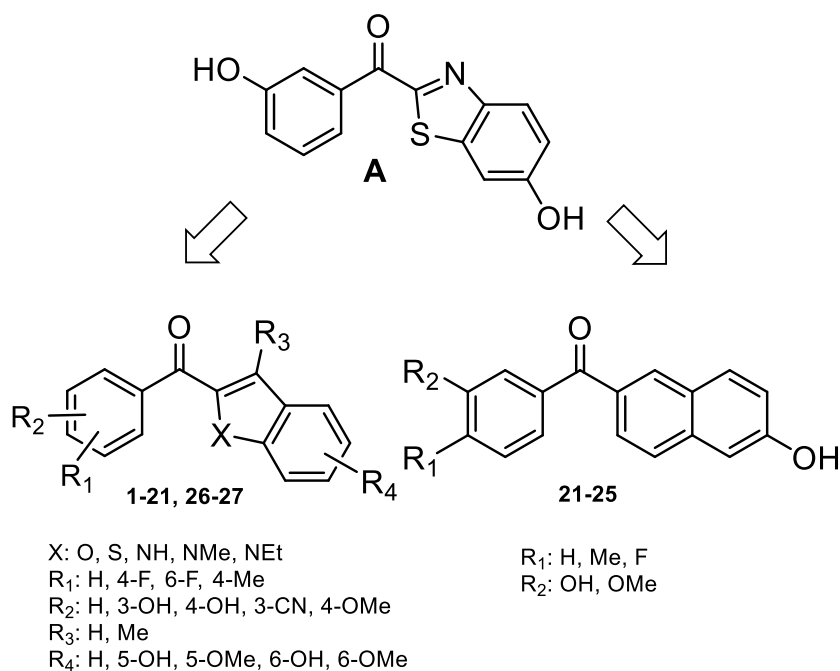


Results and Discussion

Design concept

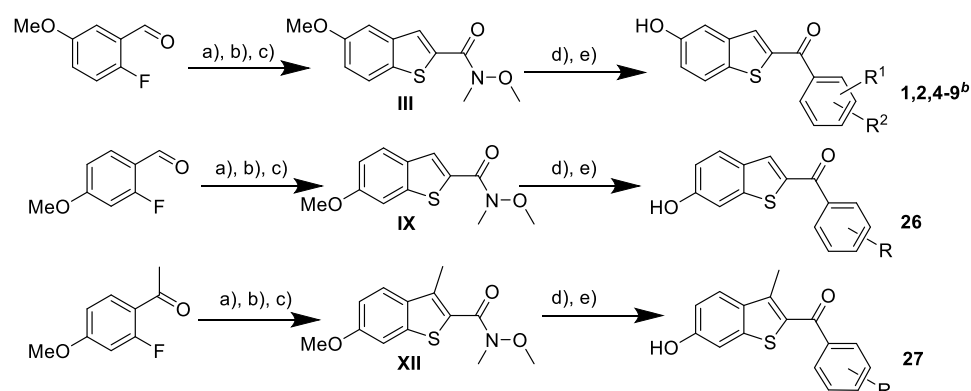
In a previous work, compound **A** has been identified as a representative for a new class of potent and selective 17β -HSD1 inhibitors.^[33] The objectives of the present study were (i) to identify alternative scaffolds and (ii) to define favorable geometric and electronic requirements for a potent inhibition. To this end, the benzothiazole in **A** was replaced with four types of bioisosteric rings: benzofuran, benzothiophene, indole and naphthalene, all differing in size, polarity, H-bonding capability, and electronic properties (Chart 2). A defined set of derivatives of each scaffold was synthesized to derive first SAR regarding the influence of substituents or the hydroxyl group positioning in the new scaffolds.

Chart 2. Compound A and synthesized compounds



Chemistry

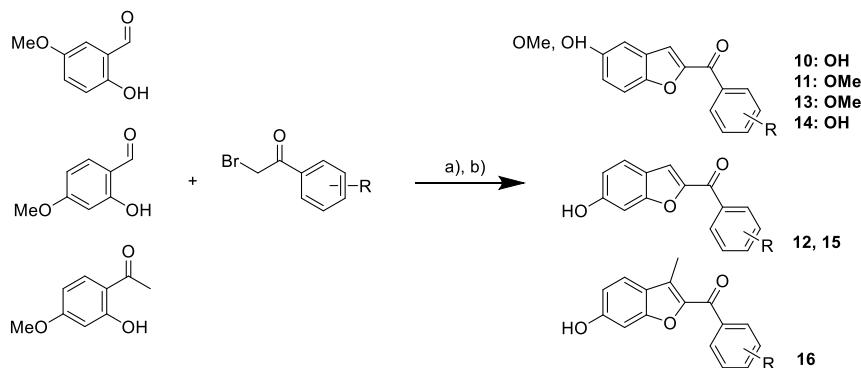
The synthesis of the compounds is depicted in Schemes 1-4. The benzothienopyridines **1**, **2** and **4-9** were synthesized according to the route presented in Scheme 1. The methoxybenzothienopyridene-2-carboxylic acid derivatives obtained as intermediates were converted into the corresponding Weinreb amides and subsequently reacted with lithiated anisoles at -78°C . The methyl ether protecting groups were then cleaved using boron tribromide to give the corresponding hydroxybenzothienopyridene ketones in varying yields. Compound **3** was synthesized in an analogous manner but starting from the commercially available benzothienopyridene-2-carboxylic acid (not shown in the Schemes).



^a Reagents and conditions: (a) Methyl thioglycolate, K_2CO_3 , DMF, 70°C , 4 h; (b) KOH, Ethanol/water 2:1, reflux, 2 h; (c) N,O-dimethylhydroxylamine hydrochloride, EDC, NEt_3 , DMAP, DCM, 0°C – RT, 18 h; (d) bromoanisole, $n\text{BuLi}$, THF, -78°C – RT, 2 h, (e) BBr_3 , -78°C , 4 h. ^b for R_1 and R_2 see Table 1.

Scheme 1. Synthesis of compounds **1**, **2**, **4-9**, **26** and **27**^a

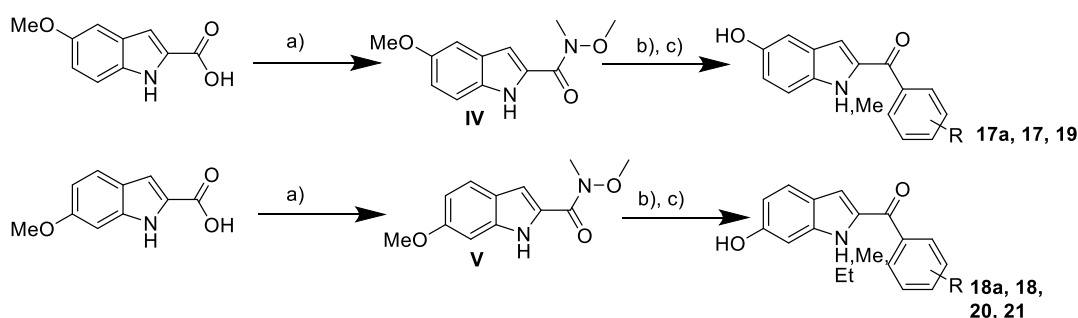
The synthesis of compounds **10-16** was performed according to the synthetic pathway shown in Scheme 2. A Rap-Stoermer reaction of commercially available salicylaldehydes or 2-hydroxy-4-methoxyacetophenones with phenacyl bromides in the presence of anhydrous potassium carbonate afforded the methoxy intermediates **10a**, **12a** and **14a-16a** (not depicted) which were demethylated using boron tribromide to yield compounds **10-16**.



^a Reagents and conditions : (a) K_2CO_3 , acetonitrile, RT, 18 h; (b) BBr_3 , $-78^\circ C$, 4 h.

Scheme 2: Synthesis of compounds **10-16**^a

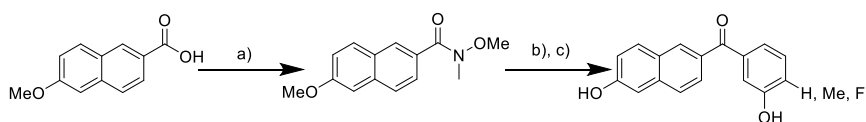
Compounds **17-21**, containing an indole core, were prepared starting from the 5-methoxy- or 6-methoxyindole-2-carboxylic acids (Scheme 3). The carboxylic acids were converted into Weinreb amides and reacted with a 3-methoxyphenyl Grignard reagent to give the corresponding ketones. The intermediate compounds **17a** and **18a** were submitted either to an ether cleavage with boron tribromide to give the desired compounds **17** and **18** or additionally subjected to N-alkylation with respective alkyl iodides in THF. Subsequent ether cleavage afforded products **19-21** in good yields.



^a Reagents and conditions : (a) N,O-dimethylhydroxylamine hydrochloride, EDC, NEt_3 , DMAP, DCM, $0^\circ C$ – RT, 18 h; (b) bromoisole, Mg, I_2 , THF, reflux – $0^\circ C$; (c) alkyl iodide, NaH, THF, $0^\circ C$ – RT, 12 h.

Scheme 3: Synthesis of compounds **17a-21**^a

Scheme 4 depicts the synthesis of compounds **22-25**. Briefly, (6-methoxynaphthalen)-2-carboxylic acid was coupled with variously substituted lithiated anisoles according to procedure D (see Experimental). The ketones were reacted with boron tribromide to give the final compounds **22-25**.



^a *Reagents and conditions:* (a) 1) N,O-dimethylhydroxylamine hydrochloride, EDC, NEt₃, DMAP, DCM, 0°C – RT, 18 h; (b) bromoanisole, nBuLi, THF, -78°C – RT, 2 h; (c) BBr₃, -78°C, 4 h.

Scheme 4: Synthesis of compounds 22-25^a

Structure–activity relationships

In a first screening, the percentage of inhibition was measured at a fixed test compound concentration of 1 μM (Table 1). Compound **A** was used as reference, showing 91% inhibition of 17β-HSD1 and 50% inhibition of 17β-HSD2 at 1 μM, respectively (Table 1). The benzothiophene system was well tolerated by the enzyme, as compound **1** was highly active (81% inhibition at 1 μM; IC₅₀ = 132 nM, Table 2). In order to optimize the potency and/ or selectivity of **1**, the substitution pattern at the phenyl ring was modified. The importance of the hydroxyl groups in the benzothiophene and phenyl moieties was revealed after biological evaluation of compounds **2** and **3**, respectively. Interestingly, the lack of a hydroxyl function at the benzothiophene did not induce a significant change in the enzyme inhibition (IC₅₀s of **3** vs. **1**: 208 vs. 132 nM, Table 2), whereas the absence of the phenolic hydroxyl almost completely abolished the inhibitory activity (**2**, 13% residual inhibition at 1 μM, Table 1). Obviously, the phenolic OH group is much more important for the potency than the OH at the benzothiophene moiety. The fact that compound **4**, in which the *meta*-hydroxyl function was replaced by *meta*-carbonitrile, revealed only a weak activity (19% inhibition at 1 μM), suggested that an H-bond donor group was essential in this area, or that the H-bond acceptor in the nitrile function was not in a proper position. Shifting of the methoxy or the hydroxyl function from the *meta*- to the *para*-position (compounds **5** and **6**, respectively) was not well tolerated, highlighting the *meta*-position as optimal substitution site for the H-bond donor function. In spite of their weak activity, the *para*-substituted analogs confirmed the importance of an H-bond donor, as the activity of the methoxy derivative **5** was reduced even stronger than that of hydroxyl analogue **6** (14% vs. 39% inhibition at 1 μM, respectively, Table 1).

Introduction of a second substituent, such as *para*-methyl, in the phenyl ring of the benzothiophene class did not improve potency compared to the prototype compound **1** (75% inhibition at 1 μM for **7**). However, the substitution by fluorine at the same position increased the inhibitory activity slightly (**8**, IC₅₀ = 89 nM, Table 2). This fluorine effect could be explained by an enhancement of the positive potential of the essential hydrogen at the adjacent hydroxyl group. However, fluorine substitution did not have a large impact on the potency in general (cf. also the 2-fluoro isomer **9**); fluorine rather acted as a bioisoster for hydrogen in the phenyl ring, which might be favorable for the enhancement of metabolic stability. The benzothiazole core was exchanged by benzofuran to afford compound **10**, which displayed a moderate inhibition of 48% at 1 μM (Table 1). In general, none of the compounds synthesized in the benzofuran series (compounds **10-16**) reached similarly high levels of potency as the benzothiophene derivatives **1**, **3**, **8** and **9**, which might be explained by the less favorable geometric variables of the benzofuran scaffold, *vide infra*. In a

second step, we aimed at testing different positions of the hydroxyl groups on the benzofuran and the phenyl moiety, which could have helped to recover some of the potency. Among the corresponding isomers **10**, **12**, **14** and **15**, the most active one was compound **14** with two hydroxyl substituents in the 5- and the *meta*-position of the benzofuran and phenyl ring, respectively. However, the inhibitory potency was still clearly lower than that of **A**.

Table 1: Inhibition of human 17 β -HSD1 and 17 β -HSD2 by compounds 1-27

Compd	R ₁	R ₂	R ₃	R ₄	X	% inhibition ^a at 1 μ M	
						17 β -HSD1 ^b	17 β -HSD2 ^c
A	-	-	-	-	-	91	50
1	H	3-OH	H	5-OH	S	81	58
2	H	H	H	5-OH	S	13	16
3	H	3-OH	H	H	S	81	70
4	H	3-CN	H	5-OH	S	19	10
5	H	4-OMe	H	5-OH	S	14	17
6	H	4-OH	H	5-OH	S	39	65
7	4-Me	3-OH	H	5-OH	S	75	36
8	4-F	3-OH	H	5-OH	S	87	84
9	2-F	5-OH	H	5-OH	S	87	60
10	H	4-OH	H	5-OH	O	48	26
11	H	4-OH	H	5-OMe	O	11	10
12	H	4-OH	H	6-OH	O	11	27
13	H	3-OH	H	5-OMe	O	34	41
14	H	3-OH	H	5-OH	O	74	38
15	H	3-OH	H	6-OH	O	66	42
16	H	3-OH	Me	6-OH	O	70	68
17	H	3-OH	H	5-OH	NH	24	25

18	H	3-OH	H	6-OH	NH	62	33
19	H	3-OH	H	5-OH	NMe	30	25
20	H	3-OH	H	6-OH	NMe	87	38
21	H	3-OH	H	6-OH	NEt	91	58
22	H	OH	-	-	-	57	46
23	4-Me	OH	-	-	-	65	34
24	4-F	OH	-	-	-	79	92
25	H	OMe	-	-	-	19	49
26	H	3-OH	H	6-OH	S	100	61
27	H	3-OH	Me	6-OH	S	97	93

[a] Mean value of three determinations, standard deviation less than 22%. [b] Human placenta, cytosolic fraction, substrate [³H]-E1, 500 nM, cofactor NADH, 500 μM. [c] Human placenta, microsomal fraction, substrate [³H]-E2, 500 nM, cofactor NAD⁺, 1500 μM.

With respect to the SAR, some of the modifications involving the hydroxyl substituents in the benzofuran derivatives produced similar effects as observed with the benzothiophene analogs, but there was also one striking difference. Analogous to the benzothiophene series, shifting the *meta*-hydroxyl substituent to the *para*-position at the phenyl ring strongly affected the activity of the benzofuran ketones (48% and 11% inhibition for compounds **10** and **12** vs. 74% and 66% for **14** and **15**, respectively). Likewise, masking of the hydrogen bond donor function on the benzofuran moiety as a methoxy group, as exemplified by **11** and **13**, also led to a reduced activity (compare with the hydroxyl analogs **10** and **15**, respectively, Table 1). However, a clear difference to the benzothiophene series was noted when the position of hydroxyl was changed from 5 in **14** to 6 in **15**. While this modification resulted in a drop of potency, the opposite was found with the benzothiophene analogs: the 6-hydroxy derivative **26** exhibited the highest inhibitory activity in this study (100% inhibition at 1 μM), and turned out to be more potent than the reference compound **A** (see also Table 2). Surprisingly, the indole scaffold showed a trend more similar to the benzothiophenes in this regard, notwithstanding that the molecule geometry resembled rather that of the benzofurans (cf. Table 3 and below); while the 5-hydroxyindole compound **17** and its *N*-methylated cognate **19** invariantly displayed weak activity (24% and 30% inhibition at 1 μM, respectively), the 6-hydroxyindole derivatives **18** and **20** were considerably more potent. This difference between the benzofurans and the indols might be determined by the furan oxygen lone pair, which is not available in the indole nitrogen and might force the benzofuran ring – in contrast to the indole ring – to accommodate an anti-periplanar position with respect to the carbonyl oxygen due to electrostatic repulsion.

The new indole core offered the opportunity to test the effect of substituents at the heteroatom. It became evident that the H-bond donor function of the indole needs to be masked by methylation

to enhance the binding affinity (cf. the methylated derivative **20** vs. **18**, Table 1), consistent with a rather hydrophobic character of the binding site. To explore the possibility of addressing an additional hydrophobic sub-pocket in the 17 β -HSD1 binding site, we replaced the methyl substituent by ethyl (**21**). Indeed, this larger substituent was tolerated as well, however at the expense of selectivity against 17 β -HSD2 (Table 2). The same observation was made after addition of a methyl at the 3-position of the benzofuran (**16**) or the benzothiophene ring (**27**). Since these alkylations were tolerated but did not improve the activity, it might be speculated that any increase in hydrophobic interactions was counteracted by less favorable H-bond formations, which, on the other hand, were important for a directed, selective interaction with 17 β -HSD1. In summary, though the indole system provided a better scaffold for 17 β -HSD1 inhibition than the benzofuran, our preliminary SAR suggested that it cannot be optimized to reach the 10 times higher potency of the benzothiophene **26**.

Table 2: IC₅₀ values and selectivity factors of selected compounds.

Compd.	IC ₅₀ ^a (nM)		SF ^d
	17 β -HSD1 ^b	17 β -HSD2 ^b	
A	44	1035	23
1	132	301	3
3	208	227	1
8	89	221	2
9	147	601	4
20	177	1822	10
21	135	469	3
26	13	500	40
27	44	85	2

[a] Mean value of three determinations, standard deviation less than 22%. [b] Human placenta, cytosolic fraction, substrate [³H]-E1, 500 nM, cofactor NADH, 500 μ M. [c] Human placenta, microsomal fraction, substrate [³H]-E2, 500 nM, cofactor NAD⁺, 1500 μ M. [d] Selectivity factor (SF): IC₅₀(17 β -HSD2)/IC₅₀(17 β -HSD1).

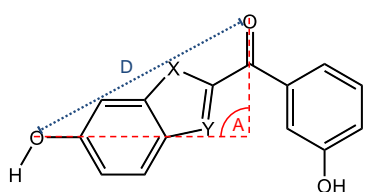
Intrigued by known hydrophobic character of the binding site and the presence of a naphthalene moiety in some highly potent 17 β -HSD1 inhibitors³², we also synthesized a few naphthol derivatives. Compound **22** turned out to be a moderate inhibitor of 17 β -HSD1 (57% inhibition at 1 μ M). Like with the bioisosteric benzothiophene scaffold, we tested the effects of small substituents (Me or F) adjacent to hydroxyl on phenyl ring. Interestingly, the naphthalene ring did not fully mimic the benzothiophene in our inhibitor series, as both the introduction of methyl and fluorine resulted in an increase in activity (65% inhibition for **23** and 79% for **24** at 1 μ M), suggesting a somewhat different

binding mode of the naphthalene derivatives. Therefore we tested whether the H-bond donor function of the *m*-OH group in the phenyl ring was dispensable; however, the change to methoxy led to a significant loss in inhibitory efficiency (**25**, 19% inhibition at 1 μ M).

Optimum geometry for 17 β -HSD1 inhibition.

Having explored the SAR of different core heterocycles in our series of analogs, we were able to derive some general structural requirements for a potent 17 β -HSD1 inhibition, which might be useful to refine the pharmacophoric model. As the most obvious effect, the type of heterocycle (or naphthalene) strongly influenced the overall geometry of the compounds. We compared in this regard the most potent benzothiazole derivative **26** with the corresponding benzothiazole (**A**), benzofuran (**15**), and indole (**18**) analogs after energy minimization. As can be seen from Table 3, both the enclosed angle and the distance between the hydroxyl substituent and the central carbonyl function is greatly determined by the type of the involved heteroatom(s). The larger angles and distances were clearly associated with the more potent compounds **A** and **26**, whereas both the benzofuran and the indole derivatives, represented by **15** and **18**, respectively, failed to reach the optimum values; this is probably one major reason for suboptimal H-bond interactions of either the hydroxyl or the ketone function, thus accounting for the generally lower potency of the latter benzoheterocycle derivatives. Consistent with this notion, the shifting of the hydroxyl substituent from the 6 to the 5-position (compounds **14** and **17**) finally could not raise the potency to the levels observed with **A** and **26**, underlining the importance of the overall geometric properties brought about by the heterocycle.

Table 3: Correlation of potencies with geometric parameters of the benzoheterocycle moiety.



Compd.	15	18	A	26
D (Å)	7.61	7.57	8.01	8.26
A	84,6°	81,2°	96,8°	105°
Potency	66% inh. at 1 μ M	62% inh. at 1 μ M	44 nM (IC ₅₀)	13 nM (IC ₅₀)
X	O	NH	S	S
Y	CH	CH	N	CH

addition, the sulfur atom adopted an anti-periplanar position with respect to the keto function, which differed from the sulfur position in A-1 (cf. Figure 2). To identify conformers with local energetic minima, an energy profiling was performed by variegating the dihedral angles of both single bonds starting from conformer 26-1. We thus found a second low-energy conformer, 26-2, exhibiting an energy content which was only marginally higher than that of 26-1 ($\Delta E = 2.8$ kJ/mol) (Figure 3). Intriguingly, this conformation 26-2 coincided with the predicted biologically active conformation. The phenolic ring enclosed a dihedral angle of about 45° , while the benzothiophene sulfur pointed to the ketone side like in A. Hence, the benzothiophene scaffold provided a great deal of conformational pre-organization favorable for binding to the 17β -HSD1 active site.

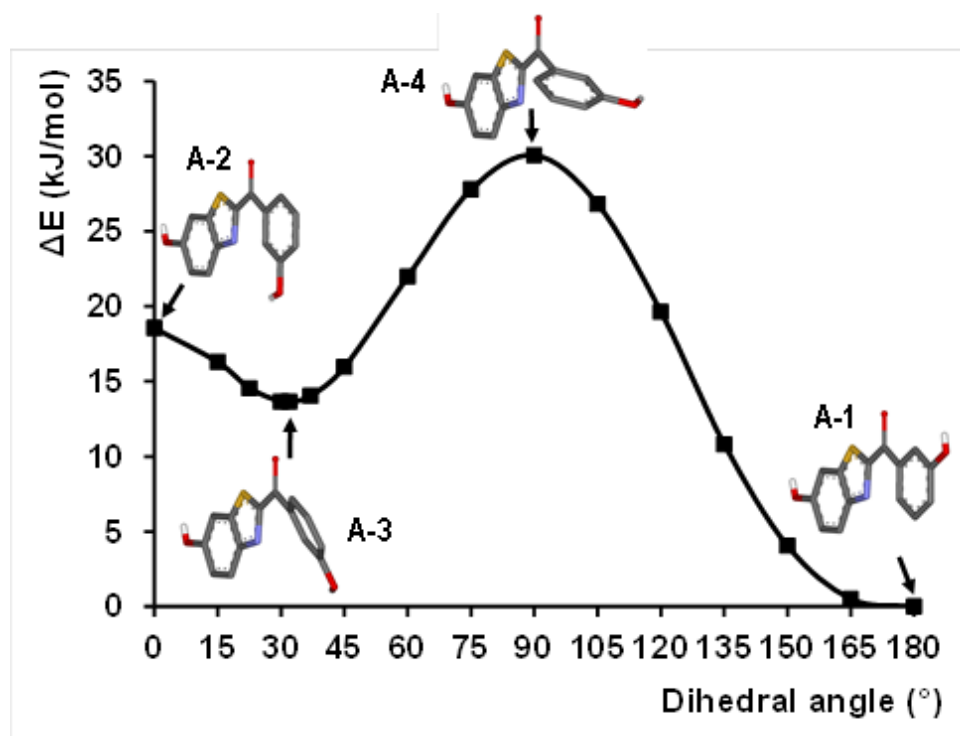


Figure 2: Energetic profile of compound A rotamers, The ordinate shows the calculated energy difference relative to the lowest-energy conformer (A-1) as a function of the dihedral angle between the phenol ring and the carbonyl plane. From left to right, the phenol ring was rotated counter-clockwise. A-4 depicts the highest-energy rotamer with a dihedral angle of 90° , while A-3 falls into a local minimum and is mostly identical to the predicted biologically active conformer.

In summary, the energetic difference between the lowest energy conformer and the biologically active conformer was considerably lower for **26** (2.8 kJ/mol) than for **A** (12.6 kJ/mol), which might partially account for the higher potency of **26**. However, the relative loss of binding affinity of **A** is much lower than these calculations may suggest; it must also be taken into consideration that in **26**, the benzothiophene ring can adopt two energetically equivalent, nearly coplanar positions with the ketone group differing by 180° (26-1 and 26-2, Figure 3). Hence, compound **A** clearly possesses the advantage of a lower entropic penalty when this molecule part binds to the 17β -HSD1 pocket, since the benzothiazole is rather fixed in one coplanar orientation. Probably this entropic advantage levels the higher energetic penalty for **A**. Further potential factors influencing this balance, such as differences in the hydration state of the two molecules, which would have a strong impact on the hydrophobic effect, can rather be excluded. The lone pair of the nitrogen in **A** is at least not fully

available to a water molecule since it is fixed and thus shielded by the predicted non-classical H-bond interaction (cf. Figure 1).

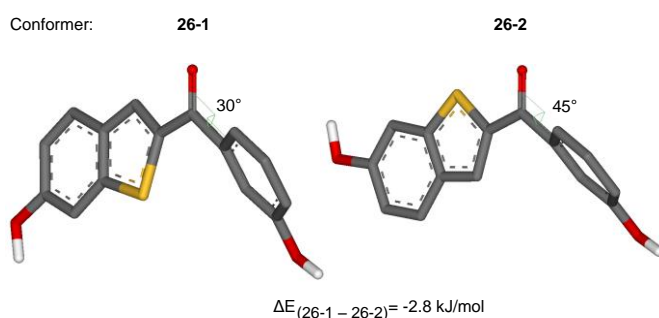


Figure 3: Calculated lowest-energy conformations of compound 26. The energies of the two identified conformers are comparable (only 2.8 kJ/mol lower with 26-1), suggesting an equal distribution in the equilibrium. Among these conformations, 26-2 is identical to the biologically active conformation as predicted previously^[33] (cf. A-3 in Figure 2).

Of note, our energy calculations for two different benzoheterocyclic classes of potent 17 β -HSD1 inhibitors converged to a consensus low-energy conformation (A-3 and 26-2, Figures 2 and 3), which was very similar to the predicted biologically active conformation, thus essentially supporting the molecular docking model as proposed by us.^[33]

Selectivity: Inhibition of human 17 β -HSD2

Since 17 β -HSD2 catalyzes the inactivation of E2 to E1, it should not be affected by 17 β -HSD1 inhibitors. Hence we assessed the activity of our new compounds against this potential off-target in a counter-screen. The IC₅₀ values as well as selectivity factors (IC₅₀ (17 β -HSD2)/IC₅₀ (17 β -HSD1)) of the most active compounds are presented in Table 2. The 6-hydroxylated compounds **20** and **26** are 10 and 40 times more potent against 17 β -HSD1 than against 17 β -HSD2, respectively. In fact, the benzothiophene derivative **26** was the most selective compound identified in this report. In contrast, the corresponding 5-hydroxy-substituted derivatives were not only less potent but also less selective (**1** and **19**). These observations indicated that the position of the hydroxyl substituent has a major impact on selectivity, especially in the benzothiophene and the indole class. Remarkably, enlargement of the alkyl at the indole nitrogen slightly improved the activity but was unfavorable for the selectivity (compare **21** with **20**, Table 2), suggesting that a similar hydrophobic sub-pocket which accommodated the alkyl substituent was present in both 17 β -HSD isoforms. Omission of the 5-hydroxyl at the benzothiophene induced a complete loss of selectivity (**3**, SF = 1), indicating that the interaction partner for this OH is only present or accessible in 17 β -HSD1. Interestingly, moving the *m*-OH group to the *para*-position in the benzothiophene class (**6**) or introduction of fluorine next to OH on the phenyl ring in the naphthalene series (**24**) changed the affinity in favor of the type 2 isoenzyme. The methoxyphenyl naphthalene derivative **25** was also a moderate inhibitor of 17 β -HSD2. A similar switch of the isoenzyme preference due to a change of the hydroxyl substitution positions was observed earlier with the (hydroxyphenyl)naphthalene class of HSD1 inhibitors which then provided access to selective HSD2 inhibitors.^[24,38] In addition, the hydroxyl of the naphthol moiety was found to be dispensable for 17 β -HSD1 inhibition like observed with the benzothiophene

derivative **3**, suggesting a similar binding mode for both compound classes. In the light of these similarities, compound **6** might serve as a starting point for the development of new 17 β -HSD2 inhibitors.

Conclusion

Using a core heterocycle replacement strategy, we were able to discover the new 6-hydroxybenzothiophene derivative **26** which displayed a better activity/selectivity profile than the starting compound **A** (IC_{50} =13 nM and SF =40 for **26** vs. IC_{50} =44 nM and SF =23 for **A**), establishing the hydroxybenzothiophene ketone derivatives as new chemical class of 17 β -HSD1 inhibitors. Using **26** as a new lead structure, the introduction of further substituents might increase the potency of this compound class to the single digit nanomolar range. In addition, a permutation of the hydroxyl substitution pattern might even provide access to a new 17 β -HSD2 inhibitor scaffold.

Furthermore, our systematic heteroatom exchange identified the optimum distance of the hydroxyl at the benzoheterocycle and the ketone oxygen (8.0 – 8.3 Å, Table 3) as well as the angle enclosed between the corresponding oxygen atom's bonds (96.8 – 105°). In addition, our calculations suggested that the dihedral angle involving the single bond linking the phenol ring should range from about 30 to 45°. The energetically favorable consensus conformation of the potent inhibitors **A** and **26** was in agreement with the predicted biologically active conformation of **A** in our previously reported binding model.^[33] Hence, the distances and vectors for all essential H-bond donor/acceptor functions crucial for biological activity could be ascertained, which will allow a refinement of our pharmacophoric model in order to search for novel active 17 β -HSD1 inhibitors *in silico*. Furthermore, our results provided evidence that the thiazole nitrogen of the hydroxybenzothiazole ketone is not relevant for the interaction with the target site, which is also in line with the predicted binding model for **A**.

Experimental Section

Chemistry

Chemical starting material was purchased from Sigma-Aldrich, CombiBlocks or Alfa Aesar and used without further purification. Purity of the compounds was determined using an Agilent 1100 series HPLC system from Agilent Technologies (UV detection: Agilent 1100 Series DAD at 254 nm,), a GC Trace Ultra from Thermo or a Waters auto-purification system from Waters Corporation. The purity of the compounds used in the biological assays was \geq 95%. Mass spectra (ESI) were measured on an AB Sciex Qtrap2000 from AB Sciex or a Waters 3100 Mass detector from Waters Corporation. Mass spectra (EI) were measured on a DSQ II from Thermo. ^1H and ^{13}C NMR spectra were recorded on either a Bruker DRX-500 (^1H , 500 MHz; ^{13}C , 126 MHz) instrument at 300 K or on a Bruker Fourier 300 (^1H , 300 MHz; ^{13}C , 75 MHz) NMR spectrometer at 300 K in the deuterated solvents indicated. Coupling constants (J) are given in hertz (Hz). Flash column chromatography was performed using silica gel 60 (Merck, 35-70 μm). Reaction/flash monitoring was done by TLC on ALUGRAM SIL G/UV₂₅₄ (Macherey-Nagel) employing UV detection

Procedure A, general synthesis of methyl benzothiophene-2-carboxylates: A suspension of 2 eq. of potassium carbonate in 20 ml of dry DMF was cooled to 0°C and 1.2 eq. of methyl thioglycolate was carefully added. The solution was stirred for 20 min at 0°C under nitrogen and a solution of 1 eq. of

the corresponding 2-fluorobenzaldehyde or 2-fluoroacetophenone in 10 ml of DMF was added dropwise. Then, the mixture was heated to 70°C and stirred for 4 hours. The suspension was cooled to room temperature and poured into 60 ml of 10 % citric acid. The aqueous layer was extracted with ethyl acetate (5x) and the combined organic layer was thoroughly washed with small amounts of water and brine (10x), and dried over magnesium sulphate. The solvent was removed *in vacuo* and the resulting yellow solid was recrystallized in ethanol to give the carboxylic ester in different yields.

Procedure B, general synthesis of benzo[b]thiophene-2-carboxylic acids: The carboxylic acids were released from the corresponding methyl benzo[b]thiophene-2-carboxylates by hydrolysis with potassium hydroxide. Therefore the methyl ester was dissolved in 5 ml of ethanol and 2.5 ml of water was added. Then 4 eq of potassium hydroxide was added and the mixture was heated to reflux for 2 hours. The solvent was removed under reduced pressure and the resulting potassium salt was dissolved in a small volume of water, cooled to 0°C before conc. HCl was carefully added dropwise to adjust the pH to 1. Then the aqueous layer was extracted with diethyl ether (5x) and the combined organic layer was dried over magnesium sulphate, filtered off, and concentrated *in vacuo*. The crude carboxylic acid was recrystallized from ethanol.

Procedure C, general synthesis of Weinreb amides: The corresponding carboxylic acid was dissolved in 5 ml of dichloromethane and cooled to 0°C. To this solution, 1.1 eq. of *N,O*-dimethylhydroxylamine hydrochloride, 0.1 eq. of dimethylaminopyridine, 1.2 eq. of *N*-(3-dimethylaminopropyl)-*N'*-ethylcarbodiimide, and 6 eq. of triethylamine were added successively. After 60 min the solution was allowed to warm to room temperature and was stirred over night at room temperature. The reaction was quenched by addition of 10 % citric acid and the organic layer was separated. The aqueous layer was neutralized by addition of saturated NaHCO₃ and extracted with dichloromethane (4x). The combined organic layer was washed with water and brine, and dried over magnesium sulfate. The solvent was removed *in vacuo* to give the Weinreb amides as solid in sufficient purity.

Procedure D, Weinreb ketone synthesis. A solution of the corresponding bromo-substituted anisole in dry THF was purged with nitrogen and cooled to -78°C. Then, 1.2 eq. of *n*-butyl lithium (2.5 M in hexanes) were added drop-wise, so that temperature did not exceed -70°C, and the solution was stirred for 1 hour at -78°C. Then 1 eq. of the corresponding Weinreb amide dissolved in 5 ml of THF was then added slowly and the reaction was stirred for 10 minutes at -78°C before it was allowed to warm to room temperature. The reaction was stopped after stirring 30 min at room temperature by addition of 10 ml of 1N HCl. The crude product was extracted with diethyl ether (4x) and the combined organic layer was washed with saturated NaHCO₃, water and brine. Then the solvent was dried over magnesium sulphate, removed *in vacuo*, and the crude product was purified by flash column chromatography.

Procedure E, methyl ether cleavage: The corresponding methyl ether was dissolved in 10 ml of dry dichloromethane and cooled to -78°C. Then, 6 eq. of boron tribromide solution (1M in dichloromethane) was slowly added, and the mixture was allowed to warm to room temperature. The progress of the reaction was monitored by TLC. When the starting material was completely converted, the reaction was stopped by addition of 10 ml of water. The crude product was extracted with ethyl acetate (4x), and the combined organic layer was subsequently washed with water and

brine, dried over magnesium sulphate, and the solvent was removed under reduced pressure. The resulting solid was purified by flash column chromatography, eluting with ethyl acetate/hexane

Procedure F, Rap Stoermer reaction for the synthesis of benzofurans: 1.1 eq. of the corresponding 2-Bromoacetophenone and 2 eq. of Cs_2CO_3 were dissolved in 5 ml of acetonitrile and stirred under nitrogen. After 30 min 1 eq. of a methoxy substituted 2-hydroxybenzaldehyde was added and the mixture was stirred over night at room temperature. After completion of the reaction a precipitate was formed and dissolved in ethyl acetate. The solution was subsequently washed with water and brine. The organic layer was dried over magnesium sulphate, the solvent was evaporated *in vacuo*, and the crude product was purified by flash column chromatography eluting with ethyl acetate/hexane 1:3 to give the benzofurans in varying yields.

Procedure G, N-alkyl nucleophilic substitution: A solution of methanone derivative (1 eq.) in anhydrous THF was treated with sodium hydride (1.4 eq.), (60% suspension in paraffine oil) at 0 °C. After 30 min, 5 eq. of methyl iodide was added and stirring was continued for 12 h at room temperature. Saturated NaHCO_3 was used to stop the reaction. The aqueous layer was extracted with ethyl acetate. The combined organic layer was dried over magnesium sulphate, filtered and concentrated to dryness. The product was purified by column chromatography

Synthesis of I, methyl 5-methoxybenzo[b]thiophene-2-carboxylate: The title compound was synthesized from 2-fluoro-5-methoxybenzaldehyde using procedure A to yield 2 g (9 mmol, 25 %) of I as a light yellow solid. ^1H NMR (Acetone- d_6 , 500MHz): δ = 8.04 (s, 1 H), 7.88 (d, $J=9.1$ Hz, 1 H), 7.51 (d, $J=2.2$ Hz, 1 H), 7.17 (dd, $J=8.8, 2.5$ Hz, 1 H), 3.91 (s, 3 H), 3.88 ppm (s, 3 H); ^{13}C NMR (Acetone- d_6 , 126MHz): δ = 163.5, 159.1, 140.9, 135.4, 135.2, 131.1, 124.4, 119.1, 107.6, 55.9, 52.8 ppm; Purity(UV) = 98 %; t_R :min, ESI-MS $[\text{M}+\text{H}]^+$: 223.08; calcd. $[\text{M}]^+$: 222.04.

Synthesis of II, 5-methoxybenzo[b]thiophene-2-carboxylic acid: The title compound was synthesized from I using procedure B to give 0.83 g (3.7 mmol, 68 %) of II as a white solid which was directly used for the synthesis of III without further characterization other than NMR. ^1H NMR (DMSO- d_6 , 300MHz): δ = 13.40 (s, 1 H), 8.01 (s, 1 H), 7.91 (d, $J=8.9$ Hz, 1 H), 7.52 (d, $J=2.4$ Hz, 1 H), 7.15 (dd, $J=8.8, 2.5$ Hz, 1 H), 3.82 ppm (s, 3 H); ^{13}C NMR (DMSO- d_6 , 75MHz): δ = 164.0, 157.9, 140.3, 136.1, 134.3, 130.4, 124.2, 118.2, 107.5, 55.8 ppm.

Synthesis of III, N,5-dimethoxy-N-methylbenzo[b]thiophene-2-carboxamide: The title compound was synthesized from II using procedure C to give 3.3 g (1.3 mmol, 53 %) of III as colorless needles after recrystallization from ethanol. ^1H NMR (Acetone- d_6 , 500MHz): δ = 8.13 (d, $J=0.6$ Hz, 1 H), 7.81 - 7.86 (m, 1 H), 7.49 (d, $J=2.5$ Hz, 1 H), 7.13 (dd, $J=8.8, 2.5$ Hz, 1 H), 3.88 (s, 3 H), 3.86 (s, 3 H), 3.36 ppm (s, 3 H); ^{13}C NMR (Acetone- d_6 , 126MHz): δ = 162.7, 158.8, 140.5, 136.2, 131.1, 123.9, 118.5, 107.3, 62.3, 55.8, 33.3 ppm; Purity(UV) = 99 %; t_R : 6.95 min, ESI-MS $[\text{M}+\text{H}]^+$: 252.06; calcd. $[\text{M}]^+$: 251.06.

Synthesis of compound 1a, (5-methoxybenzo[b]thiophen-2-yl)(3-methoxyphenyl)methanone: The title compound was synthesized according to procedure D using 3-bromoanisole and III to give 0.36 g (1.14 mmol, 64 %) of 1a as pale yellow solid. ^1H NMR (CDCl_3 , 300MHz): δ = 7.83 (s, 1 H), 7.78 (d, $J=8.9$ Hz, 1 H), 7.48 - 7.54 (m, 1 H), 7.40 - 7.48 (m, 2 H), 7.30 (d, $J=2.4$ Hz, 1 H), 7.13 - 7.20 (m, 2 H), 3.90 (s, 3 H), 3.88 ppm (s, 3 H); ^{13}C NMR (CDCl_3 , 75MHz): δ = 189.3, 159.7, 157.9, 144.0, 140.0, 139.2, 135.6, 131.9, 129.5, 123.6, 121.8, 118.7, 118.6, 113.9, 106.9, 55.6, 55.5 ppm; Purity(UV) = 98 %; t_R : 17.7 min, ESI-MS $[\text{M}+\text{H}]^+$: 299.17; calcd. $[\text{M}]^+$: 298.07.

Synthesis of compound 1, (5-hydroxybenzo[b]thiophen-2-yl)(3-hydroxyphenyl)methanone: The title compound was synthesized from **1a** according to procedure E to give 0.12 g (0.4 mmol, 70 %) of **1** as a pale yellow solid. ¹H NMR (DMSO-d₆, 300MHz): δ = 9.89 (s, 7 H), 9.69 (s, 1 H), 7.95 (d, J=0.4 Hz, 1 H), 7.86 (d, J=8.8 Hz, 1 H), 7.36 - 7.43 (m, 2 H), 7.29 - 7.34 (m, 1 H), 7.21 - 7.25 (m, 1 H), 7.04 - 7.11 (m, 2 H) ppm; ¹³C NMR (DMSO-d₆, 75MHz): δ = 189.2, 158.0, 155.9, 143.3, 140.9, 139.0, 133.3, 132.9, 130.3, 124.1, 120.3, 120.2, 119.3, 115.8, 110.8 ppm; Purity(UV) = 98 %; t_R: 13.04 min, ESI-MS [M+H]⁺: 271.14 ; calcd. [M]⁺: 270.04.

Synthesis of compound 2a, (5-methoxybenzo[b]thiophen-2-yl)(phenyl)methanone: The title compound was synthesized according to procedure D using 1-bromobenzene and **III**. The crude product was purified by flash column chromatography eluting with hexane/ethyl acetate 4:1 to give 0.22 g (0.82 mmol, 56 %) of **2a** as a white solid. ¹H NMR (CDCl₃, 500MHz): δ = 7.78 - 7.80 (m, 1 H), 7.77 (d, J=1.4 Hz, 1 H), 7.65 (d, J=0.6 Hz, 1 H), 7.62 (m, 1 H), 7.46 - 7.51 (m, 1 H), 7.37 - 7.41 (m, 2 H), 7.15 (d, J=2.4 Hz, 1 H), 7.00 (dd, J=8.8, 2.5 Hz, 1 H), 3.73 ppm (s, 3 H); ¹³C NMR (CDCl₃, 126MHz): δ = 189.4, 157.8, 143.9, 139.9, 137.8, 135.4, 132.3, 131.8, 129.1, 128.4, 123.5, 118.5, 106.8, 55.4 ppm; Purity(UV) = 98 %; t_R: 17.63 min, ESI-MS [M+H]⁺: 269.16; calcd. [M]⁺: 268.08.

Synthesis of compound 2, (5-hydroxybenzo[b]thiophen-2-yl)(phenyl)methanone: The title compound was synthesized from **2a** according to procedure E. The crude product was purified by flash column chromatography, eluting with hexane/ethyl acetate 3:1. The resulting brown solid was recrystallized from ethanol to give 0.13 g (0.5 mmol, 61 %) of **2** as a white solid. ¹H NMR (Acetone-d₆, 500MHz): δ = 8.65 (s, 1 H), 7.93 - 7.94 (m, 1 H), 7.91 - 7.92 (m, 1 H), 7.87 (d, J=0.5 Hz, 1 H), 7.84 - 7.87 (m, 1 H), 7.66 - 7.71 (m, 1 H), 7.57 - 7.61 (m, 2 H), 7.43 (d, J=2.5 Hz, 1 H), 7.16 (dd, J=8.7, 2.4 Hz, 1 H) ppm; ¹³C NMR (Acetone-d₆, 126MHz): δ = 190.7, 157.4, 145.6, 142.6, 139.8, 135.8, 134.2, 133.8, 130.8, 130.4, 125.4, 120.4, 112.0 ppm; Purity(UV) = 98 %; t_R: 14.85 min, ESI-MS [M+H]⁺: 255.15 ; calcd. [M]⁺: 254.04.

Synthesis of compound 3a, benzo[b]thiophen-2-yl(3-methoxyphenyl)methanone: The title compound was synthesized using 3-bromoanisole and *N*-methoxy-*N*-methylbenzo[b]thiophene-2-carboxamide according to procedure D. The Weinreb amide was generated from commercially available benzo[b]thiophene-2-carboxylic acid according to procedure C and directly used without further purification. The product was purified by flash column chromatography eluting with hexane/ethyl acetate 4:1 to give 0.37 g (1.37 mmol, 75%) of **3a** as a white solid. ¹H NMR (CDCl₃, 500MHz): δ = 7.93 (ddd, J=8.4, 1.9, 0.9 Hz, 0 H), 7.88 - 7.91 (m, 2 H), 7.50 - 7.53 (m, 1 H), 7.47 - 7.50 (m, 1 H), 7.45 - 7.47 (m, 1 H), 7.44 - 7.45 (m, 1 H), 7.41 - 7.43 (m, 1 H), 7.18 (ddd, J=8.2, 2.6, 0.9 Hz, 1 H), 3.90 ppm (s, 3 H); ¹³C NMR (CDCl₃, 126MHz): δ = 189.3, 159.6, 143.0, 142.7, 139.1, 139.0, 132.2, 129.5, 127.4, 126.1, 125.0, 122.9, 121.8, 113.8, 55.5 ppm; Purity(UV) : 96 %; t_R: 17.76 min, ESI-MS [M+H]⁺: 269.15; calcd. [M]⁺: 268.06.

Synthesis of compound 3 benzo[b]thiophen-2-yl(3-hydroxyphenyl)methanone: The title compound was synthesized from **3a** according to procedure E purified by flash column chromatography hexane/ethyl acetate 3:1 to give 0.13 g (0.5 mmol, 76%) of **3** as a white solid. ¹H NMR (Acetone-d₆, 500MHz): δ = 8.90 (s, 1 H), 8.02 - 8.09 (m, 3 H), 7.53 - 7.57 (m, 1 H), 7.46 - 7.50 (m, 1 H), 7.41 - 7.44 (m, 2 H), 7.37 - 7.39 (m, 1 H), 7.15 - 7.18 (m, 1 H) ppm; ¹³C NMR (Acetone-d₆, 126MHz): δ = 189.6, 158.5, 143.9, 143.2, 140.3, 140.1, 133.3, 130.7, 128.5, 127.4, 126.1, 123.7, 121.3, 120.5, 116.4 ppm; Purity(UV) = 98 %; t_R: 15.32 min, ESI-MS [M+H]⁺: 255.17; calcd. [M]⁺: 254.04.

Synthesis of compound 4a, 3-(5-methoxybenzo[b]thiophene-2-carbonyl)benzonitrile: The title compound was synthesized according to procedure D using 1-bromo-3-cyanobenzene and **III**. The crude product was purified by flash column chromatography eluting with hexane/ethyl acetate 4:1 to give 0.52 g (1.8 mmol, 83 %) of **4a** as a pale yellow solid. $^1\text{H NMR}$ (CDCl_3 , 500 MHz): δ = 8.18 (m, 1H), 8.13 (ddd, J = 1.5 Hz, J = 2.0 Hz, J = 7.5 Hz, 1H), 7.89 (m, 1H), 7.79-7.76 (m, 2H), 7.66 (m, 1H), 7.31 (d, J = 2.5 Hz, 1H), 7.18 (dd, J = 2.5 Hz, J = 9.0 Hz, 1H), 3.88 (s, 3H); $^{13}\text{C NMR}$ (CDCl_3 , 126 MHz): δ = 187.2, 158.1, 142.7, 139.9, 138.9, 135.8, 135.3, 133.1, 132.6, 132.3, 129.6, 123.6, 119.4, 117.9, 113.0, 106.9, 55.5. Purity (UV): 98 %; t_{R} : 16.76 min.

Synthesis of compound 4, 3-(5-hydroxybenzo[b]thiophene-2-carbonyl)benzonitrile: The title compound was synthesized from **4a** according to procedure E. The crude product was purified by flash column chromatography, eluting with hexane/ethyl acetate 3:1. The resulting brown solid was recrystallized from ethanol to give 0.16 g (0.57 mmol, 66 %) of **5** as a light yellow solid. $^1\text{H NMR}$ (Acetone- d_6 , 500MHz): δ = 8.67 (br. s, 1 H), 8.29 - 8.31 (m, 1 H), 8.21 - 8.24 (m, 1 H), 8.09 (m, 1 H), 7.99 (s, 1 H), 7.88 (d, J =8.8 Hz, 1 H), 7.82 - 7.86 (m, 1 H), 7.43 (d, J =2.4 Hz, 1 H), 7.18 ppm (dd, J =8.7, 2.4 Hz, 1 H); $^{13}\text{C NMR}$ (Acetone- d_6 , 126MHz): δ = 189.0, 157.5, 144.6, 142.6, 140.8, 137.2, 136.1, 134.9, 134.8, 134.2, 131.8, 125.4, 120.9, 119.5, 114.6, 112.1 ppm; Purity(UV) = 98 %; t_{R} : 14.47 min, MS(EI) $[\text{M}]^+$: 278.9; calcd. $[\text{M}]^+$: 279.04.

Synthesis of compound 5a, (5-methoxybenzo[b]thiophen-2-yl)(4-methoxyphenyl)methanone: The title compound was synthesized according to procedure D using 4-bromoanisole and **III**. The crude product was purified by flash column chromatography eluting with hexane/ethyl acetate 4:1 to give 0.24 g (0.8 mmol, 70 %) of **5a** as a white solid. $^1\text{H NMR}$ (CDCl_3 , 500MHz): δ = 7.95 - 7.97 (m, 1 H), 7.94 - 7.95 (m, 1 H), 7.78 (d, J =0.8 Hz, 1 H), 7.75 - 7.77 (m, 1 H), 7.29 (d, J =2.5 Hz, 1 H), 7.13 (dd, J =8.8, 2.5 Hz, 1 H), 7.01 - 7.03 (m, 1 H), 7.00 - 7.01 (m, 1 H), 3.91 (s, 3 H), 3.87 ppm (s, 3 H); $^{13}\text{C NMR}$ (CDCl_3 , 126MHz): δ = 190.5, 187.8, 163.0, 157.6, 144.0, 139.8, 134.9, 131.5, 130.6, 130.2, 123.3, 118.0, 113.5, 106.5, 55.3, 55.3 ppm; Purity(UV) =98 %; t_{R} : 17.48 min, ESI-MS $[\text{M}+\text{H}]^+$: 299.17; calcd. $[\text{M}]^+$: 298.07.

Synthesis of (5-Hydroxybenzo[b]thiophen-2-yl)(4-methoxyphenyl)methanone 5. The title compound was synthesized from **5a** according to procedure E and purified by flash column chromatography eluting with hexane/ethyl acetate 3:1 to give 0.1 g (0.35 mmol, 53%) of **5** as a white solid. $^1\text{HNMR}$ (CD_3COCD_3): δ = 8.62 (s, 1H), 7.97-7.95 (m, 2H), 7.87 (d, J = 0.5 Hz, 1H), 7.83 (d, J = 9.0 Hz, 1H), 7.43 (d, J = 2.0 Hz, 1H), 7.15 (dd, J = 2.5 Hz, J = 8.5 Hz, 1H), 7.12-7.10 (m, 2H), 3.93 (s, 3H); $^{13}\text{CNMR}$ (CD_3COCD_3): δ = 188.2, 164.3, 156.4, 145.0, 141.7, 134.6, 132.4, 131.8, 131.2, 124.4, 119.2, 114.7, 110.9, 56.0; MS (ESI): 284.8 $[\text{M}+\text{H}]^+$. The positions of the 5-hydroxy and the 6-methoxy substituent were clarified using NOESY experiments.

Synthesis of compound 6, (5-hydroxybenzo[b]thiophen-2-yl)(4-hydroxyphenyl)methanone: The title compound was synthesized from **5a** according to procedure E and purified by flash column chromatography eluting with hexane/ethyl acetate 3:1 to give 0.13 g (0.48 mmol, 64 %) of **6** as a white solid. $^1\text{H NMR}$ (Acetone- d_6 , 500MHz): δ = 9.29 (s, 1 H), 8.63 (s, 1 H), 7.91 - 7.92 (m, 1 H), 7.89 - 7.90 (m, 1 H), 7.87 (d, J =0.5 Hz, 1 H), 7.84 (m, 1 H), 7.41 - 7.43 (m, 1 H), 7.13 (dd, J =8.7, 2.4 Hz, 1 H), 7.02 - 7.04 (m, 1 H), 7.00 - 7.02 ppm (m, 1 H); $^{13}\text{C NMR}$ (Acetone- d_6 , 126MHz): δ = 188.1, 162.6, 156.4, 145.1, 141.7, 134.5, 132.7, 131.6, 130.3, 124.4, 119.1, 116.2, 110.9 ppm; Purity(UV) = 97 %; t_{R} : 12.79 min, ESI-MS $[\text{M}+\text{H}]^+$: 271.14; calcd. $[\text{M}]^+$: 270.04.

Synthesis of compound 7a, (3-methoxy-4-methylphenyl)(5-methoxybenzo[b]thiophen-2-yl)methanone: The title compound was synthesized according to procedure D using 4-bromoanisole and **III**. The crude product was purified by flash column chromatography eluting with hexane/ethyl acetate 4:1 to give 0.34 g (1.1 mmol, 90 %) of **7a** as a pale yellow solid. ¹H NMR (CDCl₃, 500MHz): δ = 7.82 (d, *J*=0.6 Hz, 1 H), 7.75 (d, *J*=8.8 Hz, 1 H), 7.46 (dd, *J*=7.6, 1.6 Hz, 1 H), 7.39 (d, *J*=1.6 Hz, 1 H), 7.29 (d, *J*=2.5 Hz, 1 H), 7.26 (dd, *J*=7.6, 0.7 Hz, 1 H), 7.13 (dd, *J*=8.8, 2.5 Hz, 1 H), 3.91 (s, 3 H), 3.87 (s, 3 H), 2.32 ppm (s, 3 H); ¹³C NMR (CDCl₃, 126MHz): δ = 188.7, 157.6, 157.5, 143.8, 139.7, 136.3, 135.0, 132.0, 131.0, 129.9, 123.2, 121.8, 118.1, 109.8, 106.5, 55.2, 55.2, 16.2 ppm; Purity (UV) >98 %; t_R: 18.65 min, ESI-MS [M+H]⁺: 313.18; calcd. [M]⁺: 312.08.

Synthesis of compound 7, (3-hydroxy-4-methylphenyl)(5-hydroxybenzo[b]thiophen-2-yl)methanone: The title compound was synthesized from **7a** according to procedure E. The crude product was purified by flash column chromatography, eluting with hexane/ethyl acetate 4:1. The resulting pale red solid was recrystallized from ethanol to give 0.13 g (0.46 mmol, 46 %) of **4** as a white solid. ¹H NMR (Acetone-d₆, 500MHz): δ = 8.72 (s, 1 H), 8.66 (s, 1 H), 7.88 - 7.88 (m, 1 H), 7.86 - 7.84 (m, 1 H), 7.43 - 7.42 (m, 1 H), 7.40 - 7.38 (m, 1 H), 7.38 - 7.35 (m, 1 H), 7.32 - 7.29 (m, 1 H), 7.14 (dd, *J* = 2.4, 8.7 Hz, 1 H), 2.31 (s, 3 H); ¹³C NMR (Acetone-d₆, 126MHz): δ = 189.1, 156.5, 156.3, 144.9, 141.6, 137.6, 134.7, 132.3, 131.6, 130.8, 124.4, 121.6, 119.3, 115.8, 111.0, 16.4 ppm; Purity(UV) = 98 %; t_R: 13.89 min, ESI-MS [M+H]⁺: 285.15 ; calcd. [M]⁺: 284.05.

Synthesis of compound 8a, (4-fluoro-3-methoxyphenyl)(5-methoxybenzo[b]thiophen-2-yl)methanone: The title compound was synthesized according to procedure D using 5-bromo-2-fluoroanisole and **III**. The crude product was purified by flash column chromatography eluting with hexane/ethyl acetate 4:1 to give 0.36 g (1.1 mmol, 90 %) of **8a** as a white solid. ¹H NMR (CDCl₃, 500MHz): δ = 7.75 (s, 1 H), 7.72 (d, *J*=8.8 Hz, 1 H), 7.52 (d, *J*=8.2 Hz, 1 H), 7.45 - 7.50 (m, 1 H), 7.26 (s, 1 H), 7.13 - 7.19 (m, 1 H), 7.08 - 7.13 (m, 1 H), 3.93 (s, 3 H), 3.84 ppm (s, 3 H); ¹³C NMR (CDCl₃, 126MHz): δ = 188.7, 158.8, 156.0, 148.9, 144.4, 140.8, 136.3, 135.1, 132.4, 124.4, 123.9, 119.5, 116.5, 115.0, 107.7, 57.2, 56.4 ppm; Purity(UV) = 97 %; t_R: 17.59 min, ESI-MS [M+H]⁺: 317.17; calcd. [M]⁺: 316.06.

Synthesis of compound 8, (4-fluoro-3-hydroxyphenyl)(5-hydroxybenzo[b]thiophen-2-yl)methanone: : The title compound was synthesized from **8a** according to procedure E. The crude product was purified by flash column chromatography, eluting with hexane/ethyl acetate 3:1 to give 0.21 g (0.72 mmol, 63 %) of **2** as a pale yellow solid. ¹H NMR (Acetone-d₆, 500MHz): δ = 7.90 (s, 1 H), 7.84 (d, *J*=8.7 Hz, 1 H), 7.57 (dd, *J*=8.5, 2.2 Hz, 1 H), 7.48 (ddd, *J*=8.4, 4.4, 2.2 Hz, 1 H), 7.43 (d, *J*=2.4 Hz, 1 H), 7.30 (dd, *J*=10.8, 8.4 Hz, 1 H), 7.15 ppm (dd, *J*=8.7, 2.4 Hz, 1 H); ¹³C NMR (Acetone-d₆, 126MHz): δ = 189.6, 157.8, 156.4, 147.3, 145.7, 142.9, 136.9, 136.2, 133.9, 125.7, 123.9, 120.8, 120.8, 118.3, 112.3 ppm; Purity(UV) = 98 %; t_R: 13.32 min, ESI-MS [M+H]⁺: 289.14 ; calcd. [M]⁺: 288.03.

Synthesis of compound 9a, (2-fluoro-5-methoxyphenyl)(5-methoxybenzo[b]thiophen-2-yl)methanone: The title compound was synthesized according to procedure D using 3-bromo-4-fluoroanisole and **III**. The crude product was purified by flash column chromatography eluting with hexane/ethyl acetate 4:1 to give 0.3 g (0.9 mmol, 56 %) of **9a** as a pale yellow solid. ¹H NMR (CDCl₃, 500MHz): δ = 7.74 (m, 1 H), 7.71 (dd, *J*=2.2, 0.5 Hz, 1 H), 7.24 (s, 1 H), 7.09 - 7.14 (m, 2 H), 7.06 - 7.09 (m, 1 H), 7.01 - 7.05 (m, 1 H), 3.83 (s, 3 H), 3.81 ppm (s, 3 H); ¹³C NMR (CDCl₃, 126MHz): δ = 186.3,

157.9, 155.6, 153.9, 144.2, 140.0, 136.1, 132.7, 127.1, 123.7, 119.1, 118.8, 117.3, 114.1, 107.0, 56.0, 55.5 ppm; Purity(UV) = 98 %; t_R : 17.4 min, ESI-MS $[M+H]^+$: 317.15; calcd. $[M]^+$: 316.06.

Synthesis of compound 9, (2-fluoro-5-hydroxyphenyl)(5-hydroxybenzo[b]thiophen-2-yl)methanone: The title compound was synthesized from **9a** according to procedure E. The crude product was purified by flash column chromatography, eluting with hexane/ethyl acetate 3:1 to give 0.21 g (0.72 mmol, 63 %) of **3** as a pale yellow solid. 1H NMR (Acetone- d_6 , 500MHz): δ = 8.75 (s, 1 H), 8.67 (s, 1 H), 7.86 (m, 1 H), 7.80 (dd, $J=1.7, 0.7$ Hz, 1 H), 7.41 - 7.43 (m, 1 H), 7.17 - 7.19 (m, 1 H), 7.15 - 7.16 (m, 1 H), 7.07 - 7.10 (m, 1 H), 7.06 - 7.07 (m, 1 H) ppm; ^{13}C NMR (Acetone- d_6 , 126MHz): δ = 188.4, 158.2, 156.1, 154.6, 146.5, 143.2, 136.9, 135.4, 129.8, 126.2, 121.9, 121.6, 119.6, 118.1, 112.8 ppm; Purity(UV) = 98 %; t_R : 13.19 min, ESI-MS $[M+H]^+$: 289.12 ; calcd. $[M]^+$: 288.03.

Synthesis of compound 10a, (5-Methoxybenzofuran-2-yl)(4-methoxyphenyl)methanone: The title compound was prepared by reaction of 2-hydroxy-5-methoxybenzaldehyde and 2-bromo-1-(4-methoxyphenyl)ethan-1-one according to procedure F. The product was purified by column chromatography eluting with hexane/ethyl acetate 3:1 to give 0.37 g (1.3 mmol, 65 %) of **10a** as a white solid. 1H NMR ($CDCl_3$, 500MHz) δ = 8.12 (s, 1 H), 8.11 (s, 1 H), 7.53 - 7.50 (m, 1 H), 7.47 (s, 1 H), 7.13 - 7.08 (m, 2 H), 7.03 (s, 1 H), 7.01 (s, 1 H), 3.91 (s, 3 H), 3.86 (s, 3 H) ppm; ^{13}C NMR ($CDCl_3$, 126MHz) δ = 183.1, 164.0, 157.0, 153.9, 151.5, 132.4, 130.3, 128.0, 118.5, 115.9, 114.3, 113.6, 104.4, 56.3, 56.0 ppm; Purity (UV) > 95 %, ESI-MS $[M+H]^+$: 282.9, calcd $[M]^+$ 282.09.

Synthesis of compound 10, (5-hydroxybenzofuran-2-yl)(4-hydroxyphenyl)methanone: The title compound was synthesized from **10a** according to procedure E. The crude product was purified by flash column chromatography, eluting with hexane/ethyl acetate 2:1 to give 0.23 g (0.9 mmol, 58 %) of **10** as a white solid. 1H NMR (Acetone- d_6 , 500MHz): δ = 9.26 (br. s., 1 H), 8.39 (br. s., 1 H), 8.06 - 8.08 (m, 1 H), 8.04 - 8.06 (m, 1 H), 7.49 - 7.53 (m, 2 H), 7.19 (d, $J=2.4$ Hz, 1 H), 7.08 (dd, $J=8.8, 2.5$ Hz, 1 H), 7.02 - 7.04 (m, 1 H), 7.00 - 7.02 ppm (m, 1 H); ^{13}C NMR (Acetone- d_6 , 126MHz): δ = 183.8, 164.2, 156.3, 155.8, 152.5, 134.2, 131.2, 130.2, 119.7, 117.5, 116.8, 114.7, 108.9 ppm; ESI-MS $[M+H]^+$: 254.9, calcd. $[M]^+$ 254.06.

Synthesis of (4-Hydroxyphenyl)(5-methoxybenzofuran-2-yl)methanone 11. The title compound was prepared by reaction of **10a** (0.45 g, 1.58 mmol) according to procedure E. The product was purified by flash column chromatography eluting with hexane/ethyl acetate 3:1 followed by preparative TLC to yield 0.22 g (0.8 mmol, 53 %) of **11** as a white solid. 1HNMR (CD_3COCD_3): δ = 8.39 (s, 1H), 8.13-8.11 (m, 2H), 7.53 (d, $J = 1.0$ Hz, 1H), 7.50 (d, $J = 9.0$, 1H), 7.19 (d, $J = 2.0$ Hz, 1H), 7.13-7.11 (m, 1H), 7.11-7.08 (m, 2H), 3.93 (s, 3H); 1HNMR (CD_3COCD_3): δ = 183.5, 165.5, 156.0, 155.3, 152.1, 133.5, 131.7, 129.8, 119.5, 116.6, 115.62, 114.3, 108.5, 56.9; ESI-MS: 268.9 $[M+H]^+$. The positions of the 4-hydroxy and the 5-methoxy substituent were clarified using NOESY experiments.

Synthesis of (6-Methoxybenzofuran-2-yl)(4-methoxyphenyl)methanone 12a. The title compound was prepared by reaction of 2-hydroxy-4-methoxybenzaldehyde (0.3 g, 2 mmol), 2-bromo-1-(4-methoxyphenyl)ethanone (0.46 g, 2 mmol) and K_2CO_3 (0.55 g, 4 mmol) according to procedure F. The product was purified by recrystallization in acetone to give 0.35 g (1.2 mmol, 63%) of **12a** as a white solid. 1HNMR ($CDCl_3$): δ 8.08-8.05 (m, 2H), 7.56 (d, $J = 9.0$ Hz, 1H), 7.45 (d, $J = 1.0$ Hz, 1H), 7.10 (d, $J = 1.5$ Hz, 1H), 7.02-6.99 (m, 2H), 6.95 (dd, $J = 2.0$ Hz, $J = 8.5$ Hz, 1H), 3.90 (3H, s), 3.88 (3H, S); $^{13}CNMR$ ($CDCl_3$): δ 182.8, 163.8, 161.4, 157.8, 152.7, 132.2, 130.5, 123.9, 120.8, 116.6, 114.7, 114.2, 96.1, 56.2, 55.9; ESI-MS: 283.0 $[M+H]^+$.

Synthesis of (6-Hydroxybenzofuran-2-yl)(4-hydroxyphenyl)methanone 12. The title compound was synthesized from **12a** (0.45 g, 1.58 mmol) according to procedure E. The product was purified by flash column chromatography eluting with hexane/ethyl acetate 3:1 to give 0.21 g (0.8 mmol, 53 %) of **12** as a white solid. ¹H NMR (CD₃COCD₃): δ 9.02 (s, 1H), 8.97 (s, 1H), 8.04 (s, 1H), 8.02 (s, 1H), 7.66 (d, *J* = 8.5 Hz, 1H), 7.57 (d, *J* = 1.0 Hz, 1H), 7.08 (s, 1H), 7.02 (d, *J* = 9.0 Hz, 2H), 7.07 (m, 1H), 6.96 (dd, *J* = 2.0 Hz, *J* = 8.5 Hz, 1H); ¹³C NMR (CD₃COCD₃): δ 183.8, 164.3, 161.4, 159.9, 154.8, 174.4, 131.9, 126.4, 122.4, 118.2, 117.8, 116.8, 100.3; ESI-MS: 254.9 [M+H]⁺.

Synthesis of (3-Hydroxyphenyl)(6-methoxybenzofuran-2-yl)methanone 13. The title compound was prepared by reaction of **14a** (0.26 g, 0.92 mmol) according to procedure E. The product was purified by flash column chromatography eluting with hexane/ethyl acetate 3:1 to give 0.17 g (0.6 mmol, 68 %) of **13** as a pale yellow solid. ¹H NMR (CD₃COCD₃): δ 8.75 (s, 1H), 7.72 (d, *J* = 9.0 Hz, 1H), 7.62 (d, *J* = 1.0 Hz, 1H), 7.52 (m, 1H), 7.48 (t, *J* = 1.5 Hz, 1H), 7.16 (ddd, *J* = 1.0 Hz, *J* = 2.5 Hz, *J* = 8.0 Hz, 1H), 7.02 (dd, *J* = 2.5 Hz, *J* = 9.0 Hz, 1H), 2.85 (3H, s); ¹³C NMR (CD₃COCD₃): δ 184.4, 163.2, 159.3, 159.3, 153.7, 140.9, 131.4, 125.7, 122.2, 122.1, 121.4, 118.5, 117.4, 116.2, 97.2, 57.1; ESI-MS: 268.9 [M]⁺. The positions of the 3-hydroxy and the 6-methoxy substituent were clarified using NOESY experiments.

Synthesis of 14a, (5-methoxybenzofuran-2-yl)(3-methoxyphenyl)methanone: The title compound was synthesized from 2-Bromo-3'-methoxyacetophenone and 2-hydroxy-5-methoxybenzaldehyde using procedure F to give 0.3 g (1.1 mmol, 80 %) of **14a** as colorless solid which was directly used for the next step after NMR analysis. ¹H NMR (CDCl₃, 500MHz) δ = 8.12 (s, 1 H), 8.11 (s, 1 H), 7.53 - 7.50 (m, 1 H), 7.47 (s, 1 H), 7.12 - 7.08 (m, 2 H), 7.03 (s, 1 H), 7.01 (s, 1 H), 3.91 (s, 3 H), 3.86 (s, 17 H) ppm; ¹³C NMR (CDCl₃, 126MHz) δ = 183.1, 164.0, 157.0, 153.9, 151.5, 132.4, 130.3, 128.0, 118.5, 115.9, 114.3, 113.6, 104.4, 56.3, 56.0 ppm.

Synthesis of compound 14, (5-hydroxybenzofuran-2-yl)(3-hydroxyphenyl)methanone: The title compound was synthesized from **14a** according to procedure E. The crude product was purified by flash column chromatography, eluting with ethyl acetate/hexane 1:2 to give 67 % of **14** as a white solid. ¹H NMR (Acetone-d₆, 500MHz): δ = 8.73 (s, 1 H), 8.41 (s, 1 H), 7.52 - 7.55 (m, 2 H), 7.50 (d, *J*=0.6 Hz, 1 H), 7.49 (t, *J*=2.0 Hz, 1 H), 7.42 (t, *J*=7.9 Hz, 1 H), 7.20 (dd, *J*=2.5, 0.5 Hz, 1 H), 7.15 (ddd, *J*=8.2, 2.6, 0.9 Hz, 1 H), 7.10 ppm (dd, *J*=9.0, 2.5 Hz, 1 H); ¹³C NMR (Acetone-d₆, 126MHz): δ = 184.0, 158.4, 155.1, 153.9, 151.4, 139.7, 130.6, 128.9, 121.5, 120.8, 119.0, 116.8, 116.6, 113.5, 107.8 ppm; ESI-MS: 254.9 [M+H]⁺.

Synthesis of 15a, (6-methoxybenzofuran-2-yl)(3-methoxyphenyl)methanone: The title compound was synthesized from 2-Bromo-3'-methoxyacetophenone and 2-hydroxy-4-methoxybenzaldehyde using procedure F. The product was purified by flash column chromatography eluting with hexane/ethyl acetate 3:1 to give 0.22 g (0.78 mmol, 78 %) of **15a** as a white solid. ¹H NMR (CDCl₃, 500MHz): δ = 7.59 (m, 1 H), 7.56 (d, *J*=8.7 Hz, 1 H), 7.50 (dd, *J*=2.5, 1.6 Hz, 1 H), 7.46 (d, *J*=0.9 Hz, 1 H), 7.41 (t, *J*=8.0 Hz, 1 H), 7.15 (ddd, *J*=8.2, 2.6, 0.8 Hz, 1 H), 7.09 (d, *J*=1.9 Hz, 1 H), 6.95 (dd, *J*=8.7, 2.2 Hz, 1 H), 3.88 ppm (br. s, 6 H); ¹³C NMR (CDCl₃, 126MHz): δ = 183.5, 161.2, 159.6, 157.6, 151.7, 138.7, 129.4, 123.6, 121.8, 120.3, 118.9, 117.3, 114.5, 113.8, 95.6, 55.7, 55.4 ppm; Purity (UV) > 96 %, ESI-MS [M+H]⁺: 282.9; calcd. [M]⁺: 282.9.

Synthesis of compound 15, (6-hydroxybenzofuran-2-yl)(3-hydroxyphenyl)methanone: The title compound was synthesized from **15a** according to procedure E. The crude product was purified by flash column chromatography, eluting with hexane/ethyl acetate 3:1 to give 0.14 g (0.55 mmol, 62

% of **15** as a white solid. ^1H NMR (Acetone- d_6 , 500MHz): δ = 9.04 (s, 1 H), 8.71 (s, 1 H), 7.66 (d, $J=8.5$ Hz, 1 H), 7.58 (d, $J=0.9$ Hz, 1 H), 7.480 - 7.52 (m, 1 H), 7.44 - 7.47 (m, 1 H), 7.41 (t, $J=7.8$ Hz, 1 H), 7.14 (ddd, $J=8.1, 2.6, 0.9$ Hz, 1 H), 7.06 - 7.08 (m, 1 H), 6.96 ppm (dd, $J=8.6, 2.1$ Hz, 1 H); ^{13}C NMR (Acetone- d_6 , 126MHz): δ = 183.5, 160.0, 158.5, 158.4, 152.5, 140.1, 130.6, 125.1, 121.3, 120.7, 120.5, 117.9, 116.5, 115.3, 98.6 ppm; Purity (UV) > 95 % ESI-MS $[\text{M}+\text{H}]^+$: 254.9; calcd. $[\text{M}]^+$: 254.06.

Synthesis of 16a, (6-methoxy-3-methylbenzofuran-2-yl)(3-methoxyphenyl)methanone: The title compound was synthesized from 2-Bromo-3'-methoxyacetophenone and 2'-hydroxy-4'-methoxyacetophenone using procedure F to give 0.4 g (1.4 mmol, 70 %) of **16a** as a pale yellow solid. ^1H NMR (CDCl_3 , 500MHz): δ = 7.67 - 7.70 (m, 1 H), 7.58 (dd, $J=2.5, 1.6$ Hz, 1 H), 7.52 (d, $J=8.7$ Hz, 1 H), 7.41 (t, $J=8.0$ Hz, 1 H), 7.12 (ddd, $J=8.2, 2.7, 0.9$ Hz, 1 H), 6.98 (d, $J=2.0$ Hz, 1 H), 6.94 (dd, $J=8.7, 2.2$ Hz, 1 H), 3.87 (s, 3 H), 3.85 (s, 3 H), 2.59 (s, 3 H) ppm; ^{13}C NMR (CDCl_3 , 126MHz): δ = 185.1, 161.4, 159.6, 155.9, 148.2, 139.6, 129.4, 128.0, 122.8, 122.4, 122.0, 118.8, 114.3, 113.9, 95.5, 55.9, 55.6, 10.4 ppm; Purity (UV) > 95 %, ESI-MS $[\text{M}+\text{H}]^+$: 296.9; $[\text{M}]^+$: 296.1.

Synthesis of compound 16 (6-hydroxy-3-methylbenzofuran-2-yl)(3-hydroxyphenyl)methanone. The title compound was synthesized from **16a** according to procedure E. The crude product was purified by flash column chromatography, eluting with hexane/ethyl acetate 2:1 to give 0.17 g (0.6 mmol, 67 %) of **16** as a pale yellow solid. ^1H NMR (Acetone- d_6 , 500MHz): δ = 9.00 (s, 1 H), 8.67 (s, 1 H), 7.61 (dd, $J=8.5, 0.5$ Hz, 1 H), 7.55 - 7.57 (m, 1 H), 7.53 - 7.54 (m, 1 H), 7.36 - 7.40 (m, 1 H), 7.12 (ddd, $J=8.1, 2.6, 1.0$ Hz, 1 H), 6.99 (dd, $J=2.0, 0.5$ Hz, 1 H), 6.96 (dd, $J=8.6, 2.1$ Hz, 1 H), 2.56 (s, 3 H) ppm; ^{13}C NMR (Acetone- d_6 , 126MHz): δ = 186.3, 161.2, 159.3, 157.7, 149.7, 141.7, 131.4, 129.2, 124.1, 123.8, 122.8, 121.3, 117.9, 115.8, 99.5, 11.3 ppm; Purity (UV) > 95 %, ESI-MS $[\text{M}+\text{H}]^+$: 268.9; $[\text{M}]^+$: 268.07.

Synthesis of IV, N,5-dimethoxy-N-methyl-1H-indole-2-carboxamide: The title compound was synthesized from commercial available 5-methoxy-1H-indole-2-carboxylic acid using procedure C to give 0.4 g (1.7 mmol, 83 %) of **IV** as colorless solid which was directly used without further characterisation, other than NMR. ^1H NMR ($\text{DMSO}-d_6$, 300MHz): δ = 11.41 (br. s., 1 H), 7.34 - 7.39 (m, 1 H), 7.11 (d, $J=2.4$ Hz, 1 H), 7.07 (dd, $J=2.2, 0.7$ Hz, 1 H), 6.87 (dd, $J=8.9, 2.4$ Hz, 1 H), 3.79 (s, 3 H), 3.75 (s, 3 H), 3.32 ppm (s, 3 H); ^{13}C NMR ($\text{DMSO}-d_6$, 75MHz): δ = 161.5, 154.2, 132.0, 128.9, 128.2, 115.9, 113.7, 107.0, 102.6, 61.6, 55.7, 33.4 ppm

Synthesis of compound 17a, (5-methoxy-1H-indol-2-yl)(3-methoxyphenyl)methanone: 1.2 eq. of 3-bromoanisole was dissolved in 5 ml of THF and added dropwise to a suspension of 1.3 eq. of magnesium turnings in 5 ml of THF. One crystal of iodine was added and the mixture was heated to reflux. When the magnesium was completely consumed the solution was cooled to 0°C and **IV** dissolved in 3 ml of THF was added dropwise. The reaction mixture was stirred at room temperature and the reaction was monitored by TLC. After completion, the reaction was stopped by addition of 10 % citric acid. The organic layer was separated and the aqueous layer was extracted with ethyl acetate (4x). The combined organic layer was dried over magnesium sulfate and concentrated under reduced pressure. The crude product was purified by column chromatography eluting with hexane/ethyl acetate 4:1 to give 0.9 g (3.2 mmol, 75 %) of **17a** as a pale yellow solid. ^1H NMR (CDCl_3 , 500 MHz): δ 9.64 (s, 1H), 7.59 (ddd, $J = 1.0$ Hz, $J = 1.5$ Hz, $J = 7.5$ Hz, 1H), 7.50 (dd, $J = 1.5$ Hz, $J = 2.5$ Hz, 1H), 7.43 (t, $J = 8.0$ Hz, 1H), 7.39 (m, 1H), 7.16 (ddd, $J = 1.0$ Hz, $J = 2.5$ Hz, $J = 8.0$ Hz, 1H), 7.11 (dd, $J = 1.0$ Hz, $J = 2.0$ Hz, 1H), 7.09-7.05 (m, 2H), 3.9 (s, 3H), 3.8 (s, 3H) ppm; ^{13}C NMR (CDCl_3 , 500 MHz): δ

186.9, 159.6, 154.8, 139.3, 134.7, 133.3, 129.4, 128.0, 121.9, 118.6, 118.5, 113.8, 113.2, 112.5, 102.7, 55.6, 55.5 ppm; Purity (UV) > 95 %, ESI-MS [M+H]⁺: 281.9, calcd. 281.1[M]⁺.

Synthesis of compound 17, (5-hydroxy-1H-indol-2-yl)(3-hydroxyphenyl)methanone: The title compound was synthesized from **17a** according to procedure E. The crude product was purified by flash column chromatography, eluting with ethyl acetate/hexane 1:3 to give 74 % of **17** as a pale yellow solid. ¹H NMR (Acetone-d₆, 500 MHz,): δ = 10.77 (br. s., 1 H), 8.73 (s, 1 H), 8.00 (s, 1 H), 7.48 - 7.46 (m, 1 H), 7.46 - 7.45 (m, 1 H), 7.45 - 7.42 (m, 1 H), 7.42 - 7.37 (m, 1 H), 7.13 (ddd, J = 1.1, 2.7, 8.0 Hz, 1 H), 7.11 - 7.10 (m, 1 H), 7.02 (dd, J = 0.9, 2.2 Hz, 1 H), 6.99 (dd, J = 2.4, 8.8 Hz, 1 H) ppm; ¹³C NMR (Acetone-d₆, 126MHz,) δ = 187.0, 158.3, 152.7, 140.9, 136.0, 134.3, 130.5, 129.4, 121.2, 120.0, 118.3, 116.5, 114.1, 111.8, 106.3 ppm; Purity (UV) > 95 %, ESI-MS [M+H]⁺ : 253.9, calcd. 253.07 [M]⁺.

Synthesis of intermediate compound V, N,6-dimethoxy-N-methyl-1H-indole-2-carboxamide : The title compound was synthesized from commercial available 6-methoxy-1H-indole-2-carboxylic acid using procedure C to give 0.4 g (1.7 mmol, 83 %) of **V** as colorless solid. The crude product was directly used without further characterization other than NMR. ¹H NMR (DMSO-d₆, 300MHz): δ = 11.40 (br. s., 1 H), 7.57 (d, J=8.8 Hz, 1 H), 7.14 (d, J=1.5 Hz, 1 H), 6.97 (d, J=1.5 Hz, 1 H), 6.75 (dd, J=8.8, 2.2 Hz, 1 H), 3.83 (s, 3 H), 3.81 (s, 3 H), 3.35 (s, 3 H) ppm; ¹³C NMR (DMSO-d₆, 75MHz): δ = 161.6, 158.0, 137.7, 127.6, 123.3, 122.3, 111.8, 107.8, 94.4, 61.5, 55.5, 33.4 ppm.

Synthesis of compound 18a, (6-methoxy-1H-indol-2-yl)(3-methoxyphenyl)methanone: 2 eq. of 3-bromoanisole was dissolved in 5 ml of THF and added dropwise to a suspension of 2.2 eq. of magnesium turnings in 5 ml of THF. One crystal of iodine was added and the mixture was heated to reflux. When the magnesium was completely consumed the solution was cooled to 0°C and **XV** dissolved in 3 ml of THF was added dropwise. The reaction mixture was stirred at room temperature and the reaction was monitored by TLC. After completion, the reaction was stopped by addition of 10 % citric acid. The organic layer was separated and the aqueous layer was extracted with ethyl acetate (4x). The combined organic layer was dried over magnesium sulfate and concentrated under reduced pressure. The crude product was recrystallized from ethanol to give 1.5 g of **18a** as a white solid. ¹H NMR (CDCl₃, 500MHz) δ = 9.47 (br. s., 1 H), 7.58 - 7.57 (m, 1 H), 7.57 - 7.55 (m, 1 H), 7.49 (dd, J = 1.5, 2.6 Hz, 1 H), 7.44 - 7.41 (m, 1 H), 7.15 (ddd, J = 0.9, 2.7, 8.2 Hz, 1 H), 7.13 (dd, J = 0.9, 2.2 Hz, 1 H), 6.88 (d, J = 2.2 Hz, 1 H), 6.83 (dd, J = 2.2, 8.8 Hz, 1 H), 3.89 (s, 3 H), 3.87 (s, 3 H) ppm; ¹³C NMR (CDCl₃, 126MHz) δ = 186.3, 160.0, 159.7, 139.6, 139.2, 133.8, 129.5, 124.2, 122.3, 121.8, 118.5, 113.9, 113.7, 113.2, 93.6, 55.6, 55.6 ppm; Purity (UV) > 95 % ESI-MS [M+H]⁺: 281.8; calcd. [M]⁺: 281.11.

Synthesis of compound 18, (6-Hydroxy-1H-indol-2-yl)(3-hydroxyphenyl)methanone: The title compound was synthesized from **18a** according to procedure E. The crude product was purified by flash column chromatography, eluting with hexane/ethyl acetate 3:1 to yield 0.15 g (0.59 mmol, 77%) of **18** as a white solid. ¹H NMR (Acetone-d₆, 500MHz) δ = 10.66 (br. s., 1 H), 8.80 - 8.39 (m, 2 H), 7.58 - 7.55 (m, 1 H), 7.44 - 7.42 (m, 1 H), 7.42 - 7.40 (m, 1 H), 7.40 - 7.36 (m, 1 H), 7.12 - 7.09 (m, 2 H), 7.01 - 7.00 (m, 1 H), 6.77 (dd, J = 2.2, 8.8 Hz, 1 H); ¹³C NMR (Acetone-d₆, 126MHz) δ = 187.6, 159.5, 159.2, 142.3, 142.1, 136.0, 131.7, 126.1, 123.9, 122.3, 121.0, 117.6, 114.8, 114.6, 98.6; Purity (UV) > 95 %, ESI-MS [M+H]⁺: 253.8; calcd. [M]⁺: 253.07

Synthesis of compound 19a, (5-methoxy-1-methyl-1H-indol-2-yl)(3-methoxyphenyl)methanone: The title compound was prepared from **17a** according to method G. The product was purified by

column chromatography eluting with hexane/ethyl acetate 3:1 to yield 0.2 g (0.68 mmol, 95 %) of **19a** as a pale yellow. ^1H NMR (CDCl_3 , 500MHz) δ = 7.50 (ddd, J = 0.8, 1.6, 7.6 Hz, 1 H), 7.45 (dd, J = 1.5, 2.6 Hz, 1 H), 7.42 - 7.37 (m, 1 H), 7.35 - 7.32 (m, 1 H), 7.14 (ddd, J = 1.0, 2.7, 8.3 Hz, 1 H), 7.09 (dd, J = 2.4, 9.1 Hz, 1 H), 7.06 - 7.05 (m, 1 H), 6.96 (d, J = 0.9 Hz, 1 H), 4.09 (s, 3 H), 3.88 (s, 3 H), 3.84 (s, 3 H) ppm; ^{13}C NMR (CDCl_3 , 126MHz) δ = 188.1, 159.4, 154.7, 140.8, 136.0, 135.1, 129.1, 125.9, 122.4, 118.4, 117.8, 114.1, 114.1, 111.3, 102.6, 55.7, 55.4, 32.1 ppm; Purity (UV) > 95 %, ESI-MS $[\text{M}+\text{H}]^+$: 295.8, calcd. 295.12 $[\text{M}]^+$.

Synthesis of compound 19, (5-Hydroxy-1-methyl-1H-indol-2-yl)(3-hydroxyphenyl)methanone: The title compound was synthesized from **19a** according to procedure E. Purification by column chromatography eluting with hexane/ethyl acetate 3:1 gave 0.12 g (0.45 mmol, 68 %) of **19** as a white solid. ^1H NMR (Acetone- d_6 , 500MHz) δ = 8.71 (br. s, 1 H), 8.06 (br. s, 1 H), 7.37 - 7.32 (m, 4 H), 7.10 - 7.07 (m, 1 H), 7.05 (dd, J = 0.6, 2.0 Hz, 1 H), 7.02 (dd, J = 2.2, 9.0 Hz, 1 H), 6.84 (d, J = 0.8 Hz, 1 H), 4.00 (s, 3 H) ppm; ^{13}C NMR (Acetone- d_6 , 126MHz) δ = 189.4, 159.0, 153.7, 142.8, 137.5, 137.0, 131.1, 128.4, 122.7, 120.9, 119.0, 117.8, 114.8, 113.0, 107.2, 33.2 ppm; ESI-MS $[\text{M}+\text{H}]^+$: 267.8, calcd. 267.09 $[\text{M}]^+$.

Synthesis of compound 20a, (6-Methoxy-1-methyl-1H-indol-2-yl)(3-methoxyphenyl)methanone: The title compound was prepared from **18a** according to method G. The product was purified by column chromatography eluting with hexane/ethyl acetate 3:1 to yield 0.26 g (0.88 mmol, 98 %) of **20a** as a white solid. ^1H NMR (CDCl_3 , 500MHz) δ = 7.54 - 7.52 (m, 1 H), 7.49 - 7.46 (m, 1 H), 7.43 - 7.41 (m, 1 H), 7.41 - 7.36 (m, 1 H), 7.13 (ddd, J = 0.9, 2.7, 8.2 Hz, 1 H), 7.00 (d, J = 0.8 Hz, 1 H), 6.84 (dd, J = 2.2, 8.7 Hz, 1 H), 6.79 (d, J = 2.0 Hz, 1 H), 4.09 (s, 3 H), 3.92 (s, 3 H), 3.87 (s, 3 H) ppm; ^{13}C NMR (CDCl_3 , 126MHz) δ = 187.5, 159.5, 159.4, 141.7, 141.0, 134.3, 129.0, 124.0, 122.2, 120.2, 118.2, 115.9, 114.0, 112.5, 91.8, 55.5, 55.4, 32.0 ppm; Purity (UV) > 95 %, ESI-MS $[\text{M}+\text{H}]^+$: 295.8, calcd. $[\text{M}]^+$: 295.12.

Synthesis of compound 20, (6-Hydroxy-1-methyl-1H-indol-2-yl)(3-hydroxyphenyl)methanone: The title compound was synthesized from **20a** according to procedure E. The crude product was purified by flash column chromatography, eluting with hexane/ethyl acetate 3:1 to yield 0.19 g (0.71 mmol, 81%) of **20** as a white solid. ^1H NMR (Acetone- d_6 , 500 MHz): δ = 8.68 (s, 2H), 7.54 (d, J = 8.5 Hz, 1H), 7.36 (m, 3H), 7.11-7.09 (m, 1H), 6.96 (d, J = 1.0 Hz, 1H), 6.84 (m, 1H), 6.79 (dd, 1H, J = 2.5 Hz, J = 9.0 Hz), 4.00 (s, 3H); ^{13}C NMR (Acetone- d_6 , 126 MHz): δ = 188.6, 158.9, 158.8, 143.9, 143.0, 135.8, 130.9, 125.7, 122.4, 121.5, 120.5, 117.6, 117.0, 114.1, 96.2, 33.0; Purity (UV) > 95 %, ESI-MS $[\text{M}+\text{H}]^+$: 267.9, calcd. $[\text{M}]^+$: 267.09.

Synthesis of (1-Ethyl-6-methoxy-1H-indol-2-yl)(3-methoxyphenyl)methanone 21a. The title compound was prepared by reaction of **18a** (0.38 g, 1.35 mmol), NaH 60% (0.8 g, 1.93 mmol) and ethyl iodide (0.54 ml, 6.73 mmol) according to method G. The product was purified by flash column chromatography eluting with hexane/ethyl acetate 3:1 to give 0.41 g (1.3 mmol, 98%) of **21a** as a white solid. ^1H NMR (CDCl_3): δ 7.78 (dd, J = 0.5 Hz, J = 8.5 Hz, 1H), 7.71 (ddd, J = 1.0 Hz, J = 1.5 Hz, J = 7.5 Hz, 1H), 7.66 (dd, J = 1.5 Hz, J = 3.0 Hz, 1H), 7.63 (t, J = 8.0 Hz, 1H), 7.37 (ddd, J = 1.5 Hz, J = 3.0 Hz, J = 8.5 Hz, 1H), 7.24 (d, J = 1.0 Hz, 1H), 7.09-7.06 (m, 2H), 4.85 (q, J = 7.0 Hz, 2H), 4.17 (s, 3H); ^{13}C NMR (CDCl_3): δ 187.5, 159.6, 159.5, 141.3, 140.8, 133.8, 129.1, 124.2, 122.4, 120.6, 118.3, 116.3, 114.1, 112.5, 93.0, 55.7, 55.6, 40.06, 15.6; ESI-MS: 309.7 $[\text{M}+\text{H}]^+$.

Synthesis of (1-Ethyl-6-hydroxy-1H-indol-2-yl)(3-hydroxyphenyl)methanone 21. The title compound was prepared from **21a** (0.4 g, 1.29 mmol) according to procedure E. The product was purified by flash column chromatography eluting with hexane/ethyl acetate 2:1 to give 0.3 g (1.1 mmol, 84%) of **21** pale yellow solid. ¹H NMR (CD₃COCD₃): δ 8.95 (s, 2H), 7.54 (d, *J* = 8.5 Hz, 1H), 7.37-7.33 (m, 3H), 7.11-7.08 (m, 1H), 6.96 (d, *J* = 0.50 Hz, 1H), 6.92 (m, 1H), 6.78 (dd, *J* = 2.0 Hz, *J* = 8.5 Hz, 1H), 4.55 (q, *J* = 7.0 Hz, 2H), 1.38 (t, *J* = 7 Hz, 3H). ¹³C NMR (CD₃COCD₃): δ 188.7, 159.0, 158.9, 143.3, 143.0, 135.3, 131.1, 126.0, 122.5, 121.9, 120.6, 117.7, 117.6, 114.3, 96.4, 41.3, 16.7; MS (ESI): 281.9 [M+H]⁺

Synthesis of intermediate compound VI, N,6-dimethoxy-N-methyl-2-naphthamide: The title compound was synthesized starting from commercial available 6-methoxy-2-naphthoic acid (1 g, 4.95 mmol) according to procedure C. The crude product was recrystallized from ethanol to give **VI** as a colorless solid. The crude product was directly used without further characterisation for the synthesis of **22a**, **23a** and **24a**. ¹H NMR (300 MHz, DMSO-*d*₆) δ = 8.19 (d, *J*=1.5 Hz, 1 H), 7.99 (d, *J*=8.9 Hz, 1 H), 7.90 (d, *J*=8.6 Hz, 1 H), 7.70 (dd, *J*=8.6, 1.7 Hz, 1 H), 7.42 (d, *J*=2.6 Hz, 1 H), 7.27 (dd, *J*=8.9, 2.4 Hz, 1 H), 3.93 - 3.96 (m, 3 H), 3.62 (s, 3 H), 3.35 (s, 3 H) ppm; ¹³C NMR (DMSO-*d*₆, 75MHz): δ = 169.6, 158.9, 135.7, 130.8, 129.7, 128.3, 127.8, 126.8, 125.9, 119.7, 106.3, 61.2, 55.8, 34.0 ppm.

Synthesis of 22a, (6-methoxynaphthalen-2-yl)(3-methoxyphenyl)methanone: The title compound was synthesized from **VI** and 3-bromoanisole according to procedure D. The crude product was purified by flash column chromatography eluting with ethyl acetate/hexane 1:10 to yield 0.43 g (1.46 mmol, 68 %) of **22a** as a white solid. ¹H NMR (CDCl₃, 500 MHz): δ = 8.22 (d, *J* = 1.5 Hz, 1H), 7.94 (dd, *J* = 2.0 Hz, *J* = 8.5 Hz, 1H), 7.80 (dd, *J* = 2.0 Hz, *J* = 8.5 Hz, 2H), 7.40-7.38 (m, 3H), 7.21-7.18 (m, 2H), 7.16-7.14 (m, 1H), 3.95 (s, 3H), 3.86 ppm (s, 3H); ¹³C NMR (CDCl₃, 126 MHz): δ = 196.3, 159.6, 159.5, 139.5, 137.0, 132.6, 131.9, 131.0, 129.2, 127.5, 126.9, 126.5, 122.6, 119.7, 118.5, 114.3, 105.7, 55.4, 55.3 ppm. Purity (UV) > 95 %, ESI-MS [M+H]⁺: 292.9; [M]⁺: 292.11.

Synthesis of 22, (6-hydroxynaphthalen-2-yl)(3-hydroxyphenyl)methanone: The title compound was synthesized from **22a** according to procedure E. The crude product was purified by flash column chromatography, eluting with ethyl acetate/hexane 1:3 to give 82 % of **22** as a white solid. ¹H NMR (Acetone-*d*₆, 500MHz): δ = 9.18 - 9.29 (m, 1 H), 8.85 (br. s., 1 H), 8.21 - 8.24 (m, 1 H), 7.92 - 7.96 (m, 1 H), 7.82 - 7.85 (m, 1 H), 7.79 - 7.82 (m, 1 H), 7.36 - 7.40 (m, 1 H), 7.30 (d, *J*=2.4 Hz, 1 H), 7.28 - 7.29 (m, 1 H), 7.25 - 7.27 (m, 1 H), 7.24 (dd, *J*=8.8, 2.5 Hz, 1 H), 7.12 (ddd, *J*=8.1, 2.6, 1.1 Hz, 1 H) ppm; ¹³C NMR (Acetone-*d*₆, 126MHz): δ = 196.2, 158.7, 158.3, 140.7, 138.3, 133.1, 132.7, 132.3, 130.3, 127.9, 127.3, 126.8, 121.9, 120.3, 120.0, 117.0, 110.0 ppm, Purity (UV) > 95 %, ESI-MS [M+H]⁺: 264.9; [M]⁺: 264.08.

Synthesis of 23a, (3-methoxy-4-methylphenyl)(6-methoxynaphthalen-2-yl)methanone: The title compound was synthesized from **VI** and 3-bromoanisole according to procedure D. The crude product was purified by flash column chromatography eluting with ethyl acetate/hexane 1:10 to yield 0.43 g (1.4 mmol, 71 %) of **23a** as a white solid. ¹H NMR (CDCl₃, 500 MHz): δ 8.23 (d, *J* = 1.5 Hz, 1H), 7.93 (dd, *J* = 1.5 Hz, *J* = 8.5 Hz, 1H), 7.80 (dd, *J* = 3.0 Hz, *J* = 8.5 Hz, 1H), 7.40 (d, *J* = 1.5 Hz, 1H), 7.31 (dd, *J* = 1.5 Hz, *J* = 7.5 Hz, 1H), 7.23-7.17 (m, 3H), 3.93 (s, 3H), 3.88 (s, 3H), 2.33 (s, 3H); ¹³C NMR (CDCl₃, 126 MHz): δ 197.0, 160.4, 158.6, 137.8, 133.9, 132.8, 132.5, 131.8, 130.8, 128.4, 127.7, 127.5, 124.0, 120.5, 119.5, 106.6, 56.3, 56.2, 17.4; Purity (UV) > 95 %, ESI-MS [M+H]⁺: 306.9; [M]⁺: 306.13.

Synthesis of 23, (3-hydroxy-4-methylphenyl)(6-hydroxynaphthalen-2-yl)methanone: The title compound was synthesized from **23a** according to procedure E and purified by flash column chromatography, eluting with ethyl acetate/hexane 1:3 to give 82 % of **23** as a white solid. ¹H NMR (Acetone-d₆, 500MHz): δ = 8.96 - 9.16 (m, 1 H), 8.57 (br. s., 1 H), 8.22 (d, J=0.8 Hz, 1 H), 7.92 - 7.96 (m, 1 H), 7.81 - 7.84 (m, 1 H), 7.78 - 7.81 (m, 1 H), 7.33 (d, J=1.6 Hz, 1 H), 7.31 (d, J=2.5 Hz, 1 H), 7.22 - 7.28 (m, 3 H), 2.31 ppm (d, J=0.3 Hz, 3 H); ¹³C NMR (Acetone-d₆, 126MHz): δ = 197.2, 159.7, 157.4, 139.3, 139.3, 134.7, 133.7, 133.5, 132.7, 131.6, 129.2, 128.5, 128.2, 123.6, 121.5, 117.8, 111.2, 17.7 ppm; Purity (UV) > 95 %, ESI-MS [M+H]⁺: 278.9; [M]⁺: 278.09.

Synthesis of 24a, (4-fluoro-3-methoxyphenyl)(6-methoxynaphthalen-2-yl)methanone: The title compound was synthesized from **VI** and 3-bromoanisole according to procedure D. The crude product was purified by flash column chromatography eluting with ethyl acetate/hexane 1:10 to yield 0.51 g (1.65 mmol, 84 %) of **24a** as a pale yellow solid. ¹H NMR (CDCl₃, 500 MHz): δ = 8.18 (dd, J = 1.5 Hz, J = 8.5 Hz, 1H), 7.89 (dd, J = 1.5 Hz, J = 8.5 Hz, 1H), 7.81 (dd, J = 2.0 Hz, J = 9.0 Hz, 2H), 7.55 (dd, J = 2.0 Hz, J = 8.5 Hz, 1H), 7.38-7.35 (ddd, J = 2.0 Hz, J = 4.5 Hz, J = 8.5 Hz, 1H), 7.22-7.14 (m, 3H), 3.95 (s, 3H), 3.94 ppm (s, 3H); ¹³C NMR (CDCl₃, 126 MHz): δ = 195.0, 159.6, 155.9, 153.9, 147.8, 147.7, 136.9, 134.5, 134.4, 132.4, 131.5, 130.8, 127.4, 126.9, 126.3, 123.9, 119.7, 115.5, 115.3, 114.5, 114.4, 105.6, 56.2, 55.3 ppm; Purity (UV) = 95 %, ESI-MS [M+H]⁺: 310.9; [M]⁺: 310.1.

Synthesis of 24, (4-fluoro-3-hydroxyphenyl)(6-hydroxynaphthalen-2-yl)methanone: The title compound was synthesized from **24a** according to procedure E. The crude product was purified by flash column chromatography, eluting with ethyl acetate/hexane 1:3 to give 82 % of **24** as a white solid. ¹H NMR (Acetone-d₆, 500MHz): δ = 9.05 (s, 2 H), 8.23 (d, J=0.8 Hz, 1 H), 7.94 (dd, J=8.8, 0.5 Hz, 1 H), 7.81 - 7.84 (m, 1 H), 7.79 - 7.81 (m, 1 H), 7.51 (dd, J=8.5, 2.0 Hz, 1 H), 7.32 - 7.36 (m, 1 H), 7.31 (d, J=2.5 Hz, 1 H), 7.26 - 7.29 (m, 1 H), 7.25 ppm (dd, J=6.0, 2.8 Hz, 1 H) ; ¹³C NMR (Acetone-d₆, 126MHz): δ = 195.0, 158.6, 154.9, 145.8, 138.2, 136.0, 133.0, 132.6, 132.4, 127.9, 127.4, 126.8, 123.3, 120.3, 120.1, 116.8, 110.0 ppm. Purity (UV) = 95 %, ESI-MS [M+H]⁺: 282.8; [M]⁺: 282.07.

Synthesis of (6-hydroxynaphthalen-2-yl)(3-methoxyphenyl)methanone 25. The title compound was synthesized from **22a** (0.15 g, 0.51 mmol) according to procedure E. The product was purified by flash column chromatography, eluting with hexane/ethyl acetate 2:1 to give 0.09 g (0.3 mmol, 63%) of **25** as a white solid. 8.74 (s, 1H), 8.26 (s, 1H), 7.96 (d, 1H, J = 9.0 Hz), 7.93-7.87 (m, 2H), 7.40-7.37 (m, 2H), 7.30-7.27 (m, 2H), 7.24 (dd, 1H, J = 2.5 Hz, J = 9.0 Hz), 7.15-7.13 (ddd, 1H, J = 1.0 Hz, J = 2.5 Hz, J = 8.0 Hz), 3.96 (s, 3H); ¹³CNMR (CD₃COCD₃): δ 197.8, 162.4, 159.9, 142.2, 139.6, 135.3, 134.0, 133.6, 132.0, 130.2, 129.6, 128.6, 123.6, 122.2, 121.7, 118.7, 108.4, 57.5; MS (ESI): 278.9 [M+H]⁺.

Synthesis of intermediate compound VII, methyl 6-methoxybenzothiophene-2-carboxylate: The title compound was synthesized from 2-fluoro-4-methoxy-benzaldehyde using procedure A to give 1,1 g (4.9 mmol, 60 %) of **VII** as a white solid. ¹H NMR (DMSO-d₆, 500MHz): δ = 8.07 (s, 1 H), 7.87 (d, J=8.8 Hz, 1 H), 7.59 (d, J=2.1 Hz, 1 H), 7.06 (dd, J=9.0, 2.3 Hz, 1 H), 3.84 (s, 3 H), 3.82 (s, 3 H) ppm; ¹³C NMR (DMSO-d₆, 126MHz): δ = 163.0, 159.8, 144.0, 132.8, 131.3, 130.2, 127.2, 116.4, 105.3, 56.1, 52.9 ppm Purity(FID) = 97 %, MS (EI) m/z [M]⁺ 221.96, calcd. [M]⁺ 222.04

Synthesis of intermediate compound VIII, 6-methoxy-1-benzothiophene-2-carboxylic acid: The title compound was synthesized from **VII** using procedure B to give 1,057 g (5.1 mmol, 75 %) of **VIII** as a white solid. ¹H NMR (DMSO-d₆, 500MHz): δ = 13.21 (s, 1 H), 7.98 (s, 1 H), 7.85 (d, J=8.8 Hz, 1 H), 7.57 (d, J=1.5 Hz, 1 H), 7.04 (dd, J=8.8, 2.1 Hz, 1 H), 3.82 (s, 3 H) ppm; ¹³C NMR (DMSO-d₆,126MHz): δ =

163.5, 159.0, 143.4, 132.5, 131.7, 130.1, 126.5, 115.6, 104.9, 55.5 ppm; Purity (FID) = 98 % GC-MS (EI) m/z [M-CO₂]⁺ 164.02; calcd. [M]⁺ 208.23.

Synthesis of intermediate compound IX, N,6-dimethoxy-N-methylbenzo[b]thiophene-2-carboxamide: The title compound was synthesized from VIII using procedure C to give IX as a pale yellow solid 1.1 g (0.4 mmol, 74 %). ¹H NMR (DMSO-d₆, 300 MHz): δ = 8.10 (d, J=0.6 Hz, 1 H), 7.88 (d, J=8.8 Hz, 1 H), 7.57 (d, J=2.4 Hz, 1 H), 7.05 (dd, J=8.8, 2.3 Hz, 1 H), 3.84 (s, 3 H), 3.80 (s, 3 H), 3.32 ppm (s, 3 H); ¹³C NMR (DMSO-d₆, 75MHz): δ = 161.9, 159.3, 144.1, 132.5, 131.6, 130.8, 126.9, 116.0, 104.7, 62.2, 56.0, 33.4 ppm

Synthesis of compound 26a, (6-methoxybenzo[b]thiophen-2-yl)(3-methoxyphenyl)methanone: The title compound was synthesized according to procedure D using 3-bromoanisole and IX. The crude product was purified by flash column chromatography eluting with hexane/ethyl acetate 25:1 to 0.083 g (0.27 mmol, 45 %) of 26a as a white solid. ¹H NMR (DMSO-d₆, 300MHz): δ = 8.01 (br. s., 1 H), 7.93 (d, J=8.4 Hz, 1 H), 7.62 (br. s., 1 H), 7.41 - 7.53 (m, 2 H), 7.36 (br. s., 1 H), 7.24 (d, J=8.4 Hz, 1 H), 7.07 (d, J=8.6 Hz, 1 H), 3.86 (br. s., 3 H), 3.84 ppm (br. s., 3 H); ¹³C NMR (DMSO-d₆, 75MHz): δ = 188.7, 160.3, 159.7, 144.7, 140.2, 139.3, 133.9, 133.5, 130.3, 128.2, 121.6, 118.7, 116.5, 114.1, 105.2, 56.1, 55.8 ppm; Purity(UV) = 98 %; t_R: 17.64 min, ESI-MS [M+H]⁺: 299.17; calcd. [M]⁺ 298.07.

Synthesis of compound 26, (6-hydroxybenzo[b]thiophen-2-yl)(3-hydroxyphenyl)methanone: The title compound was synthesized from 26a according to procedure E. The crude product was purified by flash column chromatography, eluting with hexane/ethyl acetate 1.5:1 to give 0.16 g (0.61 mmol, 90 %) of 26 as a white solid. ¹H NMR (DMSO-d₆, 500MHz): δ = 10.21 (br. s., 1 H), 9.88 (br. s., 1 H), 7.95 (s, 1 H), 7.87 (d, J=8.8 Hz, 1 H), 7.38 (t, J=7.9 Hz, 1 H), 7.35 (d, J=2.1 Hz, 1 H), 7.29 (d, J=7.6 Hz, 1 H), 7.22 (t, J=1.8 Hz, 1 H), 7.07 (dd, J=7.9, 1.8 Hz, 1 H), 6.97 ppm (dd, J=8.5, 2.1 Hz, 1 H); ¹³C NMR (DMSO-d₆, 126MHz): δ = 188.3, 158.2, 157.4, 144.2, 138.9, 138.9, 133.4, 132.0, 129.8, 128.0, 119.6, 119.4, 116.2, 115.2, 107.1 ppm; Purity (UV) = 98 %; t_R: 12.89 min, ESI-MS [M+H]⁺: 271.14; calcd. [M]⁺ 270.04.

Synthesis of intermediate compound X, methyl 6-methoxy-3-methylbenzo[b]thiophene-2-carboxylate: The title compound was synthesized from 2-fluoro-4-methoxy-acetophenone using procedure A to yield 1.41 g (5.96 mmol, 50 %) of X as a white solid. ¹H NMR (DMSO-d₆, 300MHz): δ = 7.82 (d, J=8.9 Hz, 1 H), 7.54 (d, J=2.2 Hz, 1 H), 7.07 (dd, J=8.9, 2.4 Hz, 1 H), 3.84 (s, 3 H), 3.84 (s, 3 H), 2.66 (s, 3 H) ppm; ¹³C NMR (DMSO-d₆, 75MHz): δ = 163.9, 160.4, 142.3, 141.8, 134.4, 125.8, 123.9, 116.2, 105.5, 56.5, 52.9, 13.8 ppm. Purity (FID) = 99 %, MS(EI) m/z [M]⁺: 235.93, calcd. [M]⁺: 236.05.

Synthesis of intermediate compound XI, 6-methoxy-3-methylbenzo[b]thiophene-2-carboxylic acid: The title compound was synthesized from X using procedure B to give 0.83 g (3.7 mmol, 68 %) of XI as a white solid. ¹H NMR (DMSO-d₆, 500MHz): δ = 7.80 (d, J=8.8 Hz, 1 H), 7.53 (d, J=2.2 Hz, 1 H), 7.06 (dd, J=9.0, 2.4 Hz, 1 H), 3.84 (s, 3 H), 2.66 ppm (s, 3 H); ¹³C NMR (DMSO-d₆, 126MHz): δ = 164.3, 159.2, 141.3, 139.8, 133.8, 125.0, 124.7, 115.1, 104.7, 55.5, 12.8 ppm. Purity (FID) = 95 %, MS(EI): m/z [M-CO₂]⁺: 178.02, [M]⁺: 222.13; calcd. [M-CO₂]⁺: 178.05, [M]⁺: 222.04.

Synthesis of intermediate compound XII, N,6-dimethoxy-N,3-dimethylbenzo[b]thiophene-2-carboxamide: The title compound was synthesized from XI using procedure C to give 0.6 g (2.26 mmol, 84 %) of XII as a colorless solid, which was directly used for the next step without further purification.

Synthesis of intermediate compound 27a, (6-methoxy-3-methylbenzo[b]thiophen-2-yl)(3-methoxyphenyl)methanone: The title compound was synthesized according to procedure D using 3-bromoanisole and **XII**. The crude product was purified by flash column chromatography eluting with hexane/ethyl acetate 25:1 to 0.074 g (0.24 mmol, 44 %) of **27a** as a colorless solid which was directly used for the synthesis of compound **27** after ¹H NMR analysis. ¹H NMR (DMSO-d₆, 300MHz): δ = 7.95 (d, J=8.9 Hz, 1 H), 7.66 (d, J=2.2 Hz, 1 H), 7.50 - 7.58 (m, 1 H), 7.38 - 7.44 (m, 1 H), 7.33 - 7.37 (m, 1 H), 7.27 - 7.32 (m, 1 H), 7.19 (dd, J=8.9, 2.4 Hz, 1 H), 3.93 (s, 3 H), 3.89 (s, 3 H), 2.52 (s, 3 H) ppm.

Synthesis of compound 27, (6-hydroxy-3-methylbenzo[b]thiophen-2-yl)(3-hydroxyphenyl)methanone: The title compound was synthesized from **27a** according to procedure E. The resulting solid was purified by flash column chromatography, eluting with hexane/ethyl acetate 5:1 to give 0.12 g (0.41 mmol, 27 %) of **27** as a white solid. ¹H NMR (DMSO-d₆, 300MHz): δ = 10.01 - 10.20 (m, 1 H), 9.72 - 9.93 (m, 1 H), 7.80 (d, J=8.9 Hz, 1 H), 7.31 (t, J=7.8 Hz, 1 H), 7.30 (d, J=2.0 Hz, 1 H), 7.18 (ddd, J=7.6, 1.9, 1.1 Hz, 1 H), 7.11 - 7.15 (m, 1 H), 7.03 (ddd, J=8.0, 2.4, 1.1 Hz, 1 H), 6.99 (dd, J=8.8, 2.2 Hz, 1 H), 2.43 ppm (s, 3 H) ppm; ¹³C NMR (DMSO-d₆, 75MHz): δ = 190.5, 158.4, 157.8, 142.6, 141.3, 140.0, 133.4, 131.9, 130.1, 125.9, 119.9, 119.9, 116.2, 115.5, 107.3, 14.6 ppm; Purity (UV) > 98 %; t_R: 13.35 min, ESI-MS [M+H]⁺: 285.15; calcd. [M]⁺ 284.05.

17β-HSD1 assay

Inhibitory activities were evaluated by an established method with minor modifications.^[39] Briefly, the purified enzyme was incubated with NADH [500 μM] in the presence of potential inhibitors at 37 °C in a phosphate buffer (50 mM) supplemented with 20% of glycerol and EDTA (1mM). Inhibitor stock solutions were prepared in DMSO. The final concentration of DMSO was adjusted to 1% in all samples. The enzymatic reaction was started by addition of unlabeled- and [2, 4, 6, 7-³H]-E1 (final concentration: 500 nM, 0.15 μCi). After 10 min, the incubation was stopped with HgCl₂ and the mixture was extracted with diethylether. After evaporation, the steroids were dissolved in acetonitrile. E1 and E2 were separated using acetonitrile/water (45:55) as mobile phase in a C18 reverse phase chromatography column (Nucleodur C18 Gravity, 3 μm, Macherey-Nagel, Duren) connected to a HPLC-system (Agilent 1100 Series, Agilent Technologies, Waldbronn). Detection and quantification of the steroids were performed using a radioflow detector (Berthold Technologies, Bad Wildbad). The conversion rate was calculated after analysis of the resulting chromatograms according to the following equation: % *conversion* = $\frac{\%E2}{\%E1+\%E2} \cdot 100$. Each value was calculated from at least three independent experiments.

17β-HSD2 assay

The 17β-HSD2 inhibition assay was performed similarly to the 17β-HSD1 procedure. The microsomal fraction was incubated with NAD⁺ [1500 μM], test compound and a mixture of unlabeled- and [2, 4, 6, 7-³H]-E2 (final concentration: 500 nM, 0.11 μCi) for 20 min at 37 °C. Further treatment of the samples and HPLC separation were carried out as mentioned above. The conversion rate was calculated after analysis of the resulting chromatograms according to the following Equation: % *conversion* = $\frac{\%E2}{\%E1+\%E2} \cdot 100$. Each value was calculated from at least three independent experiments.

Computational Methods

The *ab initio* calculations of the lowest-energy conformers and the electrostatic potentials were carried out at the B3LYP density functional scheme with the 6-31G** basis set in water, as implemented in the Gaussian 03 suite of programs.^[20,40] Lowest-energy conformers were also calculated using the Hartree-Fock approximation method and the same basis set, basically giving identical results.

References

- [1] M. Ferin, P. E. Zimmering, S. Lieberman, R. L. Vande Wiele, *Endocrinology* **1968**, *83*, 565–571.
- [2] D. B. Thomas, *Cancer* **1984**, *53*, 595–604.
- [3] A. Spadaro, M. Frotscher, R. W. Hartmann, *J Med Chem* **2012**, *55*, 2469–2473.
- [4] T. Šmuc, M. R. Pucelj, J. Šinkovec, B. Husen, H. Thole, T. L. Rižner, *Gynecol. Endocrinol.* **2007**, *23*, 105–111.
- [5] S. Marchais-Oberwinkler, C. Henn, G. Möller, T. Klein, M. Negri, A. Oster, A. Spadaro, R. Werth, M. Wetzel, K. Xu, et al., *J. Steroid Biochem. Mol. Biol.* **2011**, *125*, 66–82.
- [6] H. Peltoketo, V. Isomaa, O. Mäentausta, R. Vihko, *FEBS Lett.* **1988**, *239*, 73–77.
- [7] C. Gunnarson, M. Ahnstrom, K. Kirschner, B. Olsson, B. Nordenskjold, L. E. Rutqvist, L. Skoog, O. Stal, *Oncogene* **2003**, *22*, 34–40.
- [8] V. Speirs, A. R. Green, S. L. Atkin, *J Steroid Biochem. Mol Biol* **1998**, *67*, 267–274.
- [9] T. Suzuki, T. Moriya, N. Ariga, C. Kaneko, M. Kanazawa, H. Sasano, *Br J Cancer* **2000**, *82*, 518–523.
- [10] T. Šmuc, N. Hevir, M. Ribič-Pucelj, B. Husen, H. Thole, T. L. Rižner, *Mol Cell Endocrinol* **2009**, *301*, 59–64.
- [11] S. Gobbi, A. Cavalli, A. Rampa, F. Belluti, L. Piazzzi, A. Paluszczak, R. W. Hartmann, M. Recanatini, A. Bisi, *J Med Chem* **2006**, *49*, 4777–4780.
- [12] M. Le Borgne, P. Marchand, M. Duflos, B. Delevoye-Seiller, S. Piessard-Robert, G. Le Baut, R. W. Hartmann, M. Palzer, *Arch. Pharm. (Weinheim)*. **1997**, *330*, 141–145.
- [13] M. D. Jacobs, J. Black, O. Futer, L. Swenson, B. Hare, M. Fleming, K. Saxena, *J. Biol. Chem.* **2005**, *280*, 13728–13734.
- [14] W. Janni, P. Hepp, *Cancer Treat. Rev.* **2010**, *36*, 249–261.
- [15] J. Cuzick, I. Sestak, M. Baum, A. Buzdar, A. Howell, M. Dowsett, J. Forbes, *Lancet Oncol.* **2010**, *11*, 1135–1141.
- [16] T. Tonezzer, C. Pereira, U. Filho, A. Marx, *Eur J Gynaecol Oncol.* **2010**, *31*, 262–267.

- [17] Y. Laplante, C. Cadot, M.-A. Fournier, D. Poirier, *Bioorg. Med. Chem.* **2008**, *16*, 1849–1860.
- [18] D. Poirier, *Curr. Med. Chem.* **2003**, *10*, 453–477.
- [19] S. Gobec, P. Brozic, L. T. Rizner, *Curr. Med. Chem.* **2008**, *15*, 137–150.
- [20] E. Bey, S. Marchais-Oberwinkler, P. Kruchten, M. Frotscher, R. Werth, A. Oster, O. Algül, A. Neugebauer, R. W. Hartmann, *Bioorg. Med. Chem.* **2008**, *16*, 6423–6435.
- [21] E. Bey, S. Marchais-Oberwinkler, R. Werth, M. Negri, Y. A. Al-Soud, P. Kruchten, A. Oster, M. Frotscher, B. Birk, R. W. Hartmann, *J Med Chem* **2008**, *51*, 6725–6739.
- [22] Y. A. Al-Soud, E. Bey, A. Oster, S. Marchais-Oberwinkler, R. Werth, P. Kruchten, M. Frotscher, R. W. Hartmann, *Mol. Cell. Endocrinol.* **2009**, *301*, 212–215.
- [23] A. Oster, T. Klein, R. Werth, P. Kruchten, E. Bey, M. Negri, S. Marchais-Oberwinkler, M. Frotscher, R. W. Hartmann, *Bioorg. Med. Chem.* **2010**, *18*, 3494–3505.
- [24] M. Frotscher, E. Ziegler, S. Marchais-Oberwinkler, P. Kruchten, A. Neugebauer, L. Fetzer, C. Scherer, U. Müller-Vieira, J. Messinger, H. Thole, et al., *J Med Chem* **2008**, *51*, 2158–2169.
- [25] S. Marchais-Oberwinkler, P. Kruchten, M. Frotscher, E. Ziegler, A. Neugebauer, U. Bhoga, E. Bey, U. Müller-Vieira, J. Messinger, H. Thole, et al., *J Med Chem* **2008**, *51*, 4685–4698.
- [26] S. Marchais-Oberwinkler, M. Frotscher, E. Ziegler, R. Werth, P. Kruchten, J. Messinger, H. Thole, R. W. Hartmann, *Mol. Cell. Endocrinol.* **2009**, *301*, 205–211.
- [27] S. Marchais-Oberwinkler, M. Wetzel, E. Ziegler, P. Kruchten, R. Werth, C. Henn, R. W. Hartmann, M. Frotscher, *J. Med. Chem.* **2011**, *54*, 534–547.
- [28] J. Messinger, L. Hirvelä, B. Husen, L. Kangas, P. Koskimies, O. Pentikäinen, P. Saarenketo, H. Thole, *Mol. Cell. Endocrinol.* **2006**, *248*, 192–198.
- [29] A. Lilienkampf, S. Karkola, S. Alho-Richmond, P. Koskimies, N. Johansson, K. Huhtinen, K. Vihko, K. Wähälä, *J. Med. Chem.* **2009**, *52*, 6660–6671.
- [30] D. Deluca, A. Krazeisen, R. Breitling, C. Prehn, G. Möller, J. Adamski, *J. Steroid Biochem. Mol. Biol.* **2005**, *93*, 285–292.
- [31] A. Azzi, P. H. Rehse, D.-W. Zhu, R. L. Campbell, F. Labrie, S.-X. Lin, *Nat Struct Mol Biol* **1996**, *3*, 665–668.
- [32] S. Alho-Richmond, A. Lilienkampf, K. Wähälä, *Mol. Cell. Endocrinol.* **2006**, *248*, 208–213.
- [33] A. Spadaro, M. Negri, S. Marchais-Oberwinkler, E. Bey, M. Frotscher, *PLoS One* **2012**, *7*, e29252.
- [34] T. Klein, C. Henn, M. Negri, M. Frotscher, *PLoS One* **2011**, *6*, e22990.
- [35] A. Oster, S. Hinsberger, R. Werth, S. Marchais-Oberwinkler, M. Frotscher, R. W. Hartmann, *J. Med. Chem.* **2010**, *53*, 8176–8186.
- [36] S. Karkola, A. Lilienkampf, K. Wähälä, *ChemMedChem* **2008**, *3*, 461–472.

- [37] S. Starčević, P. Brožič, S. Turk, J. Cesar, T. Lanišnik Rižner, S. Gobec, *J. Med. Chem.* **2010**, *54*, 248–261.
- [38] M. Wetzal, S. Marchais-Oberwinkler, R. W. Hartmann, *Bioorg. Med. Chem.* **2011**, *19*, 807–815.
- [39] P. Kruchten, R. Werth, S. Marchais-Oberwinkler, M. Frotscher, R. W. Hartmann, *Mol. Cell. Endocrinol.* **2009**, *301*, 154–157.
- [40] R. Heim, S. Lucas, C. M. Grombein, C. Ries, K. E. Schewe, M. Negri, B. Birk, R. W. Hartmann, *J. Med. Chem.* **2008**, *51*, 5064–5074.

4. Final Discussion

4.1 Inhibitor Design Concept

The aim of the present study was the development of new small molecule inhibitors of the dual specificity tyrosine phosphorylation regulated kinase 1A (Dyrk1A). The new inhibitors should help to pave the way for the treatment of Down Syndrome related neurodegenerative disorders. We started our research project with a screening of our in house library lacking of classical kinase inhibitor scaffolds against Dyrk1A to identify potential new lead structures. During this approach we identified compound **EJB225**, **A/1**^a as promising initial hit compound which was moderately active towards Dyrk1A and inactive against CK2 α , which has been previously reported in association to Dyrk1A inhibition (Cozza et al., 2013; Pagano et al., 2008; Sarno et al., 2012). Ck2 α is a ubiquitous occurring kinase which is known to phosphorylate at least on 300 substrates and stabilises many other protein kinases (Meggio and Pinna, 2003; Miyata and Nishida, 2004). Since Down Syndrome requires long-term treatment, inhibition of targets that have strong impact on cell cycle control must be avoided to reduce the risk of side-effects.

Thus, the second goal was to improve the potency towards Dyrk1A while maintaining the selectivity against CK2 α and other kinases. Therefore, we applied two design strategies, depicted in Figure 4.1 for novel Dyrk1A inhibitors. The first strategy started by simple introduction of different substituents in the phenyl rings whereas the second approach focused on a ligand based approach and aimed the reduction of the H-bond acceptor distances closer to that found in the earlier described Dyrk1A inhibitor harmine (Bain et al., 2007). Thereby, the 2,4 substitution pattern of the thiophene ring was preferred to a 2,5 substitution pattern to avoid any potential plane of symmetry within the molecule which often compromises selectivity and causes promiscuous effects (Knight and Shokat, 2005). As shown in Table 4.1 compounds **1** to **10** followed the first strategy, whereas **5** to **10** were synthesized as derivatives of **EJB225** with the aim to improve the activity as well as the selectivity profile.

Within this first small compound series it was not possible to identify new more potent **EJB225** derivatives with exception of compound **4**, which is regioisomeric to the initial hit compound. But compared to **EJB225**, a strong co-inhibition of CK2 α by compound **4** was observed. As the initial hit compound **EJB225** and compounds **1-4** were originally synthesised as inhibitors of hydroxysteroid dehydrogenase 1 (HSD1) (Bey et al., 2008) we decided to focus on the second strategy, the reduction of the H-bond acceptor distances closer to that of previously reported Dyrk1A inhibitors (Bain et al., 2007; Bey et al., 2008; Ogawa et al., 2010). Applying this strategy resulted in two new compound classes (Figure 4.1) which are described in detail in chapter 3.1 and 3.2.

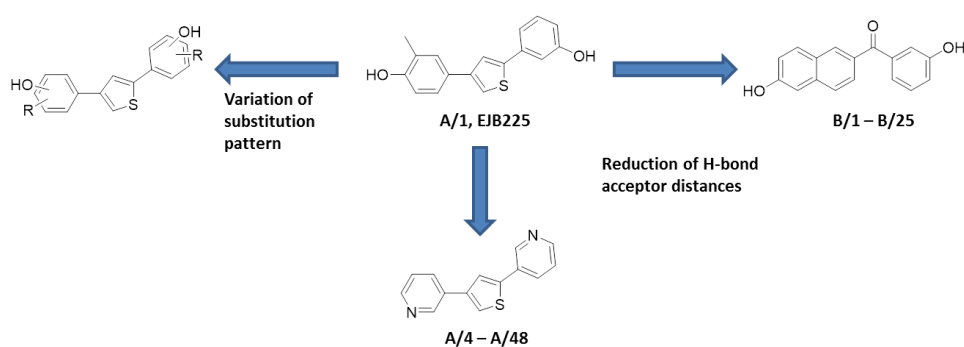
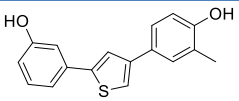
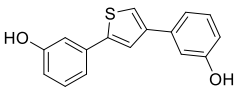
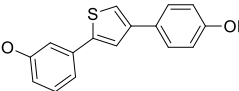
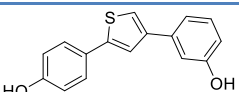
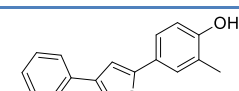
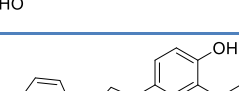
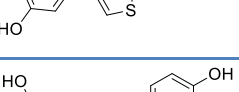
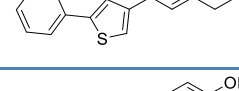
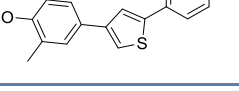
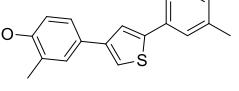
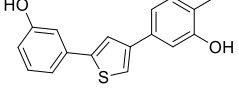


Figure 4.1: Design strategies that were applied to discover new Dyrk1A inhibitors. Reduction of the H-bond acceptor distances of the compounds resulted in the design of compound A/4 and the identification of compound B/1.

Within this first small compound series it was not possible to identify more potent **EJB225** derivatives. Only **4** showed the same inhibitory potency towards Dyrk1A. However **4** which is regioisomeric to **EJB225** turned out as CK2 α inhibitor with similar inhibitory potency. Since the initial hit compound **EJB225** and compounds **1-4** were also inhibitors of 17- β -hydroxysteroid dehydrogenase 1 (17- β -HSD1) (Bey et al., 2008) we changed the design strategy to avoid potential cross-inhibition of 17- β -HSD1 in the course of further compound development. Therefore the second strategy was applied and H-bond acceptor distances were reduced closer to that of the previously reported Dyrk1A inhibitors (Bain et al., 2007; Bey et al., 2008; Ogawa et al., 2010). Applying this strategy resulted in two compound classes (Figure 4.1) which are described in detail in chapter 3.1 and 3.2.

Table 4.1: Inhibitors, identified in a screening of in-house library (1-4) and derivatives of EJB225 (5-10)

Name	Structure	IC ₅₀ [μM]			
		Dyrk1A	Dyrk1A	Dyrk2	CK2α
EJB225, A/1		2	84	70	15
1		18	16	-	20
2		4	58	78	-
3		4	59	80	-
4		2	77	67	68
5		n.i.	28	-	-
6		5	50	50	-
7		n.i.	38	-	-
8		5	50	49	-
9		n.i.	20	-	8
10		n.i.	10	-	15

n.i.: no inhibition

4.2 Publication A: Design and Synthesis of a focused library of novel dual Dyrk1A and Dyrk1B inhibitors

In chapter 3.1, the design, synthesis and biological evaluation of a focused library of 44 substituted thiophenes (**A/4** to **A/48**) as new and potent dual Dyrk1A and Dyrk1B inhibitors is described. Starting from **EJB225**, the attention was also focused on the replacement of the phenolic moieties by more drug-like residues and simultaneous introduction of functional groups that act clearly as hydrogen bond acceptors. In addition, we expected to get more selective compounds when using only on hydrogen bond to anchor in the hinge region of the kinase. The newly designed prototype compound **A/4** bearing two 3-pyridyl rings instead of the phenyl residues turned out to be threefold more efficient against Dyrk1A ($IC_{50} = 700$ nM). Although our new lead compound was not selective within the Dyrk family, compound **A/4** showed a remarkable selectivity over CK2 α . Due to the nearly coplanar lowest energy conformation we expected an ATP competitive binding mechanism of our new hit compound which was confirmed with a Michaelis Menten kinetic experiment (Figure 4.2). Based on this result three compound series dependent on the substituent in the 2 position of the central thiophene core were synthesized. The different compound series are shortly summarised in the following:

- 3-pyridyl residue (**A/4-A/32**)
- 5-oxazole (**A/33-A/40**)
- 5 pyrimidine (**A/41-A/46**)

In addition, two individual compounds bearing a 4-isoquinoline (**A/47**) and a 5-thiazole (**A/48**) respectively in 2 position of the thiophene completed the focused compound library. The basic concept was to tune the compound potency and selectivity by adjusting the binding angle and distance of the essential hydrogen bonds to the ATP pocket.

The inhibitory potency of the compounds was initially evaluated against four kinases Dyrk1A, Dyrk1B, Dyrk2, and CK2 α . The biological results of some representative compounds out of the different compound series are summarised in Table 4.2.

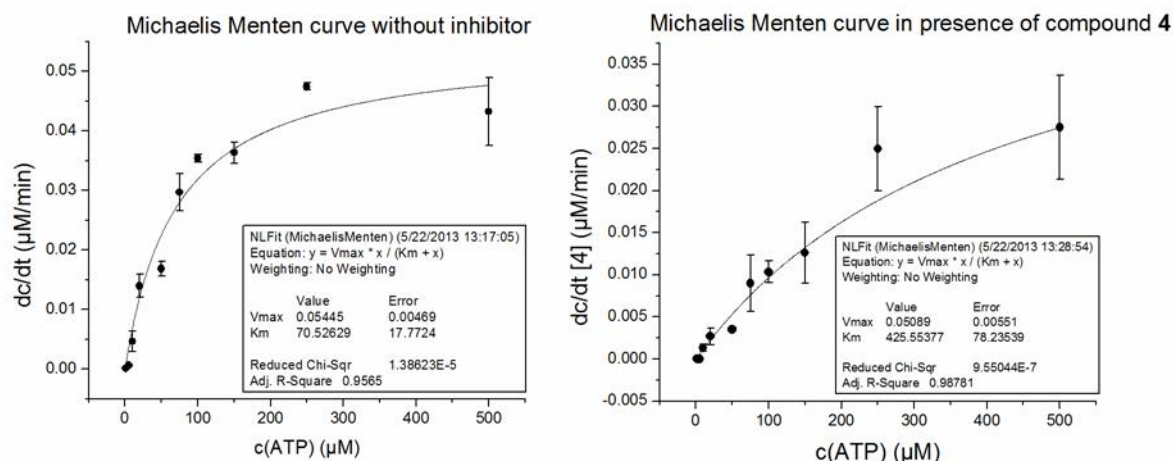
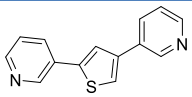
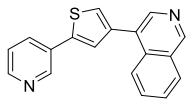
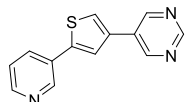
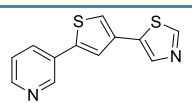
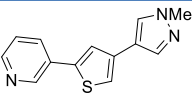
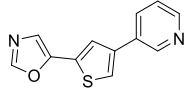
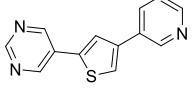
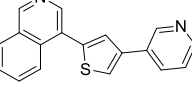
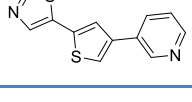


Figure 4.2: Michaelis Menten kinetic for ATP in absence (A) and in presence (B) of compound A/4. The K_m value of Dyrk1A for ATP was about 70 μM (A) and 430 μM (B), respectively. V_{max} was nearly the same in both experiments.

Compounds **A/29**, **A/30** and **A/48** turned out as the most potent Dyrk inhibitors among all compounds tested in this series. Interestingly **A/29** showed a slight selectivity for Dyrk1A and Dyrk1B over Dyrk2, whereas the constitutional isomer **A/48** was more active towards Dyrk2. Both compounds differ only in the relative position of the sulphur atom, which provoked a dramatic impact on the Dyrk2 inhibitory potency, whereas the activity towards the other kinases was not affected. This unexpected result was also observed for the both constitutional isomers **A/22** and **A/41**. Although less potent as **A/29** and **A/48**, the swapping of the sulphur position in **A/41** caused a twofold gain in activity against Dyrk1A and Dyrk1B, whereas inhibitory potency against Dyrk2 decreased by the same extent. A remarkable result showed compound **A/33** which was eightfold less active on Dyrk1A compared to its congener **A/48** even though the H-bond acceptor strength of the oxazole moiety is comparable to that of thiazole (Laurence et al., 2009). Indeed, the aromaticity of thiazole is comparable to that of pyridine, whereas the aromatic character of oxazole is significantly decreased due to the less delocalised π -electrons (Bird, 1992). Therefore, the more aromatic compound **A/48** exhibit a larger molecular surface suitable for hydrophobic contacts within adenine binding region of the ATP pocket. The selectivity of **A/29** and **A/48** was further evaluated using an extended kinase panel comprising 102 different kinases covering all kinase families of the kinome (Table 7.4, appendix). Thereby, both compounds showed only a strong inhibition of the CMGC kinases Clk1 and Clk4. This result is consistent with former scientific reports in which all Dyrk inhibitors were also identified as equally potent Clk1 and Clk4 inhibitors (Fedorov et al., 2011; Giraud et al., 2011b; Mott et al., 2009; Ogawa et al., 2010; Rosenthal et al., 2011; Wang et al., 2012).

Table 4.2. Dyrk1A, Dyrk1B, Dyrk2 and CK2 α *in vitro* inhibition by selected derivatives of A/4

Name	Structure	IC ₅₀ [μ M]			% inhibition (5 μ M)
		Dyrk1A	Dyrk1B	Dyrk2	CK2 α
A/4		0.7	0.7	0.7	19 %
A/21		3.5	3.2	2.9	6 %
A/22		1.8	3.5	1.8	n.i.
A/29		0.1	0.1	0.4	n.i.
A/30		0.3	0.4	0.2	10 %
A/33		0.8	1	1.3	n.i.
A/41		0.9	1.8	3.4	n.i.
A/47		1.5	2.4	1.2	3 %
A/48		0.1	0.07	0.04	n.i.

As Dyrk1A is mainly expressed in brain tissue, inhibitors aimed at treatment of neurodegenerative diseases must be able to cross the blood-brain barrier (Kimura et al., 2007b; Liu et al., 2008; Ryoo et al., 2007; Wegiel et al., 2008). Balanced physicochemical properties like aqueous solubility and permeability are striking features of drug-like molecules and both are necessary for intracellular activity (Lipinski, 2000). In recent literature fundamental physicochemical properties of several CNS-drugs and drug candidates were analysed to provide some clues to assess the probability of CNS activity (Ghose et al., 2012; Wager et al., 2010). Therefore logP, pK_a, and polar surface area (PSA) were calculated for **A/29**, **A/30**, **A/48** and harmine using *in silico* methods and compared (Table 4.3). The reliability of the available *in silico* methods was evaluated by comparison with experimental data previously determined for **A/4**. *In silico* prediction of solubility differed largely from the experimental

data and was not further considered. As all predicted values were in a good range a reasonable degree of CNS penetration could be expected for the selected compounds. In addition, the phase I metabolic stability of the selected compounds was determined using rat liver microsomes (Table 4.3).

Table 4.3: calculated physicochemical properties and metabolic stability of compound A/29, A/30, and A/48 in comparison to harmine

Physchem. Property	A/4	A/29	A/30	A/48	Harmine
MW [g/mol]	238.31	244.34	241.31	244.34	212.12
logP (experimental)	2.47	-	-	-	-
logP (calculated)	2.61	2.48	2.26	2.48	1.85
pK_{a1} (experimental)	3.48	-	-	-	-
pK_{a1} (calculated)	4.23 ^a	2.69	1.62	2.37	6.15
pK_{a2} (experimental)	4.8	-	-	-	-
pK_{a2} (calculated)	4.86	4.44	4.43	4.66	13.54
PSA [Å²]	25.78	25.78	30.71	25.78	37.91
Half-life [min]	-	27	53	31	18

logP, pK_a, and PSA values were calculated using JChem for Excel, PSA was determined according to the method described by Ertl *et al.* (Ertl *et al.*, 2000).

Dyrk1B has been reported to ensure survival of quiescent pancreatic cancer cells and osteosarcoma cell lines (Ewton *et al.*, 2011b). As **A/29** and **A/48** were inhibitors with equal potency against Dyrk1A and Dyrk1B, the efficiency of Dyrk inhibition in cells overexpressing Dyrk1B was examined. Dyrk1B knockdown or inhibition has been reported to induce apoptosis by activating the caspases (Gao *et al.*, 2009; Yang *et al.*, 2010). Therefore, we used U2OS osteosarcoma cells, overexpressing Dyrk1B, in the present study to evaluate the impact of Dyrk1B inhibition on apoptosis induction. We confirmed the former results by treatment of U2OS sarcoma cells with different concentrations of **A/29**, **A/48**, and **A/11** (Figure 4.3). Both active compounds were able to increase caspase 3/7 induction in a concentration dependent manner. The inactive congener **A/11** had no effect on caspase 3/7 induction.

In addition, Dyrk1B is known to reduce the production of reactive oxygen species (ROS) in quiescent pancreatic cancer cells by increasing the transcription of the antioxidant genes ferroxidase (also called ceruplasmin, CP) and superoxide dismutase 2 (SOD2) (Deng et al., 2009a). Therefore, U2OS sarcoma cells were treated with **A/29** and were examined regarding ROS production by detection with the cell permeable dihydroethidium (DHE). DHE is readily oxidised by the superoxide anion radical ($O_2^{\cdot-}$) to the DNA intercalating 2-hydroxyethidium within the cell (Rothe and Valet, 1990). The rise of fluorescence measured for increasing concentrations of **A/29** in the assay corresponded to higher ROS production indicating for Dyrk1B inhibition (Figure 4.3).

The expression pattern of seven genes was also examined, covering three distinct Dyrk1B-dependent gene regulatory pathways, were chosen to assign the observed effects triggered by the action of **A/29** and **A/48** to Dyrk1B inhibition. The corresponding genes are either linked to apoptosis induction or to ROS reduction in cells. The following genes were included:

- SOD2 (superoxide dismutase 2), antioxidant (Deng et al., 2009b);
- CP (ferroxidase, ceruplasmin), antioxidant (Deng et al., 2009b);
- CDH4 (cadherine-4) (Urbich et al., 2009);
- FGF2 (basic fibroblast growth factor) (Urbich et al., 2009), oncogenic, when overexpressed (Ornitz et al., 1996);
- BIM (BH3-only member of the BCL-2 family), proapoptotic (Gao et al., 2012);
- TRADD (tumour necrosis factor receptor type 1-associated DEATH domain protein), proapoptotic (Gao et al., 2012);
- and FasL (Fas ligand), proapoptotic (Gao et al., 2012).

As already mentioned Dyrk1B overexpression increases the up-regulation of the antioxidant genes SOD2 and CP using an as yet unidentified signalling mechanism. Incubation of U2OS osteosarcoma cells with **A/29** and **A/48** significantly decreased the mRNA expression of both antioxidant genes (Table 4.3). This result was in accordance to a previous published experiment, where Dyrk1B was silenced with shRNA in pancreatic cancer cells (Deng et al., 2009a). Therefore our experiment gave a further hint that Dyrk1B is one of the main intracellular targets of the inhibitors.

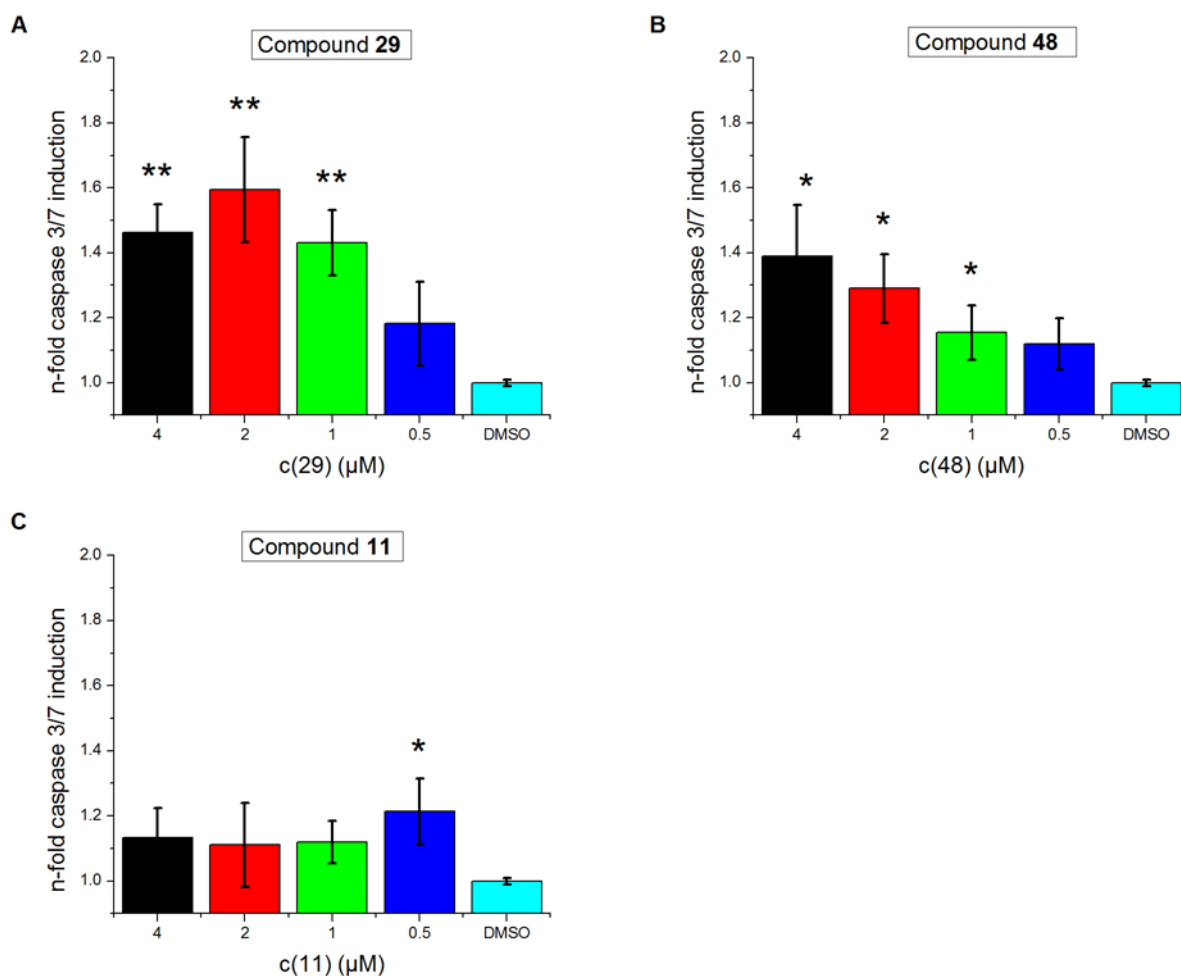


Figure 4.3: Induction of caspase 3/7 in U2OS osteosarcoma cells triggered by treatment with compound A/29 (A) and A/48 (B). The inactive congener A/11 (C) had no influence on caspase 3/7 induction. Incubation of U2OS with different concentrations of A/29 increased the production of reactive oxygen species within living cells (D). The standard deviation is given as y-error bar. One asterisk indicates significance with a p value < 0.05; two asterisks indicate significance p < 0.01.

The class II histone deacetylase 5 (HDAC5) is also a potential substrate of Dyrk1B and normally localised in the nucleus where it suppresses the transcription of CDH4 and FGF2 genes. HDAC5 is displaced from the nucleus by Dyrk1B mediated phosphorylation and leads to an increased gene expression of the potential oncogenes CDH4 and FGF2 (Deng et al., 2005, 2006). Inhibition of Dyrk1B in turn leads to a migration of HDAC5 into the nucleus and reduces the expression of CDH4 and FDF2. As shown in Table 4.3, treatment of U2OS cells with different concentrations of **A/29** and **A/48** caused a slight reduction of CDH4 and FDF2 mRNA levels and gave further evidence of selective Dyrk1B inhibition.

Since silencing or inhibition of Dyrk1B in quiescent cancer cells has been associated with the induction of caspase 3/7 the influence of Dyrk1B on the expression of three proapoptotic genes was examined. Dyrk1A and Dyrk1B phosphorylate Mammalian forkhead subclass O (FoxO) family

members of transcriptional factors in ovarian cancer cells at Ser329 (Gao et al., 2012). FoxO inhibits cell cycle progression and modulate the expression of proapoptotic genes but phosphorylation leads to its translocation from the nucleus and its deactivation.

Table 4.3. Modulation of Dyrk1B–regulated gene expression by compounds 29 and 48 as analyzed by Real-Time PCR^a

Target gene mRNA	A/29	A/29	A/48	A/48
	5 μ M	10 μ M	5 μ M	10 μ M
SOD2	-2,3 \pm 0.3	-2,3 \pm 0.4	-2,4 \pm 0.2	-2,1 \pm 0.6
CP	-2,7 \pm 0.5	-2,9 \pm 0.9	-2,0 \pm 0.4	-2,2 \pm 0.5
CDH4	-1,4 \pm 0.3	-1,5 \pm 0.4	-1,4 \pm 0.2	-1,5 \pm 0.3
FGF2	-1,4 \pm 0.2	-1,8 \pm 0.2	-1,7 \pm 0.2	-1,7 \pm 0.4
BIM	2,4 \pm 0.3	2,5 \pm 0.6	2,7 \pm 0.4	2,6 \pm 0.7
TRADD	2,5 \pm 0.4	3,0 \pm 0.4	1,2 \pm 0.3	3,0 \pm 0.7
FasL	1,2 \pm 0.1	2,7 \pm 0.6	1,2 \pm 0.2	1,9 \pm 0.4

^aValues indicate fold up-regulation (positive numbers) or down-regulation (negative numbers) of mRNA expression, relative to DMSO–treated cells. Given are mean values of at least two independent experiments, n=3, \pm S.D..

In accordance to previous results where Dyrk1B was knocked down by siRNA in ovarian cancer cells (Gao et al., 2012), treatment of U2OS osteosarcoma cells with **A/29** and **A/48** increased the expression of the FoxO1 regulated proapoptotic genes BIM, TRADD, and FasL (Table 4.3).

The results provided by the analysis of seven mRNA transcripts of three Dyrk1B-dependent pathways were in accordance to the results found recent literature. Moreover, the obtained mRNA expression pattern supported the results obtained in the caspase 3/7 and the ROS assay (Figure 4.3) and provided strong evidence that compound **A/29** and **A/48** target Dyrk1B in living cells.

In summary, discovery of **A/29** and **A/48** as new selective Cdc2-like kinase and Dyrk inhibitor scaffolds highlights the opportunity to selectively target the ATP pocket of protein kinases with exceptional small molecules. The generation of three focused libraries using automated parallel synthesis highly potent small molecules. Due to their low molecular weight and favourable physicochemical properties they are promising leadlike compounds which are suitable for further

compound optimisation (Teague et al., 1999). Furthermore they can be used as research tools to further explore the specific roles of Cdc2-like kinases and Dyrks.

4.3 Publication B: Discovery of 5-hydroxybenzothiophene ketones as novel dual inhibitors of cdc2-like kinases and Dyrk1A/1B

Chapter 3.2 describes the discovery of 5-hydroxybenzothiophene ketones as a new class of dual inhibitors of Cdc2-like kinases and Dyrks as modulators of alternative splicing. The initial design concept followed strategy depicted in Figure 4.1 to reduce the distance between the H-bond acceptor groups closer to that of harmine. Therefore our in-house compound library was screened for new scaffolds matching our criterions. The 6-hydroxybenzothiazole **A** and the 6-hydroxynaphthalene **B/1** were taken into account as scaffold suitable as Cdc2-like kinase and Dyrk1A/1B inhibitors (Figure 4.4). Compound **A** has been earlier described as potent inhibitor of 17- β -HSD (Spadaro et al., 2012a). Surprisingly only the 6-hydroxynaphthalene **B/1** turned out as moderate Clk1 and Dyrk1A inhibitor displaying an IC_{50} value of 1.9 and 2.9 μ M, respectively, whereas the 6-hydroxybenzothiazole was completely inactive. Intrigued by the finding that **B/1** was practical inactive towards the tumour suppressor kinase Dyrk2, the newly identified scaffold was further optimised. In the course of compound optimisation in terms of potency a significant gain in selectivity could also be expected (Frye, 1999). It seemed likely that compound **B/1** can accomplish only one hydrogen bond to the hinge region of the kinase. Many known core structures of kinase inhibitors take advantage of a hydrogen bond donor/acceptor tandem to bind into the kinase ATP pocket, which increases the binding affinity, while often decreasing selectivity (Zhang and Kim, 2008). Therefore, an advantage regarding the selectivity of the new inhibitor class could be expected. The optimisation strategy was focused on a systematic bioisosteric replacement of the central naphthalene core by benzothiophene, indole, and benzofuran. In addition, small substituents were introduced within the phenyl ring. Thereby the naphthalene core was replaced. Due to its importance as hydrogen bond acceptor the ketone bridge was retained as linker between the two aromatic substructures.

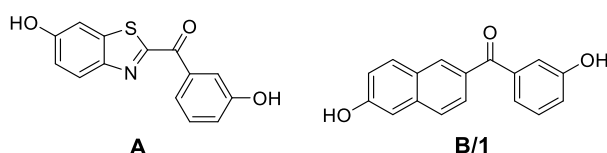


Figure 4.4: Compounds identified as new potential Clk and Dyrk inhibitor scaffolds

The 5-hydroxybenzothiophene scaffold provided the best kinase inhibitory potency against Clk1 and Dyrk1A/1B. Therefore, modifications were only introduced into the phenyl ring. Tight structure activity relationships were observed for Dyrk1A inhibition whereas Clk1 inhibition was less

susceptible for modifications within the phenyl ring (Table 4.4). Moving the hydroxyl group from the 3'-position in to the 4'-position of the phenyl ring in **B/14** resulted in a significant loss of potency against Dyrk1A of about one order of magnitude whereas the binding affinity to Clk1 only decreased by threefold.

Table 4.4: Biological activities of a representative set of 5-hydroxybezothiophene based dual Clk1/Dyrk inhibitors

Name	Structure	IC ₅₀ [μM]			% inhibition (5 μM)	
		Dyrk1A	Dyrk1B	Clk1	Dyrk2	CK2α
B/10		0.4	0.2	0.1	49	12
B/14		3.4	0.8	0.3	25	33
B/16		0.2	0.2	0.05	50	10
B/17		11	7	25 %	8	-
B/18		2	0.4	0.05	30	20
B/21		2	1	0.2	37	13
B/22		42	6 % inh. @5μM	-	15	24
B/23		0.2	0.1	0.06	46	9
B/25		0.9	1.6	0.1	41	-

The introduction of an additional methyl group to **B/10** resulted in **B/16** which represented one of the most potent Clk and Dyrk1A inhibitors in this series. The isomer **B/17** was nearly inactive indicating that a methyl group in 3'-position probably forces the inhibitor to bind in an unfavourable

conformation. To shed light on the binding orientation of the inhibitor class within the ATP pocket, the hydroxyl group of the benzothiophene moiety and of the phenyl ring was alternatively omitted (**B/21**, **B/22**). Elimination of the hydroxyl group in **B/22** resulted in a 100 fold drop in Dyrk1A inhibitory potency, whereas **B/21** showed a significantly less dramatic effect by only fivefold. Since almost all ATP competitive inhibitors take advantage of at least one hydrogen bond to the hinge region an accommodation of the 5-hydroxybenzothiophene moiety as hinge binding element is probable. Removal of this interaction can result in up to 1000 fold loss of affinity (Knight and Shokat, 2005; Noble et al., 2004). Comparing **B/10** and **B/21** in terms of Clk1 inhibitory potency, the additional hydroxyl group in the phenyl ring did not play a crucial role for activity. Therefore the phenyl ring was replaced by a simple methyl group to explore its specific importance in kinase inhibition. Interestingly, the resulting compound **B/23** was identified as the most potent dual Clk1 and Dyrk1A/1B inhibitor besides of **B/16**. Although the compound has a low molecular weight it maintained the good selectivity found for **B/16** against the both off-target kinases Dyrk2 and CK2 α . To further evaluate the selectivity within the kinome **B/16** and **B/23** were screened against a panel of 31 protein kinases at 5 μ M covering all kinase groups of the kinome (Table 7.8, chapter 7.2.3). As expected, both inhibitors also displayed strong inhibition of Clk4, which was also found to be inhibited by Clk1 inhibitors (Fedorov et al., 2011; Rosenthal et al., 2011; Tahtouh et al., 2012). The atypical kinase haspin was also identified as target of compound **B/23**.

To provide evidence that both Clk1 and Dyrk1A inhibition is required for efficient alternative splicing modulation, compound **B/16**, **B/18**, **B/23**, **B/25**, and **TG003** were incubated with embryonic fibroblasts using an earlier described protocol (Muraki et al., 2004). Different concentrations ranging from 1 to 15 μ M were chosen to probe their influence on Clk/Sty mRNA splicing. Analysis of PCR products by gel electrophoresis revealed **B/18** as inactive and **B/16** despite of its high kinase inhibitory potency was only a moderately active splicing modulator. Indeed, the sensitivity for the detection of Clk/Sty mRNA splicing modulation was largely increased by applying a new real time PCR experiment. In contrast to the PCR experiment, **B/16** triggered a fivefold increased alternative Clk1/Sty transcript at about 2 μ M. In sum, **B/16** and **B/23** were both more efficient than the earlier described Clk1 inhibitor **TG003** to increase alternative Clk1/Sty transcripts (Muraki et al., 2004). However, the maximum Clk/Sty mRNA splicing induction seems to be compound specific which turned the EC₅₀ values as not suitable to express compound efficiency (Table 4.5).

Table 4.5: Induction of Clk/Sty mRNA alternative splicing triggered by 16, 23, and 25 in comparison to TG003.

	TG003	16	23	25
C₅-fold [μM]^a	3.1	1.9	1.1	2.4
EC₅₀ [μM]^b	6.6	1.8	8.9	2.1
max. induction^c	17x	9.5x	21.4x	8.1x

^a concentration required to induce fivefold increase of the alternative Clk1 transcript levels as determined by Real-Time PCR, S.D. $\leq 10\%$; ^b concentration required for half-maximal induction of the alternative Clk1 mRNA splicing, S.D. $\leq 10\%$; ^c maximum increase of alternative Clk1 transcripts achievable with the inhibitors (fold increase over DMSO-treated samples), S.D. $< 20\%$.

In conclusion, the simplification of **B/4** by replacement of the hydroxyphenyl moiety by methyl yielded in **B/23** which represented a highly potent dual Cdc2-like and Dyrk1A/1B selective inhibitor. Although compound **B/23** was slightly less selective than **B/16** in a counter screen against 32 kinases, it can be regarded as the most promising dual Clk1/4 and Dyrk1A/1B inhibitor within the present study. Compared to TG003, which has a weaker Dyrk1A binding affinity, it provides a more efficient splicing of Clk/Sty transcripts. This result indicate that both Clk1 and Dyrk1A inhibition is required for efficient splicing modulation. Furthermore the small molecular weight of 192 g/mole and the resulting high ligand efficiency guides **B/23** to a promising leadlike compound which is a valuable starting point for further compound optimisation.

Due to the high molecular similarity of compounds **B/1** – **B/22** to the 6-hydroxybenzothiazole **A**, the new inhibitors were also evaluated against 17- β HSD1. Thereby, compound **B/16** showed an IC₅₀ of about 200 nM against 17- β -HSD1 whereas **B/23** was inactive. At this stage, it is not possible to exclude further targets other than protein kinases for **B/16** which could be a reason for the lower splicing induction. The utility of benzothiophene ketones as 17- β -HSD1 inhibitors is pursued in chapter 3.4.

4.4 Classification of the novel inhibitor classes compared to known reference inhibitors

In chapter 3.1 and 3.2 the ligand-based compound design concept was successfully applied to identify new ATP competitive kinase inhibitor scaffold suitable as Cdc2-like kinase and Dyrk inhibitors. Due to their high selectivity for certain kinases, the high ligand efficiency, and good physicochemical what provide a good starting point for further compound optimisation to increase potency as well as selectivity. In particular compound **B/18** exemplified the opportunity to design inhibitors, which are able to discriminate between Clk1 and Dyrk1A ATP pockets sharing a high shape complementarity. Since kinase assay conditions vary from study to study, in particular with respect

to ATP concentration, it is difficult to classify the potencies of the new kinase inhibitor scaffolds from 3.1 and 3.2. Therefore the inhibitory potencies of the established Cdc2-like kinase and Dyrk inhibitors harmine and TG003 found in literature were compared to the IC₅₀ values determined in this study (Table 4.6).

Table 4.6: Comparison of TG003 and harmine inhibitory potency in the present study with published IC₅₀.

IC ₅₀ (Dyrk1A)/nM		IC ₅₀ (Clk1)/nM		Selectivity factor (SF)	
TG003	Harmine	TG003	Harmine	SF(TG003)	SF (Harmine)
830 ^a	100 ^a	170 ^a	220 ^a	4.9	0.45
156 (Fedorov et al., 2011)	80 (Bain et al., 2007)	49 (Fedorov et al., 2011)	-	3.2	-
12 ^b (Mott et al., 2009)	85 (Tahtouh et al., 2012)	19 ^b (Mott et al., 2009)	72 (Tahtouh et al., 2012)	0.6	1.2
930 ^c (Ogawa et al., 2010)	350 (Ogawa et al., 2010)	20 ^c (Muraki et al., 2004)	-	46 ^b	-
-	33 (Göckler et al., 2009)	-	-	-	-

^a present study

^b K_d values for TG003 on Dyrk1A and Clk1

^c IC₅₀ values were not provided in the same study. There is a discrepancy between the assay conditions used

The obtained data suggest that our most advanced dual Cdc2-like kinase and Dyrk inhibitors within the present thesis, namely **A/29**, **A/48**, and **B/23**, have at least the same inhibitory potency as harmine and were stronger inhibitors than TG003 towards Dyrk1A as well as Clk1.

4.5 Publication C: Comparison of a MALDI-QqQ mass spectrometric kinase assay with radiometric, luminescence and LC-UV-MS kinase assays

Screening of large compound libraries is an important task in drug discovery processes. Chapter 3.3 deals with the development and optimisation of a MALDI-QqQ-based kinase assay for Dyrk1A inhibitors. The ability to use the MALDI-QqQ-based kinase assay as high-throughput screening method, which simultaneously provides molecular information is a striking feature of this technology. In addition, the MALDI-QqQ-based method was compared to different established Dyrk1A kinase assay techniques. Therefore four compounds, namely **A/29**, **A48**, **B/16** and **B/23** were chosen for the experiments. Harmine was used as reference inhibitor. The relative response ratios of substrate/product peptides during MALDI analysis are strongly influenced by the matrix compound used (Gropengiesser et al., 2009; Parker et al., 2008). Thus, three matrices, were investigated at five different concentrations for their suitability in the subsequent kinase assay (Table 4.7).

Table 4.7: Matrix compounds investigated for suitability in the kinase assay

Matrix	Abbreviation
α -cyano-4-hydroxycinnamic acid ()	α -CHCA
2,5-dihydroxybenzoic acid/ 2-hydroxy-5-methoxybenzoic 9:1	Super DHB (Karas et al., 1993) (sDHB)
α -cyano-4-hydroxycinnamic acid /3-hydroxypicolinic acid 1:1	α -CHCA/HPA

Super DHB and CHCA/HPA were previously described to suppress unfavourable phosphate loss due to fragmentation after desorption/ionization (Kapkova et al., 2006; Zhou et al., 2009).

Ionization efficiency was also dependent on the MALDI target used. Therefore, matrix compounds were probed on stainless steel plates and μ -focusing MALDI plates as sample support. The matrix preparations and type of MALDI target used in the kinase assays, which yielded in optimum ion intensity, lowest RSD, and reproducibility, are summarised in Table 4.8.

Table 4.8: Matrix compound and MALDI target combination used in the subsequent assays

Matrix	Concentration [mg/ml]	Solvent	MALDI target
CHCA	5	50 % acetonitrile	Stainless steel
Super DHB	10	70 % acetonitrile	μ -focusing plate
CHCA/HPA	20/20	70 % acetonitrile	μ -focusing plate

ATP and substrate peptide concentrations were used as previously described and assay conditions were optimised following the general instructions for kinase assay development (Glickman and Ph, 2012; Göckler et al., 2009).

To compare the different assay readout technologies experiments of a single inhibitor were performed in parallel using the same aliquots of reagents. MALDI experiments were performed in multiple reactions monitoring (MRM) mode and Selected-Ion monitoring (SIM) mode. Increasing collision induced dissociation (CID) energies were used to reveal the most intense product ion for the phosphorylated and the substrate peptide. For both substrate and phosphorylated peptide the same product ion at m/z 1442 $[y_{13}\text{-H}_2\text{O}/b_{13}]^+$ found in MRM mode turned out as most suitable due to the neutral loss of the phosphate group even at low energy CID (Boersema et al., 2009).

In recent studies the detection efficiencies of phosphorylated peptides in comparison to the substrate peptides were examined in protein kinase A assays using MALDI-MS (Craig et al., 1994; Greis et al., 2006; Rathore et al., 2008). UV detection of phosphopeptide/peptide peak area ratio at 215 nm was reported in several kinase assays to establish correction factors for exact molecular ratios for MALDI analysis (Craig et al., 1994; Gratz et al., 2010; Gropengiesser et al., 2009; Matsumoto et al., 1998).

Due to the high reproducibility of the HPLC-UV assay in our study, it was also used as reference method. Figure 4.5 exemplarily depicts the outcome of all assay techniques used within the present study (upper row). Interestingly both the HPLC-based and the radioactivity based kinase assay exhibited a nearly constant variance across the whole concentration range whereas the luminescence and MALDI based assays showed larger variances with decreasing inhibitor concentration (lower row in Figure 4.5). An intercorrelation analysis of the assay technologies revealed an excellent linear correlation between all MALDI-based methods exhibiting R values of at least 0.998 (Figure 4 in chapter 3.3) underlining its reproducibility. Correlation of the MALDI assay with the other assay techniques yielded in a concavely shaped function indicating the underrepresentation of the phosphorylated peptide in the MALDI mass spectra. Furthermore the similar IC_{50} values determined by MALDI-QqQ suggested that matrix compound and detection mode only slightly influenced the assay outcome (Table 1 in chapter 3.3). Confidence intervals and prediction intervals were additionally calculated to each IC_{50} value. The prediction intervals represent the variability introduced by future experiments and can be used to compare the IC_{50} among each other.

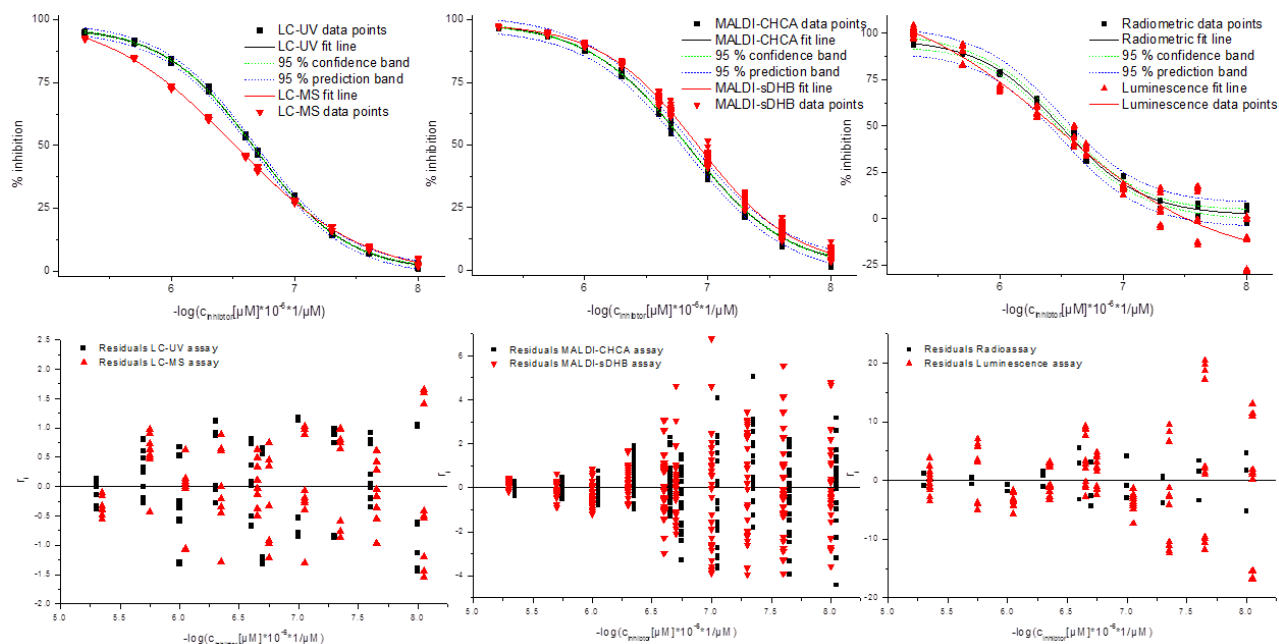


Figure 4.5: The upper row shows exemplarily IC₅₀ curves for CS375 determined using HPLC-UV, HPLC-MS, MALDI, radioactivity, and luminescence assays. Residuals of the HPLC-based and the radioactivity based assay exhibit a nearly constant variance (lower row). Residuals of MALDI and luminescence based assay increase with decreasing compound concentration.

The correction factors were calculated from the HPLC-UV assay and it was readily possible to apply them to the IC₅₀ values obtained by MALDI-QqQ. The correction factors were in the range of 1.5 – 1.8 for α -CHCA and the α -CHCA/HPA mixture and between 1.7 – 1.8 for DHB.

The calculated Z' factor is a useful tool for comparison and evaluation of the quality of assays (Zhang, 1999), Z' values for each assay were also calculated. Z' values obtained for the MALDI assays and HPLC based assays were found to be > 0.90 a value which is referred to an excellent assay. An exception are the MALDI assays for DHB in the MRM mode, where the Z' values were > 0.8. Thus, the Z' values for the MALDI assays described herein were slightly better than the Z' values in other reports using MALDI-QqQ ranging from 0.6 to 0.8 (Rathore et al., 2008, 2010). Z' values for the radiometric and the luminescence assay were ranging from 0.44 to 0.9 and were also comparable to values found in literature (Baki et al., 2007; Mallari et al., 2003; Tanega et al., 2009).

One-sided two sample t-tests were performed for inhibitor concentration of 200 nM and 250 nM respectively since the inhibition value leap is too large within the narrow concentration range. In addition, test powers and hypothetical powers for the least common denominator (N=6) and for the highest sample size (N=54) were calculated. These values are important to discriminate between two concentrations within the same assay having an identical N.

The radioactive kinase assay is limited to forty samples which can be accomplished manually at one time and therefore it provided the lowest sample number (Hastie et al., 2006). Thereby HPLC

based assays yielded the best Z' scores and test powers, however a constant bias of 1.2 ($IC_{50, \text{HPLC-MS}}/IC_{50, \text{HPLC-UV}}$) was found. This observation can be reduced to the slightly favored ESI ionization of phosphorylated peptides over their un-phosphorylated form which was earlier described (Steen et al., 2006).

In summary this study demonstrated the qualification of a high-speed MALDI-QqQ assay to evaluate the inhibitory potency of Dyrk1A inhibitors. Interestingly the choice of matrix compound had only little effect on the IC_{50} values measured. The MALDI assay was compared to radiometric, luminescence, HPLC-UV, and HPLC-MS assay. UV detection of the peptides served as reference method. Due to the lower abundance of phosphopeptides in MALDI, IC_{50} values determined in this assay were about 2-fold lower than those determined by HPLC-UV. The well elaborated assay displayed an excellent performance ($Z' > 0.91$) and allows a fast analysis of 384 well plates within 14 minutes.

4.6 Publication D: Hydroxybenzothiophene ketones as new 17- β -HSD1 inhibitors

As mentioned before the class of hydroxybenzothiophene ketones described in chapter 3.2 were partially identified as efficient inhibitors of 17- β -HSD1. Chapter 3.4 deals with the elaboration of first structure activity relationships of this new class of 17- β -HSD1 inhibitors. The benzothiazole based 17- β -HSD1 inhibitor **A** served as template for the development of a new inhibitor class (Spadaro et al., 2012a). The aim of this study was the identification of new inhibitor scaffolds and the optimisation of the electronic and geometric properties for an improved inhibition profile. Thereby the benzothiazole core was bioisosterically replaced by benzofuran, indole, benzothiophene, and naphthalene differing in size, polarity, H-bond capacity, and electronic properties. The resulting compounds **D/1-D/27** were then evaluated *in vitro* for their inhibitory potency against 17- β -HSD1 and 17- β -HSD2 and compared with the potency of **A** using a concentration of 1 μ M. The most potent compounds were used to determine IC₅₀ values against 17- β -HSD1 and 17- β -HSD2. Table 4.9 summarises the results of the IC₅₀ values found for the eight most potent compounds. It is striking that 6 compounds out of 8 were benzothiophene based inhibitors, whereas the remaining two compounds were alkylated 6-hydroxyindole based inhibitors.

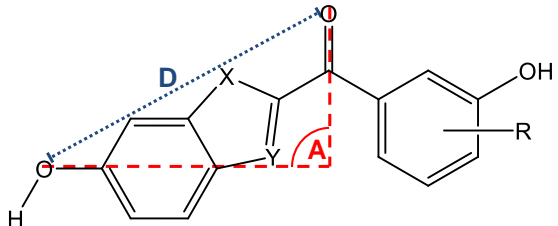
Table 4.9: Inhibitory potencies of eight compounds identified as promising 17- β -HSD1 inhibitors

Compound	R ₁	R ₂	R ₃	R ₄	X	IC ₅₀ [nM]		SF
						17- β -HSD1	17- β -HSD2	
A	-	-	-	-	-	44	1035	23
D/1	5-OH	3-OH	H	H	S	132	301	3
D/3	H	3-OH	H	H	S	208	227	1
D/8	5-OH	3-OH	4-F	H	S	89	221	2
D/9	5-OH	5-OH	2-F	H	S	147	601	4
D/20	6-OH	3-OH	H	H	NMe	177	1822	10
D/21	6-OH	3-OH	H	H	NEt	135	469	3
D/26	6-OH	3-OH	H	H	S	13	500	40
D/27	6-OH	3-OH	H	CH ₃	S	44	85	2

The 5-hydroxybenzothiophene based compounds investigated within the present study were slightly weaker inhibitors of 17- β -HSD1 compared to the initial 6-hydroxybenzothiazole **A**. However the presence of the 5-hydroxyl functionality dramatically decreased the selectivity over 17- β -HSD2. Interestingly, compound **D/3**, which lacks the 5-hydroxyl group, exhibited a similar potency towards 17- β -HSD1 indicating that this moiety is not significantly involved in inhibitor binding. However, the selectivity over 17- β -HSD2 was completely lost.

Introduction of a 6-hydroxybenzothiophene moiety, realized in compound **D/26** and **D/27**, significantly increased the inhibitory potency against 17- β -HSD1. Thereby **D/26** was identified as three times more potent as the 6-hydroxybenzthiazole based inhibitor **A** and exhibited a rather good selectivity towards 17- β -HSD2. Compound **D/27** was comparable to compound **A** in terms of potency while the increased hydrophobicity caused by the additional methyl group attenuated the selectivity over 17- β -HSD2. To address the potential reason for the preference of 17- β -HSD1 for the 6-hydroxybenzothiophene scaffolds over the other 6-hydroxybenzoheterocyclic congeners examined within this study the overall geometry of each compound class was examined and compared to the values determined for **A**. As shown in Table 4.10 the larger distances and angles between the 6-hydroxyl group and the ketone bridge are clearly associated with the more potent compounds **A** and **D/26** and may provide an optimal spatial orientation of hydrogen bonds. Since the strength of H-bonds is highly dependent on the proper spatial orientation, the smaller distances between the 6-hydroxyl group found in the benzofuran and indole based compounds seemed less favourable.

Table 4.10: Overall geometry of the different 6-hydroxybenzoheterocyclic compound classes described in this study



	A	D/15	D/18	D/26
D (Å)	8.01	7.61	7.57	8.26
A	96,8°	84,6°	81,2°	105°
Potency	44 nM (IC ₅₀)	66% inh. @ 1μM	62% inh. @ 1μM	13 nM (IC ₅₀)
X	S	O	NH	S
Y	N	CH	CH	CH

Due to the high molecular shape similarity of compound **A** and **D/26** the lowest energy conformations of both compounds were determined using an *ab initio* calculation to find a potential explanation for the three times higher potency of compound **D/26**. In brief, for compound **A** the lowest energy conformer was fully coplanar with both hydroxyl groups pointed in direction of the ketone bridge. The predicted low energy conformation (Figure 4.6, a) A-1) is probably stabilised by an intramolecular non-classical hydrogen bond involving the nitrogen of the benzothiazole moiety and the hydrogen atom in 5-position of the phenol moiety. Another local minimum of **A** was identified showing a dihedral angle of about 32° (Figure 4.6, a) A-3) which was close to the putative biological active conformation exhibiting a dihedral angle of about 45° as formerly suggested in a molecular docking study (Spadaro et al., 2012b). Hence, **A** can only bind to the target by adopting a less favourable conformation at the expense of an energy penalty. Interestingly, **D/26** can adopt two conformations which are energetically comparable (Figure 4.6, b)) and therefore an equilibrium between both conformations at room temperature could be expected.

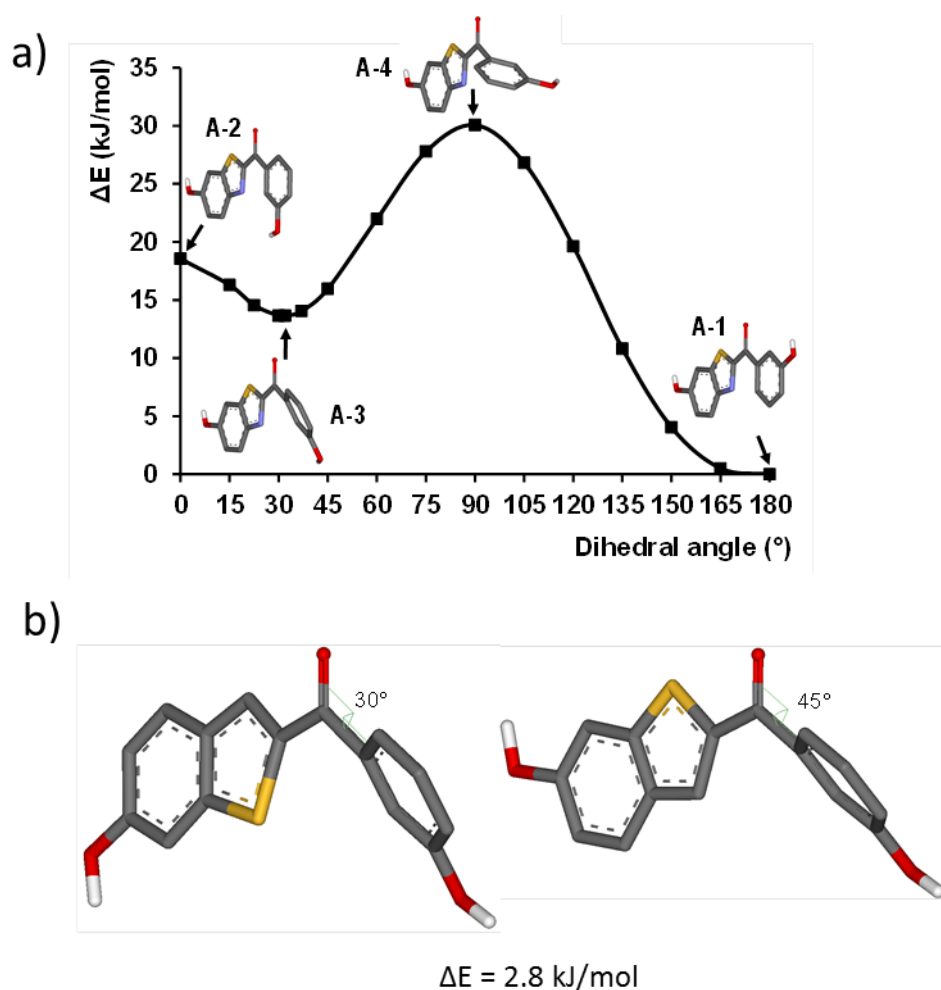


Figure 4.6: a) Conformational analysis of **A**. The energy difference relative to the lowest energy conformer **A1** is shown as a function of the dihedral angle between the phenol moiety and the carbonyl group. The conformer **A3** is similar to

the predicted biologically active conformer; b) lowest energy conformations of **D/26**. Both conformations have comparable potential energies, but only the conformation on the right corresponds to the biologically active conformation predicted previously (Spadaro et al., 2012b).

Thereby the ketone group is nearly coplanar with the benzothiophene moiety in both conformations but twisted by 180° against each other. Due to the flexibility of **D/26** between the inactive and the putative active conformation a higher entropy penalty compared to the conformational restricted **A** can be expected by binding to 17-β-HSD1. The small difference in inhibitory potency of **A** and **D/26** can be attributed to the entropic advantage of **A** which partially compensates the loss of binding enthalpy induced by adopting the unfavourable conformation **A-3** for protein binding. Different hydration stages between **A** and **D/26**, which affect the hydrophobic effect, were excluded since the lone pair of the nitrogen in **A** is involved in the non-classical hydrogen bond and therefore not fully available for surrounding water molecules.

In summary, the synthesis and biological evaluation of new benzoheterocyclic 17-β-HSD1 inhibitors was described. The systematic exchange of the heterocyclic component revealed the highly potent 6-hydroxybenzothiophene ketone **D/26** which provided optimal distance and angle between the two essential hydroxyl groups. Calculations using quantum mechanics suggested some degree of conformational pre-organization of **D/26** which potentially facilitates binding to the HSD1 active site. Therefore 6-hydroxybenzothiophene ketones can be used as templates for the design of new 17-β-HSD1 inhibitors.

5. References

- Adams, J. a (2001). Kinetic and catalytic mechanisms of protein kinases. *Chem Rev* *101*, 2271–2290.
- Adayev, T., Murakami, N., Wegiel, J., and Hwang, Y. (2006). Kinetic properties of a MNB/DYRK1A mutant suitable for the elucidation of biochemical pathways. *Biochemistry* *45*, 12011–12019.
- Akue-Gedu, R., Debiton, E., Ferandin, Y., Meijer, L., Prudhomme, M., Anizon, F., and Moreau, P. (2009). Synthesis and biological activities of aminopyrimidyl-indoles structurally related to meridianins. *Bioorg Med Chem* *17*, 4420–4424.
- Anand, P.K., Kaul, D., and Sharma, M. (2006). Green tea polyphenol inhibits Mycobacterium tuberculosis survival within human macrophages. *Int. J. Biochem Cell Biol* *38*, 600–609.
- Aranda, S., Laguna, A., and de la Luna, S. (2011). DYRK family of protein kinases: evolutionary relationships, biochemical properties, and functional roles. *FASEB J.* *25*, 449–462.
- Ashford, A., Oxley, D., Kettle, J., Hudson, K., Guichard, S., Cook, S., and Lochhead, P. (2014). A novel DYRK1B inhibitor, AZ191, demonstrates that DYRK1B acts independently of GSK3 β to phosphorylate cyclin D1 at threonine-286, not threonine-288. *Biochem J.* *457*, 43–56.
- Bain, J., McLauchlan, H., Elliott, M., and Cohen, P. (2003). The specificities of protein kinase inhibitors: an update. *Biochem J* *371*, 199–204.
- Bain, J., Plater, L., Elliott, M., Shpiro, N., Hastie, C.J., McLauchlan, H., Klevvernic, I., Arthur, J.S.C., Alessi, D.R., and Cohen, P. (2007). The selectivity of protein kinase inhibitors: a further update. *Biochem J* *408*, 297–315.
- Baki, A., Bielik, A., Molnár, L., Szendrei, G., and Keserü, G.M. (2007). A high throughput luminescent assay for glycogen synthase kinase-3beta inhibitors. *Assay Drug Dev. Technol.* *5*, 75–83.
- Becker, W. (2012). Emerging role of DYRK family protein kinases as regulators of protein stability in cell cycle control. *Cell Cycle* *11*, 3389–3394.
- Becker, W., and Joost, H.G. (1999). Structural and functional characteristics of Dyrk, a novel subfamily of protein kinases with dual specificity. *Prog Nucleic Acid Res Mol Biol* *62*, 1–17.
- Becker, W., and Sippl, W. (2011). Activation, regulation, and inhibition of DYRK1A. *FEBS J.* *278*, 246–256.
- Becker, W., Weber, Y., Wetzel, K., Eirnbter, K., Tejedor, F.J., and Joost, H.G. (1998). Sequence characteristics, subcellular localization, and substrate specificity of DYRK-related kinases, a novel family of dual specificity protein kinases. *J Biol Chem* *273*, 25893–25902.
- Ben-David, Y., Letwin, K., Tannock, L., Bernstein, A., and Pawson, T. (1991). A mammalian protein kinase with potential for serine/threonine and tyrosine phosphorylation is related to cell cycle regulators. *EMBO J* *10*, 317–325.
- Bernstein, F.C., Koetzle, T.F., Williams, G.J.B., Meyer, E.F., Brice, M.D., Rodgers, J.R., Kennard, O., Shimanouchi, T., and Tasumi, M. (1977). The Protein Data Bank. *Eur. J. Biochem.* *80*, 319–324.

Bey, E., Marchais-Oberwinkler, S., Werth, R., Negri, M., Al-Soud, Y.A., Kruchten, P., Oster, A., Frotscher, M., Birk, B., and Hartmann, R.W. (2008). Design, synthesis, biological evaluation and pharmacokinetics of bis(hydroxyphenyl) substituted azoles, thiophenes, benzenes, and aza-benzenes as potent and selective nonsteroidal inhibitors of 17 β -hydroxysteroid dehydrogenase type 1 (17 β -HSD1). *J Med Chem* 51, 6725–6739.

Bird, C.W. (1992). Heteroaromaticity, 5, a unified aromaticity index. *Tetrahedron* 48, 335–340.

Blockeel, A., Oxley, D., Cook, S., and Lochhead, P. (2011). DYRK1A and DYRK1B phosphorylate cyclin D1 on Thr286 to promote cyclin D1 turnover. In *Signalling 2011: A Biochemical Society Centenary Celebration*,.

Blunt, J.W., Copp, B.R., Munro, M.H.G., Northcote, P.T., and Prinsep, M.R. (2010). Marine natural products. *Nat. Prod. Rep.* 27, 165–237.

Boeira, J.M., da Silva, J., Erdtmann, B., and Henriques, J.A. (2001). Genotoxic effects of the alkaloids harman and harmine assessed by comet assay and chromosome aberration test in mammalian cells in vitro. *Pharmacol Toxicol* 89, 287–294.

Boeira, J.M., Viana, A.F., Picada, J.N., and Henriques, J.A. (2002). Genotoxic and recombinogenic activities of the two beta-carboline alkaloids harman and harmine in *Saccharomyces cerevisiae*. *Mutat Res* 500, 39–48.

Boersema, P.J., Mohammed, S., and Heck, A.J.R. (2009). Phosphopeptide fragmentation and analysis by mass spectrometry. *J. Mass Spec.* 44, 861–878.

De Bondt, H.L., Rosenblatt, J., Jancarik, J., Jones, H.D., Morgant, D.O., and Kim, S.-H. (1993). Crystal structure of cyclin-dependent kinase 2. *Nature* 363, 595–602.

Chang, L.-K., Wei, T.-T., Chiu, Y.-F., Tung, C.-P., Chuang, J.-Y., Hung, S.-K., Li, C., and Liu, S.-T. (2003). Inhibition of Epstein–Barr virus lytic cycle by (–)-epigallocatechin gallate. *Biochem. Biophys. Res. Commun.* 301, 1062–1068.

Chico, L.K., Van Eldik, L.J., and Watterson, D.M. (2009). Targeting protein kinases in central nervous system disorders. *Nat. Rev. Drug Discov.* 8, 892–909.

Cohen, P. (2002). Protein kinases--the major drug targets of the twenty-first century? *Nat. Rev. Drug Discov.* 1, 309–315.

Colwill, K., Pawson, T., Andrews, B., Prasad, J., Manley, J.L., Bell, J.C., and Duncan, P.I. (1996). The Clk/Sty protein kinase phosphorylates SR splicing factors and regulates their intranuclear distribution. *Embo J.* 15, 265–275.

Coombs, T.C., Tanega, C., Shen, M., Wang, J.L., Auld, D.S., Gerritz, S.W., Schoenen, F.J., Thomas, C.J., and Aubé, J. (2013). Small-molecule pyrimidine inhibitors of the cdc2-like (Clk) and dual specificity tyrosine phosphorylation-regulated (Dyrk) kinases: development of chemical probe ML315. *Bioorg Med Chem Lett* 23, 3654–3661.

Cox, K.J., Shomin, C.D., and Ghosh, I. (2010). Tinkering outside the kinase ATP box: allosteric (type IV) and bivalent (type V) inhibitors of protein kinases. *Futur. Med Chem* 3, 29–43.

Cozza, G., Sarno, S., Ruzzene, M., Girardi, C., Orzeszko, A., Kazimierczuk, Z., Zagotto, G., Bonaiuto, E., Di Paolo, M.L., and Pinna, L. a (2013). Exploiting the repertoire of CK2 inhibitors to target DYRK and PIM kinases. *Biochim. Biophys. Acta* 1402–1409.

Craig, A.G., Hoeger, C.A., Miller, C.L., Goedken, T., Rivier, J.E., and Fischer, W.H. (1994). Monitoring protein kinase and phosphatase reactions with matrix-assisted laser desorption/ionization mass spectrometry and capillary zone electrophoresis: comparison of the detection efficiency of peptide-phosphopeptide mixtures. *Biol. Mass Spectrom.* 23, 519–528.

Cuny, G.D., Robin, M., Ulyanova, N.P., Patnaik, D., Pique, V., Casano, G., Liu, J.F., Lin, X., Xian, J., Glicksman, M.A., et al. (2010). Structure-activity relationship study of acridine analogs as haspin and DYRK2 kinase inhibitors. *Bioorg Med Chem Lett* 20, 3491–3494.

Debdab, M., Carreaux, F., Renault, S., Soundararajan, M., Fedorov, O., Filippakopoulos, P., Lozach, O., Babault, L., Tahtouh, T., Baratte, B., et al. (2011). Leucettines, a class of potent inhibitors of cdc2-like kinases and dual specificity, tyrosine phosphorylation regulated kinases derived from the marine sponge leucettamine B: modulation of alternative pre-RNA splicing. *J. Med. Chem.* 54, 4172–4186.

Deng, X., Mercer, S.E., Shah, S., Ewton, D.Z., and Friedman, E. (2004). The cyclin-dependent kinase inhibitor p27Kip1 is stabilized in G(0) by Mirk/dyrk1B kinase. *J Biol Chem* 279, 22498–22504.

Deng, X., Ewton, D.Z., Mercer, S.E., and Friedman, E. (2005). Mirk/dyrk1B decreases the nuclear accumulation of class II histone deacetylases during skeletal muscle differentiation. *J. Biol. Chem.* 280, 4894–4905.

Deng, X., Ewton, D.Z., Li, S., Naqvi, A., Mercer, S.E., Landas, S., and Friedman, E. (2006). The kinase Mirk/Dyrk1B mediates cell survival in pancreatic ductal adenocarcinoma. *Cancer Res* 66, 4149–4158.

Deng, X., Ewton, D.Z., and Friedman, E. (2009a). Mirk/Dyrk1B maintains the viability of quiescent pancreatic cancer cells by reducing levels of reactive oxygen species. *Cancer Res* 69, 3317–3324.

Deng, X., Ewton, D.Z., and Friedman, E. (2009b). Mirk/Dyrk1B maintains the viability of quiescent pancreatic cancer cells by reducing levels of reactive oxygen species. *Cancer Res* 69, 3317–3324.

Dennis, P.B., Jaeschke, A., Saitoh, M., Fowler, B., Kozma, S.C., and Thomas, G. (2001). Mammalian TOR: a homeostatic ATP sensor. *Science* (80-.). 294, 1102–1105.

Dowjat, W.K., Adayev, T., Kuchna, I., Nowicki, K., Palmieriello, S., Hwang, Y.W., and Wegiel, J. (2007). Trisomy-driven overexpression of DYRK1A kinase in the brain of subjects with Down syndrome. *Neurosci. Lett.* 413, 77–81.

Duncan, P.I., Stojdl, D.F., Marius, R.M., and Bell, J.C. (1997). In vivo regulation of alternative pre-mRNA splicing by the Clk1 protein kinase. *Mol Cell Biol* 17, 5996–6001.

Echalier, A., Bettayeb, K., Ferandin, Y., Lozach, O., Clément, M., Valette, A., Liger, F., Marquet, B., Morris, J.C., Endicott, J. a, et al. (2008). Meriolins (3-(pyrimidin-4-yl)-7-azaindoles): synthesis, kinase inhibitory activity, cellular effects, and structure of a CDK2/cyclin A/meriolin complex. *J. Med. Chem* 51, 737–751.

- Ertl, P., Rohde, B., and Selzer, P. (2000). Fast calculation of molecular polar surface area as a sum of fragment-based contributions and its application to the prediction of drug transport properties. *J Med Chem* *43*, 3714–3717.
- Ewton, D.Z., Hu, J., Vilenchik, M., Deng, X., Luk, K.-C.C., Polonskaia, A., Hoffman, A.F., Zipf, K., Boylan, J.F., and Friedman, E. a (2011a). Inactivation of mirk/dyrk1b kinase targets quiescent pancreatic cancer cells. *Mol Cancer Ther* *10*, 2104–2114.
- Ewton, D.Z., Hu, J., Vilenchik, M., Deng, X., Luk, K.C., Polonskaia, A., Hoffman, A.F., Zipf, K., Boylan, J.F., and Friedman, E.A. (2011b). Inactivation of mirk/dyrk1b kinase targets quiescent pancreatic cancer cells. *Mol Cancer Ther* *10*, 2104–2114.
- Fedorov, O., Marsden, B., Pogacic, V., Rellos, P., Müller, S., Bullock, A.N., Schwaller, J., Sundström, M., and Knapp, S. (2007). A systematic interaction map of validated kinase inhibitors with Ser/Thr kinases. *PNAS* *104*, 20523–20528.
- Fedorov, O., Huber, K., Eisenreich, A., Filippakopoulos, P., King, O., Bullock, A.N., Szklarczyk, D., Jensen, L.J., Fabbro, D., Trappe, J., et al. (2011). Specific CLK inhibitors from a novel chemotype for regulation of alternative splicing. *Chem. Biol.* *18*, 67–76.
- Fischer, D., Noack, K., Runnebaum, I., Watermann, D., Kieback, D., Stamm, S., and Stickeler, E. (2004). Expression of splicing factors in human ovarian cancer. *Oncol. Rep.* *11*, 1085–1090.
- Friedman, M., Henika, P.R., Levin, C.E., Mandrell, R.E., and Kozukue, N. (2006). Antimicrobial Activities of Tea Catechins and Theaflavins and Tea Extracts against *Bacillus cereus*. *J. Food Prot.* *69*, 354–361.
- Frost, D., Meechoovet, B., Wang, T., Gately, S., Giorgetti, M., Shcherbakova, I., and Dunckley, T. (2011). β -carboline compounds, including harmine, inhibit DYRK1A and tau phosphorylation at multiple Alzheimer's disease-related sites. *PLoS One* *6*, e19264.
- Frye, S. V (1999). Structure-activity relationship homology (SARAH): a conceptual framework for drug discovery in the genomic era. *Chem. Biol.* *6*, R3–7.
- Gao, J., Zheng, Z., Rawal, B., Schell, M.J., Bepler, G., and Haura, E.B. (2009). Mirk/Dyrk1B, a novel therapeutic target, mediates cell survival in non-small cell lung cancer cells. *Cancer Biol Ther* *8*, 1671–1679.
- Gao, J., Yang, X., Yin, P., Hu, W., Liao, H., Miao, Z., Pan, C., and Li, N. (2012). The involvement of FoxO in cell survival and chemosensitivity mediated by Mirk/Dyrk1B in ovarian cancer. *Int J Oncol.* *40*, 1203–1209.
- Garcia-Blanco, M. a, Baraniak, A.P., and Lasda, E.L. (2004). Alternative splicing in disease and therapy. *Nat. Biotechnol.* *22*, 535–546.
- Geiger, J.N., Knudsen, G.T., Panek, L., Pandit, A.K., Yoder, M.D., Lord, K.A., Creasy, C.L., Burns, B.M., Gaines, P., Dillon, S.B., et al. (2001). mDYRK3 kinase is expressed selectively in late erythroid progenitor cells and attenuates colony-forming unit-erythroid development. *Blood* *97*, 901–910.

Ghose, A.K., Herbertz, T., Pippin, D.A., Salvino, J.M., and Mallamo, J.P. (2008). Knowledge Based Prediction of Ligand Binding Modes and Rational Inhibitor Design for Kinase Drug Discovery. *J. Med. Chem.* *51*, 19–21.

Ghose, A.K., Herbertz, T., Hudkins, R.L., Dorsey, B.D., and Mallamo, J.P. (2012). Knowledge-Based, Central Nervous System (CNS) Lead Selection and Lead Optimization for CNS Drug Discovery. *ACS Chem. Neurosci.* *3*, 50–68.

Giraud, F., Alves, G., Debiton, E., Nauton, L., Théry, V., Durieu, E., Ferandin, Y., Lozach, O., Meijer, L., Anizon, F., et al. (2011a). Synthesis, protein kinase inhibitory potencies, and in vitro antiproliferative activities of meridianin derivatives. *J. Med. Chem.* *54*, 4474–4489.

Giraud, F., Alves, G., Debiton, E., Nauton, L., Théry, V., Durieu, E., Ferandin, Y., Lozach, O., Meijer, L., Anizon, F., et al. (2011b). Synthesis, protein kinase inhibitory potencies, and in vitro antiproliferative activities of meridianin derivatives. *J. Med. Chem.* *54*, 4474–4489.

Glickman, J.F., and Ph, D. (2012). Assay Development for Protein Kinase Enzymes. In *Assay Guidance Manual*, J. McGee, and A. Napper, eds. (Eli Lilly & Company and the National Center for Advancing Translational Sciences), pp. 1–19.

Göckler, N., Jofre, G., Papadopoulos, C., Soppa, U., Tejedor, F.J., Becker, W., and Gockler, N. (2009). Harmine specifically inhibits protein kinase DYRK1A and interferes with neurite formation. *FEBS J.* *276*, 6324–6337.

Gold, M.G., Barford, D., and Komander, D. (2006). Lining the pockets of kinases and phosphatases. *Curr Opin Struct Biol* *16*, 693–701.

Goldberg, J., Nairn, a C., and Kuriyan, J. (1996). Structural basis for the autoinhibition of calcium/calmodulin-dependent protein kinase I. *Cell* *84*, 875–887.

Gompel, M., Leost, M., De Kier Joffe, E.B., Puricelli, L., Franco, L.H., Palermo, J., and Meijer, L. (2004). Meridianins, a new family of protein kinase inhibitors isolated from the ascidian *Aplidium meridianum*. *Bioorg Med Chem Lett* *14*, 1703–1707.

Gratz, A., Götz, C., and Jose, J. (2010). A CE-based assay for human protein kinase CK2 activity measurement and inhibitor screening. *Electrophoresis* *31*, 634–640.

Graves, J.D., and Krebs, E.G. (1999). Protein phosphorylation and signal transduction. *Pharmacol Ther.* *82*, 111–121.

Greis, K.D., Zhou, S., Burt, T.M., Carr, A.N., Dolan, E., Easwaran, V., Evdokimov, A., Kawamoto, R., Roesgen, J., and Davis, G.F. (2006). MALDI-TOF MS as a label-free approach to rapid inhibitor screening. *J. Am. Soc. Mass Spectrom.* *17*, 815–822.

Griffith, J., Black, J., Faerman, C., Swenson, L., Wynn, M., Lu, F., Lippke, J., and Saxena, K. (2004). The structural basis for autoinhibition of FLT3 by the juxtamembrane domain. *Mol Cell* *13*, 169–178.

Gropengiesser, J., Varadarajan, B.T., Stephanowitz, H., and Krause, E. (2009). The relative influence of phosphorylation and methylation on responsiveness of peptides to MALDI and ESI mass spectrometry. *J. Mass Spectrom.* *44*, 821–831.

- Guedj, F., Sebrie, C., Rivals, I., Ledru, A., Paly, E., Bizot, J.C., Smith, D., Rubin, E., Gillet, B., Arbones, M., et al. (2009). Green tea polyphenols rescue of brain defects induced by overexpression of DYRK1A. *PLoS One* 4, e4606.
- Hartmann, a M., Rujescu, D., Giannakouros, T., Nikolakaki, E., Goedert, M., Mandelkow, E.M., Gao, Q.S., Andreadis, A., and Stamm, S. (2001). Regulation of alternative splicing of human tau exon 10 by phosphorylation of splicing factors. *Mol Cell Neurosci* 18, 80–90.
- Hastie, C.J., McLauchlan, H.J., and Cohen, P. (2006). Assay of protein kinases using radiolabeled ATP: a protocol. *Nat. Protoc.* 1, 968–971.
- Hirasawa, M., and Takada, K. (2004). Multiple effects of green tea catechin on the antifungal activity of antimycotics against *Candida albicans*. *J. Antimicrob. Chemother.* 53, 225–229.
- Howell, B.W., Afar, D.E.H., Lew, J., Douville, E.M.J., Icely, P.L.E., Gray, D.A., and Bell, J.C. (1991). STY, a Tyrosine-Phosphorylating Enzyme with Sequence Homology to Serine / Threonine Kinases. *Mol Cell Biol* 11, 568–572.
- Hu, J., Nakhla, H., and Friedman, E. (2011). Transient arrest in a quiescent state allows ovarian cancer cells to survive suboptimal growth conditions and is mediated by both Mirk/dyrk1b and p130/RB2. *Int J Cancer* 129, 307–318.
- Huse, M., and Chen, Y. (1999). Crystal Structure of the Cytoplasmic Domain of the Type I TGF β Receptor in Complex with FKBP12 * Laboratories of Molecular Biophysics. *Cell* 96, 425–436.
- Huse, M., and Kuriyan, J. (2002). The conformational plasticity of protein kinases. *Cell* 109, 275–282.
- Huse, M., Muir, T.W., Xu, L., Chen, Y.G., Kuriyan, J., and Massagué, J. (2001). The TGF β receptor activation process: an inhibitor- to substrate-binding switch. *Mol Cell* 8, 671–682.
- Jimenez, J., Riveron-Negrete, L., Abdullaev, F., Espinosa-Aguirre, J., and Rodriguez-Arnaiz, R. (2008). Cytotoxicity of the beta-carboline alkaloids harmine and harmaline in human cell assays in vitro. *Exp Toxicol Pathol* 60, 381–389.
- Jin, K., Ewton, D.Z., Park, S., Hu, J., and Friedman, E. (2009). Mirk regulates the exit of colon cancer cells from quiescence. *J Biol Chem* 284, 22916–22925.
- Johnson, G. V, and Stoothoff, W.H. (2004). Tau phosphorylation in neuronal cell function and dysfunction. *J Cell Sci* 117, 5721–5729.
- Jung, H.-Y., Wang, X., Jun, S., and Park, J.-I. (2013). Dyrk2-associated EDD-DDB1-VprBP E3 ligase inhibits telomerase by TERT degradation. *J Biol Chem* 288, 7252–7262.
- Kapkova, P., Lattova, E., and Perreault, H. (2006). Nonretentive solid-phase extraction of phosphorylated peptides from complex peptide mixtures for detection by matrix-assisted laser desorption/ionization mass spectrometry. *Anal. Chem.* 78, 7027–7033.
- Karas, M., Ehring, H., Nordhoff, E., Stahl, B., Strupat, K., and Hillenkamp, F. (1993). Matrix-assisted Laser Desorption/Ionization Mass Spectrometry with Additives to hydroxy benzoic Acid. *Org. Mass Spec.* 28, 1476–1481.

Karlsson, R., Zheng, J., Xuong, N., Taylor, S.S., and Sowadski, J.M. (1993). Structure of the mammalian catalytic subunit of cAMP-dependent protein kinase and an inhibitor peptide displays an open conformation. *Acta Crystallogr. D* 49, 381–3888.

Kentrup, H., Becker, W., Heukelbach, J., Wilmes, A., Schurmann, A., Huppertz, C., Kainulainen, H., and Joost, H.G. (1996). Dyrk, a dual specificity protein kinase with unique structural features whose activity is dependent on tyrosine residues between subdomains VII and VIII. *J Biol Chem* 271, 3488–3495.

Kim, E.J., Sung, J.Y., Lee, H.J., Rhim, H., Hasegawa, M., Iwatsubo, T., Min do, S., Kim, J., Paik, S.R., and Chung, K.C. (2006a). Dyrk1A phosphorylates alpha-synuclein and enhances intracellular inclusion formation. *J Biol Chem* 281, 33250–33257.

Kim, H., Sablin, S.O., and Ramsay, R.R. (1997). Inhibition of monoamine oxidase A by beta-carboline derivatives. *Arch Biochem Biophys* 337, 137–142.

Kim, N.D., Yoon, J., Kim, J.H., Lee, J.T., Chon, Y.S., Hwang, M.-K., Ha, I., and Song, W.-J. (2006b). Putative therapeutic agents for the learning and memory deficits of people with Down syndrome. *Bioorg Med Chem Lett* 16, 3772–3776.

Kimura, R., Kamino, K., Yamamoto, M., Nuripa, A., Kida, T., Kazui, H., Hashimoto, R., Tanaka, T., Kudo, T., Yamagata, H., et al. (2007a). The DYRK1A gene, encoded in chromosome 21 Down syndrome critical region, bridges between beta-amyloid production and tau phosphorylation in Alzheimer disease. *Hum Mol Genet* 16, 15–23.

Kimura, R., Kamino, K., Yamamoto, M., Nuripa, A., Kida, T., Kazui, H., Hashimoto, R., Tanaka, T., Kudo, T., Yamagata, H., et al. (2007b). The DYRK1A gene, encoded in chromosome 21 Down syndrome critical region, bridges between beta-amyloid production and tau phosphorylation in Alzheimer disease. *Hum Mol Genet* 16, 15–23.

Knight, Z. a, and Shokat, K.M. (2005). Features of selective kinase inhibitors. *Chem. Biol.* 12, 621–637.

Knighton, D.R., Zheng, J., Eyck, L.F.T.E.N., Ashford, V.A., Xuong, N., Taylor, S.S., and Sowadski, J.M. (1991a). Crystal Structure of the Catalytic Subunit of Cyclic Adenosine Monophosphate-Dependent Protein Kinase. *Science* (80-). 253, 407–414.

Knighton, D.R., Zheng, J.H., Ten Eyck, L.F., Xuong, N.H., Taylor, S.S., and Sowadski, J.M. (1991b). Structure of a peptide inhibitor bound to the catalytic subunit of cyclic adenosine monophosphate-dependent protein kinase. *Science* (80-). 253, 414–420.

Koo, K.A., Kim, N.D., Chon, Y.S., Jung, M.-S.S., Lee, B.-J.J., Kim, J.H., and Song, W.-J.J. (2009). QSAR analysis of pyrazolidine-3,5-diones derivatives as Dyrk1A inhibitors. *Bioorg Med Chem Lett* 19, 2324–2328.

Koon, N., Schneider-Stock, R., Sarlomo-Rikala, M., Lasota, J., Smolkin, M., Petroni, G., Zaika, A., Boltze, C., Meyer, F., Andersson, L., et al. (2004). Molecular targets for tumour progression in gastrointestinal stromal tumours. *Gut* 53, 235–240.

- Kurabayashi, N., Hirota, T., Sakai, M., Sanada, K., and Fukada, Y. (2010). DYRK1A and glycogen synthase kinase 3beta, a dual-kinase mechanism directing proteasomal degradation of CRY2 for circadian timekeeping. *Mol Cell Biol* *30*, 1757–1768.
- De la Torre, R., De Sola, S., Pons, M., Duchon, A., de Lagran, M.M., Farré, M., Fitó, M., Benejam, B., Langohr, K., Rodriguez, J., et al. (2013). Epigallocatechin-3-gallate, a DYRK1A inhibitor, rescues cognitive deficits in Down syndrome mouse models and in humans. *Mol Nutr. Food Res.* 1–11.
- Lahiry, P., Torkamani, A., Schork, N.J., and Hegele, R. a (2010). Kinase mutations in human disease: interpreting genotype-phenotype relationships. *Nat. Rev Gen* *11*, 60–74.
- Lamba, V., and Ghosh, I. (2012). New directions in targeting protein kinases: focusing upon true allosteric and bivalent inhibitors. *Curr Pharm Des* *18*, 2936–2945.
- Lambert, J.D., Sang, S., and Yang, C.S. (2007). Biotransformation of Green Tea Polyphenols and the Biological Activities of Those Metabolites. *Mol. Pharm.* *4*, 819–825.
- Laurence, C., Brameld, K. a, Graton, J., Le Questel, J.-Y., and Renault, E. (2009). The pK(BHX) database: toward a better understanding of hydrogen-bond basicity for medicinal chemists. *J Med Chem* *52*, 4073–4086.
- Lee, K., Deng, X., and Friedman, E. (2000). Mirk Protein Kinase Is a Mitogen-activated Protein Kinase Substrate That Mediates Survival of Colon Cancer Cells Mirk Protein Kinase Is a Mitogen-activated Protein Kinase Substrate That Mediates Survival of Colon Cancer Cells 1. *Cancer Res* *60*, 3631–3637.
- Lei, C., and Hong-Yu, Z. (2007). Cancer Preventive Mechanisms of the Green Tea Polyphenol (-)-Epigallocatechin-3-gallate. *Molecules* *12*, 946–957.
- Leone, M., Zhai, D., Sareth, S., Kitada, S., Reed, J.C., and Pellecchia, M. (2003). Cancer Prevention by Tea Polyphenols Is Linked to Their Direct Inhibition of Antiapoptotic Bcl-2-Family Proteins. *Cancer Res.* *63* , 8118–8121.
- Liang, Y.J., Chang, H.S., Wang, C.Y., and Yu, W.C. (2008). DYRK1A stabilizes HPV16E7 oncoprotein through phosphorylation of the threonine 5 and threonine 7 residues. *Int J Biochem Cell Biol* *40*, 2431–2441.
- Van Linden, O.P.J., Kooistra, A.J., Leurs, R., de Esch, I.J.P., and de Graaf, C. (2013). KLIFS: A knowledge-based structural database to navigate kinase-ligand interaction space. *J Med Chem.*
- Lipinski, C.A. (2000). Drug-like properties and the causes of poor solubility and poor permeability. *J. Pharmacol. Toxicol. Methods* *44*, 235–249.
- Liu, F., and Gong, C.-X. (2008). Tau exon 10 alternative splicing and tauopathies. *Mol Neurodeg.* *3*, 8.
- Liu, Y., and Gray, N.S. (2006). Rational design of inhibitors that bind to inactive kinase conformations. *Nat. Chem Biol* *2*, 358–364.
- Liu, F., Liang, Z., Wegiel, J., Hwang, Y.-W.W., Iqbal, K., Grundke-Iqbal, I., Ramakrishna, N., and Gong, C.-X.X. (2008). Overexpression of Dyrk1A contributes to neurofibrillary degeneration in Down syndrome. *FASEB J* *22*, 3224–3233.

- Liu, Y., Conaway, L., Rutherford Bethard, J., Al-Ayoubi, A.M., Thompson Bradley, A., Zheng, H., Weed, S. a, and Eblen, S.T. (2013). Phosphorylation of the alternative mRNA splicing factor 45 (SPF45) by Clk1 regulates its splice site utilization, cell migration and invasion. *Nucleic Acids Res.* *41*, 4949–4962.
- Lochhead, P. a, Sibbet, G., Morrice, N., and Cleghon, V. (2005). Activation-loop autophosphorylation is mediated by a novel transitional intermediate form of DYRKs. *Cell* *121*, 925–936.
- Lord, K.A., Creasy, C.L., King, A.G., King, C., Burns, B.M., Lee, J.C., and Dillon, S.B. (2000). REDK, a novel human regulatory erythroid kinase. *Blood* *95*, 2838–2846.
- Madhusudan, Akamine, P., Xuong, N.-H., and Taylor, S.S. (2002). Crystal structure of a transition state mimic of the catalytic subunit of cAMP-dependent protein kinase. *Nat. Struct. Biol.* *9*, 273–277.
- Mallari, R., Swearingen, E., Liu, W., Ow, A., Young, S.W., and Huang, S.-G. (2003). A generic high-throughput screening assay for kinases: protein kinase a as an example. *J. Biomol. Screen.* *8*, 198–204.
- Manning, G., Whyte, D.B., Martinez, R., Hunter, T., and Sudarsanam, S. (2002). The protein kinase complement of the human genome. *Science* (80-). *298*, 1912–1934.
- Marco, E., Laine, W., Tardy, C., Lansiaux, A., Iwao, M., Ishibashi, F., Bailly, C., and Gago, F. (2005). Molecular Determinants of Topoisomerase I Poisoning by Lamellarins: Comparison with Camptothecin and Structure–Activity Relationships. *J. Med. Chem.* *48*, 3796–3807.
- Matsumoto, H., Kahn, E.S., and Komori, N. (1998). Nonradioactive phosphopeptide assay by matrix-assisted laser desorption ionization time-of-flight mass spectrometry: application to calcium/calmodulin-dependent protein kinase II. *Anal. Biochem.* *260*, 188–194.
- Matthews, D.J., and Gerritsen, M.E. (2010). Targeting Protein Kinases For Cancer Therapy.
- Meggio, F., and Pinna, L. a (2003). One-thousand-and-one substrates of protein kinase CK2? *FASEB J.* *17*, 349–368.
- Mercer, S.E., Ewton, D.Z., Deng, X., Lim, S., Mazur, T.R., and Friedman, E. (2005). Mirk/Dyrk1B mediates survival during the differentiation of C2C12 myoblasts. *J Biol Chem* *280*, 25788–25801.
- Miller, C.T., Aggarwal, S., Lin, T.K., Dagenais, S.L., Contreras, J.I., Orringer, M.B., Glover, T.W., Beer, D.G., and Lin, L. (2003). Amplification and overexpression of the dual-specificity tyrosine-(Y)-phosphorylation regulated kinase 2 (DYRK2) gene in esophageal and lung adenocarcinomas. *Cancer Res* *63*, 4136–4143.
- Mimoto, R., Taira, N., Takahashi, H., Yamaguchi, T., Okabe, M., Uchida, K., Miki, Y., and Yoshida, K. (2013). DYRK2 controls the epithelial–mesenchymal transition in breast cancer by degrading Snail. *Cancer Lett.* *339*, 214–225.
- Miralles, A., Esteban, S., Sastre-Coll, A., Moranta, D., Asensio, V.J., and Garcia-Sevilla, J.A. (2005). High-affinity binding of beta-carbolines to imidazoline I2B receptors and MAO-A in rat tissues: norharman blocks the effect of morphine withdrawal on DOPA/noradrenaline synthesis in the brain. *Eur J Pharmacol* *518*, 234–242.

Misteli, T., Cáceres, J.F., Clement, J.Q., Krainer, a R., Wilkinson, M.F., and Spector, D.L. (1998). Serine phosphorylation of SR proteins is required for their recruitment to sites of transcription in vivo. *J Cell Biol* 143, 297–307.

Miyata, Y., and Nishida, E. (2004). CK2 Controls Multiple Protein Kinases by Phosphorylating a Kinase-Targeting Molecular Chaperone , Cdc37. *Mol. Cell. Biol.* 24, 4065–4074.

Mott, B.T., Tanega, C., Shen, M., Maloney, D.J., Shinn, P., Leister, W., Marugan, J.J., Inglese, J., Austin, C.P., Misteli, T., et al. (2009). Evaluation of substituted 6-arylquinazolin-4-amines as potent and selective inhibitors of cdc2-like kinases (Clk). *Bioorg Med Chem Lett* 19, 6700–6705.

Mues, A., Young, P., Fu, D.O., Wilmanns, M., Gautel, M., Caruso, A., Uria-nickelsen, M., Mills, D.M., Ives, C., Gibson, R., et al. (1999). Structural basis for activation of the. 397, 863–869.

Muraki, M., Ohkawara, B., Hosoya, T., Onogi, H., Koizumi, J., Koizumi, T., Sumi, K., Yomoda, J., Murray, M. V, Kimura, H., et al. (2004). Manipulation of alternative splicing by a newly developed inhibitor of Clks. *J Biol Chem* 279, 24246–24254.

Nayler, O., Stamm, S., and Ullrich, A. (1997). Characterization and comparison of four serine- and arginine-rich (SR) protein kinases. *Biochem J.* 326, 693–700.

Neagoie, C., Vedrenne, E., Buron, F., Mérour, J.-Y., Rosca, S., Bourg, S., Lozach, O., Meijer, L., Baldeyrou, B., Lansiaux, A., et al. (2012). Synthesis of chromeno[3,4-b]indoles as Lamellarin D analogues: a novel DYRK1A inhibitor class. *Eur. J. Med. Chem.* 49, 379–396.

Ngo, J.C.K., Chakrabarti, S., Ding, J.-H., Velazquez-Dones, A., Nolen, B., Aubol, B.E., Adams, J. a, Fu, X.-D., and Ghosh, G. (2005). Interplay between SRPK and Clk/Sty kinases in phosphorylation of the splicing factor ASF/SF2 is regulated by a docking motif in ASF/SF2. *Mol. Cell* 20, 77–89.

Noble, M.E.M., Endicott, J. a, and Johnson, L.N. (2004). Protein kinase inhibitors: insights into drug design from structure. *Science* (80-). 303, 1800–1805.

Nolen, B., Taylor, S., and Ghosh, G. (2004). Regulation of protein kinases; controlling activity through activation segment conformation. *Mol Cell* 15, 661–675.

Obach, R.S. (1999). Prediction of human clearance of twenty-nine drugs from hepatic microsomal intrinsic clearance data: An examination of in vitro half-life approach and nonspecific binding to microsomes. *Drug Metab Dispos* 27, 1350–1359.

Ogawa, Y., Nonaka, Y., Goto, T., Ohnishi, E., Hiramatsu, T., Kii, I., Yoshida, M., Ikura, T., Onogi, H., Shibuya, H., et al. (2010). Development of a novel selective inhibitor of the Down syndrome-related kinase Dyrk1A. *Nat. Comm* 1, 86.

Ornitz, D.M., Xu, J., Colvin, J.S., McEwen, D.G., MacArthur, C.A., Coulier, F., Gao, G., and Goldfarb, M. (1996). Receptor Specificity of the Fibroblast Growth Factor Family. *J. Biol. Chem.* 271 , 15292–15297.

Oz, H.S., Chen, T., and de Villiers, W.J.S. (2013). Green tea polyphenols and sulfasalazine have parallel anti-inflammatory properties in colitis models. *Front. Immunol.* 4, 00132.

Pagano, M.A., Bain, J., Kazimierczuk, Z., Sarno, S., Ruzzene, M., Di Maira, G., Elliott, M., Orzeszko, A., Cozza, G., Meggio, F., et al. (2008). The selectivity of inhibitors of protein kinase CK2: an update. *Biochem J* 415, 353–365.

Papadopoulos, C., Arato, K., Lilienthal, E., Zerweck, J., Schutkowski, M., Chatain, N., Müller-Newen, G., Becker, W., and de la Luna, S. (2011). Splice variants of the dual specificity tyrosine phosphorylation-regulated kinase 4 (DYRK4) differ in their subcellular localization and catalytic activity. *J. Biol. Chem.* 286, 5494–5505.

Park, J., Yang, E.J., Yoon, J.H., and Chung, K.C. (2007). Dyrk1A overexpression in immortalized hippocampal cells produces the neuropathological features of Down syndrome. *Mol. Cell. Neurosci.* 36, 270–279.

Parker, L., Engel-Hall, A., Drew, K., Steinhardt, G., Helseth, D.L., Jabon, D., McMurry, T., Angulo, D.S., and Kron, S.J. (2008). Investigating quantitation of phosphorylation using MALDI-TOF mass spectrometry. *J. Mass Spectrom.* 43, 518–527.

Pozo, N., Zahonero, C., Fernández, P., Liñares, J.M., Ayuso, A., Hagiwara, M., Pérez, A., Ricoy, J.R., Hernández-laín, A., Sepúlveda, J.M., et al. (2013). Inhibition of DYRK1A destabilizes EGFR and reduces EGFR-dependent glioblastoma growth. *J. Clin. Invest.* 123, 2475–2487.

Qian, K.C., Wang, L., Hickey, E.R., Studts, J., Barringer, K., Peng, C., Kronkaitis, A., Li, J., White, A., Mische, S., et al. (2005). Structural basis of constitutive activity and a unique nucleotide binding mode of human Pim-1 kinase. *J. Biol. Chem.* 280, 6130–6137.

Qian, W., Liang, H., Shi, J., Jin, N., Grundke-Iqbal, I., Iqbal, K., Gong, C.-X., and Liu, F. (2011). Regulation of the alternative splicing of tau exon 10 by SC35 and Dyrk1A. *Nucleic Acids Res.* 39, 6161–6171.

Raingeaud, J., Gupta, S., Rogers, J.S., Dickens, M., Han, J., Ulevitch, R.J., and Davis, R.J. (1995). Pro-inflammatory Cytokines and Environmental Stress Cause p38 Mitogen-activated Protein Kinase Activation by Dual Phosphorylation on Tyrosine and Threonine. *J. Biol. Chem.* 270, 7420–7426.

Rathore, R., Corr, J.J., Scott, G., Vollmerhaus, P., and Greis, K.D. (2008). Development of an inhibitor screening platform via mass spectrometry. *J. Biomol. Screen.* 13, 1007–1013.

Rathore, R., Pribil, P., Corr, J.J., Seibel, W.L., Evdokimov, A., and Greis, K.D. (2010). Multiplex enzyme assays and inhibitor screening by mass spectrometry. *J. Biomol. Screen.* 15, 1001–1007.

Reeves, R.H., Irving, N.G., Moran, T.H., Wohn, A., Kitt, C., Sisodia, S.S., Schmidt, C., Bronson, R.T., and Davisson, M.T. (1995). A mouse model for Down syndrome exhibits learning and behaviour deficits. *Nat Genet* 11, 177–184.

Rosenthal, A.S., Tanega, C., Shen, M., Mott, B.T., Bougie, J.M., Nguyen, D.-T., Misteli, T., Auld, D.S., Maloney, D.J., and Thomas, C.J. (2011). Potent and selective small molecule inhibitors of specific isoforms of Cdc2-like kinases (Clk) and dual specificity tyrosine-phosphorylation-regulated kinases (Dyrk). *Bioorg Med Chem Lett* 21, 3152–3158.

Rothe, G., and Valet, G. (1990). Flow cytometric analysis of respiratory burst activity in phagocytes with hydroethidine and 2',7'-dichlorofluorescein. *J. Leukoc. Biol.* 47, 440–448.

- Rush, J., Moritz, A., Lee, K.A., Guo, A., Goss, V.L., Spek, E.J., Zhang, H., Zha, X.M., Polakiewicz, R.D., and Comb, M.J. (2005). Immunoaffinity profiling of tyrosine phosphorylation in cancer cells. *Nat Biotechnol* 23, 94–101.
- Ryoo, S.R., Cho, H.J., Lee, H.W., Jeong, H.K., Radnaabazar, C., Kim, Y.S., Kim, M.J., Son, M.Y., Seo, H., Chung, S.H., et al. (2008). Dual-specificity tyrosine(Y)-phosphorylation regulated kinase 1A-mediated phosphorylation of amyloid precursor protein: evidence for a functional link between Down syndrome and Alzheimer's disease. *J Neurochem* 104, 1333–1344.
- Ryoo, S.-R.R., Jeong, H.K., Radnaabazar, C., Yoo, J.-J.J., Cho, H.-J.J., Lee, H.-W.W., Kim, I.-S.S., Cheon, Y.-H.H., Ahn, Y.S., Chung, S.-H.H., et al. (2007). DYRK1A-mediated hyperphosphorylation of Tau. A functional link between Down syndrome and Alzheimer disease. *J Biol Chem* 282, 34850–34857.
- Sadler, T.M., Achilleos, M., Ragnathan, S., Pitkin, A., LaRocque, J., Morin, J., Annable, R., Greenberger, L.M., Frost, P., and Zhang, Y. (2004). Development and comparison of two nonradioactive kinase assays for I kappa B kinase. *Anal Biochem* 326, 106–113.
- Sarno, S., Mazzorana, M., Traynor, R., Ruzzene, M., Cozza, G., Pagano, M. a, Meggio, F., Zagotto, G., Battistutta, R., and Pinna, L. a (2012). Structural features underlying the selectivity of the kinase inhibitors NBC and dNBC: role of a nitro group that discriminates between CK2 and DYRK1A. *Cell Mol Life Sci* 69, 449–460.
- Shi, J., Zhang, T., Zhou, C., Chohan, M.O., Gu, X., Wegiel, J., Zhou, J., Hwang, Y.-W., Iqbal, K., Grundke-Iqbal, I., et al. (2008). Increased dosage of Dyrk1A alters alternative splicing factor (ASF)-regulated alternative splicing of tau in Down syndrome. *J Biol Chem* 283, 28660–28669.
- Simone, M., Erba, E., Damia, G., Vikhanskaya, F., Di, A.M., Riccardi, R., Bailly, C., Cuevas, C., Sousa-faro, M.F., and Incalci, M.D.Ö. (2005). Variolin B and its derivate deoxy-variolin B : New marine natural compounds with cyclin-dependent kinase inhibitor activity. *Eur. J. Cancer* 41, 2366–2377.
- Slepek, T.I., Salay, L.D., Lemmon, V.P., and Bixby, J.L. (2012). Dyrk kinases regulate phosphorylation of doublecortin, cytoskeletal organization, and neuronal morphology. *Cytoskelet.* 69, 514–527.
- Smith, B., Medda, F., Gokhale, V., Dunckley, T., and Hulme, C. (2012). Recent advances in the design, synthesis, and biological evaluation of selective DYRK1A inhibitors: a new avenue for a disease modifying treatment of Alzheimer's? *ACS Chem Neurosci* 3, 857–872.
- Spadaro, A., Frotscher, M., and Hartmann, R.W. (2012a). Optimization of hydroxybenzothiazoles as novel potent and selective inhibitors of 17 β -HSD1. *J Med Chem* 55, 2469–2473.
- Spadaro, A., Negri, M., Marchais-Oberwinkler, S., Bey, E., and Frotscher, M. (2012b). Hydroxybenzothiazoles as New Nonsteroidal Inhibitors of 17 β -Hydroxysteroid Dehydrogenase Type 1 (17 β -HSD1). *PLoS One* 7, e29252.
- Steen, H., Jebanathirajah, J.A., Rush, J., Morrice, N., and Kirschner, M.W. (2006). Phosphorylation analysis by mass spectrometry: myths, facts, and the consequences for qualitative and quantitative measurements. *Mol. Cell. Proteomics* 5, 172–181.
- Steinhilb, M.L., Dias-Santagata, D., Fulga, T.A., Felch, D.L., and Feany, M.B. (2007). Tau phosphorylation sites work in concert to promote neurotoxicity in vivo. *Mol Biol Cell* 18, 5060–5068.

- Suzuki, K., Yahara, S., Hashimoto, F., and Uyeda, M. (2001). Inhibitory Activities of (-)-Epigallocatechin-3-O-gallate against Topoisomerases I and II. *Biol. Pharm. Bull.* *24*, 1088–1090.
- Tahtouh, T., Elkins, J.M., Filippakopoulos, P., Soundararajan, M., Burgy, G., Durieu, E., Cochet, C., Schmid, R.S., Lo, D.C., Delhommel, F., et al. (2012). Selectivity, cocrystal structures, and neuroprotective properties of leucettines, a family of protein kinase inhibitors derived from the marine sponge alkaloid leucettamine B. *J Med Chem* *55*, 9312–9330.
- Taira, N., Nihira, K., Yamaguchi, T., Miki, Y., and Yoshida, K. (2007). DYRK2 is targeted to the nucleus and controls p53 via Ser46 phosphorylation in the apoptotic response to DNA damage. *Mol Cell* *25*, 725–738.
- Taira, N., Mimoto, R., Kurata, M., Yamaguchi, T., Kitagawa, M., Miki, Y., and Yoshida, K. (2012). DYRK2 priming phosphorylation of c-Jun and c-Myc modulates cell cycle progression in human cancer cells. *J Clin Invest* *122*, 859–872.
- Tanega, C., Shen, M., Mott, B.T., Thomas, C.J., MacArthur, R., Inglese, J., and Auld, D.S. (2009). Comparison of bioluminescent kinase assays using substrate depletion and product formation. *Assay Drug Dev. Technol.* *7*, 606–614.
- Teague, S., Davis, A., Leeson, P., and Oprea, T. (1999). The Design of Leadlike Combinatorial Libraries. *Angew Chem (Int. Ed.)* *38*, 3743–3748.
- Tong, L., Pav, S., White, D.M., Rogers, S., Crane, K.M., Cywin, C.L., Brown, M.L., and Pargellis, C.A. (1997). A highly specific inhibitor of human p38 MAP kinase binds in the ATP pocket. *Nat. Struct. Biol.* *4*, 311–316.
- Traut, T.W. (1994). Physiological concentrations of purines and pyrimidines. *Mol Cell Biochem* *140*, 1–22.
- Traxler, P., and Furet, P. (1999). Strategies toward the design of novel and selective protein tyrosine kinase inhibitors. *Pharmacol. Ther.* *82*, 195–206.
- Traxler, P.M., Furet, P., Mett, H., Buchdunger, E., Meyer, T., and Lydon, N. (1996). 4-(Phenylamino)pyrrolopyrimidines: Potent and Selective, ATP Site Directed Inhibitors of the EGF-Receptor Protein Tyrosine Kinase. *J. Med. Chem.* *716*, 2285–2292.
- Urbich, C., Rössig, L., Kaluza, D., Potente, M., Boeckel, J.-N., Knau, A., Diehl, F., Geng, J.-G., Hofmann, W.-K., Zeiher, A.M., et al. (2009). HDAC5 is a repressor of angiogenesis and determines the angiogenic gene expression pattern of endothelial cells. *Blood* *113*, 5669–5679.
- Wager, T.T., Chandrasekaran, R.Y., Hou, X., Troutman, M.D., Verhoest, P.R., Villalobos, A., and Will, Y. (2010). Defining Desirable Central Nervous System Drug Space through the Alignment of Molecular Properties, in Vitro ADME, and Safety Attributes. *ACS Chem Neurosci* *1*, 420–434.
- Walte, A., Rüben, K., Birner-Gruenberger, R., Preisinger, C., Bamberg-Lemper, S., Hilz, N., Bracher, F., and Becker, W. (2013). Mechanism of dual specificity kinase activity of DYRK1A. *FEBS J.*
- Wang, D., Wang, F., Tan, Y., Dong, L., Chen, L., Zhu, W., and Wang, H. (2012). Discovery of potent small molecule inhibitors of DYRK1A by structure-based virtual screening and bioassay. *Bioorg Med Chem Lett* *22*, 168–171.

- Wang, Z., Canagarajah, B.J., Boehm, J.C., Kassisà, S., Cobb, M.H., Young, P.R., Abdel-Meguid, S., Adams, J.L., and Goldsmith, E.J. (1998). Structural basis of inhibitor selectivity in MAP kinases. *Structure* 6, 1117–1128.
- Ward, A.J., and Cooper, T.A. (2010). The pathobiology of splicing. *J. Pathol.* 220, 152–163.
- Weber, J.M., Ruzindana-Umunyana, A., Imbeault, L., and Sircar, S. (2003). Inhibition of adenovirus infection and adenain by green tea catechins. *Antiviral Res.* 58, 167–173.
- Wegiel, J., Kaczmarek, W., Barua, M., Kuchna, I., Nowicki, K., Wang, K.-C., Wegiel, J., Yang, S.M., Frackowiak, J., Mazur-Kolecka, B., et al. (2011a). Link between DYRK1A overexpression and several-fold enhancement of neurofibrillary degeneration with 3-repeat tau protein in Down syndrome. *J Neuropathol Exp Neurol* 70, 36–50.
- Wegiel, J., Gong, C.-X., and Hwang, Y.-W. (2011b). The role of DYRK1A in neurodegenerative diseases. *FEBS J.* 278, 236–245.
- Wegiel, J.J., Dowjat, K., Kaczmarek, W., Kuchna, I., Nowicki, K., Frackowiak, J., Mazur Kolecka, B., Silverman, W.P., Reisberg, B., Deleon, M., et al. (2008). The role of overexpressed DYRK1A protein in the early onset of neurofibrillary degeneration in Down syndrome. *Acta Neuropathol* 116, 391–407.
- Wilson, K.P., McCaffrey, P.G., Hsiao, K., Pazhanisamy, S., Galullo, V., Bemis, G.W., Fitzgibbon, M.J., Caron, P.R., Murcko, M. a, and Su, M.S. (1997). The structural basis for the specificity of pyridinylimidazole inhibitors of p38 MAP kinase. *Chem. Biol.* 4, 423–431.
- Woods, Y.L., Cohen, P., Becker, W., Jakes, R., Goedert, M., Wang, X., and Proud, C.G. (2001). The kinase DYRK phosphorylates protein-synthesis initiation factor eIF2Bepsilon at Ser539 and the microtubule-associated protein tau at Thr212: potential role for DYRK as a glycogen synthase kinase 3-priming kinase. *Biochem J* 355, 609–615.
- Wybenga-Groot, L.E., Baskin, B., Ong, S.H., Tong, J., Pawson, T., and Sicheri, F. (2001). Structural basis for autoinhibition of the Ephb2 receptor tyrosine kinase by the unphosphorylated juxtamembrane region. *Cell* 106, 745–757.
- Xu, W., Doshi, A., Lei, M., Eck, M.J., and Harrison, S.C. (1999). Crystal structures of c-Src reveal features of its autoinhibitory mechanism. *Mol Cell* 3, 629–638.
- Yamaguchi, K., Honda, M., Ikigai, H., Hara, Y., and Shimamura, T. (2002). Inhibitory effects of (–)-epigallocatechin gallate on the life cycle of human immunodeficiency virus type 1 (HIV-1). *Antiviral Res.* 53, 19–34.
- Yamamoto, Y., Matsunaga, K., and Friedman, H. (2004). Protective effects of green tea catechins on alveolar macrophages against bacterial infections. *Biofactors* 21, 119–121.
- Yang, C., Ji, D., Weinstein, E.J., Choy, E., Hornicek, F.J., Wood, K.B., Liu, X., Mankin, H., and Duan, Z. (2010). The kinase Mirk is a potential therapeutic target in osteosarcoma. *Carcinogenesis* 31, 552–558.
- Yankner, B. (1996). Mechanisms of Neuronal Degeneration in Alzheimer’s Disease. *Neuron* 16, 921–932.

- Yoda, Y., Hu, Z.-Q., Zhao, W.-H., and Shimamura, T. (2004). Different susceptibilities of *Staphylococcus* and Gram-negative rods to epigallocatechin gallate. *J. Infect. Chemother.* *10*, 55–58.
- Yoshida, K. (2008). Role for DYRK family kinases on regulation of apoptosis. *Biochem. Pharmacol.* *76*, 1389–1394.
- Zhang, J.-H. (1999). A Simple Statistical Parameter for Use in Evaluation and Validation of High Throughput Screening Assays. *J. Biomol. Screen.* *4*, 67–73.
- Zhang, C., and Kim, S.-H. (2008). Chapter 18 The Impact of Protein Kinase Structures on Drug Discovery. In *Computational and Structural Approaches to Drug Discovery: Ligand-Protein Interactions*, (The Royal Society of Chemistry), pp. 349–365.
- Zheng, J., Knighton, D.R., Xuong, N.H., Taylor, S.S., Sowadski, J.M., and Ten Eyck, L.F. (1993). Crystal structures of the myristylated catalytic subunit of cAMP-dependent protein kinase reveal open and closed conformations. *Protein Sci.* *2*, 1559–1573.
- Zhou, L.-H., Kang, G.-Y., and Kim, K.P. (2009). A binary matrix for improved detection of phosphopeptides in matrix-assisted laser desorption/ionization mass spectrometry. *Rapid Commun. Mass Spectrom.* *23*, 2264–2272.
- Zou, Y., Ewton, D.Z., Deng, X., Mercer, S.E., and Friedman, E. (2004). Mirk/dyrk1B kinase destabilizes cyclin D1 by phosphorylation at threonine 288. *J Biol Chem* *279*, 27790–27798.

6. Acknowledgements

An dieser Stelle möchte ich mich herzlich bei den folgenden Personen bedanken:

Dr. Matthias Engel für die Bereitstellung des sehr interessanten und vielseitigen Themas, sowie seiner Betreuung und seiner Unterstützung in Form von wertvollen Anregungen, Diskussionen und dem ein oder anderen Experiment im Labor. Vielen Dank für das mir entgegengebrachte Vertrauen und den Freiraum, eigene Ideen einfließen zu lassen.

Prof. Dr. R. W. Hartmann für die Möglichkeit die Dissertation innerhalb seiner Arbeitsgruppe anzufertigen

Prof. Dr. Johann Jauch für die Übernahme des Koreferats.

Bei allen aktuellen und ehemaligen Mitgliedern der AG Engel, insbesondere bei Nadja Weber, Tamara Paul und Marica Mariano für die erfolgreiche Zusammenarbeit im Labor.

Martina Fruth, Kristina Hüsecken, Christine Maurer Benjamin Kirsch, Marica Mariano, Andreas Thomann, Benjamin Kirsch, Martin Empting , Michael Zender, Michael Storz und Mohammed Walid für die sehr gute Arbeitsatmosphäre im Büro 1.31.

Dr. Martin Frotscher, Dr. Marie Wetzel, Dr. Tobias Klein und Andreas Thomann für die gemeinsame Gestaltung, Planung und Durchführung des Praktikums Medizinische Chemie.

Michael Zender und Dr. Matthias Groh für die stets gute Laune und effiziente Zusammenarbeit im Syntheselabor.

Dr. Tobias Klein für die Freundschaft und die vielen gemeinsam in den Asphalt einmassierten Rennrad- und Laufkilometer.

Michael Storz und Dr. Matthias Groh für ihre Freundschaft und gemeinsamen sportlichen Auszeiten auch zu teilweise ungewöhnlichen Uhrzeiten.

Allen aktuellen und ehemaligen Mitarbeitern des Arbeitskreises für das gute Arbeitsklima.

David Auerbach für seine Freundschaft während unseres Studiums und die vielen gemeinsamen Aktionen abseits der Uni.

Meinen Eltern, die mir meine Ausbildung ermöglicht haben und mich in dieser Zeit immer unterstützt haben.

Meiner Frau Jana und meinem Sohn Leonard, die immer an mich geglaubt haben, für ihre Geduld und Verständnis während der Promotion.

7. Appendix

7.1 Supporting Information of publication A: Discovery and optimization of a novel, leadlike Dyrk family kinase inhibitor class with high ligand efficiency.

7.1.1 Synthetic procedures and analytical data of compounds 2, 3, 6, 7, 9-14, 16, 18, 21-24, 26-28, 31, 32, 34-40, 42-47

Procedure for the synthesis of 4-bromo-2-(3-methoxyphenyl)thiophene 2a: 5.5 ml of n-buthyllithium (2.5 M in hexane, 13.6 mmol) was added slowly to a solution of 2g (10.7 mmol) of 3-bromoanisole in 40 ml THF at -78°C under nitrogen. The mixture was stirred for 60 min and 3.56 g (15.5 mmol, 4.17 ml) of tributyl borate was added dropwise. The temperature should not exceed -70°C. The mixture was stirred at -78°C for another 90 min before it was allowed to warm to room temperature. Then, 2.3 g (21.4 mmol) of sodium carbonate dissolved in 10 ml of water, 0.49 g (0.43 mmol) of tetrakis(triphenylphosphine)palladium(0) and 2.37 g (10 mmol) of 2,4-dibromothiophene were added and the mixture was heated to reflux overnight. The reaction was stopped when no starting material could be detected. The crude mixture was dissolved in 40 ml of water extracted with diethyl ether (4x). The combined organic layer was subsequently washed with water and brine, dried over magnesium sulfate and the solvent was removed under reduced pressure. The crude product was purified by flash column chromatography eluting with ethyl acetate/hexane 1:30 to give 1.79 g (6.7 mmol), 63 % of 2a. ¹H NMR (500 MHz, DMSO-*d*₆) δ ppm 3.76 - 3.86 (m, 3 H) 6.93 (ddd, *J*=8.20, 2.36, 0.79 Hz, 1 H) 7.17 - 7.27 (m, 2 H) 7.30 - 7.39 (m, 1 H) 7.60 (d, *J*=1.26 Hz, 1 H) 7.67 (d, *J*=1.26 Hz, 1 H); ¹³C NMR (126 MHz, DMSO-*d*₆) δ ppm 55.26, 109.79, 110.63, 114.19, 117.68, 123.15, 126.14, 130.31, 133.80, 144.58, 159.79; Purity(FID): 95 %, MS(EI), *m/z* [M]⁺: 267.88, calc. 267.96.

Procedure for the synthesis of 3-methoxy-5-methylphenyl trifluoromethanesulfonate [1] 2b: 1 g (7.24 mmol) of 3-methoxy-5-methylphenol was dissolved in dichloromethane under nitrogen atmosphere and cooled to 0°C. 2.45 g (8.7 mmol) of trifluoromethanesulfonic anhydride were added dropwise and the mixture was allowed to warm to room temperature. The reaction progress was monitored by TLC. After completion, the crude mixture was dissolved in diethyl ether and poured into 4 % HCl. The organic phase was washed subsequently with brine and saturated sodium hydrogen carbonate. The organic layer was dried over magnesium sulfate, reduced under reduced pressure. The resulting product was sufficiently pure (purity > 95 %) and used without further purification, yield: 1.67 g (6.2 mmol) 85 %. ¹H NMR (500 MHz, DMSO-*d*₆) δ ppm 2.50 (d, *J*=0.63 Hz, 3 H) 3.95 (s, 3 H) 7.00 - 7.04 (m, 2 H) 7.06 - 7.10 (m, 1 H); ¹³C NMR (126 MHz, DMSO-*d*₆) δ ppm 20.91, 55.75, 104.64, 113.51, 115.13, 141.60, 149.62, 160.30, 1 C not detected; Purity(FID): 95 %, MS(EI), *m/z* [M]⁺: 269.87, calc. 270.02.

Procedure for the synthesis of 2-(3-methoxy-5-methylphenyl)-4,4,5,5-tetramethyl-1,3,2-dioxaborolane 2c: 0.2 g (0.25 mmol) of [1,1'-bis(diphenylphosphino)ferrocene] dichloropalladium(II) were suspended in dry dioxane under nitrogen. 1.67 g (6.2 mmol) of 2b, 1.88 g (18.6 mmol) of triethylamine and 2.36 g (9.3 mmol) of bis(pinacolato)diboron were added successively. The mixture was heated to reflux until the reaction was completed. Then 10 ml of water was added and the crude product was dissolved in 50 ml of dichloromethane. The organic layer was washed with water and brine, dried over magnesium sulfate and the solvent was removed under reduced pressure. The

crude product was purified by flash column chromatography eluting with ethyl acetate/hexane 1:10 to yield 0.81 g (3.27 mmol), 53 % of 2c. ^1H NMR (500 MHz, $\text{DMSO-}d_6$) δ ppm 1.50 - 1.52 (m, 15 H) 3.96 (s, 3 H) 7.08 - 7.10 (m, 1 H) 7.18 (d, $J=2.84$ Hz, 1 H) 7.31 (d, $J=0.63$ Hz, 1 H); ^{13}C NMR (126 MHz, $\text{DMSO-}d_6$) δ ppm 24.28, 54.81, 83.57, 115.57, 118.19, 127.57, 134.35, 138.54, 158.80; Purity(FID): 98 %, MS(EI), m/z $[\text{M}]^+$: 248.03, calc. 248.16.

Procedure for the synthesis of 4-(3-methoxy-5-methylphenyl)-2-(3-methoxyphenyl)thiophene 2d: 0.15 g (0.56 mmol) of 2a was dissolved in 10 ml of dioxane/water 5:1 under nitrogen. To this solution 0.14 g (0.56 mmol) of 2c, 0.12 g (1.12 mmol) of sodium carbonate and 0.032 g (0.028 mmol) of tetrakis(triphenylphosphine)palladium(0) were subsequently added and the mixture was heated to reflux. The reaction was monitored by TLC. The crude mixture was poured into water and extracted with diethyl ether (4x). The combined organic layer was washed with brine, dried over magnesium sulfate and the solvent was removed in vacuo. The crude product was purified by flash column chromatography eluting with ethyl acetate/hexane 1:25 to yield 0.164 g (0.53 mmol), 93 % of 2d; ^1H NMR (500 MHz, Methanol- d_4) δ ppm 2.25 (s, 3 H) 3.72 (s, 3 H) 3.74 (s, 3 H) 6.57 - 6.60 (m, 1 H) 6.75 - 6.78 (m, 1 H) 6.89 - 6.92 (m, 1 H) 6.97 - 7.01 (m, 1 H) 7.08 - 7.11 (m, 1 H) 7.12 - 7.16 (m, 1 H) 7.17 - 7.21 (m, 1 H) 7.40 (d, $J=1.58$ Hz, 1 H) 7.57 (d, $J=1.58$ Hz, 1 H); ^{13}C NMR (126 MHz, Methanol- d_4) δ ppm 21.67, 55.72, 55.80, 110.06, 112.25, 114.22, 114.55, 119.23, 120.58, 120.83, 123.60, 131.06, 137.04, 138.23, 140.99, 144.48, 161.61, 161.66; Purity(FID): 98 %, MS(EI), m/z $[\text{M}]^+$: 309.94, calc. 310.10.

Procedure for the synthesis of 3-(5-(3-hydroxyphenyl)thiophen-3-yl)-5-methylphenol 2: A solution of 0.15 g (0.48 mmol) of 2d in dry dichloromethane was cooled to -78°C and 2.9 mmol BBr_3 was carefully added (2.9 ml of a 1M solution in dichloromethane). The mixture was allowed to warm to room temperature. The reaction was stirred for 4 hours and the reaction was stopped by addition of 10 ml of water. The mixture was extracted with ethyl acetate and the combined organic layer was dried over magnesium sulfate. The solvent was removed under reduced pressure and purified by flash column chromatography to give 74 mg of 2 (54 %). ^1H NMR (300 MHz, Acetone) δ ppm 2.31 (s, 3 H) 6.65 (s, 1 H) 6.82 (dt, $J=7.26, 2.14$ Hz, 1 H) 7.00 - 7.02 (m, 1 H) 7.08 (dt, $J=1.68, 1.02$ Hz, 1 H) 7.19 - 7.29 (m, 3 H) 7.59 (d, $J=1.49$ Hz, 1 H) 7.75 (d, $J=1.49$ Hz, 1 H); ^{13}C NMR (75 MHz, Acetone) δ ppm 20.63, 110.19, 110.28, 114.68, 115.00, 116.92, 118.42, 119.54, 122.46, 130.12, 135.63, 136.85, 139.63, 143.19, 144.51, 157.68, 157.92; Purity(FID): 98 %, MS(EI), m/z $[\text{M}]^+$: 282.01, calc. 282.07.

Procedure for the synthesis of 4-bromo-2-(4-methoxy-3-methylphenyl)thiophene 3a: A solution of 0.83 g (4.14 mmol) of 4-bromo-2-methylanisole in 15 ml dry, nitrogen flushed THF was cooled to -78°C . A 2.5 M solution of *n*-butyllithium (1.82 ml) was carefully added and the mixture was stirred for 60 min at -78°C . Then, 0.85 g (5 mmol) of tributyl borate was slowly added and the mixture was stirred for additional 90 min at -78°C . Afterwards the mixture was allowed to warm to room temperature and 1.1 g (10.35 mmol) of sodium carbonate in 2 ml of water, 1 g (4.14 mmol) of 2,4-dibromothiophene and 0.19 g (0.16 mmol) of tetrakis(triphenylphosphine)palladium(0) was added. The mixture was heated to reflux and the reaction was monitored by TLC. The reaction was stopped when all starting materials were consumed and the crude reaction mixture was poured into water. The crude product was extracted with diethyl ether (4x) and the combined organic layer was washed with water and brine. The solvent was dried over magnesium sulfate and removed in vacuo. The crude product was purified by flash column chromatography eluting with ethyl acetate/hexane 1:30 to give 0.82 g (2.9 mmol), 70 % of 3a as a pale yellow solid. ^1H NMR (500 MHz, Methanol- d_4) δ ppm

2.11 (s, 3 H) 3.74 (s, 3 H) 6.80 (d, $J=8.51$ Hz, 1 H) 7.05 (d, $J=1.58$ Hz, 1 H) 7.13 (d, $J=1.58$ Hz, 1 H) 7.25 - 7.30 (m, 2 H); ^{13}C NMR (126 MHz, Methanol- d_4) δ ppm 16.30, 55.92, 111.23, 111.41, 122.00, 125.41, 125.44, 128.35, 128.87, 132.10, 132.48, 159.51; Purity(FID): 97 %, MS(EI), m/z $[\text{M}]^+$: 281.89, calc. 281.97.

Procedure for the synthesis of 2-(4-methoxy-3-methylphenyl)-4-(3-methoxyphenyl)thiophene 3b: A solution of 0.13 g (0.7 mmol) of 3-bromoanisole in 10 ml of dry THF was cooled to -78°C and 0.3 ml of *n*-butyllithium (2.5 M in hexane) was added dropwise. After 60 min, 0.19 g (0.85 mmol) of tributyl borate was added and the mixture was stirred for additional 90 min at -78°C . Then, the mixture was allowed to warm to room temperature and 0.2 g (0.7 mmol) of 3a, 0.19 g (1.8 mmol) of sodium carbonate in 2 ml of water and 0.023 mg (0.028 mmol) of [1,1'-bis(diphenylphosphino)ferrocene] dichloropalladium(II) were added. The mixture was heated to reflux and the reaction was monitored by TLC. The reaction was stopped when no starting materials were detected and the reaction mixture was poured into water. The crude product was extracted with ethyl acetate, washed with water and brine and dried over magnesium sulfate. The solvent was evaporated under reduced pressure and the resulting yellow oil was purified by flash column chromatography to yield 0.17 g (0.55 mmol) of 3b as white solid. ^1H -NMR (Methanol- d_4) δ ppm: 7.43 (d, $J = 1.48$ Hz, 1H), 7.35-7.33 (m, 3H), 7.19 (t, $J = 7.85$ Hz, 1H), 7.14-7.12 (m, 1H), 7.10-7.09 (m, 1H), 6.79 (d, $J = 8.14$ Hz, 1H), 6.75-6.73 (ddd, $J_1 = 8.08$ Hz, $J_2 = 2.55$ Hz, $J_3 = 1.03$ Hz, 1H), 3.73 (s, 6H), 2.12 (s, 3H); ^{13}C -NMR (Methanol- d_4) δ ppm: 161.59, 159.06, 146.42, 144.18, 138.69, 130.82, 128.99, 128.1, 128.06, 125.44, 122.04, 119.72, 113.61, 112.86, 111.35, 55.89, 55.74, 16.35; Purity(FID): 98 %, MS(EI), m/z $[\text{M}]^+$: 310.05, calc. 310.10.

Procedure for the synthesis of 4-(4-(3-hydroxyphenyl)thiophen-2-yl)-2-methylphenol 3: A solution of 0.15 g (0.48 mmol) of 3b in 8 ml of dry dichloromethane was cooled to -78°C and 2.9 ml of BBr_3 solution (1M in dichloromethane) was carefully added. The mixture was allowed to warm to room temperature and was stirred over night at 25°C . The reaction was stopped by addition of 10 ml of water and extracted with dichloromethane. The combined organic layer was washed with water and brine, dried over magnesium sulfate and the solvent was removed in vacuo. The crude product was purified by flash column chromatography eluting with ethyl acetate/hexane 1:3 to give 35 mg (0.12 mmol), 25 % of 3 as a white solid. ^1H NMR (500 MHz, Chloroform- d) δ ppm 2.17 (s, 3 H) 6.72 (ddd, $J=7.80, 2.44, 1.10$ Hz, 1 H) 6.82 (d, $J=8.20$ Hz, 1 H) 7.09 - 7.13 (m, 1 H) 7.14 - 7.24 (m, 2 H) 7.33 - 7.38 (m, 1 H) 7.46 (d, $J=2.21$ Hz, 1 H) 7.61 (d, $J=1.58$ Hz, 1 H) 7.66 (d, $J=1.26$ Hz, 1 H) 9.48 (s, 1 H) 9.54 - 9.60 (m, 1 H); ^{13}C NMR (126 MHz, Chloroform- d) δ ppm 21.19, 118.03, 119.42, 120.22, 122.10, 123.71, 125.80, 129.23, 129.75, 129.95, 133.05, 134.98, 141.77, 147.51, 149.85, 160.70, 162.95; Purity(FID): 98 %, MS(EI), m/z $[\text{M}]^+$: 282.16, calc. 282.07.

Procedure for the synthesis of 4-(4-bromothiophen-2-yl)isoquinoline 47a: 143 mg (0.83 mmol) of (isoquinolin-4-yl)boronic acid was diluted in a mixture of degassed dioxane/water (5:1) under nitrogen atmosphere. To this solution 200 mg (0.83 mmol) of 2,4-dibromothiophene, 220 mg (2.1 mmol) of Na_2CO_3 and 27 mg (0.033 mmol) of tetrakis(triphenylphosphine)palladium(0) were added successively. The mixture was heated to reflux and the reaction progress was monitored by TLC (ALUGRAM SIL G/UV $_{254}$ (Macherey-Nagel)). The reaction was stopped when all starting material was consumed and the crude reaction mixture was poured into water and extracted with ethyl acetate (4x). The combined organic extracts were washed with water and brine, dried over Magnesium sulfate and the solvent was removed under reduced pressure. The crude product was purified by

flash column chromatography eluting with ethyl acetate/hexane 1:10 to give 110 mg 46 % of 4-(4-bromothiophen-2-yl)isoquinoline as a solid. ¹H NMR (500 MHz, Methanol-*d*₄) δ (ppm) 7.18 – 7.19 (m, 1 H) 7.55 – 7.55 (m, 1 H) 7.66 (ddd, *J*=8.80, 6.90, 1.00 Hz, 1 H) 7.75 (ddd, *J*=8.43, 6.86, 1.42 Hz, 1 H) 8.05 – 8.10 (m, 2 H) 8.38 (s, 1 H) 9.16 (d, *J*=0.63 Hz, 1 H), ¹³C NMR (126 MHz, Methanol-*d*₄) δ (ppm) 111.35, 124.99, 125.78, 126.95, 129.30, 129.57, 129.80, 131.89, 133.18, 135.22, 140.04, 143.29, 153.92; Purity(FID): 99 %, MS(EI), *m/z* [M]⁺: 288.90, calc. 288.95.

Analytical data of the ISYNTH Chemspeed compounds synthesized according to the general procedure used for the synthesis of the focused library.

4-methyl-3-[5-(pyridin-3-yl)thiophen-3-yl]pyridine 6: mp 73-74°C; IR (neat) 3050, 1416, 1126, 1022, 798, 698, 616 cm⁻¹; ¹H-NMR (300 MHz, CDCl₃): δ ppm 8.90 (d, *J* = 2.42 Hz, 1H), 8.53 - 8.56 (m, 2H), 8.44 (d, *J* = 5.03 Hz, 1H), 7.89 (td, *J* = 2.00, 7.92 Hz, 1H), 7.39 (d, *J* = 1.49 Hz, 1H), 7.33 (ddd, *J* = 0.75, 4.66, 8.01 Hz, 1H), 7.29 (d, *J* = 1.49 Hz, 1H), 7.19 (d, *J* = 5.03 Hz, 1H), 2.39 (s, 3H). ¹³C-NMR (75 MHz, CDCl₃): δ ppm 20.10, 123.68, 124.18, 125.34, 125.51, 130.02, 132.30, 133.00, 139.33, 140.80, 144.76, 146.88, 148.42, 148.76, 149.57. Purity (UV): 99 %, *t*_R: 2.98 min MS (ESI+): *m/z* (%) = 255 (7), 254 (23), 253 (100) [M+H⁺], calc. 253.07.

2-methyl-5-[5-(pyridin-3-yl)thiophen-3-yl]pyridine 7: mp 121-122°C; IR (neat) 3056, 1419, 1125, 1023, 798, 699, 600 cm⁻¹; ¹H-NMR (300 MHz, CDCl₃): δ ppm 2.58 (s, 3H), 7.19 (d, *J* = 8.0 Hz, 1H), 7.32 (dd, *J* = 8.0, 4.8 Hz, 1H), 7.47 (d, *J* = 1.3 Hz, 1H), 7.54–7.61 (m, 1H), 7.77 (dd, *J* = 8.0, 2.4 Hz, 1H), 7.89 (dt, *J* = 8.0, 2.0 Hz, 1H), 8.54 (dd, *J* = 4.8, 1.5 Hz, 1H), 8.76 (d, *J* = 2.2 Hz, 1H), 8.90 (d, *J* = 2.4 Hz, 1H), ¹³C-NMR (75 MHz, CDCl₃): δ ppm 23.93, 121.26, 122.87, 123.31, 123.68, 128.40, 130.02, 133.02, 133.96, 139.90, 141.62, 146.52, 146.75, 148.69, 157.23. Purity (UV): 99 %, *t*_R = 3.03 min; MS (ESI+): *m/z* (%) = 254 (18), 253 (100) [M+H⁺], 148 (21), 127 (21), calc. 253.07.

2-methoxy-5-[5-(pyridin-3-yl)thiophen-3-yl]pyridine 9: mp 132-133°C; IR (neat) 3071, 1420, 1124, 1030, 1016, 795, 697, 609 cm⁻¹; ¹H-NMR (300 MHz, CDCl₃): δ ppm 3.97 (s, 3H), 6.80 (d, *J* = 8.6 Hz, 1H), 7.32 (dd, *J* = 8.0, 4.8 Hz, 1H), 7.37–7.40 (m, 1H), 7.51–7.57 (m, 1H), 7.79 (dd, *J* = 8.7, 2.5 Hz, 1H), 7.85–7.92 (m, 1H), 8.43 (d, *J* = 2.4 Hz, 1H), 8.54 (dd, *J* = 4.8, 1.3 Hz, 1H), 8.91 (d, *J* = 2.2 Hz, 1H), ¹³C-NMR (75 MHz, CDCl₃): δ ppm 53.55, 110.93, 120.18, 122.88, 123.65, 124.86, 130.10, 132.93, 136.69, 140.02, 141.52, 144.35, 146.91, 148.79, 163.52; Purity: 98 %, *t*_R: 5.91 min; MS (ESI+): *m/z* (%) = 271 (13), 270 (38), 269 (100) [M+H⁺], calc. 269.07.

3-ethoxy-5-[5-(pyridin-3-yl)thiophen-3-yl]pyridine 10: mp 116-117°C; IR (neat) 3075, 2980, 2937, 2889, 1606, 1505, 1467, 1431, 1329, 1285, 1135, 1042; ¹H-NMR (500 MHz, CDCl₃): δ ppm 1.39 (t, *J* = 7.1 Hz, 3H), 4.34 (q, *J* = 7.3 Hz, 2H), 6.82 (d, *J* = 8.5 Hz, 1H), 7.48 (dd, *J* = 7.9, 4.7 Hz, 1H), 7.67 (d, *J* = 1.3 Hz, 1H), 7.85 (d, *J* = 1.3 Hz, 1H), 8.00 (dd, *J* = 8.5, 2.5 Hz, 1H), 8.12 (d, *J* = 7.9 Hz, 1H), 8.42–8.50 (m, 2H), 8.88 (s, 1H), ¹³C-NMR (126 MHz, CDCl₃): δ ppm 15.01, 63.18, 111.94, 121.91, 124.61, 125.66, 126.35, 132.33, 134.96, 138.39, 141.29, 142.05, 145.30, 146.97, 149.03, 164.66; Purity: 96 %, *t*_R : 6.68 min, MS (ESI+): *m/z* (%) = 285 (10), 284 (29), 283 (100) [M+H⁺], 169 (7), calc. 283.08.

3-[4-(pyridin-4-yl)thiophen-2-yl]pyridine 11: mp 117-118°C; IR (neat) 3663, 1414, 1126, 1025, 799, 700, 614 cm⁻¹; ¹H-NMR (300 MHz, CDCl₃): δ ppm 8.87 - 8.95 (m, 1H), 8.63 (dd, *J* = 1.49, 5.40 Hz, 2H), 8.56 (dd, *J* = 1.49, 4.84 Hz, 1H), 7.88 - 7.95 (m, 1H), 7.67 (dd, *J* = 1.30, 9.13 Hz, 2H), 7.54 (dd, *J* = 1.86, 3.73 Hz, 2H), 7.37 (ddd, *J* = 0.75, 4.89, 7.96 Hz, 1H). ¹³C-NMR (75 MHz, CDCl₃): δ ppm 120.88 (2C),

122.64, 123.90, 129.93, 133.40, 140.17, 141.90, 142.96, 146.33, 148.47, 149.42 (2C). Purity (UV): 97 %, t_R = 2.81 min; MS (ESI+): m/z (%) = 241 (13), 240 (38), 239 (100) [M+H⁺], calc. 239.06.

2-methyl-4-[5-(pyridin-3-yl)thiophen-3-yl]pyridine 12: mp 162-163°C; IR (neat) 3055, 1446, 1124, 1030, 802, 697, 612 cm⁻¹; ¹H-NMR (300 MHz, CDCl₃): δ ppm 8.92 (dd, J = 0.93, 2.42 Hz, 1H), 8.53 - 8.59 (m, 2H), 7.90 - 7.96 (m, 1H), 7.62 - 7.70 (m, 2H), 7.41 (d, J = 0.56 Hz, 1H), 7.37 - 7.40 (m, 1H), 7.35 - 7.37 (m, 1H), 2.63 (s, 3H); ¹³C-NMR (75 MHz, CDCl₃): δ ppm 23.57, 118.31, 120.68, 122.75, 123.86, 123.90, 130.00, 133.42, 140.37, 141.83, 143.50, 146.39, 148.50, 148.54, 158.38. Purity: 99 %, t_R = 2.93 min; MS (ESI+): m/z (%) = 255 (6), 254 (18), 253 (100) [M+H⁺], calc. 253.07.

5-[5-(pyridin-3-yl)thiophen-3-yl]pyridine-3-carbonitrile 13: mp 217-218°C; IR (neat) 3093, 2228, 1456, 1136, 1022, 808, 705, 617; ¹H NMR (300 MHz, CDCl₃): δ ppm 9.08 (d, J = 2.24 Hz, 1H), 8.93 (d, J = 2.24 Hz, 1H), 8.83 (d, J = 2.05 Hz, 1H), 8.60 (dd, J = 1.40, 4.75 Hz, 1H), 8.13 - 8.18 (m, 1H), 7.88 - 7.95 (m, 1H), 7.62 - 7.63 (m, 1H), 7.61 (d, J = 0.93 Hz, 1H), 7.37 (dd, J = 4.84, 7.82 Hz, 1H); ¹³C NMR (75 MHz, CDCl₃): δ ppm 91.4, 110.28, 116.38, 122.36, 123.38, 123.78, 129.51, 131.50, 133.11, 136.23, 137.45, 143.01, 147.01, 149.37, 150.65; Purity: 95 %, t_R : 5.15 min; MS (ESI+): m/z (%) = 305 (12) [M+ACN+H⁺], 266 (6), 265 (20), 264 (100) [M+H⁺], calc. 264.05.

3-[5-(pyridin-3-yl)thiophen-3-yl]-5-(trifluoromethyl)pyridine 14: mp 171-172°C; IR (neat) 3056, 1468, 1119, 1023, 802, 697, 608; ¹H NMR (300 MHz, CDCl₃): δ ppm ¹H NMR (300 MHz, CHLOROFORM-d) d 9.00 (s, 1H), 8.85 (s, 1H), 8.76 (s, 1H), 8.51 (d, J = 4.47 Hz, 1H), 8.03 (s, 1H), 7.85 (d, J = 7.82 Hz, 1H), 7.55 (d, J = 2.61 Hz, 2H), 7.28 (dd, J = 4.84, 7.82 Hz, 1H); ¹³C NMR (75 MHz, CDCl₃): δ ppm 122.57, 122.99, 123.38 (d, J = 272.7 Hz, 1C), 123.72, 126.86 (q, J = 33.1 Hz, 1C), 129.62, 130.28 (q, J = 3.4 Hz, 1C), 131.22, 133.05, 138.21, 142.62, 145.07 (q, J = 3.9 Hz, 1C), 146.94, 149.18, 150.54; Purity: 98 %, t_R : 6.75 min; MS (ESI+): m/z (%) = 309 (26), 308 (70), 307 (100) [M+H⁺], calc. 307.04.

3-chloro-5-[5-(pyridin-3-yl)thiophen-3-yl]pyridine 16: mp 158-159°C; IR (neat) 3102, 1457, 1112, 1064, 1015, 800, 702, 626 cm⁻¹; ¹H NMR (300 MHz, Methanol-d₄): δ ppm 8.92 (d, J = 1.68 Hz, 1H), 8.76 (d, J = 1.86 Hz, 1H), 8.57 (dd, J = 1.49, 4.66 Hz, 1H), 8.52 (d, J = 2.05 Hz, 1H), 7.85 - 7.94 (m, 2H), 7.59 (d, J = 1.49 Hz, 1H), 7.56 (d, J = 1.49 Hz, 1H), 7.34 (ddd, J = 0.75, 5.22, 8.01 Hz, 1H); ¹³C NMR (75 MHz, Methanol-d₄): δ ppm 122.66, 123.71, 129.71, 132.24, 132.29, 133.01, 133.09, 138.37, 142.34, 145.25, 146.95, 147.30, 149.12. 1C not det.; Purity: 95, t_R : 6.01 min; MS (ESI+): m/z (%) = 276 (21), 275 (93) [M+H⁺], 274 (52), 273 (100) [M+H⁺], calc. 273.02.

methyl 5-[5-(pyridin-3-yl)thiophen-3-yl]pyridine-3-carboxylate 18: mp 210-211°C; ¹H-NMR (300 MHz, CDCl₃): δ ppm 4.00 (s, 3H), 7.36 (ddd, J = 8.0, 4.8, 0.8 Hz, 1H), 7.62 (d, J = 1.5 Hz, 1H), 7.66 (d, J = 1.5 Hz, 1H), 7.93 (ddd, J = 7.9, 2.4, 1.6 Hz, 1H), 8.50 (t, J = 2.1 Hz, 1H), 8.58 (dd, J = 4.8, 1.5 Hz, 1H), 8.93 (dd, J = 2.4, 0.8 Hz, 1H), 9.05 (d, J = 2.4 Hz, 1H), 9.16 (d, J = 2.1 Hz, 1H), ¹³C-NMR (75 MHz, CDCl₃): δ ppm 52.58, 122.59, 122.75, 123.74, 126.14, 129.81, 131.04, 133.06, 134.31, 138.78, 142.38, 147.02, 149.15, 149.42, 150.98, 165.68; Purity: >99%; t_R : 4.99 min, MS (ESI+): m/z (%) = 338 (5) [M+ACN+H⁺], 299 (16), 298 (46), 297 (100) [M+H⁺], calc. 297.06.

Procedure for the synthesis of compound 4-(5-(pyridin-3-yl)thiophen-3-yl)isoquinoline 21: To a solution of 73 mg (0.42 mmol) (isoquinolin-4-yl)boronic acid in 10 ml of Dioxane and 4 ml of water was successive added 2.5 eq. of Na₂CO₃ (1.3 mmol, 137 mg), 4 mol % of Tetrakis(triphenylphosphine)Palladium(0) (0.017 mmol, 19.4 mg), 100 mg (0.42 mmol) of 3-(4-bromothiophen-2-yl)pyridine under nitrogen atmosphere. The mixture was stirred and heated to

reflux over-night. The reaction progress was monitored by TLC analysis on ALUGRAM SIL G/UV₂₅₄ (Macherey-Nagel). The crude mixture was cooled to room temperature, washed with water and brine and extracted with ethyl acetate. The combined organic layers were dried over Magnesium sulfate and concentrated in vacuo. The crude product was purified by flash column chromatography eluting with ethyl acetate/hexane 1:5 to yield 68 mg (64 %) of 21 as a light yellow solid. mp 126-127°C; IR 3044, 1578, 1342, 1124, 1021, 799, 701, 612 cm⁻¹; ¹H NMR (500 MHz, Methanol-*d*₄) δ ppm 9.19 (d, *J* = 0.95 Hz, 1H), 8.88 (dd, *J* = 0.79, 2.36 Hz, 1H), 8.47 (dd, *J* = 1.58, 5.04 Hz, 1H), 8.45 (s, 1H), 8.11 - 8.15 (m, 2H), 8.07 - 8.10 (m, 1H), 7.78 - 7.82 (m, 1H), 7.72 (d, *J* = 1.26 Hz, 1H), 7.69 - 7.71 (m, 1H), 7.67 (d, *J* = 1.26 Hz, 1H), 7.47 (ddd, *J* = 0.95, 4.89, 8.04 Hz, 1H); ¹³C NMR (126 MHz, Methanol-*d*₄) δ ppm 125.52, 125.64, 126.89, 127.88, 129.08, 129.46, 130.01, 132.07, 132.82, 135.06, 135.56, 139.60, 141.96, 142.57, 147.11, 149.20, 153.01, 1 C not detected; Purity (FID): 95.6 %, *t*_R: 9.75 min; MS (EI), *m/z* [M]⁺: 288.00 calc.: 288.072.

5-[5-(pyridin-3-yl)thiophen-3-yl]pyrimidine 22: mp 130-131°C; IR (neat) 3059, 1442, 1131, 1020, 809, 702, 617 cm⁻¹; ¹H NMR (300 MHz, Methanol-*d*₄): δ ppm 7.35 (dd, *J* = 8.0, 4.8 Hz, 1H), 7.56-7.65 (m, 2H), 7.86-7.95 (m, 1H), 8.58 (dd, *J* = 4.8, 1.3 Hz, 1H), 8.89-8.95 (m, 1H), 8.95-9.01 (m, 2H), 9.16 (s, 1H), ¹³C NMR (75 MHz, Methanol-*d*₄): δ ppm 122.22, 122.83, 123.72, 129.20, 129.57, 133.06, 136.18, 142.81, 146.97, 149.22, 154.08, 157.43. 1C not det; Purity: 99 %, *t*_R: 3.84 min; MS (ESI+): *m/z* (%) = 242 (9), 241 (25), 240 (100) [M+H⁺], calc. 240.05.

2-chloro-5-[5-(pyridin-3-yl)thiophen-3-yl]pyridin-3-amine 23: mp 210-212°C; IR (neat) 3300, 3184, 1418, 1084, 1044, 1026, 800, 703, 590 cm⁻¹; ¹H-NMR (300 MHz, Methanol-*d*₄): δ ppm 8.90 (dd, *J* = 0.79, 2.36 Hz, 1H), 8.49 (dd, *J* = 1.58, 5.04 Hz, 1H), 8.15 (ddd, *J* = 1.58, 2.52, 8.20 Hz, 1H), 8.01 (d, *J* = 2.21 Hz, 1H), 7.88 (d, *J* = 1.26 Hz, 1H), 7.79 (d, *J* = 1.58 Hz, 1H), 7.49 - 7.53 (m, 2H); ¹³C-NMR (75 MHz, Methanol-*d*₄): δ ppm 120.93, 123.79, 124.79, 125.70, 132.20, 133.15, 134.10, 135.06, 135.48, 140.65, 142.34, 142.94, 147.05, 149.21; Purity: 99 %; *t*_R: 4.76 min; MS (ESI+): *m/z* (%) = 291 (5), 290 (35) [M+H⁺], 289 (14), 288 (100) [M+H⁺], 229 (14), calc. 288.03.

3-(4-{3-methyl-3H-imidazo[4,5-*b*]pyridin-6-yl}thiophen-2-yl)pyridine 24: mp 212-213°C; IR (neat) 3060, 1402, 1122, 1021, 799, 702, 619 cm⁻¹; ¹H-NMR (300 MHz, CDCl₃): δ ppm 3.96 (s, 3H, CH₃), 7.33-7.47 (m, 1H), 7.53 (d, *J* = 1.5 Hz, 1H, Ar_m-H), 7.67 (d, *J* = 1.5 Hz, 1H, Ar_m-H), 7.89-8.05 (m, 1H), 8.15 (s, 1H), 8.28 (d, *J* = 2.1 Hz, 1H), 8.57 (dd, *J* = 5.0, 1.6 Hz, 1H), 8.72 (d, *J* = 2.1 Hz, 1H), 8.94 (dd, *J* = 2.4, 0.8 Hz, 1H), ¹³C-NMR (75 MHz, CDCl₃): δ ppm 30.03, 121.48, 123.69, 124.01, 125.24, 127.08, 130.47, 133.66, 134.74, 140.64, 141.31, 143.19, 145.33, 146.12, 146.60, 147.97; Purity: 99 %; *t*_R: 3.68 min; MS (ESI+): *m/z* (%) = 294 (6), 293 (21) [M+H⁺], 168 (89), 147 (100), calc. 293.08.

3-[5-(pyridin-3-yl)thiophen-3-yl]pyridin-1-ium-1-olate 25: mp 168-169°C; IR (neat) 3069, 1432, 1277, 1160, 1012, 783, 708, 614 cm⁻¹; ¹H NMR (300 MHz, CDCl₃): δ ppm 8.87 (d, *J* = 1.49 Hz, 1H), 8.51 - 8.60 (m, 2H), 8.12 - 8.20 (m, 1H), 7.87 (ddd, *J* = 1.49, 2.33, 7.92 Hz, 1H), 7.55 - 7.58 (m, 1H), 7.53 - 7.55 (m, 1H), 7.51 (dd, *J* = 1.21, 8.10 Hz, 1H), 7.29 - 7.38 (m, 2H); ¹³C NMR (75 MHz, CDCl₃): δ 163.7, 149.0, 146.7, 142.5, 137.5, 136.9, 136.9, 134.6, 133.1, 129.5, 126.0, 124.1, 123.7, 123.4, 122.3; Purity: 98 %, *t*_R: 3.21 min; MS (ESI+): *m/z* (%) = 256 (17), 255 (100) [M+H⁺], calc. 255.05.

1-methyl-4-[5-(pyridin-3-yl)thiophen-3-yl]-1,2-dihydropyridin-2-one 26: mp 178-179°C; IR (neat) 3084, 1475, 1129, 1023, 804, 704, 605 cm⁻¹; ¹H-NMR (300 MHz, CDCl₃): δ ppm 8.87 (d, *J* = 2.24 Hz, 1H), 8.54 (dd, *J* = 1.30, 4.84 Hz, 1H), 7.86 - 7.93 (m, *J* = 1.90, 1.90 Hz, 1H), 7.60 (d, *J* = 1.30 Hz, 1H), 7.56 (d, *J* = 0.93 Hz, 1H), 7.30 - 7.40 (m, 2H), 6.85 (d, *J* = 1.86 Hz, 1H), 6.46 (dd, *J* = 1.96, 6.98 Hz, 1H),

3.56 (s, 3H); ^{13}C -NMR (75 MHz, CDCl_3): δ ppm 37.39, 105.01, 115.57, 122.63, 123.89, 124.26, 129.92, 133.39, 138.32, 139.69, 141.63, 145.65, 146.32, 148.44, 163.43; Purity: 99, $t_{\text{R}} = 3.69$ min; MS (ESI+): m/z (%) = 271 (9), 270 (29), 269 (100) [$\text{M}+\text{H}^+$], calc. 269.07.

3-[4-(2,3-dihydro-1-benzofuran-5-yl)thiophen-2-yl]pyridine 27: mp 136-137°C; IR (neat) 2965, 1436, 1123, 1021, 804, 704, 614 cm^{-1} ; ^1H -NMR (300 MHz, CDCl_3): δ ppm 3.26 (t, $J = 8.7$ Hz, 2H), 4.61 (t, $J = 8.7$ Hz, 2H), 6.83 (d, $J = 8.2$ Hz, 1H), 7.27–7.39 (m, 3H), 7.45 (s, 1H), 7.56 (d, $J = 1.1$ Hz, 1H), 7.85–7.97 (m, 1H), 8.53 (dd, $J = 4.7, 1.3$ Hz, 1H), 8.91 (d, $J = 1.9$ Hz, 1H); ^{13}C -NMR (75 MHz, CDCl_3): δ ppm 29.67, 71.43, 109.49, 119.22, 123.04, 123.50, 123.67, 126.33, 127.70, 128.32, 130.48, 132.93, 140.67, 143.61, 146.72, 148.40, 159.75; Purity: 99 %, $t_{\text{R}} = 6.72$ min; MS (ESI+): m/z (%) = 282 (9), 281 (24), 280 (100) [$\text{M}+\text{H}^+$], calc. 280.07.

3-[4-(1,3-thiazol-4-yl)thiophen-2-yl]pyridine 28: mp 123-124°C; IR (neat) 3076, 1441, 1121, 1023, 800, 700, 613 cm^{-1} ; ^1H -NMR (300 MHz, CDCl_3): δ ppm 8.89 - 8.95 (m, 1H), 8.82 - 8.86 (m, 1H), 8.53 (dd, $J = 1.49, 4.84$ Hz, 1H), 7.89 (ddd, $J = 1.49, 2.61, 8.01$ Hz, 1H), 7.72 - 7.80 (m, 2H), 7.40 - 7.46 (m, 1H), 7.31 (ddd, $J = 0.93, 4.84, 8.01$ Hz, 1H); ^{13}C -NMR (75 MHz, CDCl_3): δ ppm 112.43, 122.51, 123.01, 123.62, 130.08, 132.90, 137.23, 141.10, 146.81, 148.66, 151.72, 152.92; Purity: 99 %; $t_{\text{R}} = 4.69$ min; MS (ESI+): m/z (%) = 247 (14), 246 (29), 245 (100) [$\text{M}+\text{H}^+$], calc. 245.01.

3-[4-(1-methyl-1H-imidazol-5-yl)thiophen-2-yl]pyridine 31: mp 97-98°C; IR (neat) 3083, 1568, 1414, 1129, 1021, 808, 700, 611 cm^{-1} ; ^1H NMR (300 MHz, CDCl_3): δ 8.89 (s, 1H), 8.56 (d, $J = 4.28$ Hz, 1H), 7.89 (d, $J = 7.64$ Hz, 1H), 7.52 (s, 1H), 7.40 (s, 1H), 7.27 - 7.38 (m, 2H), 7.18 - 7.24 (m, 1H), 3.75 (s, 3H); ^{13}C NMR (75 MHz, CDCl_3): δ ppm 149.0, 147.0, 141.2, 133.0, 131.3, 129.8, 128.5, 124.5, 123.7, 122.3, 32.8.; Purity: 99 %, $t_{\text{R}} = 2.66$ min; MS (ESI+): m/z (%) = 243 (15), 243 (100) [$\text{M}+\text{H}^+$], calc. 242.07.

3-[4-(3H,8aH-imidazo[1,2-a]pyridin-3-yl)thiophen-2-yl]pyridine 32: mp 146-147°C; IR (neat) 2981, 1419, 1154, 1022, 807, 708, 608 cm^{-1} ; ^1H -NMR (500 MHz, Methanol- d_4): δ 8.89 (d, $J = 1.58$ Hz, 1H), 8.60 (td, $J = 1.10, 6.94$ Hz, 1H), 8.48 (dd, $J = 1.42, 4.89$ Hz, 1H), 8.13 (ddd, $J = 1.58, 2.36, 8.04$ Hz, 1H), 7.83 (d, $J = 1.26$ Hz, 1H), 7.82 - 7.83 (m, 1H), 7.81 (d, $J = 1.58$ Hz, 1H), 7.63 (td, $J = 0.99, 9.06$ Hz, 1H), 7.47 (ddd, $J = 0.79, 4.81, 7.96$ Hz, 1H), 7.41 (ddd, $J = 1.26, 6.62, 9.14$ Hz, 1H), 7.06 (dt, $J = 1.26, 6.78$ Hz, 1H); ^{13}C NMR (126 MHz, Methanol- d_4): δ ppm 15.05, 117.63, 123.05, 124.45, 125.67, 125.84, 126.05, 127.51, 131.25, 131.75, 131.85, 135.13, 142.41, 146.67, 147.13, 149.35; Purity: 99 %, $t_{\text{R}} = 2.93$ min; MS (ESI+): m/z (%) = 280 (14), 279 (33), 278 (100) [$\text{M}+\text{H}^+$], calc. 280.08.

3-chloro-5-[5-(1,3-oxazol-5-yl)thiophen-3-yl]pyridine 34: mp 118-119°C; IR (neat) 3083, 1469, 1108, 1024, 817, 738, 624 cm^{-1} ; ^1H -NMR (300 MHz, CDCl_3): δ ppm 8.59 - 8.66 (m, 1H), 7.89 (s, 1H), 7.79 - 7.86 (m, 1H), 7.51 - 7.56 (m, 1H), 7.47 - 7.51 (m, 1H), 7.37 (d, $J = 8.38$ Hz, 1H), 7.29 (s, 1H); ^{13}C -NMR (75 MHz, CDCl_3): δ ppm 121.88, 121.91, 122.84, 124.35, 129.82, 131.31, 136.20, 138.13, 146.29, 147.17, 150.19, 150.30; Purity: 98 %, $t_{\text{R}} = 7.10$ min; MS (ESI+): m/z (%) = 266 (8), 265 (63) [$\text{M}+\text{H}^+$], 264 (23), 263 (100) [$\text{M}+\text{H}^+$], calc. 263.0.

3-methyl-5-[5-(1,3-oxazol-5-yl)thiophen-3-yl]pyridine 35: mp 117-118°C; IR (neat) 3073, 1421, 1140, 1032, 810, 706, 632 cm^{-1} ; ^1H -NMR (300 MHz, CDCl_3): δ ppm 2.37 (s, 3H), 7.26 (s, 1H), 7.46 (s, 1H), 7.55 (s, 1H), 7.65 (s, 1H), 7.86 (s, 1H), 8.38 (s, 1H), 8.66 (s, 1H), ^{13}C -NMR (75 MHz, CDCl_3): δ ppm 18.37, 121.37, 121.66, 123.17, 130.29, 130.79, 133.17, 133.99, 139.62, 144.72, 146.51, 149.18,

150.05; Purity: 95 %, t_R = 3.91 min; MS (ESI+): m/z (%) = 245 (7), 244 (18), 243 (100) [M+H⁺], calc. 243.05.

5-[5-(1,3-oxazol-5-yl)thiophen-3-yl]pyrimidine 36: mp 177-178°C; IR (neat) 3112, 1447, 1098, 1007, 839, 717, 633 cm⁻¹; ¹H-NMR (300 MHz, CDCl₃): δ ppm 7.31 (s, 1H), 7.55–7.61 (m, 2H), 7.91 (s, 1H), 8.96 (s, 2H), 9.16 (s, 1H); ¹³C-NMR (75 MHz, CDCl₃): δ ppm 122.11, 122.38, 122.53, 128.89, 131.82, 135.80, 146.09, 150.29, 154.09 (2C), 157.51; Purity: 99 %, t_R = 4.85 min; MS (ESI+): m/z (%) = 232 (10), 231 (27), 230 (100) [M+H⁺], calc. 230.03.

2-(methylsulfanyl)-5-[5-(1,3-oxazol-5-yl)thiophen-3-yl]pyrimidine 37: mp 166-167°C; IR (neat) 3075, 1414, 1103, 998, 815, 627 cm⁻¹; ¹H-NMR (300 MHz, CDCl₃): δ ppm 2.60 (s, 3H), 7.30 (s, 1H), 7.48 (d, J = 1.2 Hz, 1H), 7.52 (d, J = 1.2 Hz, 1H), 7.90 (s, 1H), 8.72–8.79 (m, 2H); ¹³C-NMR (75 MHz, CDCl₃): δ ppm 14.19, 121.38, 122.03, 122.33, 124.02, 131.58, 135.97, 146.23, 150.25, 154.40 (2C), 171.61; Purity: 93 %, t_R = 6.90 min; MS (ESI+): m/z (%) = 278 (14), 277 (23), 276 (100) [M+H⁺], calc. 276.02.

5-[4-(1H-pyrazol-4-yl)thiophen-2-yl]-1,3-oxazole 38: mp 175-176°C; IR (neat) 3095; 1426; 1098; 997; 810; 723; 601 cm⁻¹; ¹H NMR (500 MHz, DMSO-d₆) δ 12.94 (br. s., 1H), 8.43 (s, 1H), 7.92 - 8.19 (m, 2H), 7.75 (d, J = 1.58 Hz, 1H), 7.65 (d, J = 1.58 Hz, 1H), 7.50 (s, 1H); ¹³C NMR (126 MHz, DMSO-d₆) δ ppm 151.3, 146.1, 134.7, 129.0, 123.9, 121.3, 118.4, 116.3; Purity: 95 %, t_R = 4.95 min; MS (ESI+): m/z (%) = 220 (8), 219 (14), 218 (100) [M+H⁺], calc. 218.03.

4-[5-(1,3-oxazol-5-yl)thiophen-3-yl]isoquinoline 39: mp 179-180°C; IR (neat) 3072, 1393, 1103, 1021, 800, 688, 637 cm⁻¹; ¹H-NMR (300 MHz, CDCl₃): δ ppm 9.26 (d, J = 0.75 Hz, 1H), 8.56 (s, 1H), 8.05 - 8.08 (m, 1H), 8.01 - 8.04 (m, 1H), 7.90 (s, 1H), 7.70 - 7.77 (m, 1H), 7.61 - 7.69 (m, 1H), 7.54 (d, J = 1.49 Hz, 1H), 7.46 (d, J = 1.30 Hz, 1H), 7.30 (s, 1H); ¹³C-NMR (75 MHz, CDCl₃): δ ppm 121.74, 124.36, 124.57, 126.45, 127.40, 127.49, 128.04, 128.40, 130.25, 130.88, 134.11, 138.26, 142.79, 146.62, 150.11, 152.45; Purity: 99 %, t_R = 4.86 min; MS (ESI+): m/z (%) = 281 (10), 280 (34), 279 (100) [M+H⁺], calc. 279.05.

5-[5-(1,3-oxazol-5-yl)thiophen-3-yl]-1H-indole 40: mp 161-162°C; IR (neat) 3142, 1429, 1114, 1039, 812, 666, 595 cm⁻¹; ¹H-NMR (300 MHz, CDCl₃): δ ppm 8.30 (br. s., 1H), 7.89 (s, 2H), 7.66 (d, J = 1.49 Hz, 1H), 7.45 - 7.49 (m, 1H), 7.41 - 7.45 (m, 1H), 7.39 (d, J = 1.30 Hz, 1H), 7.27 (s, 1H), 7.23 - 7.26 (m, 1H), 6.61 (dt, J = 1.02, 2.10 Hz, 1H); ¹³C-NMR (75 MHz, CDCl₃): δ ppm 103.00, 111.36, 118.53, 119.16, 121.08, 121.16, 124.30, 125.03, 127.38, 128.31, 129.67, 135.37, 144.38, 147.18, 149.85; Purity: 97 %, R_f = 0.68 / t_R = 7.22 min; MS (ESI+): m/z (%) = 269 (11), 268 (33), 267 (100) [M⁺], calc. 267.05.

5-[4-(5-chloropyridin-3-yl)thiophen-2-yl]pyrimidine 42: mp 210-211°C; IR (neat) 3066, 1427, 1107, 1024, 838, 715, 630 cm⁻¹; ¹H-NMR (300 MHz, CDCl₃): δ ppm 7.40 (d, J = 8.4 Hz, 1H), 7.62 (d, J = 5.0 Hz, 2H), 7.86 (dd, J = 8.1, 2.3 Hz, 1H), 8.66 (s, 1H), 9.00 (s, 2H), 9.17 (s, 1H), ¹³C-NMR (75 MHz, CDCl₃): δ = 123.30, 123.73, 124.45, 128.13, 129.83, 136.28, 138.17, 138.99, 147.24, 150.51, 153.52 (2C), 157.80; Purity: 90 %, t_R = 6.44 min; MS (ESI+): m/z (%) = 277 (8), 276 (44) [M+H⁺], 275 (19), 274 (100) [M+H⁺], calc. 274.01.

5-[4-(5-methylpyridin-3-yl)thiophen-2-yl]pyrimidine 43: mp 165-166°C; IR (neat) 3041, 1423, 1115, 1030, 789, 714, 630 cm⁻¹; ¹H-NMR (300 MHz, CDCl₃): δ ppm 2.40 (s, 3H), 7.59 (d, J = 1.5 Hz, 1H), 7.66 (d, J = 1.5 Hz, 1H), 7.68–7.74 (m, 1H), 8.38–8.45 (m, 1H), 8.69 (d, J = 1.9 Hz, 1H), 8.97–9.04 (m, 2H), 9.15 (s, 1H); ¹³C-NMR (75 MHz, CDCl₃): δ ppm 18.41, 122.79, 124.01, 128.31, 130.29, 133.27, 134.07,

137.60, 140.48, 144.77, 149.37, 153.44, 157.61; Purity: 96 %, t_R = 3.54 min; MS (ESI+): m/z (%) = 256 (5), 255 (19), 254 (100) [M+H⁺], calc. 254.07.

5-[4-(pyrimidin-5-yl)thiophen-2-yl]pyrimidine 44: mp 135-136°C; IR (neat) 3108, 1412, 1187, 1036, 839, 717, 631 cm⁻¹; ¹H-NMR (500 MHz, CDCl₃): δ ppm 7.67 (d, J =1.3 Hz, 1 H) 7.70 (d, J =1.3 Hz, 1 H) 9.00 (s, 2 H) 9.01 (s, 2 H) 9.19 (s, 1 H) 9.20 (s, 1 H); ¹³C-NMR (126 MHz, CDCl₃): δ ppm 123.31, 123.97, 127.96, 128.93, 136.65, 138.71, 153.59 (2C), 154.17 (2C), 157.70, 157.94; Purity: 97 %, t_R : 3.39 min; MS (ESI+): m/z (%) = 243 (5), 242 (16), 241 (100) [M+H⁺], calc. 241.05.

2-(methylsulfanyl)-5-[5-(pyrimidin-5-yl)thiophen-3-yl]pyrimidine 45: mp 221-222°C; IR (neat) 3083, 1409, 1171, 1033, 851, 720, 634 cm⁻¹; ¹H-NMR (300 MHz, CDCl₃): δ ppm 9.28 (s, 1H), 9.17 (s, 1H), 9.03 (s, 2H), 8.58 (s, 1H), 8.02 - 8.10 (m, 2H), 7.71 - 7.78 (m, 1H), 7.64 - 7.71 (m, 1H), 7.63 (d, J = 1.30 Hz, 1H), 7.58 (d, J = 1.49 Hz, 1H); ¹³C-NMR (75 MHz, CDCl₃): δ ppm 14.21, 122.80, 123.20, 123.99, 128.05, 136.77, 138.41, 153.54 (2C), 154.43 (2C), 157.83, 171.79; Purity: 95 %, t_R : 6.26 min; MS (ESI+): m/z (%) = 289 (12), 288 (15), 287 (100) [M+H⁺], calc. 287.03.

4-[5-(pyrimidin-5-yl)thiophen-3-yl]isoquinoline 46: mp 235-236°C; IR (neat) 3083, 1468, 1108, 1025, 816, 715, 624 cm⁻¹; ¹H-NMR (300 MHz, CDCl₃): δ ppm 7.58 (d, J = 1.3 Hz, 1H), 7.63 (d, J = 1.3 Hz, 1H), 7.65–7.78 (m, 2H), 8.02–8.10 (m, 2H), 8.58 (s, 1H), 9.03 (s, 2H), 9.17 (s, 1H), 9.28 (s, 1H), ¹³C-NMR (75 MHz, CDCl₃): δ ppm 124.29, 125.96, 127.22, 127.50, 128.14, 128.40, 128.44, 131.01, 134.13, 136.62, 137.03, 139.07, 142.75, 152.54, 153.54 (2C), 157.63; Purity: 99 %, t_R = 4.37 min; MS (ESI+): m/z (%) = 292 (7), 291 (19), 290 (100) [M+H⁺], calc. 290.07.

Procedure for the synthesis of compound 47: 47 mg (0.38 mmol) 3-Pyridylboronic acid was dissolved in degassed dioxane/H₂O (5:1) under nitrogen atmosphere. 110 mg (0.38 mmol) of 4-(4-bromothiophen-2-yl)isoquinoline, 100 mg (0.95 mmol) of Na₂CO₃ and 22 mg (0.02 mmol) of Tetrakis(triphenylphosphine)Palladium(0) were added and the mixture was stirred under reflux. The reaction progress was monitored by TLC analysis on ALUGRAM SIL G/UV₂₅₄ (Macherey-Nagel) until the whole starting material was consumed. After completion of the reaction, the crude product was washed with water and brine, extracted with ethyl acetate and purified by flash column chromatography eluting with ethyl acetate/hexane 1:3 to give 44 mg (40.3 %) of 47 as a light yellow solid; mp 99-100°C; IR(neat) 3088, 3043, 1567, 1322, 1121, 1022, 799, 702, 616 cm⁻¹; ¹H NMR (500 MHz, Methanol-*d*₄) δ ppm 9.21 (s, 1H), 8.91 (d, J = 2.21 Hz, 1H), 8.50 (s, 1H), 8.46 (dd, J = 1.10, 4.89 Hz, 1H), 8.24 (d, J = 8.51 Hz, 1H), 8.15 (d, J = 7.88 Hz, 2H), 7.97 (d, J = 0.95 Hz, 1H), 7.80 - 7.84 (m, 1H), 7.73 (d, J = 7.25 Hz, 1H), 7.71 (d, J = 0.95 Hz, 1H), 7.47 (dd, J = 5.04, 7.88 Hz, 1H); ¹³C NMR (126 MHz, Methanol-*d*₄) δ ppm 124.72, 125.33, 125.56, 127.86, 128.22, 129.27, 129.56, 129.92, 133.12, 133.26, 135.44, 135.68, 140.19, 140.21, 143.29, 147.84, 148.69, 153.63; Purity (FID): 99 %, t_R : 9.97 min; MS (EI), m/z [M]⁺: 288.08, calc. 288.07.

7.1.2 Construction of the pET45b-Dyrk1A-cd expression plasmid.

Firstly, cDNA was produced from human placenta total RNA using the “Transcriptor High Fidelity cDNA Synthesis kit” (Roche Applied Science) and oligo-dT18 primer according to the instructions of the manufacturer. Then a nested primer strategy was employed to amplify the cDNA sequence coding for the catalytic domain of Dyrk1A by PCR using the “Expand High Fidelity PCR^{PLUS} System”

(Roche Applied Science. A 0.5 µl aliquot of the cDNA synthesis mixture was first amplified in a final volume of 25 µl using 0.4 µM each primer (D1A-for, TGA_{CTT}GATCAAAACATACAAGCAT; D1A-rev: ATGAGTTTCAACAGTGACCTGTGTA), 0.2 mM of each dNTP, and 1 x Expand High Fidelity buffer². The following cycling conditions were used on an Eppendorf Mastercycler Gradient (Eppendorf AG, Germany): initial denaturation: 94 °C, 2 min; then 10 cycles of denaturation at 94 °C, 15s; annealing at 63 °C, 30s; elongation at 72 °C, 1.5 min. The cycling was continued for 15 cycles of denaturation at 94 °C, 15s; annealing at 63°C, 30s; elongation at 72 °C, 1.5 min plus 5 sec increment for each new cycle, followed by a final elongation at 72 °C for 7 min. The PCR products were purified from residual primers and primer dimers using the GeneJET™ PCR Purification Kit (Fermentas). Half of the purified product was applied to a second round of PCR using the nested primer pair D1Afor-thr-age (GAACCGGTCTGGTGCCGCGCGGATCCAGTCATAAGAAGGAACGGAAGG) and D1Arev-hind (CGTAAGCTTCTATTCATCAGCTGTTTTCTTGAAGAAAC), carrying the AgeI and HindIII restriction sites, respectively, and in the D1Afor-thr-age primer a thrombin cleavage site was also included. Now the following cycling conditions were used:

initial denaturation at 94 °C, 2 min; then 10 cycles of denaturation at 94 °C, 15s; annealing at 55 °C, 30s; elongation at 72 °C, 1 min 10 sec. The cycling was continued for 5 cycles of denaturation at 94 °C, 15s; annealing at 57°C, 30s; elongation at 72 °C, 1 min 10 sec plus 5 sec increment for each new cycle, followed by a final elongation at 72 °C for 7 min.

The final PCR product was purified by agarose gel electrophoresis, cutting out of the gel band containing the 1.1 kb product, and finally isolation of the DNA using the GeneJET™ Gel Extraction Kit (Fermentas). The PCR product was cloned into the pCR2.1 vector which is part of the TOPO® TA cloning Kit (Life Technologies), transformed into E.coli TOP10 cells, and single colonies were picked from LB agar plates containing 100 µg/ml ampicillin after growing overnight. The single colonies were grown in 5 ml LB/amp cultures overnight at 37 °C with shaking, and the plasmid DNA isolated the next day using the Plasmid Mini Kit from Qiagen. The plasmids were sequenced, and the cDNA with the correct sequence was cut out from the pCR2.1 vector using the AgeI and HindIII restriction enzymes (New England Biolabs) and subcloned using T4 DNA ligase (Fermentas) into the pET45b(+) vector (Novagen) which had been digested with the same restriction enzymes.

7.1.3 Supporting Information figures

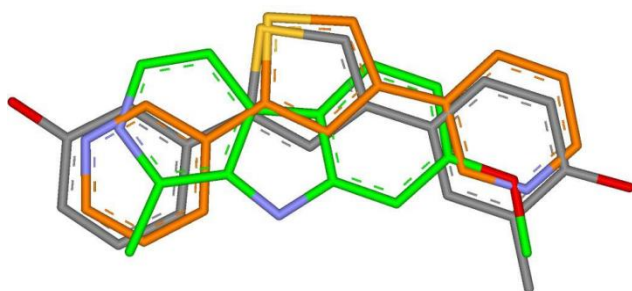


Figure 7.1: Overlay of compound 1 (grey), compound 4 (orange) and harmine (green). The hydrogen bond acceptor atoms of 4 occupy similar positions compared to harmine, whereas the hydroxyl groups of compound 1 address different spatial positions.

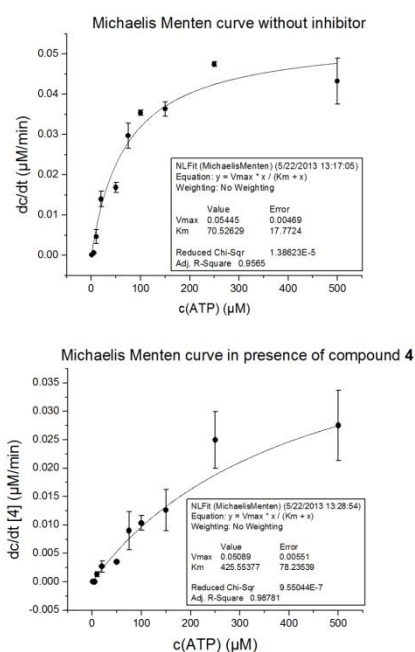


Figure 7.2. Inhibition of Dyrk1A by compound 4 is competitive with respect to the co-factor ATP. The Michaelis-Menten curves in the absence (A) vs. the presence of inhibitor 4 (B) indicate an ATP-competitive binding mechanism. The V_{max} of both kinase reactions was $0.051 \mu\text{mol/l}\cdot\text{min}$. For the kinetic experiment, kinase assays were performed with 500 nM of compound 4 or DMSO as described in the Experimental Section using ten different ATP concentrations as follows (μM ; cold ATP + $\gamma\text{-}^{32}\text{ATP}$): $1+0.003$, $5+0.017$, $10+0.033$, $20+0.066$, $50+0.165$, $75+0.248$, $150+0.5$, $250+0.825$, $500+1.65$. The kinase reactions were performed at 30°C for 2.5 min and terminated by spotting $5 \mu\text{l}$ of the reaction mixture onto P81 phosphocellulose paper, which was further treated as described. K_m and V_{max} values were calculated by fitting the data with Origin Pro 8.6 (OriginLabs). Error bars denote the standard deviation of mean.

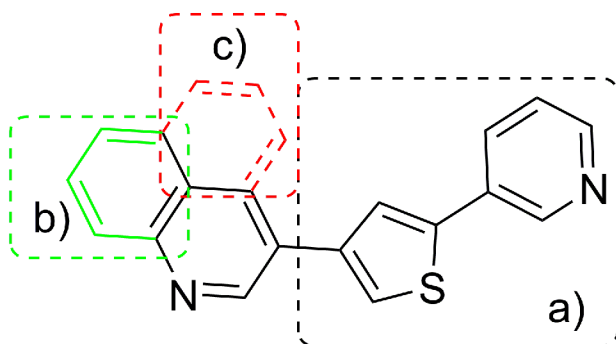


Figure 7.3. Overlay of the quinoline derivative 20 and the isoquinoline 21. a) represents the identical part of both compounds; b) additional hydrophobic part of 20 compared with 4; c) additional hydrophobic part of 21. Assuming that the same set of hydrogen bonds is formed with the nitrogen atoms, the overlay suggests that parts b) and c) are accommodated by different hydrophobic areas within the ATP binding pocket.

Compound 29

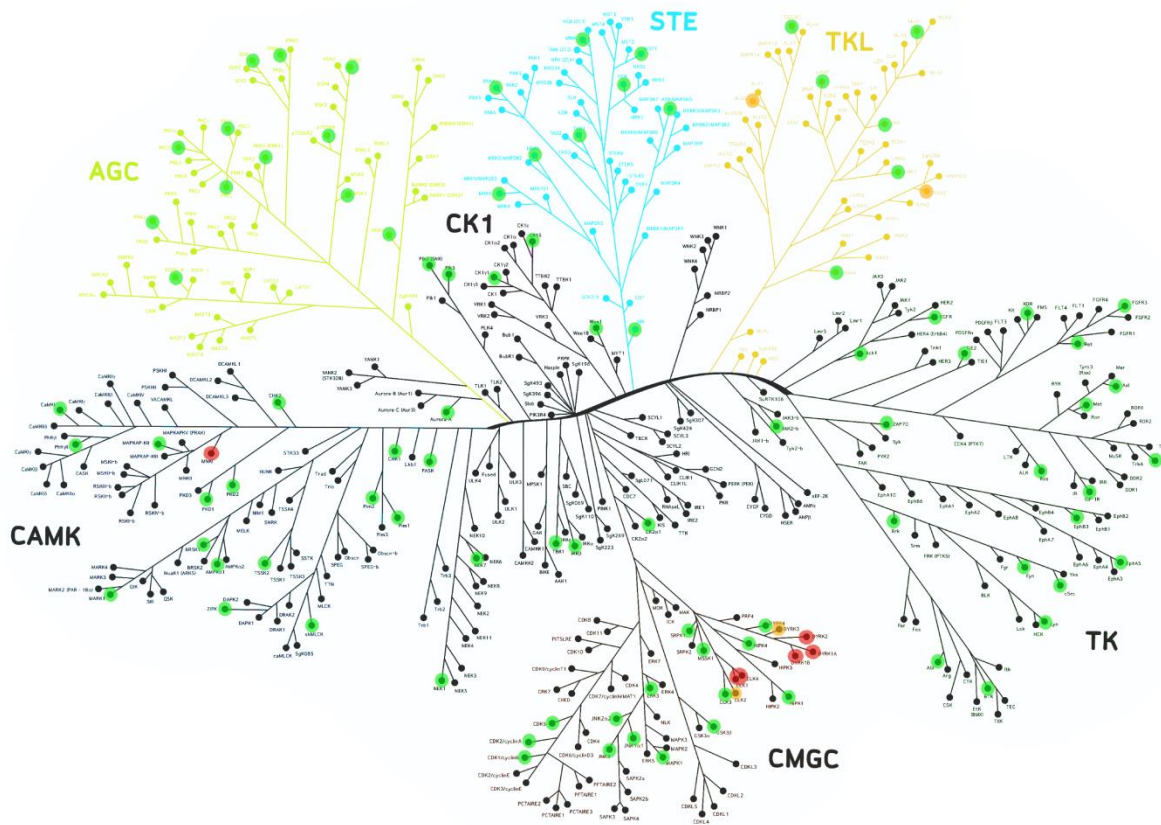


Figure 7.4. The selectivity of compound 29 is illustrated in a kinome tree dendrogram. The kinases tested are highlighted in green, orange or red circles corresponding to their inhibition at 5 μM (green: 0 - 40 % inhibition, orange: 40 - 80 % inhibition, red: > 80 % inhibition)

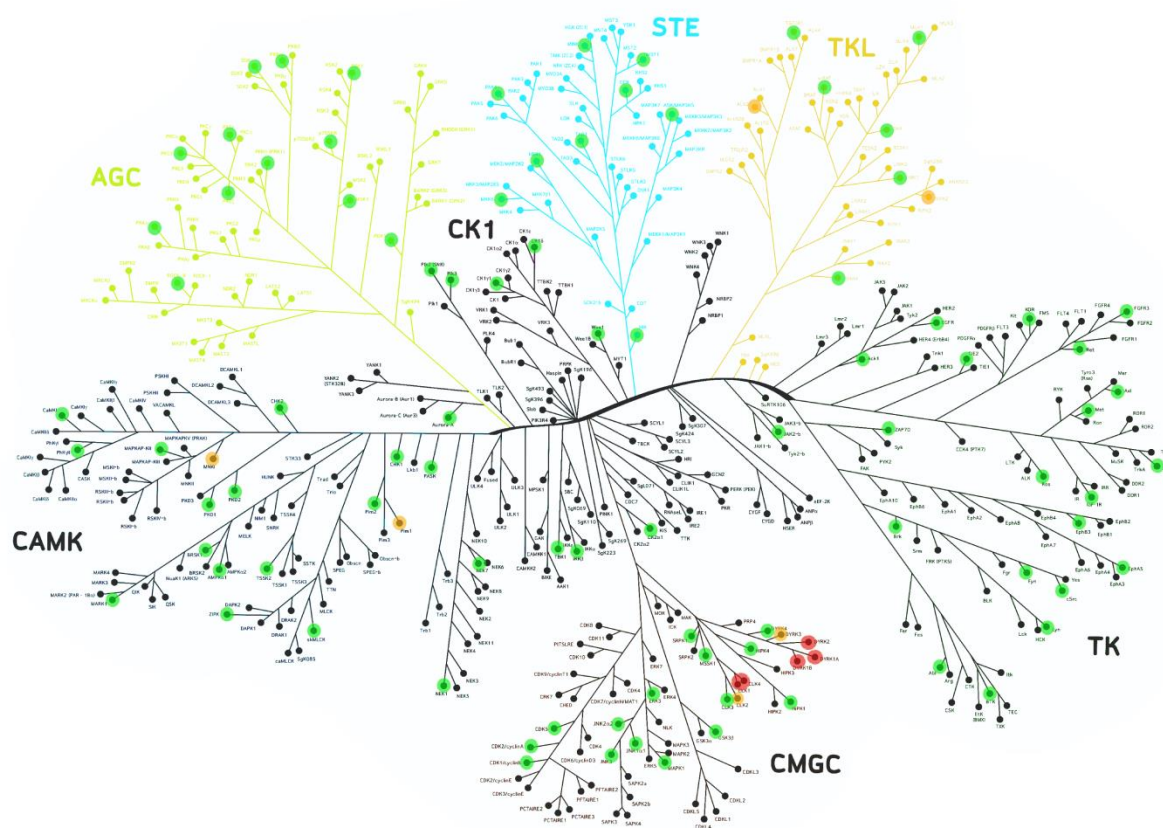


Figure 7.5. The selectivity of compound 48 is illustrated in a kinome tree dendrogram. The kinases tested are highlighted in green, orange or red circles corresponding to their inhibition at 5 μM (green: 0 - 40 % inhibition, orange: 40 - 80 % inhibition, red: > 80 % inhibition)

7.1.4 Supporting information tables

Table 7.1. Calculated Ligand efficiencies (LE) of the most potent compounds against Dyrk1A and Dyrk1B

Compound	$K_D^{a,b}$ (Dyrk1A) [nmol/l]	LE (Dyrk1A)[kcal/(mol*HA)]	$K_D^{a,b}$ (Dyrk1B) [nmol/l]	LE (Dyrk1B)[kcal/(mol*HA)] ^D
4	273	0.53	260	0.53
29	52	0.62	37.1	0.63
30	160	0.54	148	0.55
48	39	0.63	26	0.65
Harmine	42	0.63	145	0.58

^a K_D values were calculated using the Cheng-Prusoff equation. ^b The K_m value of Dyrk1A for ATP was 64 μ M (determined by a kinetic experiment, Figure 7.2). The K_m value of Dyrk1B for ATP was 59 μ M (taken from www.carnabio.com).

Table 7.2. Calculated molecular properties of the most potent compounds compared to harmine

Compound	MW ^a [g/mol]	clogP ^a	HBD ^a	HBA ^a	TPSA ^{a,b} [\AA^2]	TPSA ^c
4	238.31	2.61	0	2	54.02	25.78
29	244.34	2.48	0	2	82.26	25.78
30	241.31	2.26	0	2	58.95	30.71
48	244.34	2.48	0	2	82.26	25.78
Harmine	212.25	1.85	1	2	37.91	37.91

^a ideal ranges: MW: <300 g/mol, logP: > 0, < 3; HDB: < 3; HBA: max. 3; TPSA: 25-60 \AA^2 [2-4]. ^b TPSA was calculated according the procedure of Ertl et al. (J. Med. Chem. **2000**; 43; 3714-3717) ^c Sulfur was not considered for the calculation of TPSA.

Table 7.3. Selectivity panel of compounds 29, 30, 33, 41 and 48 against selected kinases frequently reported to be affected by Dyrk inhibitors^a

Kinase Family	Kinase	29	30	33	41	48
CMGC	Dyrk1A	90	99	84	85	97
	Dyrk1B	100	100	83	70	100
	Dyrk2	93	100	77	57	100
	Ck2 α	0	10	0	0	0
	Clk1b	96	92	88	86	94
	Clk3	12	17	5	5	31
	HIPK1	4	8	7	9	9
	CDK5	39	33	23	14	44
	GSK3 β	0	17	10	14	25
STE	MST1 (STK4)	0	-10	0	2	9
AGC	PKC β	-7	-8	-18	-7	1
CAMK	PIM1	22	52	51	14	51
	CaMK1	8	17	12	0	5
	PRKD2 (PKD2)	0	-8	0	0	0
CK1	Ck1 δ	0	-1	0	0	1
TKL	MLK1	15	16	0	3	17
TK	EGFR	0	5	0	4	15
	ROS	0	4	2	0	0
	TrkB	24	-5	23	22	0

^aGiven is the percentage of inhibition in the presence of 5 μ M inhibitor. Standard deviations for all values were < 10 %.

Table 7.4. Extended selectivity panel for compound 29 and 30 ^a

Kinase Family	Kinase	29	48
CMGC	Dyrk1A	90	97
	Dyrk1B	100	100
	Dyrk2	93	100
	DYRK3	66	69
	DYRK4	13	12
	Ck2 α	0	0
	Clk1b	96	94
	CLK2	72	78
	Clk3	12	31
	CLK4	105	99
	HIPK1	4	9
	HIPK4	7	7
	CDK5	39	44
	CDK1/cyclin B	29	42
	CDK2/cyclin A	22	33
	GSK3 β	0	25
	MAPK1 (ERK2)	-6	1
	MAPK10 (JNK3)	4	2
	MAPK12 (p38 gamma, ERK3)	-2	3
	MAPK8 (JNK1)	-1	5
	MAPK9 (JNK2)	-6	-6
	STK23 (MSSK1)	2	0
	SRPK1	3	1
STE	MAP3K5 (ASK1)	4	6

	MAP3K14 (NIK)	2	5
	MAP2K1 (MEK1)	1	2
	MAP2K6 (MKK6)	5	7
	MAP4K2 (GCK)	32	6
	MINK1	36	19
	TAOK2 (TAO1)	-6	-6
	MST1 (STK4)	0	9
	PAK4	3	4
	PASK (STLK3)	23	27
Atypical	EEF2K	0	1
AGC	ROCK2	6	9
	AKT1 (PKB alpha)	9	3
	RPS6KA1 (RSK1)	2	4
	RPS6KA5 (MSK1)	15	10
	RPS6KB1 (p70S6K)	-2	-4
	PKC β	-7	1
	SGK (SGK1)	20	22
	PRKACA (PKA)	1	3
	PRKCE (PKC epsilon)	-18	-5
	PRKCZ (PKC zeta)	-23	-25
	PDK1	-10	7
	PKN1 (PRK1)	-16	-10
CAMK	PIM1	22	51
	PIM2	7	5
	CaMK1	8	5
	MAPKAPK2	2	2

	MARK1 (MARK)	0	1
	PRKD2 (PKD2)	0	0
	CHEK1 (CHK1)	3	7
	CHEK2 (CHK2)	1	-2
	AMPK A1/B1/G1	-9	-5
	BRSK1 (SAD1)	11	-4
	DAPK3 (ZIPK)	-1	-5
	MKNK1 (MNK1)	83	47
	MYLK2 (skMLCK)	12	31
	STK22B (TSSK2)	-2	-2
	PRKD1 (PKC mu, PKD1)	-1	-5
	PASK	23	27
	PHKG2	-12	-11
Other	AURKA (Aurora A)	5	2
	WEE1	17	10
	IKBKB (IKK beta)	8	12
	NEK1	3	-5
	NEK7	0	-7
	TBK1	3	8
	PIK3CA/PIK3R1	21	12
	PLK2/SNK	-3	1
CK1	Ck1 δ	0	1
	CSNK1G1 (CK1 gamma 1)	-5	-3
TKL	ZAK	11	11
	RAF1 (cRAF) Y340D Y341D	36	37
	ACVR1 (ALK2)	51	51

	TGFBR1 (ALK5)	24	22
	MLK1	15	17
	LIMK1	11	4
	RIPK2	53	46
	IRAK4	-7	-11
TK	EGFR	0	15
	ROS	0	0
	LYN A	16	13
	KDR (VEGFR2)	6	10
	JAK2	-2	-4
	RET	-1	1
	FYN	-2	0
	TrkB	24	0
	TNK2 (ACK)	8	8
	ABL1	2	6
	AXL	-2	-11
	BTK	17	15
	EPHA5	-9	-6
	EPHB3	0	1
	FGFR3	-2	-1
	IGF1R	1	3
	MET (cMet)	1	-12
	ZAP70	4	-1
	TEK (Tie2)	-1	0
	SRC	-8	-4
PTK6 (Brk)	30	34	

^aGiven is the percentage of inhibition in the presence of 5 μ M inhibitor. Standard deviations for all values were < 10 %.

Literature

1. Thompson AL, Kabalka GW, Akula MR, Huffman JW (2005) The Conversion of Phenols to the Corresponding Aryl Halides Under Mild Conditions. *Synthesis (Stuttg)* 2005: 547–550.
2. Ertl P, Rohde B, Selzer P (2000) Fast calculation of molecular polar surface area as a sum of fragment-based contributions and its application to the prediction of drug transport properties. *J Med Chem* 43: 3714–3717.
3. Ghose AK, Herbertz T, Hudkins RL, Dorsey BD, Mallamo JP (2012) Knowledge-Based, Central Nervous System (CNS) Lead Selection and Lead Optimization for CNS Drug Discovery. *ACS Chem Neurosci* 3: 50–68.
4. Wager TT, Chandrasekaran RY, Hou X, Troutman MD, Verhoest PR, et al. (2010) Defining Desirable Central Nervous System Drug Space through the Alignment of Molecular Properties, in Vitro ADME, and Safety Attributes. *ACS Chem Neurosci* 1: 420–434.

7.2 Dual Clk1/Dyrk1A inhibition is required for efficient mRNA splicing manipulation. Discovery of a new inhibitor scaffold.

7.2.1 Biology

Recombinant Clk1 (catalog # PV3315) and Dyrk1B (catalog # PV4649) were purchased from lifetechnologies (Life Technologies GmbH, Darmstadt, Germany). RS domain derived peptide (RS tide) (catalog # 61723) was purchased from AnaSpec (Eurogentec Headquarters, Seraing, Belgium)

Protein expression and purification

Recombinant Dyrk1A and Dyrk2 were prepared according to the protocol previously described.¹

Kinase Assay

Kinase reactions were performed as earlier described in a reaction buffer containing 50 mM Tris/HCl, pH 7.4, 0.1 mM EGTA, 0.5 mM DTT, 10 mM MgCl₂, 100 μM ATP and 0.33 μM, 2 μCi [γ -³²ATP] as well as 100 μM Woodtide substrate peptide (KKISGRLSPIMTEQ-NH₂) for Dyrk assays and 100 μM RS domain derived peptide (GRSRSRSRSR) for Clk1 assays respectively.¹ Activity of recombinant kinases was 0.1 mU per reaction well and reactions were carried out at 30 °C for 15 min. Results were analyzed using a Fuji FLA-3000 PhosphorImager plate reader. Signals were quantified using AIDA software (Raytest, Version 3.52). For IC₅₀ determinations 8 to 10 different concentrations of each compound were tested in triplicates. IC₅₀ curves were plotted and analyzed using Origin Pro 8.6.0. The larger panel of kinases shown in Table S2 was screened by Life Technologies, Paisley, UK (SelectScreen® Kinase Profiling Services).

The Plasmid used to express Dyrk2¹ was a kind gift of Prof. Walter Becker, RWTH Aachen, Germany.

Real-Time PCR assay

To establish a Real-Time PCR-based assay for the quantification of splicing modulatory potencies, possible target sequences of differentially spliced transcripts were first validated using conventional PCR amplification and agarose gel detection. STO cells (derived from mouse embryonic fibroblasts) were chosen as a model since they had been successfully used previously to demonstrate the effects of TG003 on alternative pre-mRNA splicing.² For both conventional PCR and Real-Time (RT)-PCR experiments, STO cells were seeded into 6-well plates and grown to confluency in DMEM containing 10 % FCS and antibiotics. The cells were treated with the test compounds or DMSO (0.1% DMSO as final conc.) in the same medium for 4 h at 37°C in the incubator, then the supernatant was removed, the cells were harvested by trypsinization, transferred to Eppendorf tubes and total RNA isolated without prior freezing using the RNeasy Mini Kit (Qiagen, Cat. No. 74104). 1 µg of total RNA was transcribed to cDNA using the QuantiTect Rev. Transcription Kit (Qiagen, Cat. No. 205311) in combination with random primers, and 20 ng of cDNA (assuming quantitative reverse transcription) were used per PCR. Among several primer pairs tested, the pair targeting the Clk/Sty cDNA as published by Pilch et al.³ was giving the most consistent results: CLK-For, 5'-GCA TAG TAG CAA GTC CTC TG-3'; CLK-Rev, 5'-TAC TGC TAC ACG TCT ACC TC-3'. Using this primer pair, differential splicing as caused by the effectors was sensitively detected by an increase in the total amplified cDNA which mainly consisted of the 274 bp product including the Clk1/Sty exon2 (cf. Figure S1).^{2,3}

The conventional PCR was performed using the "JumpStart REDTaq ReadyMix" reaction mix from Sigma (Cat. No. P0982) using 10µM of each primer. The following cycling conditions were used on an Eppendorf Mastercycler Gradient (Eppendorf AG, Germany): initial denaturation: 94 °C, 2 min; then 35 cycles of denaturation at 94 °C, 30s; annealing at 56 °C, 30s; elongation at 72 °C, 50 sec. As a control for the amount of cDNA, additional PCRs were performed in parallel under the same conditions, except that β-actin primers of the following sequences were used: β-actin forward: 5'-TGC GTG ACA TTA AGG AGA AG-3'; β-actin reverse: 5'-GTC AGG CAG CTC GTA GCT CT-3'; size of amplified product: 107 bp. Half of the PCR volumes (25µL) were resolved on 1.5% agarose gels and stained using ethidium bromide.

Real-Time (RT)-PCR was performed in a StepOnePlus Real-Time PCR System (Life Technologies) using 20 ng cDNA per reaction with the SYBR green RT-PCR Kit (Peqlab, Cat. No. 07-KK4603-01) according to the manufacturer's protocol, using the following cycling conditions: initial denaturation: 95 °C, 40 sec, followed by 45 cycles of denaturation at 95 °C, 2 sec, and annealing/extension at 60 °C, 40 sec. Primers were as above. The increase in the amount of specific cDNA corresponding to the alternative Clk/Sty transcripts relative to the samples derived from DMSO-treated cells was calculated after normalization to the β-actin values obtained with the same cDNA samples. To calculate EC₅₀ values and the concentration required to induce a 5-fold increase ("C_{5-fold}"), different concentrations of TG003, **16**, **18**, **23**, and **25** were used for the cell treatments, ranging from 0.5 to 15 µM.

7.2.2 Chemistry

Chemical starting materials were purchased from Sigma-Aldrich, CombiBlocks or Alfa Aesar and used without further purification. Purity of the compounds was determined using an Agilent 1100 series HPLC system from Agilent Technologies, a GC Trace Ultra from Thermo or a Waters

autopurification system from Waters Corporation. The purity of the compounds used in the biological assays was $\geq 95\%$. Mass spectra (ESI) were measured on an AB Sciex Qtrap2000 from AB Sciex or a Waters 3100 Mass detector from Waters Corporation. Mass spectra (EI) were measured on a DSQ II from Thermo. ^1H and ^{13}C NMR spectra were recorded on either a Bruker DRX-500 (^1H , 500 MHz; ^{13}C , 126 MHz) instrument at 300 K or on a Bruker Fourier300 (^1H , 300 MHz; ^{13}C , 75 MHz) NMR spectrometer at 300 K in the deuterated solvents indicated. IR spectra were recorded on a Perkin Elmer Spectrum 100 FT-IR spectrometer, Perkin Elmer, Rodgau, Germany. Flash column chromatography was performed using silica gel 60 (Merck, 35-70 μm). Reaction/flash monitoring was done by TLC on ALUGRAM SIL G/UV254 (Macherey-Nagel) employing UV detection.

The detailed synthesis of the following compounds is described in Miralinaghi *et al.*⁴

Compound Number	IUPAC name
1	(6-hydroxynaphthalen-2-yl)(3-hydroxyphenyl)methanone
2	(3-hydroxy-4-methylphenyl)(6-hydroxynaphthalen-2-yl)methanone
3	(4-fluoro-3-hydroxyphenyl)(6-hydroxynaphthalen-2-yl)methanone
4	(6-hydroxybenzo[b]thiophen-2-yl)(3-hydroxyphenyl)methanone
5	(6-hydroxybenzofuran-2-yl)(3-hydroxyphenyl)methanone
6	(6-hydroxy-1H-indol-2-yl)(3-hydroxyphenyl)methanone
7	(6-hydroxy-1-methyl-1H-indol-2-yl)(3-hydroxyphenyl)methanone
8	(6-hydroxy-3-methylbenzo[b]thiophen-2-yl)(3-hydroxyphenyl)methanone
9	(6-hydroxy-3-methylbenzofuran-2-yl)(3-hydroxyphenyl)methanone
10	(5-hydroxybenzo[b]thiophen-2-yl)(3-hydroxyphenyl)methanone
11	(5-hydroxybenzofuran-2-yl)(3-hydroxyphenyl)methanone
12	(5-hydroxy-1H-indol-2-yl)(3-hydroxyphenyl)methanone
13	(5-hydroxy-1-methyl-1H-indol-2-yl)(3-hydroxyphenyl)methanone
14	(5-hydroxybenzo[b]thiophen-2-yl)(4-hydroxyphenyl)methanone
15	(5-hydroxybenzofuran-2-yl)(4-hydroxyphenyl)methanone
16	(3-hydroxy-4-methylphenyl)(5-hydroxybenzo[b]thiophen-2-yl)methanone

17	(4-hydroxy-3-methylphenyl)(5-hydroxybenzo[b]thiophen-2-yl)methanone
18	(2-fluoro-5-hydroxyphenyl)(5-hydroxybenzo[b]thiophen-2-yl)methanone
19	(4-fluoro-3-hydroxyphenyl)(5-hydroxybenzo[b]thiophen-2-yl)methanone
20	3-(5-hydroxybenzo[b]thiophene-2-carbonyl)benzotrile
21	(5-hydroxybenzo[b]thiophen-2-yl)(phenyl)methanone
22	benzo[b]thiophen-2-yl(3-hydroxyphenyl)methanone
24	(5-methoxybenzo[b]thiophen-2-yl)(3-methoxyphenyl)methanone
25	N,5-dimethoxy-N-methylbenzo[b]thiophene-2-carboxamide

Procedure A, general synthesis of methyl benzothiophene-2-carboxylates: A suspension of 2 eq. of potassium carbonate in 20 ml of dry DMF was cooled to 0°C and 1.2 eq. of methyl thioglycolate was carefully added. The solution was stirred for 20 min at 0°C under nitrogen and a solution of 1 eq. of the corresponding 2-fluorobenzaldehyde or 2-fluoro-acetophenone in 10 ml of DMF was added drop-wise. Then, the mixture was heated to 70°C and stirred for 4 hours. The suspension was cooled to room temperature and poured into 60 ml of 10 % citric acid. The aqueous layer was extracted with ethyl acetate (5x) and the combined organic layer was thoroughly washed with small amounts of water and brine (10x), and dried over magnesium sulphate. The solvent was removed in vacuo and the resulting yellow solid was recrystallized in ethanol to give the carboxylic ester in different yields.

Procedure B, general synthesis of benzo[b]thiophene-2-carboxylic acids: The carboxylic acids were released from the corresponding methyl benzo[b]thiophene-2-carboxylates by hydrolysis with potassium hydroxide. Therefore the methyl ester was dissolved in 5 ml of ethanol and 2.5 ml of water was added. Then 4 eq of potassium hydroxide was added and the mixture was heated to reflux for 2 hours. The solvent was removed under reduced pressure and the resulting potassium salt was dissolved in a small volume of water, cooled to 0°C before conc. HCl was carefully added dropwise to adjust the pH to 1. Then the aqueous layer was extracted with diethyl ether (5x) and the combined organic extracts were dried over magnesium sulphate, filtered off, and concentrated in vacuo. The crude carboxylic acid was recrystallized from ethanol.

Procedure C, general synthesis of Weinreb amides: The corresponding carboxylic acid was dissolved in 5 ml of dichloromethane and cooled to 0°C. To this solution, 1.1 eq. of N,O-dimethylhydroxylamine hydrochloride, 0.1 eq. of dimethylaminopyridine, 1.2 eq. of N-(3-dimethylaminopropyl)-N'-ethylcarbodiimid, and 6 eq. of triethylamine were added successively. After 60 min the solution was allowed to warm to room temperature and was stirred over night at RT. The reaction was quenched by addition of 10 % citric acid and the organic layer was separated.

The aqueous layer was neutralized by addition of saturated NaHCO_3 and extracted with dichloromethane (4x). The combined organic layer was washed with water and brine, and dried over magnesium sulphate. The solvent was removed in vacuo to give the Weinreb amides as solid in sufficient purity.

Procedure F, Rap Stoermer reaction for the synthesis of intermediate compounds: 1.1 eq. of the corresponding 2-Bromoacetophenone and 2 eq. of Cs_2CO_3 were dissolved in 5 ml of acetonitrile and stirred under nitrogen. After 30 min 1 eq. of a methoxy substituted 2-hydroxybenzaldehyde was added and the mixture was stirred over night at room temperature. After completion of the reaction a precipitate was formed and dissolved in ethyl acetate. The solution was subsequently washed with water and brine. The organic layer was dried over magnesium sulphate, the solvent was evaporated in vacuo, and the crude product was purified by flash column chromatography eluting with ethyl acetate/hexane 1:3 to give the intermediate compounds in varying yields.

Synthesis of II, methyl 5-methoxybenzo[b]thiophene-2-carboxylate: The title compound was synthesized from 2-fluoro-5-methoxybenzaldehyde using procedure A to yield 2 g (9 mmol, 25 %) of **II** as a light yellow solid. ^1H NMR (Acetone- d_6 , 500MHz): δ = 8.04 (s, 1 H), 7.88 (d, $J=9.1$ Hz, 1 H), 7.51 (d, $J=2.2$ Hz, 1 H), 7.17 (dd, $J=8.8, 2.5$ Hz, 1 H), 3.91 (s, 3 H), 3.88 ppm (s, 3 H); ^{13}C NMR (Acetone- d_6 , 126MHz): δ = 163.5, 159.1, 140.9, 135.4, 135.2, 131.1, 124.4, 119.1, 107.6, 55.9, 52.8 ppm; Purity(UV) > 98 %; t_{R} :min, ESI-MS $[\text{M}+\text{H}]^+$: 223.08; calcd. $[\text{M}]^+$: 222.04.

Synthesis of III, 5-methoxybenzo[b]thiophene-2-carboxylic acid: The title compound was synthesized from **II** using procedure B to give 0.83 g (3.7 mmol, 68 %) of **III** as a white solid which was directly used for the synthesis of **IV** without further characterization other than NMR. ^1H NMR (DMSO- d_6 , 300MHz): δ = 13.40 (s, 1 H), 8.01 (s, 1 H), 7.91 (d, $J=8.9$ Hz, 1 H), 7.52 (d, $J=2.4$ Hz, 1 H), 7.15 (dd, $J=8.8, 2.5$ Hz, 1 H), 3.82 ppm (s, 3 H); ^{13}C NMR (DMSO- d_6 , 75MHz): δ = 164.0, 157.9, 140.3, 136.1, 134.3, 130.4, 124.2, 118.2, 107.5, 55.8 ppm.

Synthesis of IV, N,5-dimethoxy-N-methylbenzo[b]thiophene-2-carboxamide: The title compound was synthesized from **III** using procedure C to give 3.3 g (1.3 mmol, 53 %) of **IV** as colourless needles after recrystallization from ethanol. ^1H NMR (Acetone, 500MHz): Shift = 8.13 (d, $J=0.6$ Hz, 1 H), 7.81 - 7.86 (m, 1 H), 7.49 (d, $J=2.5$ Hz, 1 H), 7.13 (dd, $J=8.8, 2.5$ Hz, 1 H), 3.88 (s, 3 H), 3.86 (s, 3 H), 3.36 ppm (s, 3 H); ^{13}C NMR (Acetone, 126MHz): Shift = 162.7, 158.8, 140.5, 136.2, 131.1, 123.9, 118.5, 107.3, 62.3, 55.8, 33.3 ppm; Purity(UV) > 99 %; t_{R} : 6.95 min, ESI-MS $[\text{M}+\text{H}]^+$: 252.06; calcd. $[\text{M}]^+$: 251.06.

Synthesis of intermediate compound VI, 2-bromo-1-(4-hydroxy-3-methylphenyl)ethan-1-one: The procedure for the synthesis of **VI** was taken from Bakke and co-workers.⁵ 5 g (33 mmol) of commercial available 1-(4-hydroxy-3-methylphenyl)ethan-1-one in 100 ml of chloroform was added to a boiling solution of 2 eq. of copper (II) bromide in ethyl acetate. The mixture was refluxed overnight. The progress of the reaction was monitored by TLC. Then, the crude reaction mixture was stirred and warmed over charcoal, filtered off, and the solvent was removed under reduced pressure. The resulting solid was recrystallized from heptane/ethyl acetate 2:1 to yield **VI** as a light purple solid. ^1H NMR (DMSO- d_6 , 300MHz) Shift = 7.77 - 7.74 (m, 1 H), 7.70 (dd, $J = 2.2, 8.4$ Hz, 1 H), 6.91 (d, $J = 8.4$ Hz, 1 H), 5.03 (s, 2 H), 2.16 (s, 3 H); IR (NaCl): (C-Br-stretching 672 cm^{-1}).

Synthesis of intermediate compound VII, 2-mercapto-5-nitrobenzaldehyde: The synthesis was carried out as described by Reinhard and co-workers in 2004.⁶ A mixture of 1 g (5.91 mmol) of 2-

fluoro-5-nitrobenzaldehyde and 1.1 eq. of sodium sulphide nonahydrate in 15 ml of DMSO were stirred under nitrogen at room temperature. After completion of the reaction the solution was poured into ice water acidified with 2N HCl and extracted with diethyl ether (3x). The combined organic layer was dried, filtered and concentrated in vacuo to give the crude **VII** as yellow solid which was directly used for the synthesis of **VIII** without further purification.

Synthesis of intermediate compound VIII, (4-hydroxy-3-methylphenyl)(5-nitrobenzo[b]thiophen-2-yl)methanone: **VII** was dissolved in acetonitrile at 0°C and 1 eq. of K₂CO₃ was added. The mixture was stirred for 30 minutes at 0°C and **VI** dissolved in acetonitrile was added drop-wise and the mixture was stirred at room temperature. After 3 hours a precipitate was formed, which was filtered off and washed subsequently with cold acetonitrile and a mixture of water and acetonitrile. The crude product was analyzed by ¹H NMR and then directly used without further characterization for the next step. ¹H NMR (300MHz, DMSO-d₆) Shift = 8.99 (d, J = 1.9 Hz, 1 H), 8.40 - 8.23 (m, 3 H), 7.80 - 7.64 (m, 2 H), 6.82 (d, J = 8.2 Hz, 1 H), 2.18 (s, 3 H).

Synthesis of compound 11a, (5-aminobenzo[b]thiophen-2-yl)(4-hydroxy-3-methylphenyl)methanone: The procedure for the synthesis of **11a** was earlier described by Dey and co-workers in 2012.⁷ 3 eq. of FeSO₄ x 7H₂O and 0.24 eq. of citric were dissolve in 100 ml of water and purged with nitrogen. Then 5 eq. of NaBH₄ was quickly added and the resulting suspension was stirred for 5 min at room temperature. Stirring was stopped and the water was carefully decanted. The iron on the bottom of the flask was washed twice with degassed water suspended in 10 ml of water again. Then **VIII** was added and the suspension was stirred at room temperature. The reaction was monitored by TLC. After completion of the reaction, the mixture filtered and the filtrate was extracted with ethyl acetate (4x). The combined organic layer was dried over magnesium sulphate, and the solvent was removed under reduced pressure. The crude product was recrystallized from ethanol to give 3.6 g (12.6 mmol, 85 %) of **11a**. ¹H NMR (DMSO-d₆, 500MHz): δ = 10.32 (s, 1 H), 7.79 (s, 1 H), 7.63 - 7.70 (m, 3 H), 7.09 (d, J=2.1 Hz, 1 H), 6.95 (d, J=8.2 Hz, 1 H), 6.90 (dd, J=8.5, 2.1 Hz, 1 H), 5.24 (br. s., 2 H), 2.21 ppm (s, 3 H); ¹³C NMR (DMSO-d₆, 126MHz): δ = 187.7, 160.6, 147.1, 143.1, 141.0, 132.7, 131.3, 130.2, 129.8, 128.8, 124.9, 123.3, 118.5, 114.8, 108.3, 16.4 ppm; Purity (UV) : 90 %; t_R: 10.58 min, ESI-MS [M+H]⁺: 284.21; calcd. [M]⁺: 283.07.

Synthesis of compound 11, (4-hydroxy-3-methylphenyl)(5-hydroxybenzo[b]thiophen-2-yl)methanone: The procedure for the synthesis of **11** was earlier described by Martin-Smith and co-workers in 1956.⁸ 0.5 g (1.8 mmol) of **11a** were refluxed in 100 ml of a 40 % (w/v) NaHSO₃ solution for 48 hours. The reaction was stopped by diluting the mixture with 200 ml of water, and an excess of sodium hydroxide was added. The mixture was heated to reflux for an hour. The solution was allowed to cool to room temperature and the resulting precipitate was filtered off. The filtrate was acidified using concentrated HCl and the newly formed precipitate was collected and recrystallized from ethanol to yield 0.14 g (0.49 mmol, 28 %) of **11** as a white solid. ¹H NMR (DMSO-d₆, 300MHz): δ = 10.54 (br. s., 2 H), 8.07 - 8.25 (m, 2 H), 7.97 (br. s., 1 H), 7.61 - 7.81 (m, 2 H), 7.47 (d, J=8.4 Hz, 1 H), 7.02 (d, J=7.8 Hz, 1 H), 2.21 ppm (s, 3 H); ¹³C NMR (DMSO-d₆, 75MHz): δ = 187.4, 161.1, 145.1, 140.1, 139.6, 132.8, 131.7, 131.5, 130.0, 128.1, 125.0, 124.6, 122.4, 119.5, 115.0, 16.4 ppm; Purity (UV) 95 %; t_R: 10.48 min, ESI-MS [M+H]⁺: 285.10; calcd. [M]⁺: 284.05.

Synthesis of intermediate compound IX, methyl 5-nitrobenzo[b]thiophene-2-carboxylate: The title compound was synthesized from 2-fluoro-5-nitrobenzaldehyde according to procedure A to yield 14

g (59 mmol, 99 %) of **IX** as a white solid. After confirmation of the identity by NMR, the compound was directly used without further characterisation in the next step. ^1H NMR (DMSO- d_6 , 300MHz) δ = 9.00 - 8.96 (m, 1 H), 8.43 (s, 1 H), 8.38 - 8.33 (m, 1 H), 8.33 - 8.27 (m, 1 H), 3.92 (s, 3 H) ppm; ^{13}C NMR (DMSO- d_6 , 75MHz) δ = 162.3, 147.3, 146.0, 138.9, 136.7, 132.1, 125.0, 122.1, 121.5, 53.5 ppm.

Synthesis of intermediate compound X, methyl 5-aminobenzo[b]thiophene-2-carboxylate: The procedure for the synthesis of **11a** was earlier described by Dey and co-workers in 2012.⁷ 3 eq. of $\text{FeSO}_4 \cdot 7\text{H}_2\text{O}$ and 0.24 eq. of citric were dissolve in 100 ml of water and purged with nitrogen. Then 5 eq. of NaBH_4 was quickly added and the resulting suspension was stirred for 5 min at room temperature. Stirring was stopped and the water was carefully decanted. The iron on the bottom of the flask was washed twice with degassed water suspended in 10 ml of water again. Then **IX** was added and the suspension was stirred at room temperature. The reaction was monitored by TLC. After completion of the reaction, the mixture filtered and the filtrate was extracted with ethyl acetate (4x). The combined organic layer was dried over magnesium sulphate, and the solvent was removed under reduced pressure. The crude product was recrystallized from ethanol to give 5.35 g (25.8 mmol, 86 %) of **X** as a white solid. ^1H NMR (DMSO- d_6 , 300MHz) δ = 7.92 (s, 1 H), 7.65 (d, J = 8.6 Hz, 1 H), 7.06 (br. s., 1 H), 6.89 (d, J = 8.8 Hz, 1 H), 5.26 (br. s., 2 H), 3.85 (s, 3 H) ppm; ^{13}C NMR (DMSO- d_6 , 75MHz) δ = 163.2, 147.3, 140.4, 132.7, 130.6, 130.0, 123.4, 118.4, 107.8, 52.9 ppm.

Synthesis of intermediate compound XI, 5-hydroxybenzo[b]thiophene-2-carboxylic acid: The procedure for the synthesis of **XI** was earlier described by Martin-Smith and co-workers in 1956.⁸ 3 g (14.5 mmol) of **X** were refluxed in 150 ml of a 40 % (w/v) NaHSO_3 solution for 48 hours. The reaction was stopped by diluting the mixture with 230 ml of water, and an excess of sodium hydroxide was added. The mixture was heated to reflux for an hour. The solution was allowed to cool to room temperature and the resulting precipitate was filtered off. The filtrate was acidified using concentrated HCl and the newly formed precipitate was collected and recrystallized from ethanol to yield 1.6 g (8.25 mmol, 57 %) of **XI** as colourless needles. ^1H NMR (DMSO- d_6 , 300MHz) δ = 9.91 - 9.38 (m, 2 H), 8.00 (s, 1 H), 7.87 (d, J = 8.6 Hz, 1 H), 7.48 (d, J = 2.0 Hz, 1 H), 7.16 (dd, J = 2.1, 8.7 Hz, 1 H) ppm; ^{13}C NMR (DMSO- d_6 , 75MHz) δ = 164.0, 140.1, 139.4, 136.0, 135.0, 130.2, 124.1, 120.1, 113 ppm; Purity (UV) > 95 %, t_R : 2.75 min; ESI-MS $[\text{M}+\text{H}]^+$: 194.04; calcd. $[\text{M}]^+$: 194.00.

Synthesis of compound 16, 1-(5-hydroxy-1-benzothiophen-2-yl)ethan-1-one: The title compound was synthesized starting from **XI** using the procedure described by Rubottom and co-workers in 1983.⁹ Therefore **XI** was dissolved in dry THF and cooled to -78°C . Then 8 eq. of methyl lithium was added dropwise and the reaction was stirred for 30 min at -78°C , before it was allowed to warm to room temperature. The mixture was stirred for another 30 min at RT, before 27 eq. of TMSCl were added. Then a solution of 1N HCl was carefully added and the aqueous layer was extracted with ethyl acetate (4x). The combined organic layer was dried over magnesium sulphate and the solvent was removed in vacuo. The crude product was purified on a waters autopurification system to give compound **16** as yellow solid. ^1H NMR (Methanol- d_4 , 300 MHz) δ = 8.02 (br. s., 1H), 7.71 (d, J = 7.82 Hz, 1H), 7.31 (br. s., 1H), 7.05 (d, J = 7.45 Hz, 1H), 2.65 (br. s., 3H) ppm ; ^{13}C NMR (Methanol- d_4 , 75 MHz,) δ = 193.3, 155.4, 144.2, 140.7, 134.2, 130.2, 123.2, 118.3, 109.5, 25.3 ppm; Purity (UV): > 95 %; t_R : 7.96 min; ESI-MS $[\text{M}-\text{H}]^-$: 191.0; calcd. $[\text{M}]^+$: 192.02.

7.2.3 Tables

Table 7.5. Potencies of the reference compound TG003 in different studies depending on the experimental conditions, to facilitate a comparison of our compound's potencies with those reported in the cited studies.

	Reference compound	TG003	
	IC ₅₀ (Dyrk1A)/nM	IC ₅₀ (Clk1)/nM	Selectivity factor (SF)
This study	830	170	4.9
Fedorov et al. ¹⁰	156	49	3.2
Mott et al. ¹¹	12 ^a	19 ^a	0.6
Ogawa et al. ¹² / Muraki et al. ²	930 ^b	20 ^b	46 ^b

^a K_d values for TG003 on Dyrk1A and Clk1

^b IC₅₀ values were not provided in the same study. There is a discrepancy between the assay conditions used in the two papers of the group

Table 7.6. 17-β HSD1 and -2 inhibition by compounds 16, 23, and 25

Compound	% 17-β HSD1 inhibition	% 17-β HSD2 inhibition
16	IC ₅₀ = 195 nM	IC ₅₀ = 1200 nM
23	33 % @ 5μM	11 % @ 5μM
25	0 % @ 5μM	7 % @ 5μM

Table 7.7. Comparison of potencies dependent on the ATP concentration in the cell free assay for 16 and harmine in different studies.

	ATP concentration [μM] ¹	16	Harmine
		IC ₅₀ [nM]	
This study	100	170	100
	10	83	39
Ogawa et al. ¹²	10	-	350
Göckler et al. ¹³	100	-	33
Bain et al. ¹⁴	50	-	80
Tahtouh et al. ¹⁵	15	-	34

¹ One obvious factor which strongly influences the measured potencies of ATP-competitive inhibitors under cell-free conditions is the ATP concentration. This explains, at least in part, the apparently lower potencies obtained with our standard assay conditions (100 μM ATP), as can be seen from the reference compound harmine, a well-established, potent ATP competitive inhibitor of Dyrk1A. However, working at ATP concentrations under the Km value of the kinase for ATP (37 μM ¹² - 59 μM ¹⁶) leads to a strong over-estimation of the potencies and, concomitantly, to a large drop of activities when changing to cell-based assays.

Table 7.8. Selectivity of compounds 16 and 23 against a panel of 31 selected protein kinases^a covering all kinase families from the kinome tree.

Kinase Family	Kinase	16	23
		% inhibition at 5 μM ^b	
CMGC	Dyrk1A	96	95
	Dyrk1B	99	98
	Dyrk2	50	46
	DYRK3	12	23
	DYRK4	11	16
	Ck2 α	10	9
	Clk1	98	99
	CLK2	67	85
	CLK3	16	43
	CLK4	90	97

	HIPK1	10	1
	GSK3 β	3	16
STE	MST4	5	9
AGC	PKC β	-8	19
CAMK	PIM1	44	59
	PIM2	10	23
	CaMKI	-2	1
	STK17A (DRAK1)	47	65
	PKD2	6	32
	MYLK2 (skMLCK)	19	36
	MLCK (MLCK2)	53	49
	MYLK (MLCK)	15	12
Other	Haspin	69	83
CK1	CSNK1D (CK1 delta)	-1	16
	CSNK1G2 (CK1 gamma 2)	3	26
	CSNK1G3 (CK1 gamma 3)	13	12
	CSNK1E (CK1 epsilon)	8	15
TKL	MLK1	10	-3
TK	EGFR	20	-3
	ROS	9	4
		-8	-18

^a the screening list was especially composed to include all kinases that were frequently reported as off-targets for diverse chemical classes of Dyrk inhibitors.¹³⁻¹⁷ Hence, the low hit rate besides the main targets Dyrk1A/1B and Clk1/4 (basically limited to Haspin for **23**) suggests a very high degree of selectivity. In comparison, reference compound TG003 also inhibited CSNK1D and CSNK1G2 (IC₅₀= 150 and 270 nM, respectively)¹¹. ^b All screenings were performed in the presence of 100 μ M ATP.

Table 7.9. IC₅₀ values (nM) of 16 and 23 against Dyrk1A, Clk1, and the off-target Haspin.

	16	23
Dyrk1A	230	230

Dyrk1B	170	104
Clk1	52	64
Haspin	2500	800

7.2.4 Figures

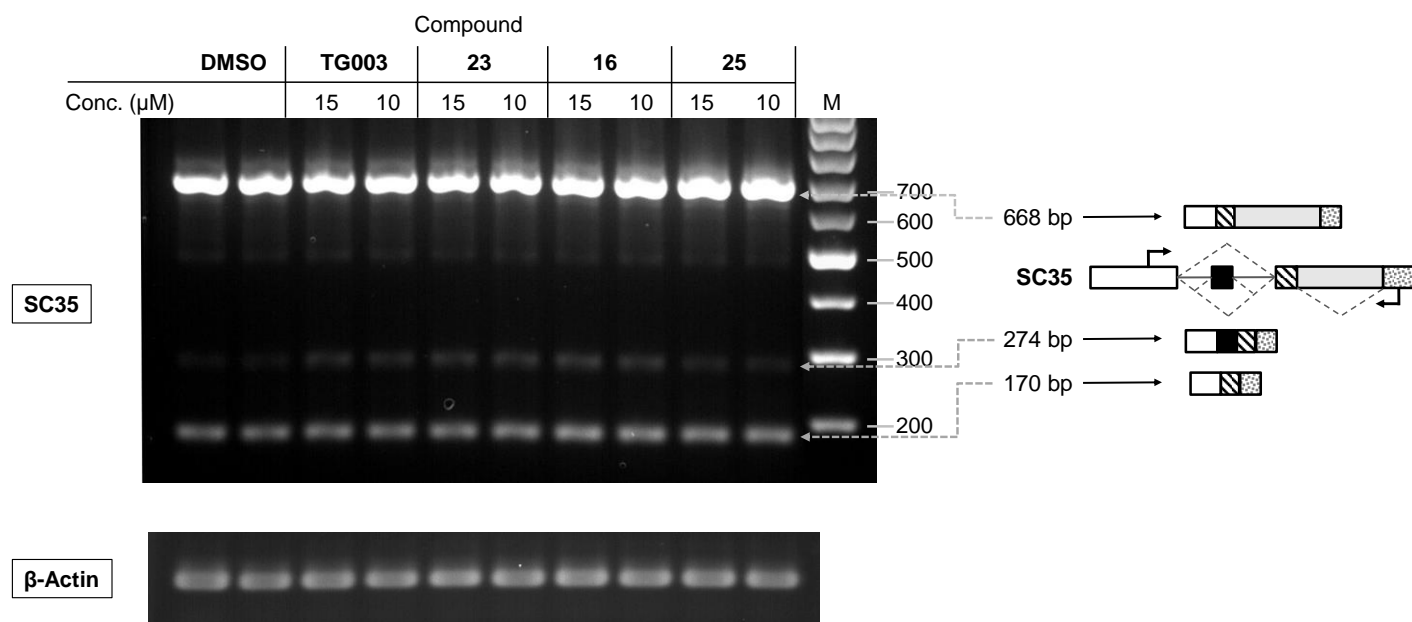


Figure S1. Modulation of SC35 mRNA splicing pattern by the Dyrk1A/Clk1 inhibitors. After treatment of STO cells with the compounds (concentrations as indicated in the Figure), total RNA was isolated and reverse transcribed to cDNA as described above. The PCR amplification was performed as described above, and the products resolved by agarose gel electrophoresis followed by ethidium bromide staining. Amplification of β -actin was used as a control for the cDNA amounts.

As can be seen, the potent compounds 23 and 16 as well as the reference compound TG003 but not the less potent Dyrk1A inhibitor 18 induced a marked increase in the 274 bp transcript at the expense of the shorter splicing variant lacking exon 2 (183 bp). Results shown are representative of at least two independent experiments; on the right panel, samples derived from duplicate cell treatments were applied. M: 1 kb DNA-ladder from Peqlab (Cat.No. 25-2030); relevant bp sizes of the marker are indicated at the right border.

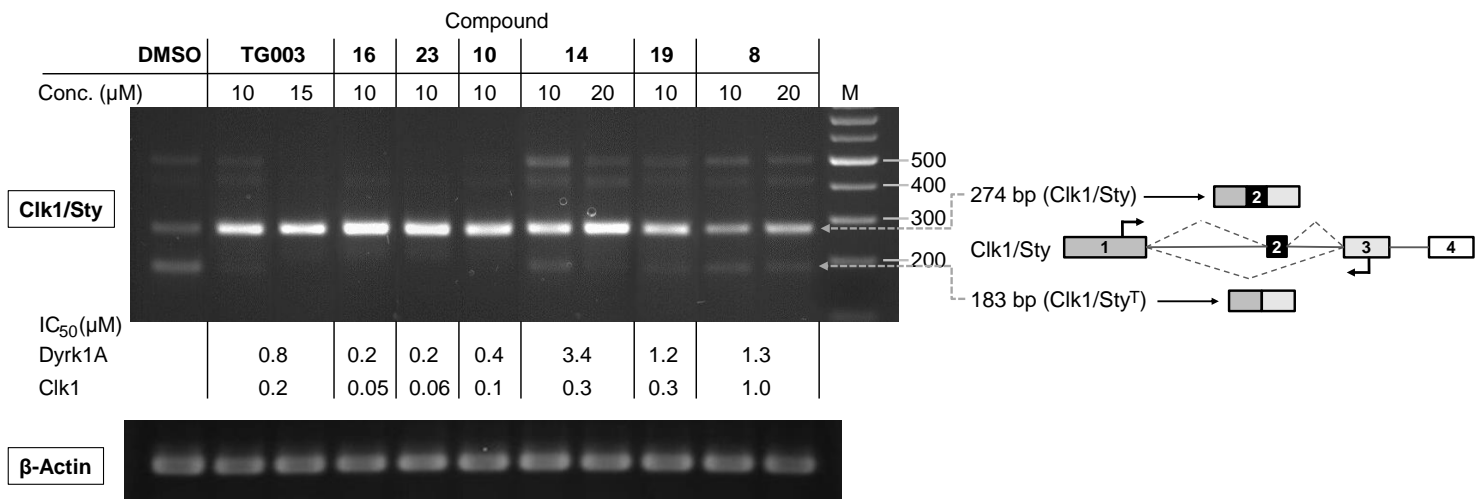


Figure S2. The strength of the Clk1/Sty mRNA splicing modulation correlates with the potency to inhibit Dyrk1A and Clk1. After treatment of STO cells with the compounds (concentrations as indicated in the Figure), total RNA was isolated from the cells and reverse transcribed to cDNA as described above. The PCR was performed as described above, and the products resolved by agarose gel electrophoresis followed by ethidium bromide staining. Amplification of β -actin was used as a control for the cDNA amounts.

More potent compounds were grouped to the left, including the reference compound TG003. Treatment with the compounds led to a disappearance of all alternative splicing products, triggering the production of only the full length Clk1 mRNA. ... strongly induced the generation of the full length Clk1 mRNA, at the expense of all alternative splicing products. The most potent compound was 23,

As can be seen, the potent compounds 23 and 16 as well as the reference compound TG003 but not the less potent Dyrk1A inhibitor 18 induced a marked increase in the 274 bp transcript at the expense of the shorter splicing variant lacking exon 2 (183 bp). Results shown are representative of at least two independent experiments; on the right panel, samples derived from duplicate cell treatments were applied. M: 1 kb DNA-ladder from Peqlab (Cat.No. 25-2030); relevant bp sizes of the marker are indicated at the right border.

7.2.5 References

- (1) Schmitt, C.; Kail, D.; Mariano, M.; Empting, M.; Weber, N.; Paul, T.; Hartmann, R. W.; Engel, M. Design and Synthesis of a library of lead-like 2,4-bisheterocyclic substituted thiophenes as selective Dyrk/Clk inhibitors. *PLoS One* **2014**, *9*, e87851.
- (2) Muraki, M.; Ohkawara, B.; Hosoya, T.; Onogi, H.; Koizumi, J.; Koizumi, T.; Sumi, K.; Yomoda, J.; Murray, M. V.; Kimura, H.; Furuichi, K.; Shibuya, H.; Krainer, A. R.; Suzuki, M.; Hagiwara, M. Manipulation of alternative splicing by a newly developed inhibitor of Clks. *J Biol Chem* **2004**, *279*, 24246–24254.
- (3) Pilch, B.; Allemand, E.; Facompré, M.; Facompre, M.; Bailly, C.; Riou, J.; Soret, J.; Tazi, J. Specific Inhibition of Serine- and Arginine-rich Splicing Factors Phosphorylation , Spliceosome Assembly , and Splicing by the Antitumor Drug NB-506 Specific Inhibition of Serine- and Arginine-rich Splicing Factors Phosphorylation , Spliceosome Assembly ,. *Cancer Res* **2001**, *61*, 6876–6884.
- (4) Miralinaghi, P.; Schmitt, C.; Engel, M.; Frotscher, M.; Hartmann, R. W. Systematic replacement of the heterocycle core in the 6-hydroxybenzothiazole ketone type inhibitors of 17 β -Hydroxysteroid Dehydrogenase Type 1 (17 β -HSD1) reveals 6-hydroxybenzothiophene ketones as a new potent class of inhibitors with optimal molecule geo. *ChemMedChem* **2014**, *Submitted*.
- (5) Bakke, B. a; McIntosh, M. C.; Turnbull, K. D. Improved alkylation and product stability in phosphotriester formation through quinone methide reactions with dialkyl phosphates. *J. Org. Chem.* **2005**, *70*, 4338–4345.
- (6) Reinhard, E.; Kolodziej, S.; Anderson, D.; Stehle, N.; Vernier, W.; Lee, L.; Hegde, S. Method of using aminocyanopyridine compounds as mitogen activated protein kinase-activated protein kinase-2 inhibitors. *PCT/US2003/039166* **2004**.
- (7) Dey, R.; Mukherjee, N.; Ahammed, S.; Ranu, B. C. Highly selective reduction of nitroarenes by iron(0) nanoparticles in water. *Chem Comm* **2012**, *48*, 7982–7984.
- (8) Martin-Smith, M.; Gates, M. Benzothiophene-4,5-quinones. *J. Am. Chem. Soc.* **1956**, *78*, 5351–5357.
- (9) Rubottom, G. M.; Kim, C. Preparation of Methyl Ketones by the Sequential Treatment of Carboxylic Acids with Methylolithium and Chlorotrimethylsilane. *J. Org. Chem.* **1983**, *48*, 1550–1552.

- (10) Fedorov, O.; Huber, K.; Eisenreich, A.; Filippakopoulos, P.; King, O.; Bullock, A. N.; Szklarczyk, D.; Jensen, L. J.; Fabbro, D.; Trappe, J.; Rauch, U.; Bracher, F.; Knapp, S. Specific CLK inhibitors from a novel chemotype for regulation of alternative splicing. *Chem. Biol.* **2011**, *18*, 67–76.
- (11) Mott, B. T.; Tanega, C.; Shen, M.; Maloney, D. J.; Shinn, P.; Leister, W.; Marugan, J. J.; Inglese, J.; Austin, C. P.; Misteli, T.; Auld, D. S.; Thomas, C. J. Evaluation of substituted 6-arylquinazolin-4-amines as potent and selective inhibitors of cdc2-like kinases (Clk). *Bioorg Med Chem Lett* **2009**, *19*, 6700–6705.
- (12) Ogawa, Y.; Nonaka, Y.; Goto, T.; Ohnishi, E.; Hiramatsu, T.; Kii, I.; Yoshida, M.; Ikura, T.; Onogi, H.; Shibuya, H.; Hosoya, T.; Ito, N.; Hagiwara, M. Development of a novel selective inhibitor of the Down syndrome-related kinase Dyrk1A. *Nat. Comm* **2010**, *1*, 86.
- (13) Göckler, N.; Jofre, G.; Papadopoulos, C.; Soppa, U.; Tejedor, F. J.; Becker, W.; Gockler, N. Harmine specifically inhibits protein kinase DYRK1A and interferes with neurite formation. *FEBS J.* **2009**, *276*, 6324–37.
- (14) Bain, J.; Plater, L.; Elliott, M.; Shpiro, N.; Hastie, C. J.; McLauchlan, H.; Klevernic, I.; Arthur, J. S. C.; Alessi, D. R.; Cohen, P. The selectivity of protein kinase inhibitors: a further update. *Biochem J* **2007**, *408*, 297–315.
- (15) Tahtouh, T.; Elkins, J. M.; Filippakopoulos, P.; Soundararajan, M.; Burgy, G.; Durieu, E.; Cochet, C.; Schmid, R. S.; Lo, D. C.; Delhommel, F.; Oberholzer, A. E.; Pearl, L. H.; Carreaux, F. F.; Bazureau, J.; Knapp, S.; Meijer, L.; Ralf, S.; Pearl, H. Selectivity, Cocrystal Structures, and Neuroprotective Properties of Leucettines, a Family of Protein Kinase Inhibitors Derived from the Marine Sponge Alkaloid Leucettamine B. *J Med Chem* **2012**, *55*, 9312–9330.
- (16) Adayev, T.; Wegiel, J.; Hwang, Y.-W. Harmine is an ATP-competitive inhibitor for dual-specificity tyrosine phosphorylation-regulated kinase 1A (Dyrk1A). *Arch. Biochem. Biophys.* **2011**, *507*, 212–218.
- (17) Bain, J.; McLauchlan, H.; Elliott, M.; Cohen, P. The specificities of protein kinase inhibitors: an update. *Biochem J* **2003**, *371*, 199–204.
- (18) Anastassiadis, T.; Deacon, S. W.; Devarajan, K.; Ma, H.; Peterson, J. R. Comprehensive assay of kinase catalytic activity reveals features of kinase inhibitor selectivity. *Nat Biotechnol* **2011**, *29*, 1039–1045.

(19) Pagano, M. A.; Bain, J.; Kazimierczuk, Z.; Sarno, S.; Ruzzene, M.; Di Maira, G.; Elliott, M.; Orzeszko, A.; Cozza, G.; Meggio, F.; Pinna, L. A. The selectivity of inhibitors of protein kinase CK2: an update. *Biochem J* **2008**, *415*, 353–365.

(20) Cuny, G. D.; Robin, M.; Ulyanova, N. P.; Patnaik, D.; Pique, V.; Casano, G.; Liu, J. F.; Lin, X.; Xian, J.; Glicksman, M. A.; Stein, R. L.; Higgins, J. M. Structure-activity relationship study of acridine analogs as haspin and DYRK2 kinase inhibitors. *Bioorg Med Chem Lett* **2010**, *20*, 3491–3494.

8. Lebenslauf

Persönliche Daten

Geburtsdatum: 12. Oktober 1982

Familienstand: Verheiratet, 1 Kind

Ausbildung

Juni 2009 bis August 2014: ➤ Promotionsstudium, Titel der Dissertation: Development of new Lead-Like Dual Inhibitors of the cdc2-like Kinase 1 (Clk1) and Dual Specificity Y-phosphorylation Regulated Kinases 1A and 1B (Dyrk1A and Dyrk1B), Abschlussnote: Magna cum laude
➤ Fortbildung zum iQA (ISO 9000 Normenfamilie)

September 2003 bis März 2009: ➤ Chemiestudium an der Universität des Saarlandes. Abschluss Diplomchemiker (Gesamtnote 1,2)
➤ Titel der Diplomarbeit: Massenspektrometrische Methoden zur Analytik von Proteinacetylierungen

Oktober 2002 bis August 2003: ➤ Zivildienst: Rettungsdienst bei der Berufsfeuerwehr Saarbrücken, Ausbildung zum Rettungshelfer

September 1993 bis Juni 2002: ➤ Gymnasium am Schloss, Saarbrücken; Allgemeine Hochschulreife (Gesamtnote 2,2)

Praktische Erfahrung

Juni 2009 bis Oktober 2013: ➤ Wissenschaftlicher Mitarbeiter am Institut für pharmazeutische und medizinische Chemie an der Universität des Saarlandes unter Leitung von Prof. Dr. R. W. Hartmann
➤ Mitarbeit an der präklinischen Entwicklung von Dyrk- und Cdc2-like Kinasehemmstoffen zur Behandlung neurodegenerativer Erkrankungen und Krebs
➤ Organische Synthese und Analytik der Verbindungen (HPLC/MS, GC/MS und NMR Techniken (1D, 2D)) unter GLP Bedingungen
➤ Entwicklung und Validierung einer MALDI-Triple Quadrupole basierten Methode zur Analyse von Kinaseassays (Publikation [3])
➤ Expression und chromatographische Aufreinigung von Proteinen (IEX, SEC)
➤ Entwicklung und Validierung der Radioaktivitäts- und Lumineszenzassays
➤ Erste Erfahrung in Personalführung durch Anleitung einer Laborantin bei der Durchführung der biochemischen *in vitro* Assays.
➤ Leitung und Koordination des Vertiefungspraktikums medizinische Chemie für Studierende der Chemie, als auch des Praktikums „Medicinal Chemistry and Molecular Modelling“ für Studierende der Chemie und Pharmazie
➤ Erfolgreiche Mitarbeit an einem DFG-Antrag (EN381/3-1)

Juni 2008 bis März 2009:	<ul style="list-style-type: none"> ➤ Diplomarbeit unter Leitung von Prof. Dr. Andreas Tholey ➤ MALDI-TOF-MS/MS zur Identifizierung von Proteinacetylierungen ➤ Protein Identifikation mittels PFF und PMF
Nov. 2007 bis März 2008:	<ul style="list-style-type: none"> ➤ Leitung der Übung „Grundlagen der Chemie“ für Studierende des Maschinenbaus und der biomedizinischen Technik an der Hochschule für Technik und Wirtschaft des Saarlandes (HTW Saar)

Sonstiges

Fremdsprachen- kenntnisse:	<ul style="list-style-type: none"> ➤ Deutsch – Muttersprache ➤ Englisch – fließend in Wort und Schrift ➤ Französisch – fließend in Wort und Schrift
Sonstige Kenntnisse:	<ul style="list-style-type: none"> ➤ Microsoft Office, Origin Pro, Laborgerätesoftware, Windows, Linux ➤ ICH Quality Documents (Q1, Q2, Q7, Q10)
Zertifikate:	<ul style="list-style-type: none"> ➤ Sachkundenachweis nach §5 der „Chemikalien-Verbotsordnung“ ➤ QM und iQA (ISO 9000 Normenfamilie)
Mitgliedschaften in Verbänden:	<ul style="list-style-type: none"> ➤ Mitglied der Gesellschaft Deutscher Chemiker (GDCh)
Ehrenamtliche Tätigkeiten:	<ul style="list-style-type: none"> ➤ Von 2003 bis 2009 Vorstandsmitglied im Badmintonverein SuS Obere Saar e.V.

Hobbies

- Rudern, Badminton (aktiv in einer Verbandsligamannschaft)
-

Referenzen

-
1. Prof. Dr. Rolf W. Hartmann, Helmholtz Institute for Pharmaceutical Research Saarland, 66123 Saarbrücken; Rolf.hartmann@helmholtz-hzi.de
 2. Dr. Matthias Engel, Institut für pharmazeutische und medizinische Chemie, Universität des Saarlandes, 66123 Saarbrücken; ma.engel@mx.uni-saarland.de
 3. Prof. Dr. Simon Cämmerer, Instituto de Química Caixa Postal 6154 Campinas, SP 13083-970 Sala I-209; simon.cammerer@iqm.unicamp.br

Christian Schmitt

Saarbrücken, 18.08.2014

Publikationen

- [1] Christian Schmitt, Dagmar Kail, Marica Mariano, Martin Empting, Nadja Weber, Tamara Paul, Matthias Engel and R.W. Hartmann; Design and Synthesis of a Library of Lead-Like 2,4-Bisheterocyclic Substituted Thiophenes as Selective Dyrk/Clk inhibitors. *PlosOne.*, **2014**, 9(3): e87851. doi:10.1371/journal.pone.0087851
- [2] Christian Schmitt, Parisa Miralinaghi, Marica Mariano, Matthias Engel and R.W. Hartmann; Hydroxybenzothiophene ketones are efficient pre-mRNA splicing modulators due to dual inhibition of Dyrk1A and Clk1/4. *Medicinal Chemistry Letters*, **2014**, accepted; DOI: 10.1021/ml500059y
- [3] David Gode, Christian Schmitt, Matthias Engel and Dietrich A. Vollmer, Screening Dyrk1A inhibitors by MALDI-QQQ mass spectrometry. Systematic comparison to established radiometric, luminescence and LC-UV-MS assays *Analytical and Bioanalytical Chemistry*, **2014**, 406(12):2841-2852.; DOI: 10.1007/s00216-014-7703-1
- [4] Parisa Miralinaghi^a, Christian Schmitt^a, R.W. Hartmann, Martin Frotscher and Matthias Engel; Systematic replacement of the heterocycle core in the 6-hydroxybenzothiazole ketone type inhibitors of 17 β -Hydroxysteroid Dehydrogenase Type 1 (17 β -HSD1) reveals 6-hydroxybenzothiophene ketones as a new potent class of inhibitors with optimal molecule geometry and conformational pre-organization. *ChemMedChem*, **2014**, accepted; DOI: 10.1002/cmdc.201402050 (^aboth authors equally contributed to this work)
- [5] Marica Mariano, Christian Schmitt, Miralinaghi Parisa, Marco Catto, R.W. Hartmann, Angelo Carotti, Matthias Engel; First selective dual inhibitors of tau phosphorylation and beta-amyloid aggregation, two major pathogenic mechanisms in Alzheimer's disease. *ACS Chemical Neuroscience*, **submitted**

Posterbeiträge

- [1] Schmitt C., Hartmann R.W., Engel M.; Development of Selective Dyrk1A Inhibitors, 5th Summer School "Medicinal Chemistry", September **2010**, Regensburg, Germany
- [2] Schmitt C., Mariano M., Carotti A., Engel, M.; Discovery of Hydroxybenzothiophene Ketones as New Dyrk1A Inhibitors For the Treatment of Down Syndrome Related Alzheimer's Disease, September, International Symposium on Medicinal Chemistry (ISMC), **2012**, Berlin, Germany